SOURCE OF SCHEELITE IN THE TURBIDITE-HOSTED OROGENIC AU DEPOSITS OF OTAGO, NEW ZEALAND: AN INTEGRATED METAMORPHIC SOURCE MODEL EXPLAINING THE PRESENCE OR ABSENCE OF SCHEELITE IN TURBIDITE-HOSTED OROGENIC AU DEPOSITS

Ben J. Cave

(BSc. Honours, University of Adelaide)

ARC Centre of Excellence in Ore Deposits (CODES)

School of Physical Sciences (Earth Sciences)

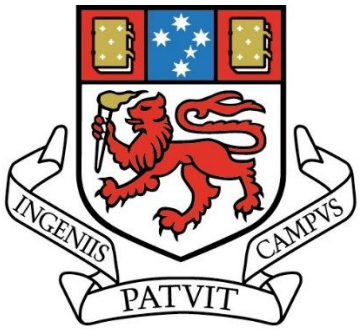

UNIVERSITY OF TASMANIA

Submitted in fulfilment of the requirements for the degree of

Doctor of Philosophy

University of Tasmania

May, 2016

Declaration

This thesis does not contain any material that has been accepted for degree or diploma by the University or any other institution, except where it has been duly acknowledged in the thesis. To the best of the author's knowledge it also contains no previously published material written by another person, except where it is acknowledged in the text of the thesis.

Ben J. Cave

Date: 02-09-2016

Authority of Access

The publisher of the papers comprising Chapter 7 (The Canadian Mineralogist) and Chapter 8 (Mineralium Deposita) holds the copyright for that content, and access to the material should be sought from the respective journals. The remaining non published content of the thesis may be made available for loan and limited copying and communication in accordance with the Copyright Act 1968.

Statement of Co-authorship

The following people and institutions contributed to the publication of work undertaken as part of this thesis:

Ben Cave, University of Tasmania = **Candidate**

Aleksandr Stepanov, University of Tasmania = **Author 1**

Dave Craw, University of Otago = **Author 2**

Ross Large, University of Tasmania = **Author 3**

Jacqueline Halpin, University of Tasmania = **Author 4**

Jay Thompson, University of Tasmania = **Author 5**

Iain Pitcairn, Stockholm University = **Author 6**

Sean Johnson, University of Tasmania = **Author 7**

Chris White, Nova Scotia Department of Natural Resources = **Author 8**

Stafford McKnight, Federation University Australia = **Author 9**

Author details and their roles:

Paper 1, Release of Trace Elements through the Subgreenschist Facies Breakdown of Detrital Rutile to Metamorphic Titanite in the Otago Schist, New Zealand:

Located in Chapter 7

Candidate was the primary author (75%) and combined with authors 1, 2, and 3 contributed to the idea, its formalization, and development (15%). Author 4 provided U-Pb

geochronological ages for zircons, and assisted in the refinement and presentation (10%). Author 5 assisted in the refinement of the methodology section (5%).

Paper 2, A Metamorphic Mineral Source for W in the Turbidite-hosted Orogenic Au Deposits of the Otago Schist, New Zealand:

Located in Chapter 8

Candidate was the primary author (80%) and combined with authors 2, 3, 6, and 7 contributed to the idea, its formalization, and development (15%). Author 5 assisted in the refinement of the methodology section (5%).

Paper 3, The Source of W in Turbidite-hosted Orogenic Au Mineralization: Implications for Metamorphic Processes and Metal Sources in the Meguma and Bendigo-Ballarat Terranes:

Located in Chapter 9

Candidate was the primary author (80%) and combined with author 3, 8, and 9 contributed to the idea, its formalization and development (15%). Author 5 assisted in the refinement of the methodology section (5%).

We the undersigned agree with the above stated "proportion of work undertaken" for each of the above published (or submitted) peer-reviewed manuscripts contributing to this thesis:

Ross Large

Primary Supervisor

School of Physical Sciences

University of Tasmania

Leonid Danyushevsky

Co-Supervisor/ Head of Earth Sciences

School of Physical Sciences

University of Tasmania

Abstract

The Otago Schist in the South Island of New Zealand is a Mesozoic-aged accretionary belt comprised predominately of metaturbiditic graywackes and argillites, with subordinate metabasic horizons and ultramafic slices. A complete crustal section is exposed from prehnite-pumpellyite facies on the flanks to upper greenschist facies (biotite-garnet-albite) in the center of the belt. Quartz veins are abundant throughout the schist, some of which are enriched in a variety of metals including W, Au, As, Ag, Hg, and Sb. Historically, W (scheelite; $CaWO_4$) has been exploited from some of these veins, with in excess of 3,000 tons of scheelite concentrate having been produced.

Previous research on metal sources for these deposits has defined the sources for most of these metals. Sources are well-constrained for Au, As, Ag, Hg, and Sb, with the metamorphic recrystallization of sedimentary pyrite (to metamorphic pyrrhotite) having been shown to mobilize these metals. The source for W, however, has not been constrained.

The primary aim of this thesis is to investigate the source of W (scheelite) in the turbidite-hosted orogenic Au deposits of the Otago Schist. Major lithologies have been sampled and analyzed from the lowest metamorphic grade to the highest metamorphic grade observed in the Otago Schist. Combined laser ablation inductively coupled plasma mass spectrometry (LA-ICP-MS) traverses, images, and spot analyzes, show that detrital rutile is the most important host mineral for W in the subgreenschist facies rocks, and that its prograde metamorphic recrystallization to titanite releases significant amounts of W. Mass balance calculations indicate that this mineral reaction has potential to mobilize over 1,100 tons of W from every 1 km^3 (0.41 g of W per ton of rock) of subgreenschist facies rock metamorphosed to greenschist facies conditions. Scheelite development closely follows the progression of this W-liberating reaction, with early formation of scheelite micrograins

within the fabric of the rock evolving to locally and regionally sourced scheelite-bearing veins. Scheelite is present in the Otago Schist in two major vein forms, that is, syn-metamorphic and late-metamorphic veins. Syn-metamorphic veins sampled at Fiddlers Flat and Lake Hāwea show distinct differences in chemical composition to scheelite from late metamorphic veins at the Macraes Mine, with the Macraes scheelite being enriched in REEs, Y, and Sr. This enrichment in the Macraes scheelite is likely sourced from the breakdown of the Ca-silicate minerals epidote and titanite by the ore forming fluid.

Tungsten enrichments (in the form of scheelite) are common in Archean to Cenozoic aged turbidite-hosted orogenic Au deposits, worldwide. The source model developed for the W-bearing turbidite-hosted orogenic deposits of the Otago Schist was evaluated through investigating the source and mobilization mechanism in two additional turbidite-hosted orogenic Au provinces, one containing orogenic Au mineralization with associated subordinate W (Meguma Terrane, Canada) and the other containing orogenic Au mineralization without associated W (Bendigo-Ballarat Terrane, Australia). Similar to the Otago Schist, in both of these terranes, detrital rutile is the most important host mineral for W in the lowest metamorphic grade rocks, and its prograde metamorphic recrystallization (to ilmenite) releases significant amounts of W (1.9 g and 0.18 g of W per ton of rock, Meguma Terrane and Bendigo-Ballarat Terrane, respectively). This release of W in the Meguma Terrane is likely the source of W in the orogenic Au deposits. The lack of W in the orogenic Au deposits of the Bendigo-Ballarat Terrane possibly reflects the Au in these deposits as being sourced from lower greenschist facies metasediments (Castlemaine metasediments), and further potentially precludes previous models that have suggested source rocks for Au in these deposits as being either Castlemaine metasediments at the upper greenschist-amphibolite transition or underlying Cambrian metavolcano-sedimentary rocks. However, the lack of scheelite in the Bendigo-Ballarat Terrane could also result from other factors, such as

variations in the conditions of formation of the mineralized veins (P, T, pH, redox, host-rock composition) that may not favor the transport and/or precipitation of W. These factors were unable to be resolved in this study.

The results presented within this thesis support recent models for turbidite-hosted orogenic Au mineralization, whereby prograde metamorphic recrystallization of diagenetic or detrital metal-rich mineral phases [pyrite to pyrrhotite, Au, As, Ag, Hg, and Sb; rutile to titanite or ilmenite (this study), W] can release significant amounts of these metals into the concurrently developing metamorphic fluids that can be subsequently focused into regional structures and form orogenic Au ± W deposits.

Acknowledgements

I would like to thank my family, girlfriend Georgia, and friends, for their constant support and encouragement over the 3.5 years, which has been instrumental in my ability to produce this completed thesis. Georgia is additionally thanked for her invaluable assistance in the field.

My supervisory team consisting of Professor Ross Large, Professor Leonid Danyushevsky, and Dr Aleksandr Stepanov, are thanked for their constant support and guidance. Likewise, Professor Dave Craw at the University of Otago, New Zealand, and Dr Iain Pitcairn at the University of Stockholm are thanked for sharing their enthusiasm, as well as immense wealth of knowledge of the geology of the Otago Schist.

I am indebted to Al Cusion and Michelle Chapple-Smith at the UTAS lapidary who consistently produced perfect laser mounts, which was fundamental for this research. Mr Jay Thompson, Dr Sarah Gilbert, and Dr Ivan Belousov are thanked for their assistance with LA-

ICP-MS analyzes, as is Dr Karsten Goemann and Dr Sandrin Feig for their assistance with SEM work.

Advice and samples provided by Dr Chris White, Professor Rebecca Jamieson, and Mr Stafford McKnight, is acknowledged and proved invaluable for this research. In addition, I am extremely thankful for the scheelite samples provided by Ms Lauren Farmer (via Dave Craw), which were instrumental in unravelling the story behind the source of W in the Otago Schist.

Funding for this research, for which I am extremely thankful, was provided by a University of Tasmania, Centre of Excellence post-graduate grant, and a Society of Economic Geology, Student Research Grant (SRG_15-28) from the Newmont Mining Corporation.

Table of Contents

List of Tables

Chapter 5

Chapter 6

Chapter 7

Chapter 8

List of Figures

Chapter 2

Chapter 3

Chapter 4

Chapter 5

from prehnite-pumpellyite facies (A, B, C) to upper greenschist facies (M, N, O). A, prehnite-pumpellyite facies turbidites (near-complete Bouma Sequence) from the Fiddlers Flat section. Bedding is largely preserved. B, argillite-graywacke contact in prehnite-pumpellyite facies rocks from Fiddlers Flat. C, photomicrograph (transmitted light) showing argillite-graywacke contact in prehnite-pumpellyite facies rocks from Fiddlers Flat. D, pumpellyite-actinolite facies turbidites (near-complete Bouma Sequence) from the Fiddlers Flat section. E, cut surface (perpendicular to foliation/bedding) of pumpellyite-actinolite facies greywacke-psammite, showing foliation development that largely obscures bedding. F, photomicrograph of pumpellyite-actinolite greywacke-psammite from Fiddlers Flat, showing foliation development and elongation (parallel to foliation) of minerals. Relict bedding features can still be observed. G, lower greenschist facies outcrop near pumpellyite-actinolite/ lower greenschist facies boundary along the Lake Hāwea section. Minor syn-metamorphic veins (qtz-ab-ttn-ep-sch) are observed. H, close-up of lower greenschist facies psammitic schist from Lake Hāwea, showing segregation laminae development. I, photomicrograph of lower greenschist facies psammitic schist from Lake Hāwea, showing qtz-ab±cld and cld-ttn-k-mca-act-czo-gr segregation laminae. J, lower greenschist facies outcrop along Lake Hāwea section, displaying a higher degree of textural reconstruction than lower greenschist facies samples in G, H, and I. K, close-up of lower greenschist facies psammitic schist from Lake Hāwea, showing textural reconstruction of the rock and the syn-metamorphic veins. L, photomicrograph of lower greenschist facies psammitic schist from Lake Hāwea, showing qtz-ab and cld-ttn-k-mca-act-czo-gr segregation laminae that display a higher degree of textural reconstruction. M, upper greenschist facies psammitic schist from Clyde Dam that display a higher degree of textural reconstruction than the lower greenschist facies

Chapter 7

Chapter 8

Fig. 46. Scanning electron images of mineralogical texture within the Meguma (A-M) and Bendigo-Ballarat terranes (N-T). Meguma Terrane: (A) Heavy mineral band (highlighted) in lower greenschist facies Halifax Group slate (CUN-03) containing zircon, rutile, apatite, and other minerals. (B) Anhedral poikilitic rutile grain containing inclusions of muscovite, chlorite, and quartz, in regionally metamorphosed lower greenschist facies Halifax Group psammite (CUN-13). (C) Rounded rutile grain within regionally metamorphosed lower greenschist facies Halifax Group slate (CUN-03). Rounded rutile grain displaying prominent zonation patterns under SEM; zonation is truncated by the rounded grain boundaries. (D) Rounded anhedral slightly poikilitic rutile grain, with subhedral to euhedral fine laths adjoining it, within regionally metamorphosed lower greenschist facies Halifax Group slate (CUN-03). (E) Rounded slightly poikilitic rutile grain, with very minor subhedral to euhedral rutile laths adjoining it, within regionally metamorphosed lower greenschist facies Halifax Group slate (CUN-03). Prominent zonation patterns are observed under SEM, with zonation being truncated by the rounded grain boundaries. (F) Polycrystalline rutile mantling quartz and pyrrhotite in regionally metamorphosed lower greenschist facies Halifax Group psammite (CUN-13). (G) Subhedral poikilitic rutile grain containing inclusions of muscovite, chlorite, and quartz, in regionally metamorphosed lower greenschist facies Goldenville Group psammite/ argillite (MG-3). (H) Anhedral poikilitic ilmenite grain containing inclusions of muscovite and quartz, and mantled by biotite, in regionally metamorphosed upper greenschist facies Goldenville Group psammite (MG-7). (I) Rotated subhedral poikilitic ilmenite grain containing inclusions of muscovite, chlorite, biotite, and quartz, in regionally metamorphosed upper greenschist facies Goldenville Group psammite (CUN-14). Anhedral to subhedral rutile laths are observed along ilmenite grain boundaries. (J) Subhedral poikilitic ilmenite grain containing inclusions

of muscovite, chlorite, biotite, and quartz, in regionally metamorphosed upper greenschist facies Goldenville Group psammite (CUN-15). Rare rutile relict grains are observed within some ilmenite grains, and are textural dissimilar to the commonly observed rutile laths that grow along ilmenite grain boundaries. (K) Subhedral poikilitic rutile grain containing inclusions of muscovite, chlorite (with minor recrystallization to biotite), and quartz, in hornfelsed (biotite-in isograd) Halifax Group shale (KIL-E04P). Rutile shows very minor recrystallization to ilmenite (insert). (L) Subhedral poikilitic ilmenite grain containing inclusions of muscovite, biotite (with minor inclusions of muscovite and chlorite), rutile, and quartz, in hornfelsed (above biotite-in isograd) Halifax Group shale (SS). (M) Subhedral poikilitic ilmenite grain containing inclusions of muscovite, biotite, quartz and, rare rutile, in hornfelsed (well-above the biotite-in isograd) Halifax Group shale (OEC11-2B). Bendigo-Ballarat Terrane: (N) Rare heavy mineral band (highlighted) in regionally metamorphosed lower greenschist facies Castlemaine Group psammite (259W1-798), containing zircon, rutile, apatite, and other minerals. (O) Enlargement of the heavy mineral band shown in Fig. 45N. (P) Rounded rutile grain within regionally metamorphosed lower greenschist facies Castlemaine Group psammite (NBD005-140.1). Rutile grains commonly display minor fracturing. (Q) Subhedral rutile grain within regionally metamorphosed lower greenschist facies Castlemaine Group psammite (NBD005-140.1). Rutile grains commonly display rounding and minor fracturing. (R) Rare heavy mineral band (highlighted) in hornfelsed (well-above the biotite-in isograd) Castlemaine Group psammite (H8), containing zircon, apatite, ilmenite, and other minerals. (S) Band containing ilmenite and phyllosilicate minerals (for example, muscovite and biotite) in hornfelsed (well-above the biotite-in isograd) Castlemaine Group psammite (H9B). Not shown in this picture is that these bands run parallel to rare heavy mineral bands (for example, Fig. 45R). (T)

Chapter 1: BACKGROUND AND SCOPE

1.1 Background

Turbidite-hosted orogenic Au deposits are a well-studied class of Au deposits that fall under the broader umbrella of orogenic Au deposits. These deposits are an important source for global Au along with being exploited for significant quantities of other metals, including W, Ag, and Sb. Ore metal signatures in these deposits are well summarized (for example, Phillips and Groves 1983; Craw 1992; Groves et al. 1998; Goldfarb et al. 2005) with orogenic Au deposits being enriched in variable amounts of As, Ag, Sb, Te, W, Mo, and Bi, and importantly low base-metal contents (Goldfarb and Groves 2015). Various models have been proposed to account the source(s) of these metal enrichments, with recent studies suggesting metals mobilized during metamorphism represent the source of the metals enriched in these deposits (for example, Pitcairn et al. 2006, 2014, 2015b; Large et al. 2011). These studies, however, invariably focused on Au, As, and Sb, leaving the sources of other metals enriched in these deposits (for example, W) to be poorly constrained.

The Otago Schist of southern New Zealand provides an ideal natural laboratory in which to investigate the hypothesis of a metamorphic source for W in orogenic Au deposits. No volumetrically significant syn-orogenic magmas or spatially contemporaneous lamprophyric dyke swarms are recognized within the Otago Schist. W-bearing orogenic Au deposits are common in the Otago Schist and have historically been exploited for W, including the currently producing Macreas Au mine. Metamorphic sequences are well-exposed and only minor lithological variation occurs across the belt. Importantly, the mobility of trace elements with metamorphism and mineralization are very well studied providing a robust framework for this

study.

Systematic decreases in elements enriched in the Otago orogenic deposits are observed in the metasedimentary (Au, As, Ag, Hg, Mo, Sb, and W; Pitcairn et al. 2006) and metabasaltic (Au, Sb, and Hg; Pitcairn et al. 2015a) rocks of the Otago Schist, with increasing metamorphic grades. These observations have largely led to the prevailing consensus among recent researchers that the metasedimentary country-rocks hosting these deposits are the major source metals, with a subordinate input of Au, Sb, and Hg from metabasalts also possible. Previous investigations on the occurrence of W in the Otago Schist have suggested that the source rocks for W is either; enriched source rocks (metavolcanics and cherts; Henley et al. 1976; Wood 1983) or non-enriched source rocks [for example, Paterson and Rankin 1979; Paterson 1982, 1986; Craw and Norris 1991). Observation of systematic decreases in W with increasing metamorphic grade in the metasediments (Breeding and Ague 2002; Pitcairn et al. 2006) and not the metabasalts (Pitcairn et al. 2015a), coupled with the observation that W-bearing mineralization throughout the Otago Schist is not spatially associated with any particular rock type (Craw and Norris 1991) strongly suggests non-enriched metasedimentary rocks are the source rocks for W in the Otago Schist. Diagenetic pyrite is identified as the major mineralogical host for Au, As, Ag, Hg, Mo, and Sb in the lowest metamorphic grade metasedimentary rocks (Pitcairn et al. 2010; Large et al. 2012). Recrystallization of diagenetic pyrite to metamorphic pyrrhotite through regional greenschist facies metamorphism releases these elements into the concurrently developing metamorphic fluids effectively mobilizing them from the sedimentary pile, with focusing of these metal-rich fluids into metamorphic structures resulting in orogenic ore formation (Pitcairn et al. 2006, 2010; Large et al., 2012). Large et al. (2012) found no enrichment of W in diagenetic pyrite, as such, W could not have been sourced from diagenetic pyrite to pyrrhotite transition.

This notion that W could be sourced from the sedimentary pile is significant, as elevated concentrations of W ± Bi, Te in ore metals signatures have previously been cited by many authors to imply a magmatic source for mineralizing fluids and metals (for example, Finlayson 1908; Reed 1958; Hedenquist and Lowenstern 1994; Blevin and Chappell 1995; Ishihara 1998).

1.2 Aims and Methods

This study is aimed at identifying the primary mineralogical source of W (scheelite) mineralization in the turbidite-hosted W-rich orogenic Au deposits of Otago, New Zealand. In pursuit of identifying the source of W in the orogenic Au deposits of Otago, New Zealand, this project will:

- Identify and characterize major W-bearing mineral phases in the lowest metamorphic grade metasedimentary rocks.
- Characterize changes these major W-bearing mineral phases undergo with prograde metamorphism. Do they recrystallize and potentially provide a viable W mobilizing reaction?
- Characterize the geochemistry and nature of scheelite in the Otago region, including describing where it is first occurs.
- Discuss the significance of W availability and how it contributes to the model for W depletion and transport in the Otago Schist put forward by Breeding and Ague (2002) and Pitcairn et al (2006).

A key assumption in this study is that the systematic depletions of W shown in the Otago Schist metasediments, with increasing metamorphic grade (Breeding and Ague 2002; Pitcairn et al. 2006), represents W being mobilized from these rocks. The results and associated conclusions of these authors were crucial in designing the research program reported in this thesis.

In addition, this study will test the W source model developed for the Otago deposits, on the similarly W-bearing (scheelite) turbidite-hosted orogenic Au deposits of the Meguma Terrane of Nova Scotia, Canada, and the W deficient turbidite-hosted orogenic Au deposits of the Bendigo-Ballarat Terrane of Victoria, Australia.

1.3 Structure of the Thesis

This thesis consists of three papers (Chapters 7, 8, and 9) that have been or will soon be published. Whilst care was taken to avoid repetition where possible, the nature of producing a thesis by papers has produced some repetition throughout this thesis.

Chapter 2 provides a generalized introduction to orogenic Au deposits; briefly introducing previous nomenclature, their economic significance, and discussing general characteristics that make them a coherent and important class of Au deposit. In this chapter, current and previous genetic models for fluid and metal sources are reviewed, and a summary is provided discussing the most likely source of fluids and metals in the deposits of the Otago Schist, New Zealand.

Chapter 3 deals with the association of W with orogenic Au deposits. Incorporation of W into mineral phases from previous literature is also discussed, with potential enriched sources of W identified. Transportation of W in hydrothermal fluids is also briefly discussed, with previous literature on fluid compositions, metal species, and solubilities of scheelite drawn upon.

Chapter 4 provides a general introduction to the geological evolution of southern New Zealand and development of the Otago Schist. In addition this Chapter (4) discusses orogenic Au-W mineralization in the Otago Schist and the source of W enrichment in the Otago Schist.

Chapter 5 details samples obtained in the Otago Schist including, discussing the rationale

behind the sampling procedure and provides more detailed geology of individual sites selected for systematic sampling programs.

Chapter 6 identifies the major W host mineral phase(s) in the metasedimentary rocks of the Otago Schist of varying metamorphic grade, using Laser Ablation Inductively Coupled Plasma Mass Spectrometer (LA-ICP-MS) traverses, combined with reflected and scanning electron microscopy (SEM), and statistical analyses. In addition, laser traverses are utilized to confirm that W is depleted at the subgreenschist-greenschist facies boundary consistent with the previous study of Breeding and Ague (2002) that showed W mobility at the same metamorphic grade. This chapter is purposely placed prior to Chapter 7, to help the reader understand why the rutile to titanite recrystallization reaction is looked at in depth.

Chapter 7 consists of a manuscript published in The Canadian Mineralogist that details the subgreenschist to greenschist facies recrystallization of detrital rutile to metamorphic titanite, and trace element releases associated with this process. Additionally, trace element data from detrital rutile is used to infer provincial source rocks for the Torlesse Terrane, Otago Schist.

Chapter 8 consists of a manuscript accepted in Mineralium Deposita that builds upon the trace element recrystallization reaction described in Chapter 7. Laser ablation inductively coupled plasma mass spectrometry traverses and mapping techniques are presented within to show W distribution with increasing metamorphic grade and identify and confirm that the detrital rutile to metamorphic titanite mineral recrystallization reaction is the most important W-liberating mineral reaction in the Otago Schist. Development of scheelite and its geochemistry (and Ca-silicate phases) is also discussed within this chapter, with special attention afforded to its incipit development and the timing and pervasiveness of the recrystallization of detrital rutile to metamorphic titanite. Together, evidence presented within this chapter and Chapter 7 is

discussed to propose a source model for W in the Otago Schist and discuss its implications to the currently accepted genetic model for the formation of orogenic mineralization in the Otago Schist.

Chapter 9 consist of a manuscript soon to be submitted to Economic Geology. This manuscript evaluates the rigor of the source model for W in the turbidite-hosted orogenic Au mineralization presented in Chapter 8, through investigating the source and mobilization mechanism in two additional turbidite-hosted orogenic Au provinces, one containing orogenic Au mineralization with associated subordinate W (Meguma Terrane) and the other containing orogenic Au mineralization without associated W (Bendigo-Ballarat Terrane).

Chapter 10 consists of a concise summary of the major findings presented within this thesis.

Detailed information regarding samples collected in this study, along with all LA-ICP-MS and EMPA analyses are presented within in the Appendices, which are contained on a CD-ROM inside the back cover of this thesis.

References

BLEVIN, P. L. & CHAPPELL, B. W. 1995. Chemistry, origin, and evolution of mineralized granites in the Lachlan Fold Belt, Australia; the metallogeny of I-and S-type granites. *Economic Geology,* 90**,** 1604-1619.

BREEDING, C. M. & AGUE, J. J. 2002. Slab-derived fluids and quartz-vein formation in an accretionary prism, Otago Schist, New Zealand. *Geology,* 30**,** 499-502.

CRAW, D. 1992. Fluid evolution, fluid immiscibility and gold deposition during Cretaceous-Recent tectonics and uplift of the Otago and Alpine Schist, New Zealand. *Chemical Geology,* 98**,** 221-236.

CRAW, D. & NORRIS, R. J. 1991. Metamorphogenic Au-W veins and regional tectonics: mineralisation throughout the uplift history of the Haast Schist, New Zealand. *New Zealand Journal of Geology and Geophysics,* 34**,** 373-383.

FINLAYSON, A. M. 1908. The geology of the quartz veins of the Otago goldfields. *Transactions of the New Zealand Institute,* 41**,** 64-84.

GOLDFARB, R. J., BAKER, T., DUBE, B., GROVES, D. I., HART, C. J. & GOSSELIN, P. 2005. Distribution, character, and genesis of gold deposits in metamorphic terranes. *Economic Geology 100th Anniversary Volume***,** 407-450.

GOLDFARB, R. J. & GROVES, D. I. 2015. Orogenic gold: Common or evolving fluid and metal sources through time. *Lithos,* 233**,** 2-26.

GROVES, D. I., GOLDFARB, R. J., GEBRE-MARIAM, M., HAGEMANN, S. G. & ROBERT, F. 1998. Orogenic gold deposits: a proposed classification in the context of their crustal distribution and relationship to other gold deposit types. *Ore Geology Reviews,* 13**,** 7-27.

HEDENQUIST, J. W. & LOWENSTERN, J. B. 1994. The role of magmas in the formation of hydrothermal ore deposits. *Nature,* 370**,** 519-527.

HENLEY, R., NORRIS, R. & PATERSON, C. 1976. Multistage ore genesis in the New Zealand geosyncline a history of post-metamorphic lode emplacement. *Mineralium Deposita,* 11**,** 180-196.

ISHIHARA, S. 1998. Granitoid series and mineralization in the Circum-Pacific Phanerozoic granitic belts. *Resource Geology,* 48**,** 219-224.

LARGE, R., THOMAS, H., CRAW, D., HENNE, A. & HENDERSON, S. 2012. Diagenetic pyrite as a source for metals in orogenic gold deposits, Otago Schist, New Zealand. *New Zealand Journal of Geology and Geophysics,* 55**,** 137-149.

LARGE, R. R., BULL, S. W. & MASLENNIKOV, V. V. 2011. A carbonaceous sedimentary source-rock model for Carlin-type and orogenic gold deposits. *Economic Geology,* 106**,** 331-358.

PATERSON, C. J. 1982. Oxygen isotopic evidence for the origin and evolution of a scheelite ore-forming fluid, Glenorchy, New Zealand. *Economic geology,* 77**,** 1672-1687.

PATERSON, C. J. 1986. Controls on gold and tungsten mineralization in metamorphic-hydrothermal systems, Otago, New Zealand. *Geological Association of Canada special paper,* 32**,** 25-39.

PATERSON, C. J. & RANKIN, P. C. 1979. Trace element distribution in the schist surrounding a quartz-scheelite lode, Glenorchy, New Zealand. *New Zealand Journal of Geology and Geophysics,* 22**,** 329-338.

PHILLIPS, G. N. & GROVES, D. I. 1983. The nature of Archaean gold-bearing fluids as deduced from gold deposits of Western Australia. *Journal of the Geological Society of Australia,* 30**,** 25-39.

PITCAIRN, I. K., TEAGLE, D. A. H., CRAW, D., OLIVO, G. R., KERRICH, R. & BREWER, T. S. 2006. Sources of metals and fluids in orogenic gold deposits: insights from the Otago and Alpine Schists, New Zealand. *Economic Geology,* 101**,** 1525-1546.

PITCAIRN, I. K., OLIVO, G. R., TEAGLE, D. A. H. & CRAW, D. 2010. Sulfide evolution during prograde metamorphism of the Otago and Alpine Schists, New Zealand. *The Canadian Mineralogist,* 48**,** 1267-1295.

PITCAIRN, I. K., CRAW, D. & TEAGLE, D. A. 2014. The gold conveyor belt: large-scale gold mobility in an active orogen. *Ore Geology Reviews,* 62**,** 129-142.

PITCAIRN, I. K., CRAW, D. & TEAGLE, D. A. 2015a. Metabasalts as sources of metals in

orogenic gold deposits. *Mineralium Deposita*, 50**,** 373-390.

PITCAIRN, I., SKELTON, A. & WOHLGEMUTH-UEBERWASSER, C. 2015b. Mobility of gold during metamorphism of the Dalradian in Scotland. *Lithos*, 233**,** 69-88.

REED, J. J. 1958. Granites and mineralization in New Zealand. *New Zealand Journal of Geology and Geophysics*, 1**,** 47-64.

WOOD, B. 1983. Widespread scheelite in Mesozoic schists of South Island, New Zealand [abs.]. *Pacific Science Congress, Proceedings and Abstracts*, 1983**,** 258.

Chapter 2: OROGENIC AU DEPOSITS

2.1 Aims

This chapter has two major aims; (1) provide a generalized introduction to orogenic Au deposits, and (2) review previous and current models for the formation of orogenic Au deposits, focusing on the source(s) of fluids and metals. In doing this, previous nomenclature for these deposits will briefly be introduced, along with their economic significance and the general characteristics that make them a coherent and important class of Au deposit.

2.2 Introduction to Orogenic Au Deposits

The term 'orogenic Au deposits' was first proposed by Groves et al. (1998) in an attempt to clarify and reduce the confusion surrounding the application of various nomenclature to Au deposits that Groves et al. (1998) considered as belonging to a single coherent class of deposits. Previous nomenclature for orogenic Au deposits includes, Au-only, lode-Au, mesothermal Au, shear-zone hosted, structurally-controlled, metamorphic Au, slate-belt hosted, greenstone hosted Au, and mother lode-type deposits. These deposits form an important source for global Au (in excess of 29% of Au ever produced; Foster 2002) and are exploited for significant quantities of other metals, including W, Ag, and Sb. In terms of world-class Au deposits (producing, or containing greater than 100t Au), orogenic Au deposits are the most important class of deposits with sixty-three orogenic Au deposits being classified as world-class Au deposits, as of 2008, which is the largest number of any Au deposit type globally (Groves 2008).

Orogenic Au deposits have formed episodically over more than 3 billion years of Earth's history at convergent plate margins in accretionary and collisional orogens that have experienced

compressional to transpressional deformation processes (Groves et al. 1998; Goldfarb et al. 2001). These deposits show a strong structural control and are typified by quartz-dominate veins systems containing lesser amounts (5-15%) of carbonate minerals (for example, calcite and ankerite) and low contents of sulfide minerals (≤3-5% sulfide minerals, for example; pyrite, pyrrhotite, arsenopyrite) (Groves et al. 1998; Goldfarb et al. 2001). In subgreenschist to greenschist facies hosted systems, albite, paragonite, white mica or fuchsite, chlorite, scheelite, and tourmaline are also common gangue mineral phases; whereas in amphibolite facies hosted systems, amphibolite, diopside, biotite/phlogopite, tourmaline, and garnet are the most common gangue mineral phases (Groves et al. 1998; Goldfarb et al. 2001). Ore metals signatures in these deposits are well summarized (for example, Phillips and Groves 1983; Craw 1992; Groves et al. 1998; Goldfarb et al. 2005) with orogenic Au deposits observed as being enriched in Au, together with variable amounts of As, Ag, Sb, Te, W, Mo, and Bi, and importantly low base-metal contents (Goldfarb and Groves 2015).

Important to note is that orogenic Au deposits share many similarities with the coherent and genetically distinct reduced intrusion-related Au systems (RIRGS), particularly in terms of fluid compositions, metal assemblages (Au, As, Ag, Bi, Te ± Sb, W), and alteration (Hart and Goldfarb 2005). This has led to considerable confusion in distinguishing intrusion-related Au and orogenic Au vein deposits (variably discussed in Goldfarb et al. 2001, 2005; Groves et al. 2003; Hart and Goldfarb 2005). Goldfarb et al. (2001) highlights the common, consistent temporal and spatial metal zonation patterns commonly recognized in RIRGS as being a point of departure between the two. In addition, orogenic Au deposits often occur in the same orogens as Au-rich porphyry and epithermal-vein deposits (Fig. 1). Porphyry and epithermal deposits, however, are spatially more restricted, and only occur over a very narrow depth range, and well

within the continental margin arc. In contrast, orogenic Au deposits are observed forming in the fore arc region over an extended range of depths (Groves et al. 1998). Gold-rich volcanogenic massive sulfide (VMS) deposits in instances, may also be observed as having a spatial association with orogenic Au deposits (Fig. 1), but typically these two deposit types form tens of millions years apart, with VMS deposits forming earlier within the oceanic rocks prior to collision-and-accretion on the growing continental margins (Groves et al. 2000).

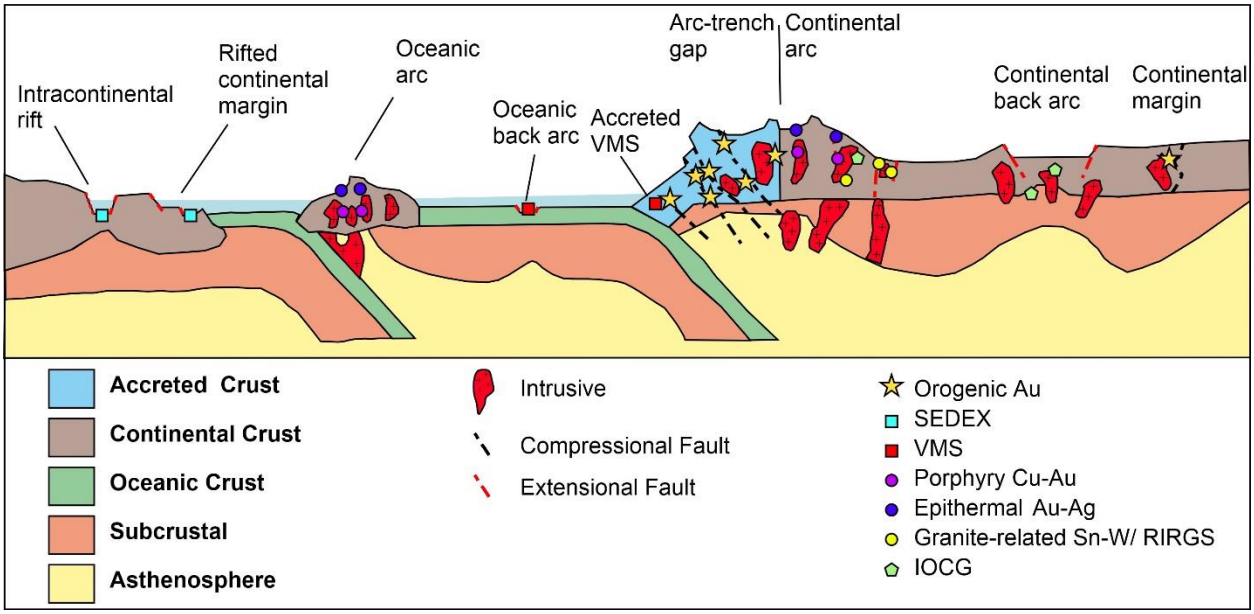

Fig. 1. The tectonic settings of Au-rich mineral deposits. Epithermal veins, Au-rich porphyry and skarn deposits, form in the shallow (≤5 km) parts of both island and continental arcs in compressional through extensional settings. In contrast, orogenic Au deposits are emplaced during collisional events throughout much of the middle to upper crust. Modified from Goldfarb and Groves (2015).

2.3 Characteristics of Orogenic Au Deposits

Orogenic Au deposits, as stated earlier, are recognized by numerous workers as being a coherent group of deposits, sharing numerous characteristics common to one another. Important coherent characteristics that define orogenic Au deposits identified by previous workers (Groves et al. 1998; Jia 2002; Bierlein et al. 2004; Mortensen et al. 2010) are summarized as follows:

- Structurally controlled mineralization, hosted within regional-scale compressional to transpressional structures in metamorphosed volcanic-plutonic or sedimentary terranes, within accretionary and collisional orogenic belts.
- Strong lithological control, mineralization usually restricted to certain stratigraphic units within a province, typically units containing permeable or chemically reactive lithologies, or both.
- Mineralization, syn-accretionary near peak metamorphism, in brittle to ductile shear zones.
- Distributed in belts of great geological complexity, with gradients of lithology, strain, and metamorphic grade, reflecting an orogenic environment.
- Gold precipitation is syn-kinematic, typically in structures with high-angle oblique displacement, commonly with reverse slip, but with some examples in transcurrent fault regimes.
- Mineralogy typified by quartz-dominated vein systems with subordinate carbonate (5-15% carbonate minerals, for example, calcite and ankerite) and sulfide minerals (≤3-5% sulfide minerals, for example, pyrite, pyrrhotite, and arsenopyrite). Gangue vein mineral phases are restricted, relative to metamorphic grade with greenschist facies deposits commonly containing accessory amounts of albite, paragonite, white mica or fuchsite, chlorite, scheelite, and tourmaline, whilst amphibolite facies deposits commonly containing accessory amounts of, diopside, biotite/phlogopite, tourmaline, and garnet.
- Characterized by enrichment in Au, As, Ag (± Sb, Te, W, Mo, Bi, and B), whilst base metals Cu, Pb, and Zn commonly display only minor enrichment relative to background levels.

- Ore forming hydrothermal fluids are dilute aqueous carbonic fluids, with uniformly low fluid salinities (typically: 3-7 wt% NaCl equivalent), and $CO_2 + CH_4$ contents of 5-30 mole %, with up to 55 mole % of N_2.
- Abundant quartz-carbonate veins and show evidence for formation from fluids at pressures from supra-lithostatic to sub-lithostatic within brittle-ductile shear zones.
- Mineralization formed over a uniquely broad range of upper to mid-crustal pressures and temperatures, primarily 1.5 ± 0.5 kbar, 350° ± 50°C, but can occur over 1-5 kbar, 200-650°C.
- Vein systems commonly have vertical extents greater than 2 km, and display cryptic lateral and vertical zoning.

2.4 Review of Genetic Models for Fluid and Metal Sources

Despite extensive research devoted to understanding these deposits, many uncertainties still remain surrounding their formation, in particular the sources of their metals and fluids. Various models have been proposed to explain the source(s) of fluids and metals in orogenic Au deposits. The most popular are the metamorphic crustal devolatilization model (Kerrich and Fryer 1979; Kerrich and Fyfe, 1981; Phillips and Groves 1983; Phillips et al. 1987; Phillips 1993; Kerrich et al. 2005; Pitcairn et al. 2006; Phillips and Powell 2010), magmatic hydrothermal fluid models (Burrows et al. 1986; Burrows and Spooner 1987; Spooner 1993), the slab subduction model (Breeding and Ague 2002; Hyndman et al. 2015), the mantle derived fluids and metals model (Cameron and Hattori 1987; Cameron 1993; Krogh 1993) and a meteoric water circulation model (Nesbitt et al. 1986; Nesbitt 1988; Nesbitt and Muehlenbachs 1989; So and Yun 1997) (for example, Fig. 2).

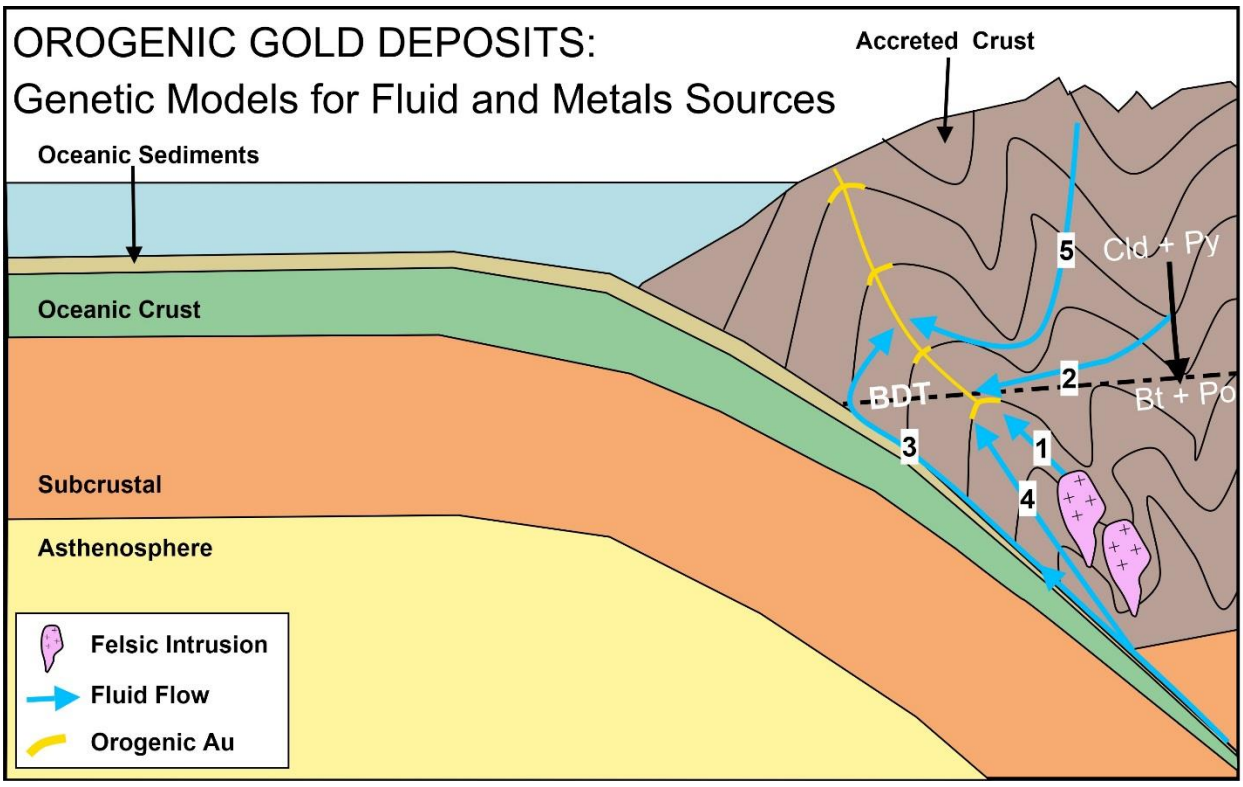

Fig. 2. Summary Diagram for various metals/fluid source models for orogenic Au deposits. 1- Magmatic Hydrothermal Model, 2- Metamorphic Crustal Devolatilization Model, 3- Slab Subduction Model, 4- Mantle Derived Fluids and Metals Model, 5- Deep Meteoric Water Circulation Model. Abbreviations: BDT- Brittle-ductile transition, Cld- chlorite, Py pyrite, Bt- biotite, Po-pyrrhotite.

2.4.1 Magmatic Hydrothermal

Two models invoking a magmatic hydrothermal origin have previously been proposed by workers (Burrows et al. 1986; Burrows and Spooner 1987; Cameron and Hattori 1987; Rock and Groves 1988; Rock et al. 1989; Spooner 1993) to explain the sources of hydrothermal fluids, and metal enrichments associated with orogenic Au deposits.

The devolatilization of deep crystallizing felsic intrusions model (Burrows et al. 1986; Burrows and Spooner 1987; Cameron and Hattori 1987), is based on empirical evidence gained from field relations, stable isotope compositions of carbon, and the similarity of the element suite of orogenic Au deposits to certain granite-related ore deposit types (Burrows et al. 1986;

Burrows and Spooner 1987; Ridley and Diamond 2000). In this model, fluids are proposed to be sourced by exsolution, from deep crystallizing granitic magmas (second boiling), with metals being concentrated into the magmatic fluid due to their inherent incompatibility during crystallization, or leached from country rocks during fluid propagation, or both.

Felsic intrusions implicated as the source(s) of fluids and metals in some deposits, include Archean tonalite-trondhjemite-granodiorite magmas (Burrows and Spooner 1987) and oxidized alkaline suites (Cameron and Hattori 1987; Ridley and Diamond 2000). However, many orogenic Au deposits initially identified as having a magmatic origin based on their spatial association with felsic intrusions, for example in Burrows et al. (1986), have since been discounted due to high-precision dating of the age of spatially associated felsic intrusions and Au-mineralization (Colvine 1988). More evolved reduced ilmenite-bearing granites have also been implicated as a potential source of fluids and metals in this model, however, following the introduction of the reduced intrusion-related Au deposits model (Thompson et al. 1999) these deposits which were originally classified as orogenic Au deposits have been reclassified into the separate, reduced intrusion-related Au deposit class.

Alternate to the devolatilization of felsic magmas model, Rock and Groves (1988) proposed a model in which fluids are released during the crystallization of Au-rich shoshonitic lamprophyre magmas or the interaction of these magmas with crustal rocks or both, with metals thought to have been concentrated in the magmatic fluid due to their inherent incompatibility during crystallization, or have been leached from country rocks during fluid propagation, or both. This model is largely based on the temporal and spatial association of lamprophyres with Au deposits, in conjunction with empirical data of average Au abundance in lamprophyres, which Rock et al. (1989) suggests is several orders of magnitude higher than common igneous rocks.

Rock et al. (1989) also implies that the composition of lamprophyre volatiles and incompatible elements (high H_2O, CO_2, F, K, Rb, and Ba, and moderate S contents) closely mimics that of ore fluids associated with the deposition of Au in orogenic Au-bearing veins. Subsequent analysis of Au and other trace elements commonly associated with orogenic Au deposits (Au, Ag, B, and W) by Wyman and Kerrich (1988), however, found that fresh lamprophyres are not intrinsically enriched in Au (mean Au ≈ 3.8 ppb), or Ag, B, and W that are typically associated with orogenic Au deposits, and suggested that the elevated Au contents reported by Rock and Groves (1988) resulted from analyzing altered lamprophyres. Wyman and Kerrich (1988) further propose that the commonly observed spatial and temporal association of lamprophyres and orogenic Au deposits noted by Rock and Groves (1988) and Rock et al. (1989) reflects a shared tectonic setting, and not a genetic relationship. Additionally, many lamprophyres are derived from subduction zone magmatism and not Au-enriched mantle; and most Au-bearing lamprophyres are located in continental rift and oceanic arc environments, which are tectonic settings that lack orogenic Au (Goldfarb and Groves 2015).

2.4.2 Metamorphic Crustal Devolatilization from Metasedimentary or Metavolcanic Rocks

Metamorphism of crustal rocks at varying metamorphic facies (predominantly at the greenschist-amphibolite facies transition) is an alternative model proposed by multiple workers (Morris and Henley 1976; Kerrich and Fryer 1979; Kerrich and Fyfe 1981; Phillips and Groves 1983; Groves and Phillips 1987; Phillips et al. 1987; Phillips 1993; Pitcairn et al. 2006; Phillips and Powell 2010; Large et al. 2011) to explain the source of fluids and metals in the formation of orogenic Au deposits. In this model, it is generally suggested that Au and other ore components (for example, S and As) are released into concurrently developing metamorphic fluid(s) during

greenschist to amphibolite facies metamorphism (for example, Powell et al. 1991, Tomkins 2010), and most orogenic Au deposits are hosted within greenschist facies metamorphosed host-rock (Goldfarb and Groves 2015). The source of metals in this model is thought to originate from the leaching of metals from crustal rocks during the generation of fluid. Recent geochemical studies in the Otago Schist of New Zealand, provide a compelling case for this source for metals, with systematic decreases in elements enriched in the Otago orogenic deposits documented in the metasedimentary rocks of the Otago Schist, with increasing metamorphic grades (Au, As, Ag, Hg, Mo, Sb, and W; Pitcairn et al. 2006). Diagenetic pyrite is identified as the major mineralogical host for Au, As, Ag, Hg, Mo, and Sb in the lowest metamorphic grade metasedimentary rocks of the Otago Schist (Pitcairn et al. 2010; Large et al. 2012). Recrystallisation of diagenetic pyrite to metamorphic pyrrhotite through regional greenschist facies metamorphism releases these elements into the concurrently developing metamorphic fluids (Pitcairn et al. 2010; Large et al. 2012). This process effectively mobilizes these elements from the sedimentary pile, with subsequent focusing of these metal-rich fluids into metamorphic structures resulting in orogenic ore formation (Pitcairn et al. 2006, 2010; Large et al. 2012). Similar metal-rich diagenetic pyrites are observed in other orogenic Au provinces (for example, Bendigo-Ballarat Terrane; Thomas et al. 2011; Large et al. 2011), suggesting similar processes may be operating for sediment hosted deposits (predominately Phanerozoic in age and younger). One void present in this model, however, is that neither Pitcairn et al. (2010) nor Large et al. (2012) were able to resolve the ultimate source of W which is a metal commonly associated with the orogenic Au deposits of Otago, New Zealand.

Limited volcanic rocks, compared to sedimentary rocks in many Phanerozoic-aged orogenic Au hosting terranes, coupled with recent evidence showing As is not mobilized from

metabasaltic rocks in the Otago Schist during prograde metamorphism (Pitcairn et al. 2015a) suggests that the metasedimentary rocks may be the major source of metals in Phanerozoic-aged orogenic hosting terranes. Precambrian terranes that are highly-endowed in orogenic Au are most commonly developed in supracrustal sequences termed greenstone belts (Goldfarb and Groves 2015). These belts are characteristically comprised of thick-successions of lower arc- to back-arc volcanic rock dominated sequences that host most of the major deposits and are overlain by thick, largely unmineralized metasedimentary rock successions (except in parts of West Africa and northeastern South America) (Goldfarb and Groves 2015). Therefore, although a sedimentary rock source for Au-bearing metamorphic fluids is plausible for Phanerozoic orogenic Au provinces, where world-class to giant deposits are hosted in thick turbidite sequences, it is not considered a viable source for Archean provinces and it is also unlikely for many Paleoproterozoic provinces (Goldfarb and Groves 2015).

Additional evidence supporting a metamorphic model for orogenic Au deposits includes; orogenic Au deposits being spatially and temporally associated with syn-accretionary near-peak metamorphism within metamorphic terranes; alignment of deposits along regional faults and shear zones temporal associated with regional metamorphism suggesting fluid migration occurred from considerable depth and was related to regional metamorphism; fluid-inclusions displaying lithostatic ore-fluid pressures; ore fluids having δD and $\delta 18O$ values within the metamorphic field; and variability of H, C, O, Sr, and Pb isotopes of the deposits consistent with lithologically heterogeneous crust.

2.4.3 Slab Subduction

The slab subduction model is an alternative model that has been proposed by numerous workers (for example, Breeding and Ague 2002, Hyndman et al. 2015) to explain the occurrence

of orogenic deposits throughout the world, including the deposits of the Otago Schist (that is, Breeding and Ague 2002). In the simplest sense, the slab subduction model is essentially a variant on the metamorphic crustal devolatilization model previously described, in that progressive metamorphism of the subducting oceanic lithosphere and (or) overlying oceanic sediments (containing metal-rich pyrite and hydrated minerals such as chlorite) provides a fertile source for both fluids and metals (Goldfarb and Groves 2015). Large volumes of metals and fluids mobilized from the subducting slab travel up-dip along the slab-mantle boundaries (Peacock 1990; Sibson 2004; Peacock et al. 2011), eventually entering fault zones at shallower levels near the base of the crust, and subsequently precipitating as orogenic Au deposits (Goldfarb and Groves 2015).

Problematic to the slab subduction model is that available analytical data doesn't unequivocally support this model above other models. The most compelling evidence for the slab subduction model often cited are the Jiaodong deposits of the North China block (Wang et al. 1998; Goldfarb et al. 2001, 2005; Goldfarb and Santosh 2014; Groves and Santosh 2015). These orogenic deposits, although somewhat controversial in nature are Cretaceous in age (approximately, 120-126 Ma) and hosted by basement rock that experienced high-grade metamorphism during the Precambrian (Goldfarb and Groves 2015). Thus, prograde metamorphism of supracrustal host rocks (that is, the metamorphic crustal devolatilization model) could not have provided the required metals and fluids to produce these Au deposits, implying these metals and fluids are subcrustal in origin (Goldfarb and Groves 2015). Evaluation of potential subcrustal sources for these deposits by Goldfarb and Santosh (2014) and Groves and Santosh (2015) concluded that the most plausible source for these metals and fluids was from metal and fluid -rich oceanic lithosphere and (or) overlying oceanic sediments, with these

fluids and metals mobilized during progressive metamorphism related to their subduction (Goldfarb and Groves 2015).

Debate among researchers of whether subcrustal fluid and metal source(s) implied for the Jiaodong deposits are suitable to explain the formation of many orogenic Au provinces is current, with suggestions that the Jiaodong deposits support a model that best explains most of the tectonic- to deposit-scale features of orogenic Au deposits throughout Earth's history (Groves and Santosh 2015) or a departure from the metamorphic crustal devolatilization model (Goldfarb and Santosh 2014).

2.4.4 Mantle Derived Fluids

The mantle derived fluids model is another model proposed to explain the genesis of orogenic Au systems (for example, Cameron and Hattori 1987, Cameron 1993, Krogh 1993). This model like the slab subduction model, in the simplest sense is a variant on the metamorphic crustal devolatilization model previously described, in that progressive metamorphism of the crust (to granulite facies) provides a fertile source for both fluids and metals. Introduction of an initially CO_2 rich mantle derived fluid is proposed to induce granulite facies metamorphism in the lower crust (Cameron and Hattori 1987; Cameron 1993; Krogh, 1993). Devolatilization suggested accompanying granulite facies metamorphism, produces metamorphic fluids that mix with the mantle derived fluids and leach metals (for example, Au, As, Ag, W) from the crustal rocks, with subsequent focusing of these metal-rich fluids into metamorphic structures resulting in orogenic ore formation (Cameron and Hattori 1987; Cameron 1993; Krogh, 1993). However, recent studies have questioned several fundamental mechanisms and pieces of evidence that support this model. For example, Hoernes and Van Reenen (1992) suggests that influxes of CO_2 into the lower crust will not induce granulite facies metamorphism. In addition, geochemical

depletions in granulite facies rocks in the elements contained within the ore metal signatures (cited as indicating leaching) have been shown as being depleted significantly prior to granulite facies metamorphism (for example, Knudsen and Andersen 1999, Pitcairn et al. 2006, 2015). Furthermore, fluid inclusion data previously cited as indicating a mantle input into the fluids (for example, de Ronde et al. 2000) has also recently been discredited following more rigorous analytical techniques (for example, Goodwin 2010, Goodwin et al. 2016). The mantle derived fluids model, as such, is not considered a viable model amongst the vast majority of current orogenic Au researchers.

2.4.5 Deep Meteoric Water Circulation

The infiltration and circulation of meteoric water deep into the crust is another model proposed (Nesbitt et al. 1986; Nesbitt 1988; Nesbitt and Muehlenbachs 1989; So and Yun 1997) for the genesis of orogenic Au systems. Infiltration of meteoric water deep into the crust in this model, is proposed to occur along transcurrent faults under conditions of low water/rock ratios. Highly depleted δD values obtained from fluid inclusions within orogenic Au veins is the major evidence for a meteoric source for fluids in this model. In this model, like the metamorphic crustal devolatilization, slab subduction, and the mantle derived fluid models, metals are thought to be leached from crustal rocks, with heating of the circulating fluid due to geothermal gradients, thought to promote the solubility of metals in the fluids.

Problematic to the deep meteoric water circulation model are several key uncertainties best highlighted by Jia (2002). For example, in several regions fluid inclusion data from adjacent Au deposits have considerable and widely varying δD values, which are inconsistent with latitudinally controlled δD values of meteoric waters (Weston et al. 1998; Zhang et al. 1989). Low δD values in ore fluids also could result from isotopic exchange with δD-depleted organic

bearing sedimentary rocks in the crust (Peters 1993); or measured bulk extracted fluid inclusions were dominated by secondary inclusions formed in the presence of meteoric water during uplift of the deposits, rather than representing primary ore fluids (Goldfarb et al. 1991; Weston et al. 1998).

Additionally the mixing of meteoric waters with fluids of metamorphic or magmatic origin has also been proposed (Nesbitt and Muehlenbachs 1989; Koons and Craw 1991) as an important mode for precipitating metals out of solution and to account for isotopic data indicating a possible meteoric fluid source. However, this mixed meteoric model also does not account for all the uncertainties listed above.

2.4.6 Summary of Genetic Models

Orogenic Au deposits have long been recognized as an import class of Au deposit in greenstone and turbidite orogenic belts. Despite this recognition and the depth of investigation into this important class of deposit, the mode for their formation is still not clearly understood and is a topic of continual debate in the literature, as are many other aspects of orogenic Au deposits. Debate on the source of metals and fluids is suggested by Goldfarb and Groves (2015) as a relic of the initial classification of orogenic Au deposits. This initial classification focused on lumping deposits that displayed certain features together to form a competent class. However, as Goldfarb and Groves (2015) explore, it is unlikely that orogenic Au deposits formed via a single constant fluid and metal source, as opposed to a variety of fluid and metal sources that produce similar ore fluids and metal signatures; especially considering orogenic Au deposits are recorded in terranes spanning >3 billion years of the Earth's history, throughout which time tectonic and lithospheric settings have undergone considerable change.

In turbidite-hosted terranes of Phanerozoic-age, such as the Otago Schist deposits, there

is a general consensus among the majority of recent researchers that metals mobilized during metamorphism represent the source of the metals enriched in these deposits (for example, Pitcairn et al. 2006, 2014, 2015a; Thomas et al. 2011; Large et al. 2011, 2012). However, one current and important void in this model is the source of W that could not be explained by the transition of pyrite to pyrrhotite.

References

BIERLEIN, F. P., CHRISTIE, A. B. & SMITH, P. K. 2004. A comparison of orogenic gold mineralisation in central Victoria (AUS), western South Island (NZ) and Nova Scotia (CAN): implications for variations in the endowment of Palaeozoic metamorphic terrains. *Ore Geology Reviews,* 25**,** 125-168.

BREEDING, C. M. & AGUE, J. J. 2002. Slab-derived fluids and quartz-vein formation in an accretionary prism, Otago Schist, New Zealand. *Geology,* 30**,** 499-502.

BURROWS, D., WOOD, P. & SPOONER, E. 1986. Carbon isotope evidence for a magmatic origin for Archaean gold-quartz vein ore deposits. *Nature,* 321**,** 851-854.

BURROWS, D. R. & SPOONER, E. T. C. 1987. Generation of a magmatic H2O-CO2 fluid enriched in Au, Mo, and W within an Archean sodic granodiorite stock, Mink Lake, northwestern Ontario. *Economic Geology,* 82**,** 1931-1957.

CAMERON, E. 1993. Precambrian gold: perspectives from the top and bottom of shear-zones. *Canadian Mineralogist,* 31**,** 917-917.

CAMERON, E. M. & HATTORI, K. 1987. Archean gold mineralization and oxidized hydrothermal fluids. *Economic Geology,* 82**,** 1177-1191.

COLVINE, A. C. 1988. Archean lode gold deposits in Ontario, *Ontario Geological Survey Miscellaneous Paper 139,* 136 p.

CRAW, D. 1992. Fluid evolution, fluid immiscibility and gold deposition during Cretaceous-Recent tectonics and uplift of the Otago and Alpine Schist, New Zealand. *Chemical Geology,* 98**,** 221-236.

DE RONDE, C. E. J., FAURE, K., BRAY, C. J. & WHITFORD, D. J. 2000. Round Hill shear zone-hosted gold deposit, Macraes Flat, Otago, New Zealand: evidence of a magmatic ore fluid. *Economic Geology,* 95**,** 1025-1048.

FOSTER, R. P. 2002. Precambrian shields: gold metallogeny, exploration potential and economic realities. *Metallogeny of Precambrian Shields, Ukraine 2002*. Unpublished keynote lecture.

GOLDFARB, R. J. & SANTOSH, M. 2014. The dilemma of the Jiaodong gold deposits: are they unique? *Geoscience Frontiers,* 5**,** 139-153.

GOLDFARB, R. J. & GROVES, D. I. 2015. Orogenic gold: common or evolving fluid and metal sources through time. *Lithos,* 233**,** 2-26.

GOLDFARB, R. J., NEWBERRY, R. J., PICKTHORN, W. J. & GENT, C. A. 1991. Oxygen, hydrogen, and sulfur isotope studies in the Juneau gold belt, southeastern Alaska; constraints on the origin of hydrothermal fluids. *Economic Geology,* 86**,** 66-80.

GOLDFARB, R. J., GROVES, D. I. & GARDOLL, S. 2001. Orogenic gold and geologic time: a global synthesis. *Ore Geology Reviews,* 18**,** 1-75.

GOLDFARB, R. J., BAKER, T., DUBE, B., GROVES, D. I., HART, C. J. & GOSSELIN, P. 2005. Distribution, character, and genesis of gold deposits in metamorphic terranes. *Economic Geology 100th Anniversary Volume***,** 407-450.

GOODWIN, N. R. J. 2010. A combined noble gas and halogen study of orogenic gold mineralisation in the Alpine and Otago Schists, New Zealand. *Ph.D. Thesis*, The

University of Manchester, United Kingdom.

GOODWIN, N. R. J., BURGESS, R., CRAW, D., TEAGLE, D. A. H., & BALLENTINE C. J. 2016. Noble gases fingerprint a metasedimentary fluid source in the Macraes orogenic gold deposit, New Zealand. Mineralium Deposita, *In Press.* Avaliable from: http://link.springer.com/article/10.1007%2Fs00126-016-0648-x [Accessed 3 May 2016].

GROVES, D. I. 2008. Unpublished Orogenic Gold Workshop for Lappland Goldminers AB, June 2008.

GROVES, D. I. & PHILLIPS, G. N. 1987. The genesis and tectonic control on Archaean gold deposits of the Western Australian shield—a metamorphic replacement model. *Ore Geology Reviews,* 2**,** 287-322.

GROVES, D. I. & SANTOSH, M. 2015. Province-scale commonalities of some world-class gold deposits: Implications for mineral exploration. *Geoscience Frontiers,* 6**,** 389-399.

GROVES, D. I., GOLDFARB, R. J., GEBRE-MARIAM, M., HAGEMANN, S. G. & ROBERT, F. 1998. Orogenic gold deposits: a proposed classification in the context of their crustal distribution and relationship to other gold deposit types. *Ore Geology Reviews,* 13**,** 7-27.

GROVES, D. I., GOLDFARB, R. J., KNOX-ROBINSON, C. M., OJALA, J., GARDOLL, S., YUN, G. Y. & HOLYLAND, P. 2000. Late-kinematic timing of orogenic gold deposits and significance for computer-based exploration techniques with emphasis on the Yilgarn Block, Western Australia. *Ore Geology Reviews,* 17**,** 1-38.

GROVES, D. I., GOLDFARB, R. J., ROBERT, F. & HART, C. J. R. 2003. Gold deposits in metamorphic belts: overview of current understanding, outstanding problems, future research, and exploration significance. *Economic Geology,* 98**,** 1-29.

HART, C. & GOLDFARB, R. 2005. Distinguishing intrusion-related from orogenic gold

systems [abs.]. *New Zealand Minerals Conference Proceedings, 2005*. 125-133.

HOERNES, S. & VAN REENEN, D. 1992. The oxygen-isotopic composition of granulites and retrogressed granulites from the Limpopo Belt as a monitor of fluid-rock interaction. *Precambrian Research,* 55**,** 353-364.

HYNDMAN, R. D., MCCRORY, P., WECH, A., KAO, H. & AGUE, J. 2015. Cascadia subducting plate fluids channelled to forearc mantle corner: ETS and silica deposition. *Journal of Geophysical Research: Solid Earth*, 120**,** 4344-4358.

JIA, Y. 2002. Nitrogen isotope characteristics of orogenic lode gold deposits and terrestrial reservoirs. *Ph.D. Thesis*, University of Saskatchewan, Canada.

KERRICH, R. & FRYER, B. 1979. Archaean precious-metal hydrothermal systems, Dome Mine, Abitibi Greenstone Belt. II. REE and oxygen isotope relations. *Canadian Journal of Earth Sciences,* 16**,** 440-458.

KERRICH, R. & FYFE, W. 1981. The gold-carbonate association: Source of CO2, and CO2 fixation reactions in Archaean lode deposits. *Chemical Geology,* 33**,** 265-294.

KERRICH, R., GOLDFARB, R. J. & RICHARDS, J. P. 2005. Metallogenic provinces in an evolving geodynamic framework. *Economic Geology,* 100**,** 1097-1136.

KNUDSEN, T.-L. & ANDERSEN, T. 1999. Petrology and geochemistry of the Tromøy gneiss complex, South Norway, an alleged example of Proterozoic depleted lower continental crust. *Journal of Petrology,* 40**,** 909-933.

KOONS, P. O. & CRAW, D. 1991. Gold mineralization as a consequence of continental collision: an example from the Southern Alps, New Zealand. *Earth and Planetary Science Letters,* 103**,** 1-9.

KROGH, T. 1993. High precision U-Pb ages for granulite metamorphism and deformation in the

Archean Kapuskasing structural zone, Ontario: implications for structure and development of the lower crust. *Earth and Planetary Science Letters,* 119**,** 1-18.

LARGE, R. R., BULL, S. W. & MASLENNIKOV, V. V. 2011. A carbonaceous sedimentary source-rock model for Carlin-type and orogenic gold deposits. *Economic Geology,* 106**,** 331-358.

LARGE, R., THOMAS, H., CRAW, D., HENNE, A. & HENDERSON, S. 2012. Diagenetic pyrite as a source for metals in orogenic gold deposits, Otago Schist, New Zealand. *New Zealand Journal of Geology and Geophysics,* 55**,** 137-149.

MORRIS, R. & HENLEY, R. 1976. Dewatering of a metamorphic pile. *Geology,* 4**,** 333-336.

MORTENSEN, J. K., CRAW, D., MACKENZIE, D. J., GABITES, J. E. & ULLRICH, T. 2010. Age and origin of orogenic gold mineralization in the Otago Schist Belt, South Island, New Zealand: constraints from lead isotope and 40Ar/39Ar dating studies. *Economic Geology,* 105**,** 777-793.

NESBITT, B. E. 1988. Gold deposit continuum: A genetic model for lode Au mineralization in the continental crust. *Geology,* 16**,** 1044-1048.

NESBITT, B. E. & MUEHLENBACHS, K. 1989. Origins and movement of fluids during deformation and metamorphism in the Canadian Cordillera. *Science,* 245**,** 733-736.

NESBITT, B. E., MUROWCHICK, J. B. & MUEHLENBACHS, K. 1986. Dual origins of lode gold deposits in the Canadian Cordillera. *Geology,* 14**,** 506-509.

PEACOCK, S. A. 1990. Fluid processes in subduction zones. *Science,* 248**,** 329-337.

PEACOCK, S. M., CHRISTENSEN, N. I., BOSTOCK, M. G. & AUDET, P. 2011. High pore pressures and porosity at 35 km depth in the Cascadia subduction zone. *Geology,* 39**,** 471-474.

PETERS, S. 1993. Polygenetic melange in the Hodgkinson goldfield, northern Tasman orogenic zone. *Australian Journal of Earth Sciences,* 40**,** 115-129.

PHILLIPS, G. N. 1993. Metamorphic fluids and gold. *Mineralogical Magazine- London,* 57**,** 365-365.

PHILLIPS, G. N. & GROVES, D. I. 1983. The nature of Archaean gold-bearing fluids as deduced from gold deposits of Western Australia. *Journal of the Geological Society of Australia,* 30**,** 25-39.

PHILLIPS, G. N. & POWELL, R. 2010. Formation of gold deposits: a metamorphic devolatilization model. *Journal of Metamorphic Geology,* 28**,** 689-718.

PHILLIPS, G. N., GROVES, D. I. & BROWN, I. J. 1987. Source requirements for the Golden Mile, Kalgoorlie: significance to the metamorphic replacement model for Archean gold deposits. *Canadian Journal of Earth Sciences,* 24**,** 1643-1651.

PITCAIRN, I. K., TEAGLE, D. A. H., CRAW, D., OLIVO, G. R., KERRICH, R. & BREWER, T. S. 2006. Sources of metals and fluids in orogenic gold deposits: insights from the Otago and Alpine Schists, New Zealand. *Economic Geology,* 101**,** 1525-1546.

PITCAIRN, I. K., OLIVO, G. R., TEAGLE, D. A. H. & CRAW, D. 2010. Sulfide evolution during prograde metamorphism of the Otago and Alpine Schists, New Zealand. *The Canadian Mineralogist,* 48**,** 1267-1295.

PITCAIRN, I. K., CRAW, D. & TEAGLE, D. A. 2014. The gold conveyor belt: large-scale gold mobility in an active orogen. *Ore Geology Reviews,* 62**,** 129-142.

PITCAIRN, I. K., CRAW, D. & TEAGLE, D. A. 2015a. Metabasalts as sources of metals in orogenic gold deposits. *Mineralium Deposita,* 62**,** 373-390.

PITCAIRN, I., SKELTON, A. & WOHLGEMUTH-UEBERWASSER, C. 2015b. Mobility of

gold during metamorphism of the Dalradian in Scotland. *Lithos,* 233**,** 69-88.

POWELL, R., WILL, T. & PHILLIPS, G. 1991. Metamorphism in Archaean greenstone belts: calculated fluid compositions and implications for gold mineralization. *Journal of Metamorphic Geology,* 9**,** 141-150.

RIDLEY, J. R. & DIAMOND, L. W. 2000. Fluid chemistry of orogenic lode gold deposits and implications for genetic models. *Reviews in Economic Geology,* 13**,** 141-162.

ROCK, N. M. S. & GROVES, D. I. 1988. Can lamprophyres resolve the genetic controversy over mesothermal gold deposits? *Geology,* 16**,** 538-541.

ROCK, N. M. S., GROVES, D. I., PERRING, C. S. & GOLDING, S. D. 1989. Gold, lamprophyres, and porphyries: what does their association mean. *Economic Geology Monograph,* 6**,** 609-625.

SIBSON, R. H. 2004. Controls on maximum fluid overpressure defining conditions for mesozonal mineralisation. *Journal of Structural Geology*, 26**,** 1127-1136.

SO, C.-S. & YUN, S.-T. 1997. Jurassic mesothermal gold mineralization of the Samhwanghak Mine, Youngdong area, Republic of Korea; constraints on hydrothermal fluid geochemistry. *Economic Geology,* 92**,** 60-80.

SPOONER, E. T. C. 1993. Magmatic sulphide/volatile interaction as a mechanism for producing chalcophile element enriched, Archean Au-quartz, epithermal Au□Ag and Au skarn hydrothermal ore fluids. *Ore Geology Reviews,* 7**,** 359-379.

THOMAS, H. V., LARGE, R. R., BULL, S. W., MASLENNIKOV, V., BERRY, R. F., FRASER, R., FROUD, S. & MOYE, R. 2011. Pyrite and pyrrhotite textures and composition in sediments, laminated quartz veins, and reefs at Bendigo gold mine, Australia: insights for ore genesis. *Economic Geology*, 106**,** 1-31.

THOMPSON, J., SILLITOE, R., BAKER, T., LANG, J. & MORTENSEN, J. 1999. Intrusion-related gold deposits associated with tungsten-tin provinces. *Mineralium Deposita,* 34**,** 323-334.

TOMKINS, A. G. 2010. Windows of metamorphic sulfur liberation in the crust: implications for gold deposit genesis. *Geochimica et Cosmochimica Acta,* 74**,** 3246-3259.

WANG, L., QIU, Y., MCNAUGHTON, N., GROVES, D., LUO, Z., HUANG, J., MIAO, L. & LIU, Y. 1998. Constraints on crustal evolution and gold metallogeny in the Northwestern Jiaodong Peninsula, China, from SHRIMP U–Pb zircon studies of granitoids. *Ore Geology Reviews,* 13**,** 275-291.

WESTON, R., CEDELL, T., MCCUAIG, T. & KERRICH, R. 1998. PTt-deformation-fluid characteristics of lode gold deposits: evidence from alteration systematics. *Ore Geology Reviews,* 12**,** 381-453.

WYMAN, D. & KERRICH, R. 1988. Alkaline magmatism, major structures, and gold deposits; implications for greenstone belt gold metallogeny. *Economic Geology,* 83**,** 454-461.

ZHANG, X., NESBITT, B. E. & MUEHLENBACHS, K. 1989. Gold mineralization in the Okanagan Valley, southern British Columbia; fluid inclusion and stable isotope studies. *Economic Geology,* 84**,** 410-424.

Chapter 3: AN INTRODUCTION TO W: ABUNDANCE IN THE COSMOS AND EARTH'S CRUST; ASSOCIATION WITH OROGENIC AU DEPOSITS; INCORPORATION INTO MINERAL PHASES; TRANSPORTATION IN HYDROTHERMAL FLUIDS

3.1 Aims

This chapter has three major aims; (1) introduce the element W and discuss its metal association in orogenic Au deposits, (2) discuss previous data on the incorporation of W into mineral phases that could act as potential mineralogical sources, and (3) discuss fluid characteristics and mechanisms involved in the transportation and deposition of W, in orogenic Au-W deposits.

3.2 Introduction to W, and W in Orogenic Au Deposits

Tungsten (W) is a rare element in the earth's crust with average upper continental crust abundances ascribed by Hu and Gao (2008) of 1.4 ppm. However, due to its highly incompatible nature (König et al. 2008 and references therein), W is commonly observed being concentrated in the fractionation products of igneous processes, with the highest values most commonly observed in the most evolved rocks (for example, average abundances in granitoids, mafic rocks and ultramafic rocks are 1.5, 0.5-1.0, and 0.1-0.8 ppm, respectively; De Vos et al. 2006). Clastic sedimentary rocks (for example, psammites and shales) commonly contain concentrations similar to those observed in granitoids (approximately 1-2 ppm; De Vos et al. 2006).

The low abundance of W observed in the earth's crust is predominantly ascribed to the

following factor: W like other elements heavier than ^{56}Fe are exclusively synthesized during core collapse supernova processes, these are rare and short astrophysical events, therefore elements produced in these events (for example, ^{74}W) are inherently rare in the cosmos. On Earth, W forms two main oxidation states ($^{+4}$ and $^{+6}$), of these states $^{+6}$ is by far the most common, with the $^{+4}$ oxidization state usually only associated with the rare W sulfide minerals (for example, tungstenite). Tungsten present in the $^{+6}$ oxidization state is almost exclusively as the tungstate (WO_4^{2-}) ion which is present in the 6-fold or 4-fold coordination. Compared to other metals, W is found in quite few minerals in significant proportions, with wolframite $(Fe,Mn)WO_4$), scheelite ($CaWO_4$), ferberite ($FeWO_4$), and hübnerite ($MnWO_4$), being the most common; of these, wolframite and scheelite are economically the most important ore minerals for W, with scheelite being the far more prevalent of these two in orogenic Au deposits.

Gold deposits associated with elevated W are formed under a wide range of geological processes and are distributed all over the world. These elements (Au and W) are common to a range of important Au ore deposits types, including orogenic Au deposits (Groves et al. 1998; Hronsky et al. 2012) and reduced intrusion-related Au deposits (Lang et al. 2000; Mair et al. 2011; Hart and Goldfarb 2005;), of which the former is the focus of this thesis. Orogenic Au-W mineralization is recognized in nearly all major orogenic provinces of varying ages and host rock composition (greenstones, metasediments, and granitoids), including numerous world-class (>100 t Au) orogenic Au deposits [for example, ***Archean Deposits***: Golden Mile, Australia (Brugger et al. 2000); McIntyre–Hollinger, Canada (Bell et al. 1989); Champions Reef, India (Narayanaswami et al. 1960). ***Proterozoic Deposits***: Omai, Guyana (Voicu et al. 1999); Telfer, Australia (Schindler et al. 2012); Olympiada, Russia (Genkin et al. 1998). ***Paleozoic Deposits***: Sukhoi Log (Distler et al. 2005); Muruntau, Uzbekistan (Kempe et al. 2001). ***Mesozoic–Tertiary***:

Macraes, New Zealand (McKeag et al. 1989); Treadwell, United States of America (Barnett and Miller 2003); Grass Valley, United States of America (Farmin 1941)]. Tungsten in these deposits is predominantly found as scheelite ($CaWO_4$) within structurally controlled auriferous quartz-carbonate veins.

3.3 Tungsten Incorporation into Accessory Mineral Phases

Current models on metal sources for turbidite-hosted orogenic deposits (as described in Chapter 2) suggest the recrystallization of diagenetic or detrital minerals is the source of the majority of metals enriched in these deposits (Goldfarb and Groves 2015). However, a mineralogical source for W is not constrained and as such, understanding the incorporation of W into accessory mineral phases is paramount. Previous literature on the concentration and partitioning of W into accessory silicate, oxide, and sulfide minerals is limited, with the majority of available data concerning sulfide and oxide minerals. Sulfide minerals are not considered a viable source for W in the orogenic Au deposits of the Otago Schist, following the detailed investigations of Pitcairn et al. (2010) and Large et al. (2012), and as such, are not discussed in the following section.

Several studies have identified rutile, titanite, and ilmenite as being able to incorporate appreciable amounts of W into their lattices (for example, Lyakhovich and Balanova 1969, Kwak 1983, Rice et al. 1998, Zack et al. 2004, Lucassen et al. 2010). Incorporation of W into these titanium-rich minerals, is proposed by Shannon (1976) as occurring due to W and Ti having similar ionic radii in the six-fold coordination, with Ti^{4+} having an ionic radius of 0.605 Å, whereas W^{4+}, W^{5+}, and W^{6+} have 0.66, 0.62, and 0.60 Å, respectively. Tungsten-rich rutile (hydrothermal in origin), has been observed and described in several orogenic Au deposits [for example, Hemlo, Canada (Urban et al. 1992); Big Bell, Australia (Scott et al. 2011; Scott and Radford 2007)] and intrusion-related Au deposits (for example, Kori Kollo, Boliva; Rice et al.

1998) around the world. Tungsten concentrations in rutile from these deposits varies drastically from below detection limit, up to 57,000 ppm W, and can be associated with up to 48,900 ppm Sb, 31,370 ppm V, 117,400 ppm Nb, and 13,200 ppm Fe (Rice et al. 1998). Similarly, rutile of metamorphic origin has been observed containing enrichments (10's to 100's ppm) in W (for example, Zack et al. 2004, Xiao et al. 2006, Luvizotto et al. 2009). Tungsten-rich titanite (hydrothermal in origin) has been observed and described in several Sn-W skarns around the world [for example, Mt. Lindsay, Tasmania (Kwak 1983); Mactung, Yukon, Canada (Linnen and Che 2009); Ray Gulch, Yukon, Canada (Linnen and Che 2009); Risby, Yukon, Canada (Linnen and Che 2009)]. Tungsten concentrations in titanite from these deposits varies drastically from below detection limit, up to 1,030 ppm W, and can be associated with up to 11,500 ppm Nb, 72,900 ppm Sn, 20,300 ppm, Y, and 16,900 ppm Fe (Kwak 1983; Linnen and Che 2009). Similarly, titanite of metamorphic origin has been observed containing enrichments (10's ppm) in W (Lyakhovich and Balanova 1969; Lucassen et al. 2010;). Interestingly titanite described in the study of Lucassen et al. (2010), formed after rutile and contains significantly less W (mean 2.8 ppm) than its parent mineral phase (rutile, mean 54.9 ppm) (Lucassen et al. 2010). Concentrations of W in ilmenite from a variety of granitic rock types (for example, biotite, leucocratic, and alaskite granites) have previously been published (Lyakhovich and Balanova 1969), with 10's of ppm W observed in ilmenite from all granitic rock types.

These anomalous W concentrations in rutile and ilmenite are concordant with available experimental data on the partitioning of trace elements between rutile, ilmenite, ulvospinel, karrooite, ferropseudobrookite, orthopyroxene, and silicate melts (Klemme et al. 2005, 2006). Partitioning coefficients calculated from these studies (Klemme et al. 2005, 2006) for W, between selected minerals and the quenched liquid [D (mineral/ quenched liquid)], reveals W

behaves quite compatibly with rutile and ilmenite (0.5-43 and 0.09-11.4, respectively), whilst being quite incompatible with other minerals [0.10 (ulvospinel), N/A (karrooite), 0.07-0.16 (ferropseudobrookite) and 0.004 (orthopyroxene)].

Tungsten-rich silicate minerals (hydrothermal in origin) have been observed and described in several Sn-W skarns around the world [for example, Mt. Lindsay, Tasmania (Kwak 1983); Cigga Head, southwest England (Alderton et al. 1980); St Michael, southwest England (Alderton et al. 1980)]. Anomalous concentrations of W were recorded in most silicate minerals phases analyzed, including biotite (up to 475 ppm W; Kwak 1983), K-feldspar (up to 950 ppm W; Kwak 1983), pyroxene (up to 1,190 ppm W; Kwak 1983), garnet (up to 1,900 W; Kwak 1983), amphibole (up to 475 ppm W; Kwak 1983), chlorite (up to 790 ppm W; Kwak 1983), stilpnomelane (up to 555 ppm W; Kwak 1983), and muscovite (up to 80 ppm W; Alderton et al. 1980). Values for W for these silicate minerals from sources metamorphic in origin is currently limited, with further research needed to constrain W concentration in these minerals.

Summary

Previous research on the incorporation of W into accessory minerals phases' highlights rutile and to a lesser degree ilmenite, titanite, chlorite, biotite, K-feldspar, pyroxene, muscovite, garnet, amphibole, and stilpnomelane, as mineral phases capable of incorporating significant concentrations of W. However, it is important to note that the majority of previous research on W concentrations in minerals has been conducted on minerals of hydrothermal origin. Metamorphic minerals commonly display much lower degrees of enrichments (for example, hydrothermal rutile is observed containing 10,000's ppm W versus metamorphic rutile which is observed containing 100's ppm W). Thus the W-rich silicate minerals (chlorite, biotite, K-feldspar, pyroxene, muscovite, garnet, amphibole, and stilpnomelane) are not as likely to be the

most important hosts for W, when compared to rutile, titanite, and ilmenite.

3.4 Transportation of W in Hydrothermal Fluids

A general mobility of W in hydrothermal fluids in multiple geological environments (for example, metamorphic fluids: Breeding and Ague 2002, Pitcairn et al. 2006; submarine hydrothermal fluids: Kishida et al. 2004; mantle derived fluids: Kamber et al. 2005; groundwater: Arnórsson and Óskarsson 2007; subduction zones: König et al. 2008, Bali et al. 2012) has been established, evidenced from positive correlations between W and highly fluid-mobile elements (for example, B, Be, As, Hg, and Sb). The solubility of W has been shown to increase with temperature, NaCl concentration, and decreasing pH (Wood and Samson 2000; Seiler et al. 2005). Furthermore, in high pressure-temperature settings (for example, subduction zones) that lack rutile, W is always strongly partitioned into the fluid, almost entirely independent of salinity (NaCl concentration) and oxygen fugacity.

3.4.1 Tungsten Speciation

Metal-bearing complexes are critical in increasing metal solubilities in hydrothermal fluids sufficiently, to allow the transportation of metals from the source rocks to the site of deposition (the ore deposit). Previous research of metal complexes in orogenic deposits has focused on Au-bearing metal complexes, with minimal work undertaken on understanding the important metal complexes for W. Historical studies emulating characteristics of orogenic and granite-related deposits (for example, Berkem 1943, Bokii and Anikin 1956, Ravich and Yastrebova 1961, Glinkina 1969) emphasize the importance of W-chloride complexes. However, experimental studies conducted with chloride-rich solutions (for example, Foster 1977) suggests that under temperature ranges typical for orogenic Au deposits (350 to 550 °C), tungstate

complexes (for example, H_2WO_4 and WO_4^{2-}) are the most important complexes (Fig. 3). Wood and Samson (2000) provide a detailed review of in excess of 200 pre-2000 studies on the geochemistry of W. Modelling by Wood and Samson (2000) highlights the importance of tungstate complexes, and suggests that tungstate complexes (H_2WO_4, HWO_4^-, WO_4^{2-}, $NaHWO_4$, and $NaWO_4^-$) are sufficient enough to account for concentrations of W as high as 100's to 1,000's of ppm. Therefore, W-chloride, -fluoride, or -carbonate complexes, or more exotic species (-sulfide) are not required to transport a sufficient amount of W to produce an ore deposit. Alternatively, Redkin and Kostromin (2010) thorough experimental methods and modelling, suggest that at similar pressure and temperature conditions to orogenic system (for example, 1 kbar at 500°C) W solubility is predominately controlled by isopolyanionic W-complexes ($H_3W_3^{VI}O_{12}^{3-}$, $W_3O_9^{3-}$, and $[W^VW_4^{VI}O_{16}]^{3-}$), however this study was conducted on acid chloride solutions, which differ dramatically to the chemistry of orogenic fluids.

The modelling of Wood and Samson (2000) additionally suggests that W solubility is highly dependent on temperature, NaCl concentration, and the pH of the fluids, with the solubility of W strongly increasing together with increases in temperature, NaCl concentrations, and decreasing pH, with pressure playing a subordinate role on solubility.

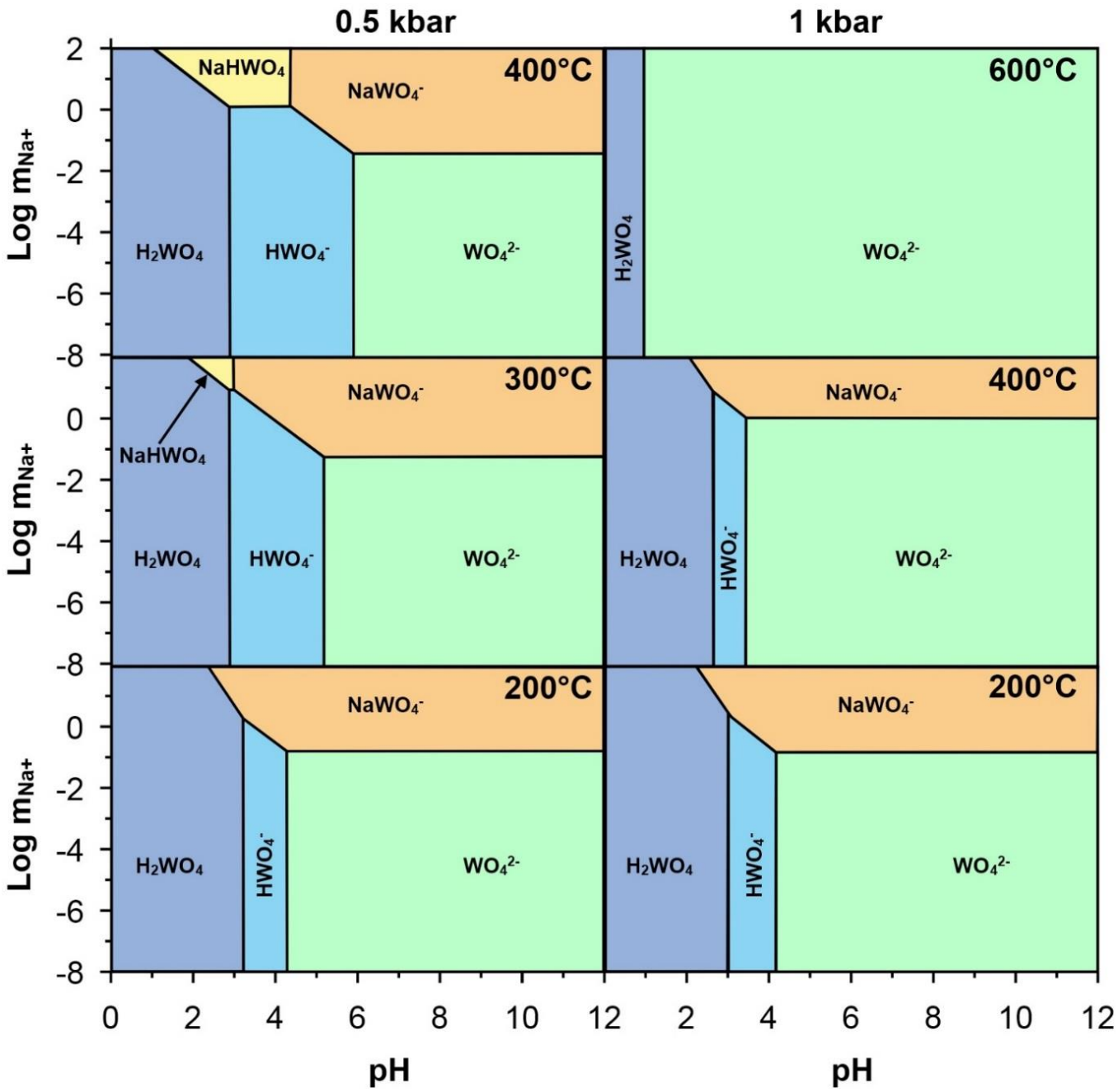

Fig. 3. Predominance fields for various W species as a function of pH and sodium ion concentration at selected pressures and temperatures. All activity coefficients are assumed to be at a constant ionic strength of 0.5 m. At this ionic strength, activity coefficients were calculated by Woods and Samson (2000) using the extended Debye-Hückel equation: $log\ \gamma_i = \frac{-Az_i^2\sqrt{I}}{1+\mathring{a}B\sqrt{I}} + b_\gamma I$,. In addition, it is assumed that total dissolved W concentrations are low enough that isopolytungstates are not predominant. Diagram modified from Woods and Samson (2000).

3.4.2 Fluid Characteristics

The composition of hydrothermal fluids involved in the formation of orogenic Au deposits has long been considered a critical area of study. The reasons for this include, fluid compositions provide a valuable insight in the generation of fluid, source of fluid, transportation of metals, fluid evolution along the flow paths between source and deposit, and deposition of metals. Surprisingly, fluid characteristics of orogenic Au deposits of all ages and settings, show consistency in chemical composition.

Fluids associated with orogenic Au-W mineralization are described as being low in salinity, with 3-7 wt% NaCl equivalent being typical of orogenic Au deposits. Various techniques have been employed to determine the dominant electrolytes present, with Na^+ been shown as being the dominant cation, K^+ the next dominant, although an order of magnitude lower than Na^+, and Ca^{2+}, Mg^{2+}, and other cations having concentration of $\leq$ 100ppm (Ridley and Diamond 2000). Crush-leach analyzes (Yardley et al. 1993) and ion chromatography techniques have also been employed to determine Cl^- as the dominant anion in solution, with charge balance calculation and the common presence of daughter nahcolite crystals in fluid inclusion studies suggesting HCO_3^- as the next most abundant anion (Ridley and Diamond 2000). Boron has also been observed from multi-element analyzes to be a significant solute (Yardley et al. 1993; Ridley and Diamond 2000). Fluid pH is commonly near-neutral (approximately 5.5), with pH calculation largely based on the thermodynamic equilibrium between the fluid and alterations mineralogy (Neall and Phillips 1987), and from bicarbonate content of fluid inclusions with nahcolite daughter crystals (Ridley and Ojala 1997). Ridley and Diamond (2000) notes that these estimates of pH neglect the effects of CO_2 on ion association and therefore pH. Carbon dioxide is a ubiquitous component of mineralizing fluids associated with orogenic Au-W

mineralization. Fluid inclusion from orogenic Au-W deposits from around the world are commonly characterized by carbon dioxide-rich fluid inclusions, however, CO_2 concentrations in fluid inclusion can be quite variable among Au provinces and even within individual districts (commonly prescribed to unmixing during extreme pressure fluctuation that can lead to entrapment of much more CO_2-rich fluid inclusions; Goldfarb and Groves 2015). The majority of orogenic deposits, however, have concentrations between 4 and 15 mol percent gas in the mixed parent fluids (Ridley and Diamond 2000). Concentrations of N_2, H_2S, and CH_4 are variable but generally low and subordinate to CO_2 in fluid inclusion analysis (Goldfarb and Groves 2015).

Pressure- temperature conditions associated with orogenic Au mineralization have been estimated from fluid inclusion and stable isotope studies as ranging from 1 kbar at 200 °C to 5 kbars at 650°C (Groves et al. 1998; Jia 2002). Orogenic Au mineralization containing scheelite, however appears to have more restricted pressure and temperature conditions, with scheelite most commonly found as a gangue mineral in subgreenschist facies to upper greenschist facies hosted deposits (Groves et al. 1998; Jia 2002).

3.4.3 Summary

Previous studies have shown W to being mobile in hydrothermal fluids from a variety of geological environments. Modelling and experimental studies on the speciation of W, combined with fluid characteristics of orogenic Au-W deposits suggests tungstate complexes (H_2WO_4, HWO_4^-, WO_4^{2-}, $NaHWO_4$, and $NaWO_4^-$) facilitate the transportation of a sufficient amount of W to produce an ore deposit. Additionally, modelling conditions closest to those present in orogenic systems suggests that W solubility is highly dependent on temperature, NaCl concentration, and the pH of the fluids, with the solubility strongly increasing concurrent with increases in

temperature, NaCl concentrations, and decreasing pH, with pressure playing a subordinate role on solubility.

References

ARNÓRSSON, S. & ÓSKARSSON, N. 2007. Molybdenum and tungsten in volcanic rocks and in surface and <100 °C ground waters in Iceland. *Geochimica et Cosmochimica Acta,* 71**,** 284–304.

ALDERTON, D. H. M., PEARCE, J. A. & POTTS, P. J. 1980. Rare earth element mobility during granite alteration: evidence from southwest England. *Earth and Planetary Science Letters,* 49**,** 149-165.

BALI, E., KEPPLER, H. & AUDETAT, A. 2012. The mobility of W and Mo in subduction zone fluids and the Mo–W–Th–U systematics of island arc magmas. *Earth and Planetary Science Letters,* 351–352**,** 195–207.

BARNETT, J. C. & MILLER, L. D. 2003. Alaska Resource Data File, Juneau quadrangle, Alaska. *US Geological Survey,* Open-File Report 2003-456, 587 p.

BELL, K., ANGLIN, C. & FRANKLIN, J. 1989. Sm-Nd and Rb-Sr isotope systematics of scheelites: possible implications for the age and genesis of vein-hosted gold deposits. *Geology,* 17**,** 500-504.

BREEDING, C. M. & AGUE, J. J. 2002. Slab-derived fluids and quartz-vein formation in an accretionary prism, Otago Schist, New Zealand. *Geology,* 30**,** 499-502.

BRUGGER, J., LAHAYE, Y., COSTA, S., LAMBERT, D. & BATEMAN, R. 2000. Inhomogeneous distribution of REE in scheelite and dynamics of Archaean hydrothermal systems (Mt. Charlotte and Drysdale gold deposits, Western Australia). *Contributions to Mineralogy and Petrology,* 139**,** 251-264.

CRAW, D. & NORRIS, R. J. 1991. Metamorphogenic Au-W veins and regional tectonics: mineralisation throughout the uplift history of the Haast Schist, New Zealand. *New Zealand Journal of Geology and Geophysics,* 34**,** 373-383.

DE VOS, W., TARVAINEN, T., SALMINEN, R., REEDER, S., DE VIVO, B., DEMETRIADES, A., PIRC, S., BATISTA, M., MARSINA, K. & OTTESEN, R. 2006. Geochemical atlas of Europe, Part 2: interpretation of geochemical maps, additional tables, figures, maps, and related publications. *Geological Survey of Finland,* Espoo, 690 p.

DISTLER, V., MITROFANOV, G., YUDOVSKAYA, M., LISHNEVSKY, E. & PROKOF'EV, V. 2005 [abs.]. Deep structure and ore-forming processes of the Sukhoi Log gold-platinum deposit, Russia. *Proceedings of the Eighth Biennial SGA Meeting Beijing, China,* 2005**,** 921-923.

FARMIN, R. 1941. Host-rock inflation by veins and dikes at Grass Valley, California. *Economic Geology,* 36**,** 143-174.

FOSTER, R. 1977. Solubility of scheelite in hydrothermal chloride solutions. *Chemical Geology,* 20**,** 27-43.

GENKIN, A. D., BORTNIKOV, N. S., CABRI, L. J., WAGNER, F. E., STANLEY, C. J., SAFONOV, Y. G., MCMAHON, G., FRIEDL, J., KERZIN, A. L. & GAMYANIN, G. N. 1998. A multidisciplinary study of invisible gold in arsenopyrite from four mesothermal gold deposits in Siberia, Russian Federation. *Economic Geology,* 93**,** 463-487.

GOLDFARB, R. J. & GROVES, D. I. 2015. Orogenic gold: common or evolving fluid and metal sources through time. *Lithos,* 233**,** 2-26.

GROVES, D. I., GOLDFARB, R. J., GEBRE-MARIAM, M., HAGEMANN, S. G. & ROBERT, F. 1998. Orogenic gold deposits: a proposed classification in the context of their crustal distribution and relationship to other gold deposit types. *Ore Geology Reviews,* 13**,** 7-27.

HART, C. & GOLDFARB, R. 2005. Distinguishing intrusion-related from orogenic gold systems [abs.]. *New Zealand Minerals Conference Proceedings,* 2005**,** 125-133.

HRONSKY, J. M., GROVES, D. I., LOUCKS, R. R. & BEGG, G. C. 2012. A unified model for gold mineralisation in accretionary orogens and implications for regional-scale exploration targeting methods. *Mineralium Deposita,* 47**,** 339-358.

HU, Z. & GAO, S. 2008. Upper crustal abundances of trace elements: a revision and update. *Chemical Geology,* 253**,** 205-221.

JIA, Y. 2002. Nitrogen isotope characteristics of orogenic lode gold deposits and terrestrial reservoirs. *Ph.D. Thesis,* University of Saskatchewan, Canada.

KAMBER, B. S., GREIG, A. & COLLERSON, K. D. 2005. A new estimate for the composition of weathered young upper continental crust from alluvial sediments, Queensland, Australia. *Geochimica et Cosmochimica Acta,* 69**,** 1041–1058.

KISHIDA, K., SOHRIN, Y., OKAMURA, K. & ISHIBACHI, J. 2004. Tungsten enriched in submarine hydrothermal fluids. *Earth and Planetary Science Letters,* 222**,** 819–827.

KEMPE, U., BELYATSKY, B., KRYMSKY, R., KREMENETSKY, A. & IVANOV, P. 2001. Sm–Nd and Sr isotope systematics of scheelite from the giant Au (–W) deposit Muruntau (Uzbekistan): implications for the age and sources of Au mineralization. *Mineralium Deposita,* 36**,** 379-392.

KLEMME, S., GÜNTHER, D., HAMETNER, K., PROWATKE, S. & ZACK, T. 2006. The partitioning of trace elements between ilmenite, ulvospinel, armalcolite and silicate melts

with implications for the early differentiation of the moon. *Chemical Geology,* 234**,** 251-263.

KLEMME, S., PROWATKE, S., HAMETNER, K. & GÜNTHER, D. 2005. Partitioning of trace elements between rutile and silicate melts: implications for subduction zones. *Geochimica et Cosmochimica Acta,* 69**,** 2361-2371.

KÖNIG, S., MÜNKER, C., SCHUTH, S. & GARBE-SCHÖNBERG, D. 2008. Mobility of tungsten in subduction zones. *Earth and Planetary Science Letters,* 274**,** 82-92.

KWAK, T. A. 1983. The geology and geochemistry of the zoned, Sn-W-F-Be skarns at Mt. Lindsay, Tasmania, Australia. *Economic Geology,* 78**,** 1440-1465.

LANG, J. R., BAKER, T., HART, C. & MORTENSEN, J. K. 2000. An exploration model for intrusion-related gold systems. *SEG Newsletter,* 40**,** 6-15.

LARGE, R., THOMAS, H., CRAW, D., HENNE, A. & HENDERSON, S. 2012. Diagenetic pyrite as a source for metals in orogenic gold deposits, Otago Schist, New Zealand. *New Zealand Journal of Geology and Geophysics,* 55**,** 137-149.

LINNEN, R. & CHE, X. 2009. Evaluation of titanite as an indicator mineral for tungsten-skarn mineralization. *In:* Yukon Exploration and Geology 2009, K.E. MacFarlane, L.H. Weston and L.R. Blackburn (eds.), *Yukon Geological Survey,* 223-228.

LUCASSEN, F., DULSKI, P., ABART, R., FRANZ, G., RHEDE, D. & ROMER, R. L. 2010. Redistribution of HFSE elements during rutile replacement by titanite. *Contributions to Mineralogy and Petrology,* 160**,** 279-295.

LUVIZOTTO, G. L., ZACK, T., MEYER, H. P., LUDWIG, T., TRIEBOLD, S., KRONZ, A., MÜNKER, C., STOCKLI, D. F., PROWATKE, S., KLEMME, S., JACOB, D. E. & VON EYNATTEN, H. 2009. Rutile crystals as potential trace element and isotope

mineral standards for microanalysis. *Chemical Geology,* 261**,** 346-369.

LYAKHOVICH, V. & BALANOVA, T. 1969. On the average content of W, Mo, Sn, Ta, Nb and Zn in sphene and ilmenite from granitic rocks. *Geochemistry International,* 7**,** 281-287.

MAIR, J. L., FARMER, G. L., GROVES, D. I., HART, C. J. & GOLDFARB, R. J. 2011. Petrogenesis of postcollisional magmatism at Scheelite Dome, Yukon, Canada: evidence for a lithospheric mantle source for magmas associated with intrusion-related gold systems. *Economic Geology,* 106**,** 451-480.

MCKEAG, S., CRAW, D. & NORRIS, R. 1989. Origin and deposition of a graphitic schist-hosted metamorphogenic Au-W deposit, Macraes, East Otago, New Zealand. *Mineralium Deposita,* 24**,** 124-131.

NARAYANASWAMI, S., ZIAUDDIN, M. & RAMACHANDRA, A. V. 1960. Structural control and localization of gold-bearing lodes, Kolar gold field, India. *Economic Geology,* 55**,** 1429-1459.

NEALL, F. B. & PHILLIPS, G. N. 1987. Fluid-wall rock interaction in an Archean hydrothermal gold deposit; a thermodynamic model for the Hunt Mine, Kambalda. *Economic Geology,* 82**,** 1679-1694.

PITCAIRN, I. K., TEAGLE, D. A. H., CRAW, D., OLIVO, G. R., KERRICH, R. & BREWER, T. S. 2006. Sources of metals and fluids in orogenic gold deposits: insights from the Otago and Alpine Schists, New Zealand. *Economic Geology,* 101**,** 1525-1546.

PITCAIRN, I. K., OLIVO, G. R., TEAGLE, D. A. H. & CRAW, D. 2010. Sulfide evolution during prograde metamorphism of the Otago and Alpine Schists, New Zealand. *The Canadian Mineralogist,* 48**,** 1267-1295.

RICE, C. M., DARKE, K. E. & STILL, J. W. 1998. Tungsten-bearing rutile from the Kori Kollo gold mine, Bolivia. *Mineralogical Magazine,* 62**,** 421-429.

RIDLEY, J. R. & DIAMOND, L. W. 2000. Fluid chemistry of orogenic lode gold deposits and implications for genetic models. *Reviews in Economic Geology,* 13**,** 141-162.

RIDLEY, J. R. & OJALA, J. 1997. Fluid pH estimation from nahcolite-bearing aqueous-carbonic inclusions, the example of the Granny Smith gold deposits, Western Australia [abs.]. *European Current Research on Fluid Inclusions- Biennial Conference,* 1997. 284-285.

SCHINDLER, C., HAGEMANN, S. & MAXLOW, J. 2012. Preliminary results from fluid inclusion petrography and microthermometry on quartz and calcite from different types of orebodies at the Telfer Au-Cu deposit, Paterson Orogen, Western Australia [abs.]. *Biennial Conference on Asian Current Research on Fluid Inclusions, 2012.* 1-2.

SCOTT, K., RADFORD, N., HOUGH, R. & REDDY, S. 2011. Rutile compositions in the Kalgoorlie Goldfields and their implications for exploration. *Australian Journal of Earth Sciences,* 58**,** 803-812.

SCOTT, K. M. & RADFORD, N. W. 2007. Rutile compositions at the Big Bell Au deposit as a guide for exploration. *Geochemistry: Exploration, Environment, Analysis,* 7**,** 353-361.

SEILER, R. L., STOLLENWERK, K. & GARBARINO, J. 2005. Factors controlling tungsten concentrations in ground water, Carson Desert, Nevada. *Applied Geochemistry,* 20**,** 423–441.

URBAN, A. J., HOSKINS, B. F. & GREY, I. E. 1992. Characterization of V-Sb-W-bearing rutile from the Hemlo gold deposit, Ontario. *The Canadian Mineralogist,* 30**,** 319-326.

VOICU, G., BARDOUX, M., JEBRAK, M. & CREPEAU, R. 1999. Structural, mineralogical

and geochemical studies of the Paleoproterozoic Omai gold deposit, Guyana. *Economic Geology,* 94**,** 1277-1303.

WOOD, S. A. & SAMSON, I. M. 2000. The hydrothermal geochemistry of tungsten in granitoid environments: I. Relative solubilities of ferberite and scheelite as a function of T, P, pH, and mNaCl. *Economic Geology,* 95**,** 143-182.

XIAO, Y., SUN, W., HOEFS, J., SIMON, K., ZHANG, Z., LI, S. & HOFMANN, A. W. 2006. Making continental crust through slab melting: constraints from niobium–tantalum fractionation in UHP metamorphic rutile. *Geochimica et Cosmochimica Acta,* 70**,** 4770-4782.

YARDLEY, B., BANKS, D., BOTTRELL, S. & DIAMOND, L. 1993. Post-metamorphic gold-quartz veins from NW Italy: the composition and origin of the ore fluid. *Mineralogical Magazine- London,* 57**,** 407-407.

ZACK, T., VON EYNATTEN, H. & KRONZ, A. 2004. Rutile geochemistry and its potential use in quantitative provenance studies. *Sedimentary Geology,* 171**,** 37-58.

Chapter 4: GEOLOGICAL SETTING OF THE OTAGO REGION

4.1 Aims

This chapter has three major aims; (1) briefly introduce the geological evolution of southern New Zealand, with emphasis placed on the terranes and tectonic events that formed the Otago Schist, (2) summarize orogenic Au-W mineralization in the Otago Schist, and (3) summarize previous studies on the source of W in the Otago Schist.

4.2 Geological Setting

Basement lithologies of New Zealand comprise Cambrian to Early Cretaceous volcanic, plutonic, and sedimentary rocks that were deposited, intruded, and erupted along the Panthalassan/proto-Pacific-plate margin of continental Gondwana (Korsch and Wellman 1988; Mortimer 1993; Adams et al. 1998a, 1998b; Mortimer 2000; Pitcairn 2004; Vaughan et al. 2005; Pitcairn et al. 2006, 2014). Traditionally, the basement of the South Island, New Zealand, has been grouped into two provinces, the Western Province and the Eastern Province that are separated by a complex zone (Median Tectonic Zone) of Carboniferous to Early Cretaceous subduction-related calc-alkaline plutons with subordinate volcanic and sedimentary rocks (Coombs et al. 1976; Bishop 1985; Bradshaw 1989; Pitcairn 2004) (Fig. 4). A central arc terrane group consisting of volcanics and volcaniclastic sediments of the Dun Mountain- Maitai, Murihiku, and Brook Street terranes (Fig. 4) intervenes between the Median Tectonic Zone and the eastern terranes (Coombs et al. 1976; Pitcairn 2004). The Western Province is comprised of two terranes of predominantly Lower Palaeozoic metasedimentary rocks that are intruded by Devonian, Carboniferous and Early Cretaceous granitoids (Cooper 1989; Muir et al. 1994;

Waight et al. 1997; Allibone and Tulloch 2004; Pitcairn 2004, Vaughan et al. 2005), together with subordinate Cambrian volcanic and metamorphic rocks (Gibson and Ireland 1996; Ireland et al. 1998; Münker and Cooper 1999; Pitcairn 2004; Vaughan et al. 2005). The Eastern Province consists of arc, fore-arc, and accretionary complexes, relating to a prolonged period (Permian to Cretaceous) of subduction along the Panthalassan/proto-Pacific-plate margin of continental Gondwana. The Eastern Province is of particular significance as it contains the lithofacies at the center of this study, the Otago Schist (MacKinnon 1983; Pitcairn 2004; Vaughan et al. 2005).

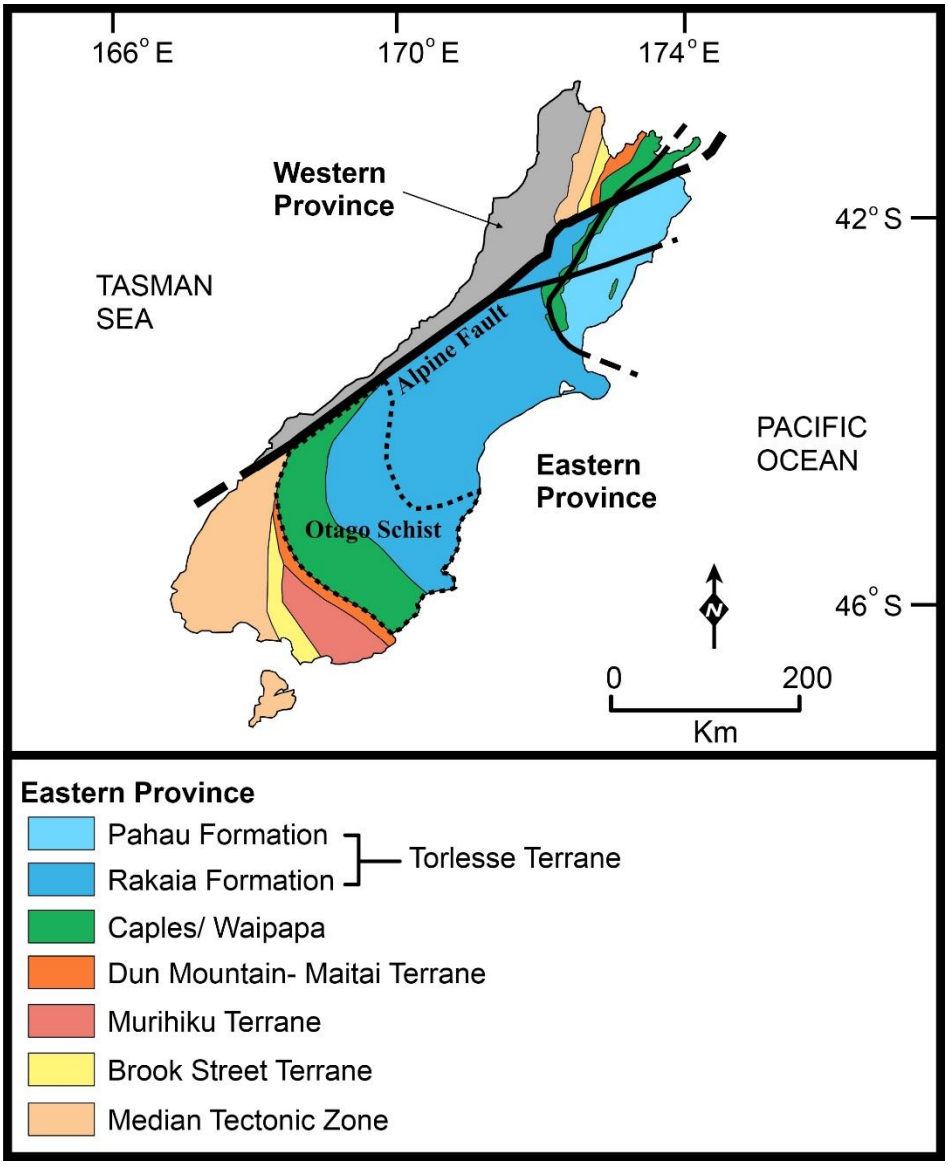

Fig. 4. Geology of the South Island of New Zealand. The Median Tectonic Zone marks the boundary between the Eastern and Western Provinces. Contains aspects from MacKinnon (1983), Mortimer et al. (1999), and Pitcairn (2004).

4.3 Basement Geology of the Otago Region

In the Otago region basement geology is dominated by the Torlesse and Caples terranes, and their metamorphic equivalents (Otago and Alpine Schists), with the Dun Mountain– Maitai Terrane flanking the southern and southwestern margins of the Caples Terrane and making up a subordinate component. The Torlesse and Caples terranes are allochthonous terranes, dominated by graywacke turbidite sequences that are postulated to have been deposited off the eastern edge of southern Gondwana in the New Zealand geosyncline (MacKinnon 1983; Adams et al. 1998a, 1998b; Mortimer 2000; Pitcairn 2004). Comparison of the composition of the Caples Terrane to the Torlesse Terrane reveals intrinsic compositional differences between the two, with the Torlesse Terrane being quartz-rich and the Caples Terrane more volcaniclastic (Korsch and Wellman 1988; Roser and Korsch 1988, 1999; Roser and Cooper 1990; Mortimer and Roser 1992; Pitcairn 2004). The transition from the more volcaniclastic Caples Terrane, to the more mature, quartz-rich Torlesse Terrane, is often cited as supporting the depositional model that postulates an increasing cratonic Gondwana influence eastwards toward the Torlesse Terrane and a westwards increasing arc-influence on the Caples Terrane (MacKinnon 1983; Korsch and Wellman 1988; Wandres 2002; Pitcairn 2004).

4.3.1 The Dun Mountain - Maitai Terrane

The Dun Mountain - Maitai Terrane is a thick (up to 10 km) succession of rocks, comprising the Dun Mountain Ophiolite Belt and the overlying Maitai Group (Fig. 4). Bound to the west by Triassic and Jurassic volcanogenic sedimentary rocks of the Murihiku Terrane, and

in turn by the Brook Street Terrane (Fig. 4); the Dun Mountain - Maitai Terrane is exposed discontinuously in the South Island of New Zealand, over a length in excess of 480 km, with the northern and southern segments of the terrane being offset dextrally 450 km by the Alpine Fault (Fig. 4) (Kimbrough et al. 1992; Tulloch et al. 1999; Wandres 2002; Pitcairn 2004). Dating of zircons in plagiogranites from the Dun Mountain Ophiolite Belt and granite clasts from a conglomerate higher in the Maitai Group, has yielded ages of 285-275 and 265 Ma, respectively; constraining the eruption and maximum deposition age of the Dun Mountain - Maitai Terrane to a relatively short interval of time (≈ 20 Ma) in the Permian, thought to have been concurrent with a period of extension in the volcanic-arc marginal basin (Kimbrough et al. 1992). Analyzes on marine organic matter of the Maitai Group imply a high-paleo latitude setting for the terrane and deposition at intermediate depth in the ocean (approximately 400 m; Krull et al. 2000).

4.3.2 Caples Terrane

The Caples Terrane in the southern New Zealand (Figs. 4, 5) occurs as an arcuate belt of rocks, extending from the Pacific coast near Dunedin, approximately 250 km northwest where it meets the Alpine Fault (Wandres 2002). Bound to the northeast by the Torlesse Terrane and to the southwest by the Dun Mountain - Maitai Terrane (Fig. 4); the Caples Terrane is predominately comprised of volcanogenic graywackes and argillites, with subordinate basic horizons (now all variably metamorphosed) that were deposited as a submarine fan in structurally controlled lower trench slope basins and on the trench floor (Turnbull 1980; Pitcairn 2004).

A relatively evolved calc-alkaline arc system is proposed as the source of the sediments and minor basic volcanic horizons of the Caples Terrane, based on evidence largely derived from geochemical analyzes (for example, Roser and Korsch 1988). Age constraints for the deposition

of the Caples Terrane largely based on fossil evidence that indicate deposition occurred over an extended period of time from the Permian (*Atomodesma bivalve*) to early Triassic age (*Rhaetian radiolarians*) (Campbell and Campbell 1970). Detrital zircon U-Pb ages support this, with the youngest zircon age components from Caples Terrane graywackes yielding ages from 251 to 215 Ma (Adams et al. 2009b, 2013). Bulk compositions of the Caples Terrane graywackes are described in terms of the major components (quartz, feldspar, and lithics), with these components observed varying between 10-35% quartz, 15-20% feldspar, and 50-75% lithics, with lithic fragments being derived predominantly from mafic, intermediate, and felsic volcanic rocks that contain common detrital hornblende and pyroxene (Turnbull 1980; MacKinnon 1983).

4.3.3 Torlesse Terrane

The Torlesse Terrane is the dominant terrane in the Eastern Province, bound in the south by the Caples Terrane and to the west by the Alpine Fault (Fig. 4), and extending eastwards from the Alpine Fault more than 1,300 km past Chatham Island (Bishop 1985). In southern New Zealand, the Torlesse Terrane is comprised of two formations: the older Permain to Late Triassic, Rakaia Formation, and the younger Late Jurassic to Early Cretaceous Pahau Formation (Fig. 4) (Adams et al. 1998b). In the Otago region, the Rakaia Formation is the only sub-terrane of the Torlesse Terrane present and as such will be the only petrofacies described in detail.

The Rakaia Formation in the Otago Schist is comprised predominately of graywackes and argillites, with subordinate basic horizons (now all variably metamorphosed) that were deposited as a submarine fan (Turnbull 1980; Pitcairn 2004). These graywackes are more feldspathic and quartz rich than the Caples Terrane, with detrital modes varying between 24-40% quartz, 24-40% feldspar, and 17-26% lithics, and lithic fragments derived predominantly from silicic volcanic-plutonic rocks (MacKinnon 1983; Graham 1985; Mortimer and Roser 1992; Yokoyama

1994; Roser and Korsch 1999; Grapes et al. 2001; Wandres 2002). Regionally, minor lithologies of oceanic association (for example, basalt, limestone, and chert) are observed in fault or mélange zones (Silberling et al. 1988; Mortimer 1993; Adams et al. 2013).

Age constraints for the deposition of the Rakaia Formation (Torlesse Terrane), like the Caples Terrane are largely based on fossil evidence that suggests deposition occurred over an extended period of time from the Permian to Early Triassic, with the youngest Triassic fossils being *Rhaetian radiolarians* (Campbell and Campbell 1970). Detrital zircon U-Pb ages and $^{40}Ar/^{39}Ar$ mica ages, however, suggest that sedimentation of the Rakaia Formation in the South Island continued into the Early Jurassic (Kamp 2001). Source rocks for the Torlesse Terrane are often suggested to be I-type calc-alkaline granitoid, with age patterns of detrital zircon and muscovite implying a Permian –Triassic (230-270 Ma) age of source rocks, with minor components at 420-440 Ma and 500-550 Ma (Ireland 1992; Adams et al. 1998a, 1998b, 2009a, 2013). The source rocks of the Rakaia Formation are contentious, with the Lachlan Fold Belt of southeastern Australia, the Ross/Delmarian Orogeny of Antarctica, and the New England Fold Belt of northeastern Australia all proposed as the provincial source (Adams et al. 2013 and references therein).

An additional terrane is proposed in the Otago region based on a higher occurrence of mafic schist. This terrane, the Aspiring Terrane is comprised of psammitic schist, greenschist, minor chert, marble, and ultramafic schist, and has been suggested to be a distinct oceanic assemblage that was juxtaposed next to the psammite dominated Torlesse and Caples terranes (Craw 1984; Norris and Craw 1987). However, detailed geochemical studies by Mortimer and Roser (1992) revealed that these rocks are chemically indistinguishable from the Torlesse Terrane and as such do not belong to a distinct terrane (Pitcairn 2004). For the purposes of this

study, the Aspiring Terrane rocks are considered to be part of the Torlesse Terrane.

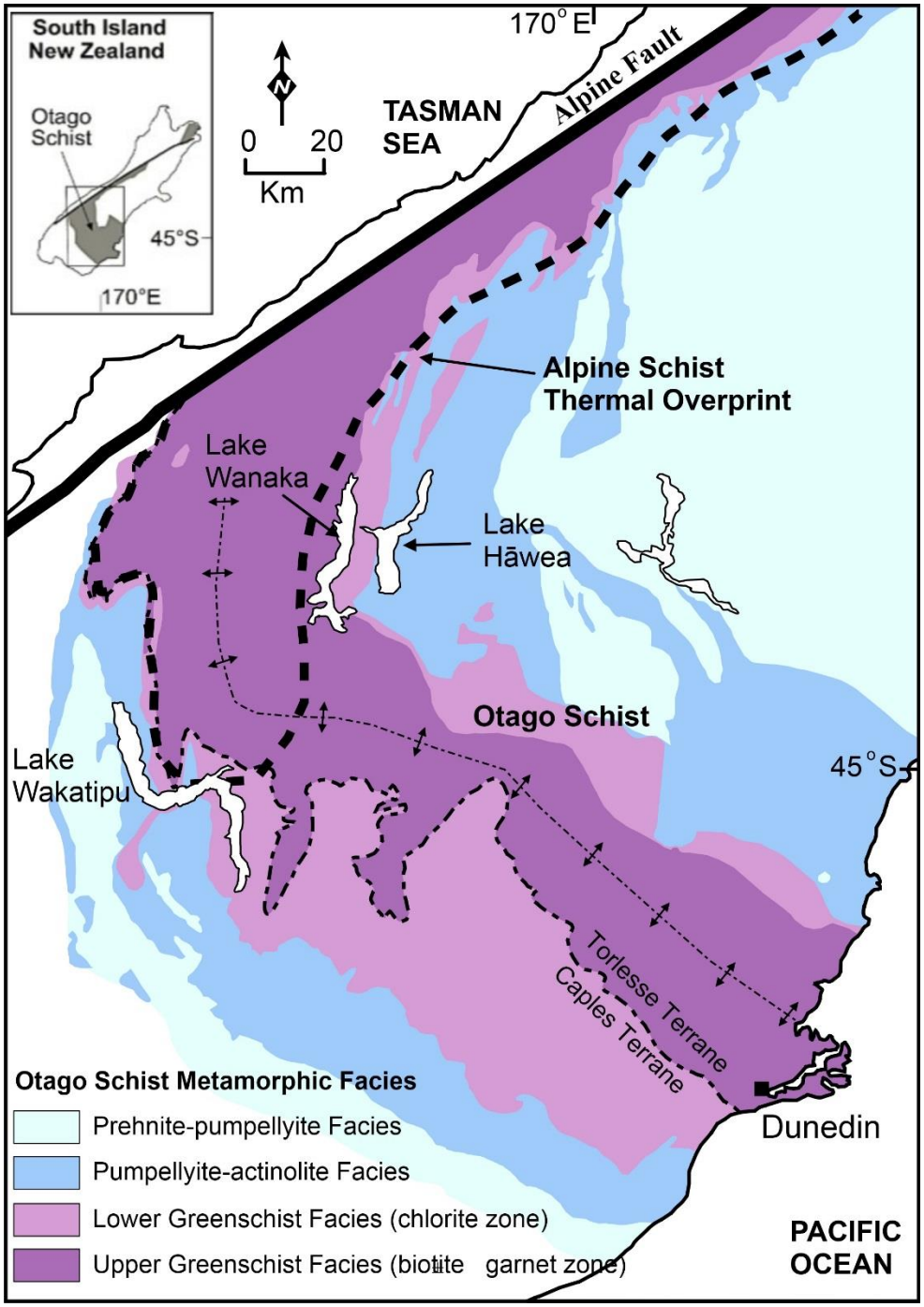

Fig. 5. Geological map of the Otago Schist, South Island, New Zealand, showing the Caples and Torlesse terranes, metamorphic facies, the major northwest trending anticlinorium, the Alpine Fault – Austro-Pacific plate contact and the thermal overprint on the Otago Schist by the development of the Alpine Schist. Aspects from Pitcairn (2004).

4.3.4 Otago Schist

The Otago Schist is a major feature of the Eastern Province of southern New Zealand that extends from the Pacific coast near Dunedin, approximately 250 km northwest where it merges with Alpine Schist, covering an area in excess of 20,000 Km^2. Formed as a result of the Mesozoic collision and accretion of the Torlesse and Caples terranes during the Rangitata Orogeny (Mortimer 1993), the Otago Schist belt (Fig. 5) is predominately comprised of metaturbiditic graywackes and argillites, with subordinate metabasic horizons and ultramafic slices (Turnbull 1979; MacKinnon 1983; Craw 1984; Mortensen et al. 2010). Metamorphic grade of the Otago Schist belt ranges from prehnite-pumpellyite facies along the flanks to upper greenschist facies (biotite–garnet–albite) in the center (Fig. 5) (MacKinnon 1983; Craw 1984; Mortimer 2000; Mortensen et al. 2010; Pitcairn et al. 2015), equivalent to peak metamorphic conditions of approximately 450°C and 8–10 kbar (Bishop 1972; Yardley 1982; Craw 1998; Pitcairn et al. 2015). Argon-Ar dating of the metamorphism of the Otago Schist suggests metamorphism occurred between 200 to 120 Ma (Little et al., 1999; Gray and Foster 2004; Pitcairn et al. 2010), with the timing of peak metamorphism poorly constrained, but most likely occurring considerably later (at approximately 160-140 Ma) in the higher metamorphic grade rocks than in the lower metamorphic grade rocks (at approximately 180 Ma; Little et al. 1999, Gray and Foster, 2004, Pitcairn et al. 2010). The metamorphic transition between the higher metamorphic grade core and lower grade flanks has been accentuated by post-metamorphic extensional faulting, some of which was dominated by middle Cretaceous low-angle normal faults that facilitated exhumation of the Otago Schist (Deckert et al. 2002; Gray and Foster 2004; MacKenzie and Craw 2005; Mortensen et al. 2010). Extensional deformation continued through the Late Cretaceous and into the Tertiary as a result of the crustal thinning associated with the

breakup of Gondwana in the southwest Pacific (Laird and Bradshaw 2004; Landis et al. 2008; Mortensen et al. 2010). Following peak metamorphism, little retrogression has occurred, owing to the rapid nature of the uplift of the Otago Schist (Pitcairn et al. 2010).

The increase in metamorphic grade, from the prehnite-pumpellyite facies precursor rocks of the Otago Schist to the upper greenschist facies (biotite-garnet-albite) rocks located within the core of the Otago Schist belt (Fig. 5), is accompanied in all lithologies by progressive metamorphic recrystallization and foliation development (Bishop 1972; Turnbull et al. 2001; Henne et al. 2011). Textural zone gradients have previously been established in the Otago Schist based progressive metamorphic recrystallization foliation development (Bishop 1972; Henne, Craw and MacKenzie 2011; Turnbull, Mortimer and Craw 2001). These zones were developed to allow rapid identification in the field, to aid in mapping (Bishop 1972; Henne, Craw and MacKenzie 2011; Turnbull, Mortimer and Craw 2001. Textural zones broadly are coincidental in the Otago Schist (for example, TZI- prehnite- pumpellyite facies, TZII- pumpellyite-actinolite, TZIII- lower greenschist facies, TZIV- upper greenschist facies). However this not always the case (for example, Turnbull, Mortimer and Craw 2001). Following this, textural zone gradients are not used to describe rocks in this thesis, with this approach is taken to reduce confusion and avoid any potential inconsistencies with metamorphic grade. Rocks belonging to the prehnite-pumpellyite metamorphic facies at outcrop scale are observed as unfoliated graywackes and subordinate argillites (MacKinnon 1983; Turnbull et al. 2001; Henne et al. 2011). Original sedimentary textures associated with the deposition of these rock packages are largely preserved, with little metamorphic recrystallization observed, except in the sedimentary matrix (MacKinnon 1983; Turnbull et al. 2001; Henne et al. 2011). The breakdown of detrital plagioclase, K-feldspar, biotite, garnet, and amphibole is observed throughout the development of the prehnite-

pumpellyite facies (Bishop 1972), with plagioclase being completely albitized early on and K-feldspar, biotite, garnet, and amphibole persisting into the pumpellyite-actinolite facies rocks (Bishop 1972). The disappearance of prehnite marks the onset of the pumpellyite-actinolite facies with incipient development of foliation also being coincidental with this metamorphic facies transition (MacKinnon 1983; Turnbull et al. 2001; Henne et al. 2011). Rocks within the pumpellyite-actinolite facies zone are observed at outcrop scale as being dominated by weakly foliated graywackes and argillites, verging on psammites and slates, respectively (Bishop 1972). Detrital K-feldspar, biotite, and garnet are observed breaking down early in the pumpellyite-actinolite facies rocks (Bishop 1972) and detrital quartz grains commonly have undulose extinction (Turnbull et al. 2001; Stallard et al. 2005). Additionally, there is evidence for development of a weak alignment of metamorphic micas (Turnbull et al. 2001).

A transition from weakly foliated to strongly foliated rocks is observed in the pumpellyite-actinolite facies, these strongly foliated pumpellyite-actinolite facies occur near the boundary of lower greenschist facies rocks and are marked by a greater metamorphic recrystallization and the increased development of foliation, to the extent that it dominates the fabric of the rock (Turnbull et al. 2001). The sedimentary features in these rocks are largely obscured at outcrop scale (MacKinnon 1983; Turnbull et al. 2001; Henne et al. 2011). In thin section, detrital quartz grains are observed being partially to fully recrystallized to sub-grains, and metamorphic micas have developed a strong preferred orientation in the rocks (Turnbull et al. 2001; Stallard and Shelley 2005; Stallard et al. 2005). Pumpellyite-actinolite facies rocks transition to lower greenschist facies rocks through the gradual disappearance of pumpellyite, and the appearance of clinozoisite (Bishop 1972; Turnbull et al. 2001). Lower greenschist facies rocks are pervasively foliated, and locally tightly folded with incipient development of a second

foliation parallel to fold axial surfaces (Craw and Norris 1991; Turnbull et al. 2001; Henne et al. 2011). Detrital quartz and mica are no longer stable at these conditions having been pervasively recrystallized to metamorphic quartz and micas (Stallard and Shelley 2005; Stallard et al. 2005; Turnbull et al. 2001). Appearance of biotite in the greenschist facies rocks marks the transition of lower greenschist facies to upper greenschist facies, with upper greenschist facies rocks being more pervasively recrystallized and coarser in grain than the lower greenschist facies rocks (Turnbull et al. 2001).

Structurally, the major feature of the Otago Schist is the major northwest trending anticlinorium in the center of the metamorphic belt (Fig. 5) (Pitcairn 2004). Foliation in the centrally located greenschist rocks is horizontal in sense, with foliation transitioning to steeply dipping in the subgreenschist facies rocks flanking the northeast and southwest margins of the schist belt (Pitcairn 2004). Juxtaposition of the Caples and Torlesse terranes was syn-metamorphic and resulted in the formation of complex high strain zones along the terrane boundaries (Cox et al. 1991; Pitcairn, 2004). Development of these complex high strain zones, took place under ductile deformation conditions along the base of nappe structures or on lower limbs of recumbent folds (Cox et al. 1991; Pitcairn, 2004). Structural complexity in the Otago Schist is observed to increase with metamorphic grade and structural depth towards the axis. Five major phases of deformation are recognized in the Otago and Alpine Schists; F1 and F2 are steeply plunging syn-metamorphic macroscopic folding phases, F3 and F4 are late metamorphic deformation phases, and F5 is a series of post-metamorphic chevron and kink folds (Cooper 1974; Cooper et al. 1987; Cox et al. 1991; Pitcairn 2004). Bedding is commonly destroyed by F1 cleavage at the prehnite-pumpellyite to pumpellyite-actinolite facies transition, and F1 fabrics transposed by F2 folds and cleavage within the greenschist facies (Cox 1993). Structural style is

a function of rock type with more competent psammitic schists appearing less strained than adjacent pelitic lithologies. F2 and F3 recumbent folds and nappe sheets occur on a mountain-range scale and are common mesoscopic structures (Cox 1993; Pitcairn 2004).

4.3.5 Alpine Schist

The Alpine Schist is exposed as a narrow, southeast to northwest trending metamorphic belt extending in excess of 200 km's along and tens of km's to the east of the Alpine Fault. In the Otago region, the Alpine Schist overprints westerly portions of the earlier formed Otago Schist (Fig. 5). Metamorphic grade of the Alpine Schist in the Otago Region, is observed increasing westerly towards the Alpine Fault (Grapes and Watanabe 1992; Grapes, 1995). Peak metamorphic conditions are estimated at approximately 620°C and 9.2 kbars (Grapes 1995) indicating that peak metamorphism of the Alpine Schist occurred at higher temperatures but slightly lower pressures than that of the Otago Schist. Radiometric dating of mineral phases (garnet, monazite, titanite, and hornblende) suggests metamorphism of the Alpine Schist occurred between approximately 100 to 70 Ma, with a major episode of high metamorphic grade mineral growth occurring at approximately 86 Ma (Vry et al. 2004) and most likely coinciding with the oblique collision of the Hikurangi Plateau and the continental margin of Gondwana (Murphy 2010). Metamorphism in the late Cenozoic occurred synchronous with the uplift of the Southern Alps (Little et al. 2002a, 2002b) and resulted in the exhumation and further deformation of the Alpine Schist after peak metamorphic conditions (Murphy 2010). This late Cenozoic event resulted in the overprinting of earlier Alpine Schist metamorphic fabrics, as well as forming an approximately 1-2 km thick mylonite zone that is exposed in the hanging wall of the Alpine Fault (Murphy 2010).

4.4 Au-W Mineralization in the Otago Schist

Orogenic Au-mineralization is widespread throughout the greenschist facies (and to a lesser extent, the subgreenschist facies) rocks of the Otago Schist, with >200 exposed mineralized quartz-carbonate veins being recognized (for example, Fig. 6) (Rattenbury and Isaac 2012). These Au-bearing veins and placer deposits derived from the weathering of these veins were the subject of the Victorian Otago Au rush, a major period of development in the Otago Region (Reed 1956). Gold-bearing veins hosted in the Otago Schist display a strong structural control, with mineralization hosted in brittle-ductile shear zones and extensional veins formed at relatively shallow crustal levels (Craw et al. 2006, Pitcairn et al. 2016, 2014). Two discrete and relatively short-lived mineralizing events are recognized as being responsible for the majority of orogenic mineralization in the Otago Schist (one occurring between 142 and 135 Ma, and the other occurring between 106 and 101 Ma), with both mineralizing events generating brittle-ductile shear zones and extensional veins (Mortensen et al. 2010). Comprising a series of open pits and underground developments along a regional-scale mineralized Early Cretaceous (142-135 Ma) shear zone (The Hyde-Macraes Shear Zone; Fig. 6), the Macraes Mine is the most significant deposit in the Otago Schist having produced in excess of 70 t of Au (Pitcairn et al. 2014) and containing reserves in excess of 160 t at approximately 1.1 g/t (OceanaGold 2015). In addition to Au at the Macraes Mine, a variety of other trace elements (including As, Sb, Hg, Se, Mo, W, Cr, and Bi) are enriched in the ore metals signature, a feature that is common in orogenic mineralization in the Otago Schist (McKeag et al. 1989; Craw 1992, 2002; Craw et al. 1999; Pitcairn et al., 2006, 2010, 2014, 2015). Scheelite is the major mineral responsible for the enrichment of W in these orogenic occurrences, with scheelite recorded as an accessory mineral (and occasionally ore mineral) in >170 localities throughout the Otago Schist (Rattenbury and

Isaac 2012). Previously W has been mined in the Otago Schist with production (>3,000 t of scheelite concentrate) predominantly derived from the mines surrounding Glenorchy and the Macraes Mine (Fig. 6) (Mutch 1969; Williamson, 1939).

Tungsten-bearing veins in the Otago Schist are predominantly comprised of quartz with subordinate amounts of carbonate (ankerite and calcite), scheelite, pyrite, and arsenopyrite, minor chalcopyrite, sphalerite, galena, and stibnite (McKeag et al. 1989; Craw and Norris 1991; MacKenzie and Craw 1993; Craw 2002; Craw et al. 2004). Many veins contain schist breccia fragments (Angus et al. 1997; de Ronde et al. 2000; Craw 2002; Craw et al. 2004; Petrie et al. 2005; Begbie and Craw 2006). Gold is observed as small (<20 µm) blebs in sulfides, and more rarely as coarser (up to 3 mm) free Au grains in quartz (Craw and Norris 1991). Veins generally crosscut the schistosity and fill faults or fractures (Angus et al. 1997; de Ronde et al. 2000; Craw 2002; Craw et al. 2004; Petrie et al. 2005; Begbie and Craw 2006). Areas in which scheelite has economically been exploited (for example, Glenorchy and Macraes), commonly contain several parallel or subparallel faults, branching, to form a large complex of vein systems over several km^2 (Craw and Norris 1991).

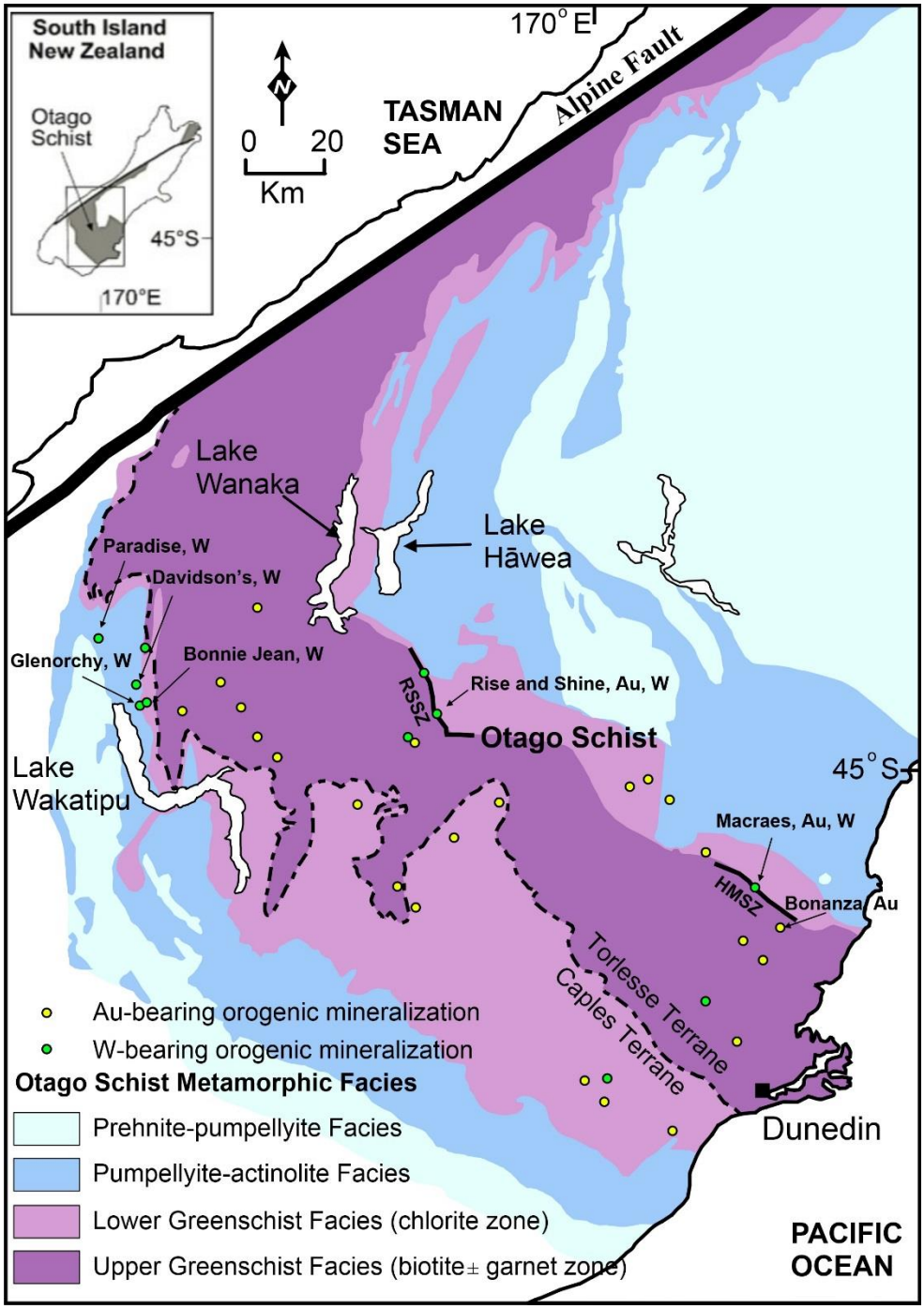

Fig. 6. Geological map of the Otago Schist and Alpine Schists, South Island, New Zealand, showing the Caples and Torlesse terranes, metamorphic facies, selected W-bearing and Au- bearing orogenic ore deposits, selected mineralized shear zones, the Alpine Fault – Austro-Pacific plate contact. Abbreviations: HMSZ- Hyde-Macraes Shear Zone, RSSZ- Rise and Shine Shear Zone.

4.5 Previous and Current Source Models for W (scheelite) in Orogenic Deposits of the Otago Schist

Investigations detailing a source for W in turbidite-hosted orogenic deposits are limited; perhaps owing to W only occasionally being a primary element of economic significance. Source rock models suggested for W in the orogenic deposits of the Otago Schist include; the metamorphic devolatilization of non-enriched sedimentary (Paterson and Rankin 1979; Paterson 1982, 1986; Craw and Norris 1991; Pitcairn et al. 2006, 2014; Large et al. 2012), or enriched sedimentary (Henley et al. 1976) or volcanic rocks (Henley et al. 1976), lateral secretion deriving W from the enclosing and adjacent schistose rocks (Marshall 1918; Morgan 1920), and hypothesized felsic magmas crystallizing at depth (Finlayson 1908; Reed 1958).

Successive studies within the Otago Schist of New Zealand, have assessed various aspects of each of these source models, discounting all but one. Hypothesized felsic magmas crystallizing at depth (Finlayson 1908; Reed 1958) are not favored among recent researchers largely owing to a distinct lack of any evidence for any spatially or temporally significant magmatism in the Otago region. Similarly, the lateral secretion model (Marshall 1918; Morgan 1920) has been discounted following the detailed trace element geochemical study of Paterson and Rankin (1979) in the Glenorchy scheelite field and their accompanying mass balance calculations. Geological mapping (for example, Craw 1984) similarly discounts the devolatilization of metavolcanic and enriched sedimentary rocks (for example, cherts) as metal sources for the orogenic deposits, with these lithologies observed to be volumetrically insignificant to account for the widespread occurrence of W-Au deposits throughout the Otago Schist. Recent whole rock geochemical studies of metabasaltic rocks with prograde metamorphism (Pitcairn et al. 2015) further discounts metavolcanics as source rocks, with

Pitcairn et al. (2015) observing no depletion in W with increasing metamorphic grade, thus they could not have been the source for W in the Otago deposits. This leaves the devolatilization of non-enriched sedimentary rocks (graywackes and argillites) with prograde metamorphism as the only remaining model, and is currently the favored source model (for example, Pitcairn et al. 2006, 2014; Large et al. 2012; Craw et al. 2015). Recent detailed geochemical studies (Breeding and Ague 2002; Pitcairn et al. 2006) have shown non-enriched sedimentary rocks in the Otago Schist, systematically decrease in their whole rock W concentrations (along with other elements observed in the orogenic deposits of the Otago Schist) with increasing metamorphic grade, with these decreases occurring between subgreenschist to greenschist facies conditions (Breeding and Ague 2002). The recrystallization of diagenetic pyrite to metamorphic pyrrhotite, as briefly discussed in Chapter 2, has been shown to mobilize Au, As, Ag, Sb, and Hg during its metamorphic recrystallization. However, one current and important void in this model, is that the source of W could not be explained by the transition of pyrite to pyrrhotite, with significant concentrations of W not being detected by either Pitcairn et al. (2010) or Large et al. (2012) in any of the sulfide minerals; suggesting that if the model is correct, W must be located elsewhere within the sedimentary pile in another diagenetic or detrital mineral, with prograde recrystallization to another mineral phase(s) as the mechanism for its release.

References

ADAMS, C., BARLEY, M., FLETCHER, I. & PICKARD, A. 1998a. Evidence from U–Pb zircon and 40Ar/39Ar muscovite detrital mineral ages in metasandstones for movement of the Torlesse suspect terrane around the eastern margin of Gondwanaland. *Terra Nova,* 10**,** 183-189.

ADAMS, C., CAMPBELL, H., GRAHAM, I. & MORTIMER, N. 1998b. Torlesse, Waipapa and

Caples suspect terranes of New Zealand: integrated studies of their geological history in relation to neighbouring terranes. *Episodes,* 21**,** 235-240.

ADAMS, C., MORTIMER, N., CAMPBELL, H. & GRIFFIN, W. 2009a. Age and isotopic characterisation of metasedimentary rocks from the Torlesse Supergroup and Waipapa Group in the central North Island, New Zealand. *New Zealand Journal of Geology and Geophysics,* 52**,** 149-170.

ADAMS, C. J., CAMPBELL, H. J. & GRIFFIN, W. L. 2009b. Tracing the Caples Terrane through New Zealand using detrital zircon age patterns and radiogenic isotope signatures. *New Zealand Journal of Geology and Geophysics,* 52**,** 223-245.

ADAMS, C., KORSCH, R. & GRIFFIN, W. 2013. Provenance comparisons between the Nambucca Block, Eastern Australia and the Torlesse Composite Terrane, New Zealand: connections and implications from detrital zircon age patterns. *Australian Journal of Earth Sciences,* 60**,** 241-253.

ALLIBONE, A. & TULLOCH, A. 2004. Geology of the plutonic basement rocks of Stewart Island, New Zealand. *New Zealand Journal of Geology and Geophysics,* 47**,** 233-256.

ANGUS, P., DE RONDE, C. & SCOTT, J. 1997. Exploration along the Hyde Macraes shear [abs.]. *New Zealand Minerals and Mining Conference Proceedings,* 1997. 151-157.

BEGBIE, M. & CRAW, D. 2006. Geometry and petrography of stockwork vein swarms, Macraes mine, Otago Schist, New Zealand. *New Zealand Journal of Geology and Geophysics,* 49**,** 63-73.

BISHOP, D. 1972. Progressive metamorphism from prehnite-pumpellyite to greenschist facies in the Dansey Pass area, Otago, New Zealand. *Geological Society of America Bulletin,* 83**,** 3177-3198.

BISHOP, D. 1985. Provisional terrane map of South Island, New Zealand.

BRADSHAW, J. 1989. Origin and metamorphic history of an Early Cretaceous polybaric granulite terrain, Fiordland, southwest New Zealand. *Contributions to Mineralogy and Petrology,* 103**,** 346-360.

BREEDING, C. M. & AGUE, J. J. 2002. Slab-derived fluids and quartz-vein formation in an accretionary prism, Otago Schist, New Zealand. *Geology,* 30**,** 499-502.

CAMPBELL, J. K. & CAMPBELL, J. 1970. Triassic tube fossils from Tuapeka rocks, Akatore, south Otago. *New Zealand Journal of Geology and Geophysics,* 13**,** 392-399.

COOMBS, D., LANDIS, C., NORRIS, R., SINTON, J., BORNS, D. & CRAW, D. 1976. The Dun Mountain Ophiolite Belt, New Zealand, its tectonic setting, constitution, and origin, with special reference to the southern portion. *American Journal of Science,* 276**,** 561-603.

COOPER, A. 1974. Multiphase deformation and its relationship to metamorphic crystallisation at Haast River, South Westland, New Zealand. *New Zealand Journal of Geology and Geophysics,* 17**,** 855-880.

COOPER, R. 1989. Early Paleozoic terranes of New Zealand. *Journal of the Royal Society of New Zealand,* 19**,** 73-112.

COOPER, A., BARREIRO, B., KIMBROUGH, D. & MATTINSON, J. 1987. Lamprophyre dike intrusion and the age of the Alpine fault, New Zealand. *Geology,* 15**,** 941-944.

COX, S. C. 1993. Veins, fluid, fractals, scale & schist: an investigation of fluid-rock interaction during deformation of the Torlesse Terrane, New Zealand. *Ph.D. Thesis,* University of Otago, New Zealand.

COX, S., WALL, V., ETHERIDGE, M. & POTTER, T. 1991. Deformational and metamorphic

processes in the formation of mesothermal vein-hosted gold deposits—examples from the Lachlan Fold Belt in central Victoria, Australia. *Ore Geology Reviews,* 6**,** 391-423.

CRAW, D. 1984. Lithologic variations in Otago Schist, Mt Aspiring area, northwest Otago, New Zealand. *New Zealand Journal of Geology and Geophysics,* 27**,** 151-166.

CRAW, D. 1992. Fluid evolution, fluid immiscibility and gold deposition during Cretaceous-Recent tectonics and uplift of the Otago and Alpine Schist, New Zealand. *Chemical Geology,* 98**,** 221-236.

CRAW, D. 1998. Structural boundaries and biotite and garnet 'isograds' in the Otago and Alpine Schists, New Zealand. *Journal of Metamorphic Geology,* 16**,** 395-402.

CRAW, D. 2002. Geochemistry of late metamorphic hydrothermal alteration and graphitisation of host rock, Macraes gold mine, Otago Schist, New Zealand. *Chemical Geology,* 191**,** 257-275.

CRAW, D. & NORRIS, R. J. 1991. Metamorphogenic Au-W veins and regional tectonics: mineralisation throughout the uplift history of the Haast Schist, New Zealand. *New Zealand Journal of Geology and Geophysics,* 34**,** 373-383.

CRAW, D., WINDLE, S. & ANGUS, P. 1999. Gold mineralization without quartz veins in a ductile-brittle shear zone, Macraes Mine, Otago Schist, New Zealand. *Mineralium Deposita,* 34**,** 382-394.

CRAW, D., MACKENZIE, D. & PETRIE, B. 2004. Disseminated gold mineralisation in a schist-hosted mesothermal deposit, Macraes Mine, Otago, New Zealand [abs.]. *Proceedings of the PACRIM 2004 Congress,* 2004. 135-141.

CRAW, D., BEGBIE, M. & MACKENZIE, D. 2006. Structural controls on Tertiary orogenic gold mineralization during initiation of a mountain belt, New Zealand. *Mineralium*

Deposita, 41**,** 645-659.

CRAW, D., MORTENSEN, J., MACKENZIE, D. & PITCAIRN, I. 2015. Contrasting geochemistry of orogenic gold deposits in Yukon, Canada and Otago, New Zealand. *Geochemistry: Exploration, Environment, Analysis,* 15**,** 150-166.

DE RONDE, C. E. J., FAURE, K., BRAY, C. J. & WHITFORD, D. J. 2000. Round Hill shear zone-hosted gold deposit, Macraes Flat, Otago, New Zealand: evidence of a magmatic ore fluid. *Economic Geology,* 95**,** 1025-1048.

DECKERT, H., RING, U. & MORTIMER, N. 2002. Tectonic significance of Cretaceous bivergent extensional shear zones in the Torlesse accretionary wedge, central Otago Schist, New Zealand. *New Zealand Journal of Geology and Geophysics,* 45**,** 537-547.

FINLAYSON, A. M. 1908. The geology of the quartz veins of the Otago goldfields. *Transactions of the New Zealand Institute,* 41**,** 64-84.

GIBSON, G. & IRELAND, T. 1996. Extension of Delamerian (Ross) orogen into western New Zealand: evidence from zircon ages and implications for crustal growth along the Pacific margin of Gondwana. *Geology,* 24**,** 1087-1090.

GRAHAM, I. J. 1985. Rb-Sr geochronology and geochemistry of Torlesse metasediments from the central North Island, New Zealand. *Chemical Geology,* 52**,** 317-331.

GRAPES, R. & WATANABE, T. 1992. Paragenesis of titanite in metagreywackes of the Franz Josef-Fox Glacier area, Southern Alps, New Zealand. *European Journal of Mineralogy,* 4**,** 547-555.

GRAPES, R. H. 1995. Uplift and exhumation of Alpine schist, Southern Alps, New Zealand: thermobarometric constraints. *New Zealand Journal of Geology and Geophysics,* 38**,** 525-533.

GRAPES, R., ROSER, B. & KASHAI, K. 2001. Composition of monocrystalline detrital and authigenic minerals, metamorphic grade, and provenance of Torlesse and Waipapa graywacke, Central North Island, New Zealand. *International Geology Review,* 43**,** 139-175.

GRAY, D. & FOSTER, D. 2004. 40Ar /39Ar thermochronologic constraints on deformation, metamorphism and cooling/exhumation of a Mesozoic accretionary wedge, Otago Schist, New Zealand. *Tectonophysics,* 385**,** 181-210.

HENLEY, R., NORRIS, R. & PATERSON, C. 1976. Multistage ore genesis in the New Zealand geosyncline a history of post-metamorphic lode emplacement. *Mineralium Deposita,* 11**,** 180-196.

HENNE, A., CRAW, D. & MACKENZIE, D. 2011. Structure of the Blue Lake Fault Zone, Otago Schist, New Zealand. *New Zealand Journal of Geology and Geophysics,* 54**,** 311-328.

IRELAND, T. R. 1992. Crustal evolution of New Zealand: evidence from age distributions of detrital zircons in Western Province paragneisses and Torlesse greywacke. *Geochimica et Cosmochimica Acta,* 56**,** 911-920.

IRELAND, T., FLÖTTMANN, T., FANNING, C., GIBSON, G. & PREISS, W. V. 1998. Development of the early Paleozoic Pacific margin of Gondwana from detrital-zircon ages across the Delamerian orogen. *Geology,* 26**,** 243-246.

KAMP, P. J. 2001. Possible Jurassic age for part of Rakaia Terrane: implications for tectonic development of the Torlesse accretionary prism. *New Zealand Journal of Geology and Geophysics,* 44**,** 185-203.

KIMBROUGH, D. L., MATTINSON, J. M., COOMBS, D. S., LANDIS, C. A. & JOHNSTON,

M. R. 1992. Uranium-lead ages from the Dun Mountain ophiolite belt and Brook Street terrane, South Island, New Zealand. *Geological Society of America Bulletin,* 104**,** 429-443.

KORSCH, R. & WELLMAN, H. 1988. The geological evolution of New Zealand and the New Zealand region. *The ocean basins and margins.* Springer.

KRULL, E., RETALLACK, G., CAMPBELL, H. & LYON, G. 2000. δ13Corg chemostratigraphy of the Permian-Triassic boundary in the Maitai Group, New Zealand: Evidence for high-latitudinal methane release. *New Zealand Journal of Geology and Geophysics,* 43**,** 21-32.

LAIRD, M. & BRADSHAW, J. 2004. The break-up of a long-term relationship: the Cretaceous separation of New Zealand from Gondwana. *Gondwana Research,* 7**,** 273-286.

LANDIS, C., CAMPBELL, H., BEGG, J., MILDENHALL, D., PATERSON, A. M. & TREWICK, S. 2008. The Waipounamu Erosion Surface: questioning the antiquity of the New Zealand land surface and terrestrial fauna and flora. *Geological Magazine,* 145**,** 173-197.

LARGE, R., THOMAS, H., CRAW, D., HENNE, A. & HENDERSON, S. 2012. Diagenetic pyrite as a source for metals in orogenic gold deposits, Otago Schist, New Zealand. *New Zealand Journal of Geology and Geophysics,* 55**,** 137-149.

LITTLE, T., HOLCOMBE, R. & ILG, B. 2002a. Ductile fabrics in the zone of active oblique convergence near the Alpine Fault, New Zealand: identifying the neotectonic overprint. *Journal of Structural Geology,* 24**,** 193-217.

LITTLE, T., HOLCOMBE, R. & ILG, B. 2002b. Kinematics of oblique collision and ramping inferred from microstructures and strain in middle crustal rocks, central Southern Alps,

New Zealand. *Journal of Structural Geology,* 24**,** 219-239.

LITTLE, T. A., MORTIMER, N. & MCWILLIAMS, M. 1999. An episodic Cretaceous cooling model for the Otago-Marlborough Schist, New Zealand, based on 40Ar/39Ar white mica ages. *New Zealand Journal of Geology and Geophysics,* 42**,** 305-325.

MACKENZIE, D. J. & CRAW, D. 1993. Structural control of gold-scheelite mineralisation in a major normal fault system, Barewood, eastern Otago, New Zealand. *New Zealand Journal of Geology and Geophysics,* 36**,** 437-445.

MACKENZIE, D. & CRAW, D. 2005. Structural and lithological continuity and discontinuity in the Otago Schist, Central Otago, New Zealand. *New Zealand Journal of Geology and Geophysics,* 48**,** 279-293.

MACKINNON, T. C. 1983. Origin of the Torlesse terrane and coeval rocks, South Island, New Zealand. *Geological Society of America Bulletin,* 94**,** 967-985.

MARSHALL, P. 1918. The geology of the Tuapeka district, central Otago Division. *New Zealand Geological Survey Bulletin,* 19**,** 79 p.

MCKEAG, S., CRAW, D. & NORRIS, R. 1989. Origin and deposition of a graphitic schist-hosted metamorphogenic Au-W deposit, Macraes, East Otago, New Zealand. *Mineralium Deposita,* 24**,** 124-131.

MORGAN, P. 1920. Scheelite mines of Otago. *14th Annual Report, New Zealand Geological Survey,* 10**,** 338 p.

MORTENSEN, J. K., CRAW, D., MACKENZIE, D. J., GABITES, J. E. & ULLRICH, T. 2010. Age and origin of orogenic gold mineralization in the Otago Schist Belt, South Island, New Zealand: constraints from lead isotope and 40Ar/39Ar Dating Studies. *Economic Geology,* 105**,** 777-793.

MORTIMER, N. 1993. Jurassic tectonic history of the Otago schist, New Zealand. *Tectonics,* 12**,** 237-244.

MORTIMER, N. 2000. Metamorphic discontinuities in orogenic belts: example of the garnet–biotite–albite zone in the Otago Schist, New Zealand. *International Journal of Earth Sciences,* 89**,** 295-306.

MORTIMER, N. & ROSER, B. 1992. Geochemical evidence for the position of the Caples–Torlesse boundary in the Otago Schist, New Zealand. *Journal of the Geological Society,* 149**,** 967-977.

MUIR, R., IRELAND, T., WEAVER, S. & BRADSHAW, J. 1994. Ion microprobe U-Pb zircon geochronology of granitic magmatism in the Western Province of the South Island, New Zealand. *Chemical Geology,* 113**,** 171-189.

MÜNKER, C. & COOPER, R. 1999. The Cambrian arc complex of the Takaka Terrane, New Zealand: an integrated stratigraphical, paleontological and geochemical approach. *New Zealand Journal of Geology and Geophysics,* 42**,** 415-445.

MURPHY, D. B. 2010. Metamorphism and the PT History of Alpine Schist from the Newton Range, Southern Alps, New Zealand. *M.Sc. Thesis*, Victoria University of Wellington, New Zealand.

MUTCH, A. R. 1969. The Scheelite Resources of the Glenorchy District West Otago, New Zealand. *New Zealand Geological Survey Report*, 40**,** 68 p.

NORRIS, R. & CRAW, D. 1987. Aspiring Terrane: an oceanic assemblage from New Zealand and its implications for terrane accretion in the southwest Pacific. *In:* Leitch, E. C., Schneiber, E. *ed.* Terrane Accretion and Orogenic Belts**.** *Americian Geophysical Union***,** 19**,** 169-177.

OCEANA GOLD. 2015. Updated resource & reserve statement March 2015. *OceanaGold*, https://www.oceanagold.com/wp-content/uploads/OceanaGold-Announces-Updated-Resource-Reserve-Statement.pdf. Accessed 7th April 2016.

PATERSON, C. J. 1982. Oxygen isotopic evidence for the origin and evolution of a scheelite ore-forming fluid, Glenorchy, New Zealand. *Economic Geology,* 77**,** 1672-1687.

PATERSON, C. J. 1986. Controls on gold and tungsten mineralization in metamorphic-hydrothermal systems, Otago, New Zealand. *Geological Association of Canada Special Paper,* 32**,** 25-39.

PATERSON, C. J. & RANKIN, P. C. 1979. Trace element distribution in the schist surrounding a quartz-scheelite lode, Glenorchy, New Zealand. *New Zealand Journal of Geology and Geophysics,* 22**,** 329-338.

PETRIE, B., CRAW, D. & RYAN, C. 2005. Geological controls on refractory ore in an orogenic gold deposit, Macraes mine, New Zealand. *Mineralium Deposita,* 40**,** 45-58.

PITCAIRN, I. K. 2004. Sources of fluids and metals in orogenic gold deposits: the Otago Schists, New Zealand. *Ph.D. Thesis,* University of Southhampton, United Kingdom.

PITCAIRN, I. K., TEAGLE, D. A. H., CRAW, D., OLIVO, G. R., KERRICH, R. & BREWER, T. S. 2006. Sources of Metals and Fluids in Orogenic Gold Deposits: Insights from the Otago and Alpine Schists, New Zealand. *Economic Geology,* 101**,** 1525-1546.

PITCAIRN, I. K., OLIVO, G. R., TEAGLE, D. A. H. & CRAW, D. 2010. Sulfide evolution during prograde metamorphism of the Otago and Alpine Schists, New Zealand. *The Canadian Mineralogist,* 48**,** 1267-1295.

PITCAIRN, I. K., CRAW, D. & TEAGLE, D. A. 2014. The gold conveyor belt: large-scale gold mobility in an active orogen. *Ore Geology Reviews,* 62**,** 129-142.

PITCAIRN, I. K., CRAW, D. & TEAGLE, D. A. 2015. Metabasalts as sources of metals in orogenic gold deposits. *Mineralium Deposita, 50***,** 373-390.

RATTENBURY, M. & ISAAC M. 2012. The QMAP 1: 250 000 geological map of New Zealand project. *New Zealand Journal of Geology and Geophysics,* 55**,** 393-405.

REED, A. H. 1956. The Story of Early Dunedin. *A.H. & A.W. Reed for the Alfred & Isabel & Marian Reed Trust*. 295 p.

REED, J. J. 1958. Granites and mineralization in New Zealand. *New Zealand Journal of Geology and Geophysics,* 1**,** 47-64.

ROSER, B. & COOPER, A. 1990. Geochemistry and terrane affiliation of Haast Schist from the western Southern Alps, New Zealand. *New Zealand Journal of Geology and Geophysics,* 33**,** 1-10.

ROSER, B. & KORSCH, R. 1988. Provenance signatures of sandstone-mudstone suites determined using discriminant function analysis of major-element data. *Chemical Geology,* 67**,** 119-139.

ROSER, B. & KORSCH, R. 1999. Geochemical characterization, evolution and source of a Mesozoic accretionary wedge: the Torlesse terrane, New Zealand. *Geological Magazine,* 136**,** 493-512.

SILBERLING, N., NICHOLS, K., BRADSHAW, J. & BLOME, C. 1988. Limestone and chert in tectonic blocks from the Esk Head subterrane, South Island, New Zealand. *Geological Society of America Bulletin,* 100**,** 1213-1223.

STALLARD, A. & SHELLEY, D. 2005. The initiation and development of metamorphic foliation in the Otago Schist, Part 1: competitive oriented growth of white mica. *Journal of Metamorphic Geology,* 23**,** 425-442.

STALLARD, A., SHELLEY, D. & REDDY, S. 2005. The initiation and development of metamorphic foliation in the Otago Schist, Part 2: evidence from quartz grain-shape data. *Journal of Metamorphic Geology,* 23**,** 443-459.

TULLOCH, A., KIMBROUGH, D., LANDIS, C., MORTIMER, N. & JOHNSTON, M. 1999. Relationships between the Brook Street Terrane and Median Tectonic Zone (Median Batholith): evidence from Jurassic conglomerates. *New Zealand Journal of Geology and Geophysics,* 42**,** 279-293.

TURNBULL, I. 1979. Petrography of the Caples terrane of the Thomson Mountains, northern Southland, New Zealand. *New Zealand Journal of Geology and Geophysics,* 22**,** 709-727.

TURNBULL, I. 1980. Structure and interpretation of the Caples terrane of the Thomson Mountains, northern Southland, New Zealand. *New Zealand Journal of Geology and Geophysics,* 23**,** 43-62.

TURNBULL, I., MORTIMER, N. & CRAW, D. 2001. Textural zones in the Haast Schist—a reappraisal. *New Zealand Journal of Geology and Geophysics,* 44**,** 171-183.

VAUGHAN, A. P., LEAT, P. T. & PANKHURST, R. J. 2005. Terrane processes at the margins of Gondwana: introduction. *Geological Society, London, Special Publications,* 246**,** 1-21.

VRY, J., BAKER, J., MAAS, R., LITTLE, T., GRAPES, R. & DIXON, M. 2004. Zoned (Cretaceous and Cenozoic) garnet and the timing of high grade metamorphism, Southern Alps, New Zealand. *Journal of Metamorphic Geology,* 22**,** 137-157.

WAIGHT, T. E., WEAVER, S., IRELAND, T., MAAS, R., MUIR, R. & SHELLEY, D. 1997. Field characteristics, petrography, and geochronology of the Hohonu Batholith and the adjacent Granite Hill complex, North Westland, New Zealand. *New Zealand Journal of Geology and Geophysics,* 40**,** 1-17.

WANDRES, M. C. A. 2002. Provenance study of the Torlesse Terranes and implications for the origin of the continental crust of eastern New Zealand. *Ph.D Thesis,* University of Canterbury, New Zealand.

WILLIAMSON, J. H. 1939. The geology of the Naseby subdivision, Central Otago, New Zealand. *New Zealand Geological Survey Bulletin,* 39**,** 141 p.

YARDLEY, B. D. 1982. The early metamorphic history of the Haast Schists and related rocks of New Zealand. *Contributions to Mineralogy and Petrology,* 81**,** 317-327.

YOKOYAMA, K. 1994. Preliminary study of the sandstones in the Torlesse terrane, New Zealand. *Geoscience Reports of Shizuoka University,* 20**,** 63-70.

Chapter 5: SAMPLING AND GEOLOGY OF OTAGO SCHIST SAMPLE SITES

5.1 Aims

This chapter aims to provide information on samples obtained in the Otago Schist including, discussing rational behind the sampling procedure and more detailed geology of individual sites selected for systematic sampling programs.

5.2 Sample Collection

Tungsten, as discussed in Chapters 2 and 4, has been shown to have been mobilized from the metasedimentary rocks of the Otago Schist during prograde subgreenschist to greenschist facies metamorphism (Breeding and Ague 2002). Following this key observation, fieldwork and sampling was planned and undertaken on two sections in the Otago Schist, Lake Hāwea and Fiddlers Flat (Fig. 7). Combined, these areas depict the progressive metamorphism of Otago Schist from prehnite-pumpellyite facies to lower greenschist facies (Fig. 8). Dominant lithologies from these sections were sampled, with samples collected from Fiddlers Flat and Lake Hāwea having protolith compositions ranging from argillite to graywacke, and metamorphic grades ranging from prehnite-pumpellyite to lower greenschist facies (Fig. 9). This approach was undertaken to allow the identification of W-rich diagenetic or detrital mineral(s) and any prograde recrystallization they may undergo that could liberate W, as is predicted in the studies of Pitcairn et al. (2010) and Large et al. (2012).

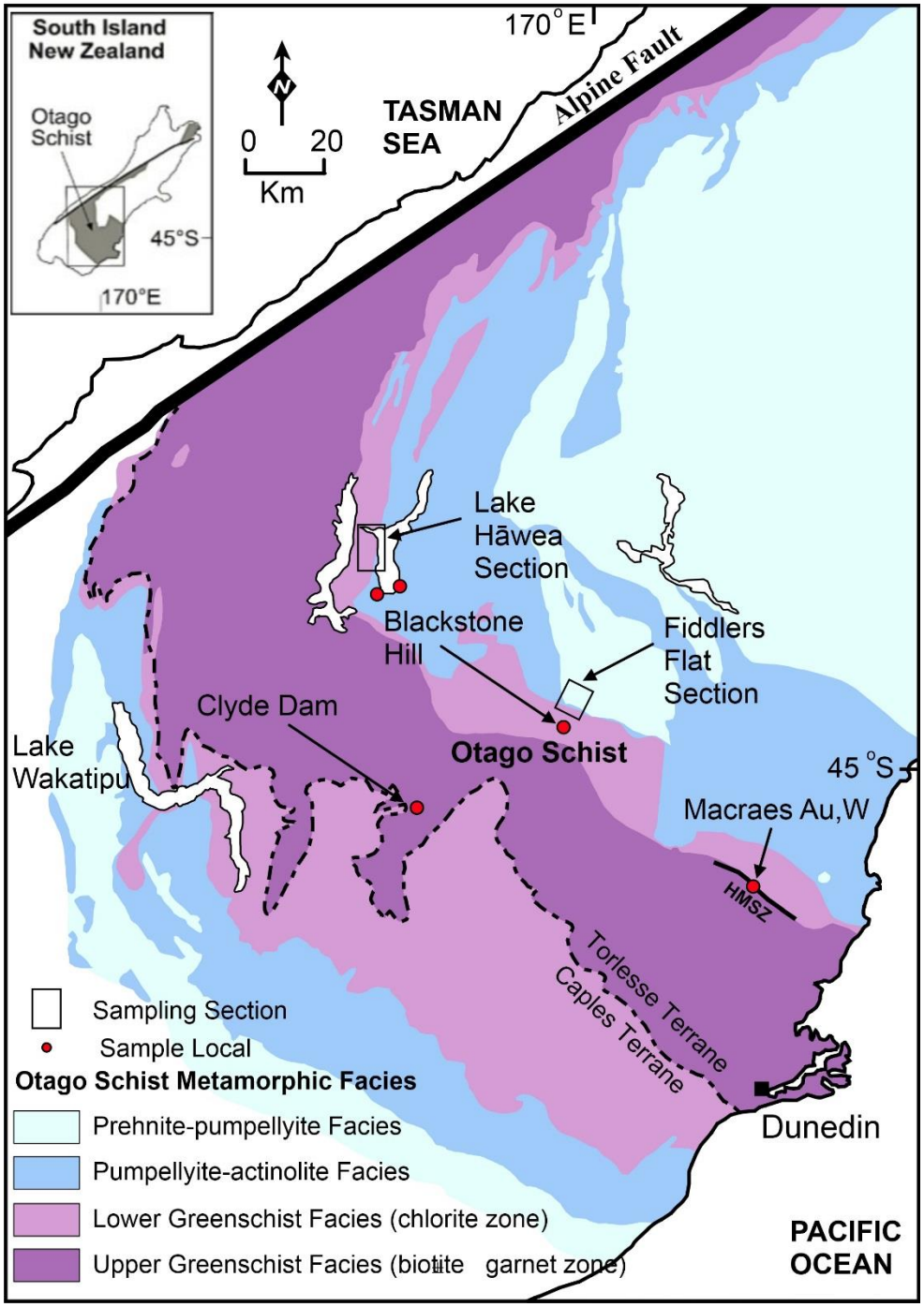

Fig. 7. Geological map of the Otago Schist and Alpine Schist, South Island, New Zealand, showing the Caples and Torlesse terranes, metamorphic facies, sample sections (boxes), sample sites (red dots), the Alpine Fault – Austro-Pacific plate contact.

Scheelite was observed and sampled from both the Fiddlers Flat and Lake Hāwea sections (Fig. 8), and also from auriferous veins in the Macraes Mine (Macraes underground). Scheelite has previously been observed and discussed at the Macraes Mine (for example, Begbie and Craw 2006) and the Lake Hāwea section (Craw and Norris 1991), however prior to this study, scheelite had not been observed along the Fiddlers Flat section, nor hosted in such low metamorphic grade rocks in the Otago Schist.

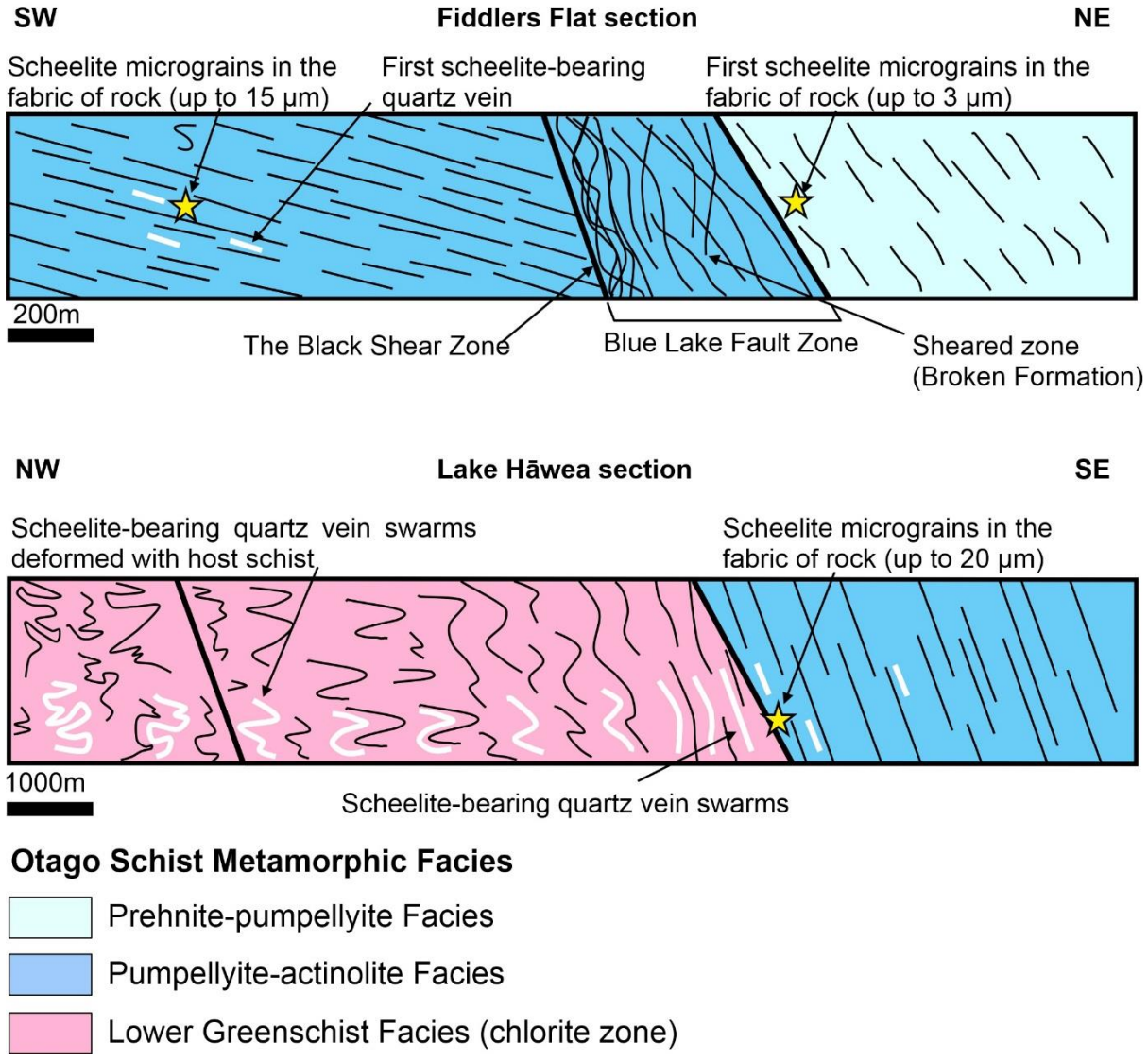

Fig. 8. Schematic diagram showing metamorphic facies and some geological features of the Fiddlers Flat and Lake Hāwea sections. Modified after Henne et al. (2011).

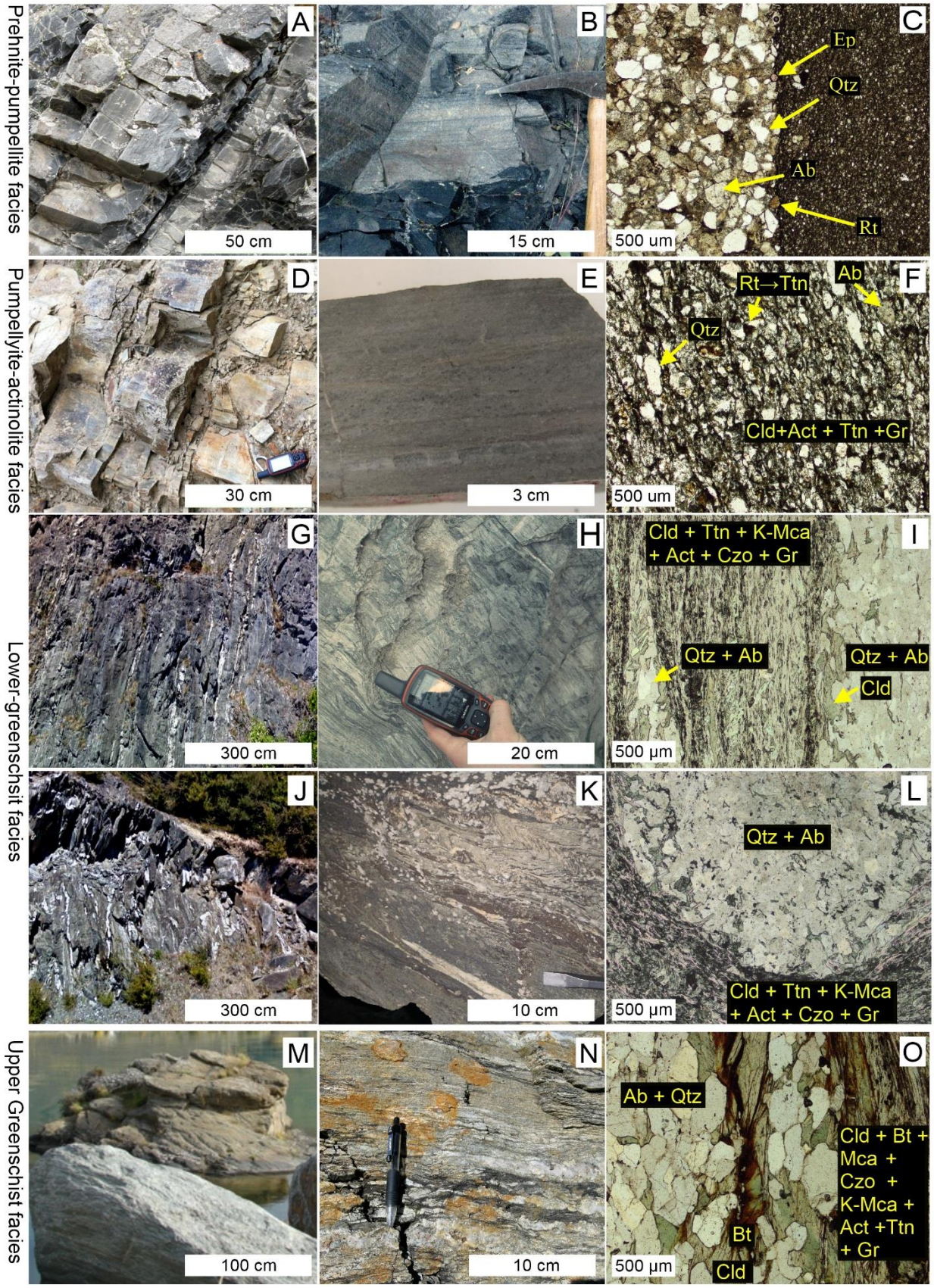
Prehnite-pumpellite facies
Pumpellyite-actinolite facies
Lower-greenschsit facies
Upper Greenschist facies
A
50 cm
B
15 cm
C
Ep
Qtz
Ab
Rt
500 um
D
30 cm
E
3 cm
F
Rt→Ttn
Ab
Qtz
Cld+Act + Ttn +Gr
500 um
G
300 cm
H
20 cm
I
Cld + Ttn + K-Mca
+ Act + Czo + Gr
Qtz + Ab
Qtz + Ab
Cld
500 µm
J
300 cm
K
10 cm
L
Qtz + Ab
Cld + Ttn + K-Mca
+ Act + Czo + Gr
500 µm
M
100 cm
N
10 cm
O
Ab + Qtz
Cld + Bt +
Mca +
Czo +
K-Mca +
Act +Ttn
+ Gr
Bt
Cld
500 µm

Fig. 9. Representative appearance of dominant lithologies (argillite and greywacke to phyllitic and psammitic schists) of the Otago Schist with increasing metamorphic grade from prehnite-pumpellyite facies (A, B, C) to upper greenschist facies (M, N, O). A, prehnite-pumpellyite facies turbidites (near-complete Bouma Sequence) from the Fiddlers Flat section. Bedding is largely preserved. B, argillite-graywacke contact in prehnite-pumpellyite facies rocks from Fiddlers Flat. C, photomicrograph (transmitted light) showing argillite-graywacke contact in prehnite-pumpellyite facies rocks from Fiddlers Flat. D, pumpellyite-actinolite facies turbidites (near-complete Bouma Sequence) from the Fiddlers Flat section. E, cut surface (perpendicular to foliation/bedding) of pumpellyite-actinolite facies greywacke-psammite, showing foliation development that largely obscures bedding. F, photomicrograph of pumpellyite-actinolite greywacke-psammite from Fiddlers Flat, showing foliation development and elongation (parallel to foliation) of minerals. Relict bedding features can still be observed. G, lower greenschist facies outcrop near pumpellyite-actinolite/ lower greenschist facies boundary along the Lake Hāwea section. Minor syn-metamorphic veins (qtz-ab-ttn-ep-sch) are observed. H, close-up of lower greenschist facies psammitic schist from Lake Hāwea, showing segregation laminae development. I, photomicrograph of lower greenschist facies psammitic schist from Lake Hāwea, showing qtz-ab±cld and cld-ttn-k-mca-act-czo-gr segregation laminae. J, lower greenschist facies outcrop along Lake Hāwea section, displaying a higher degree of textural reconstruction than lower greenschist facies samples in G, H, and I. K, close-up of lower greenschist facies psammitic schist from Lake Hāwea, showing textural reconstruction of the rock and the syn-metamorphic veins. L, photomicrograph of lower greenschist facies psammitic schist from Lake Hāwea, showing qtz-ab and cld-ttn-k-mca-act-czo-gr segregation laminae that display a higher degree of textural reconstruction. M, upper greenschist facies psammitic schist from Clyde Dam that display a higher degree of textural reconstruction than the lower greenschist facies samples. N, close-up of upper greenschist facies psammitic schist from Clyde Dam. O, photomicrograph of upper greenschist facies psammitic schist from Clyde Dam, showing qtz-ab and cld-bt-ttn-k-mca-act-czo-gr segregation laminae that display a higher degree of textural reconstruction and are coarser grained than the lower greenschist facies samples. Abbreviations are as follows: Ep- Epidote, Qtz- Quartz, Ab- Albite, Rt- Rutile, Ttn- Titanite, Act- Actinolite, Gr- Graphite, Cld- Chlorite, K-Mca- K-Mica, Czo- Clinozoisite, Bt- Biotite, Mca- Mica.

Sampling areas are shown on Figure 7, with individual sample locations listed in Table 1 and Appendix 1. Detailed descriptions of the geology of sampling areas are given in the following section.

Table 1. Otago Schist regional metamorphic and mineralized samples. Sample number, sample id, locality, UTM WGS84 coordinates for zone 59G, metamorphic grade, and lithology. Abbreviations are as follows: P.P- prehnite-pumpellyite, P.A- pumpellyite-actinolite, C.GS- lower greenschist, B.GS- upper greenschist.

Sample No.	Sample Id	Locality	Easting	Northing	Met. Grade	Lithology
1	FFPP001	Fiddlers Flat	412393	5029356	P.P	graywacke/ argillite
2	F1-A	Fiddlers Flat	412260	5028560	P.P	argillite
3	F1-B	Fiddlers Flat	412260	5028560	P.P	argillite
4	F1-D	Fiddlers Flat	412260	5028560	P.P	argillite
5	F2-A	Fiddlers Flat	412260	5028560	P.P	graywacke/ argillite
6	F2-B	Fiddlers Flat	412260	5028560	P.P	graywacke/ argillite
7	F3	Fiddlers Flat	412260	5028560	P.P	argillite
8	F4	Fiddlers Flat	412260	5028560	P.P	argillite
9	F5-A	Fiddlers Flat	412260	5028560	P.P	graywacke/ argillite
10	F5-B	Fiddlers Flat	412260	5028560	P.P	graywacke/ argillite
11	F5-C	Fiddlers Flat	412260	5028560	P.P	graywacke/ argillite
12	FFB-001	Fiddlers Flat	411880	5028026	P.P/P.A	graywacke/ argillite
13	FFPA-001	Fiddlers Flat	411171	5026987	P.A	Semi-schist graywacke
17	FFPA-002	Fiddlers Flat	411059	5027015	P.A	Semi-schist graywacke
14	FFPA-003	Fiddlers Flat	411068	5027018	P.A	Semi-schist graywacke
15	FFPA-004	Fiddlers Flat	411088	5027008	P.A	Semi-schist graywacke
16	FFPA-005	Fiddlers Flat	411042	5027039	P.A	Semi-schist graywacke
18	RS-6	Lake Hāwea	366520	5060800	P.A	Semi-schist argillite
19	RS-3	Lake Hāwea	360970	5058860	P.A/C.GS	Semi-schist argillite
20	LH-PA001	Lake Hāwea	360613	5074718	P.A/C.GS	Semi-schist argillite
21	LH-PA002	Lake Hāwea	360601	5074727	P.A/C.GS	Semi-schist argillite
22	LH-PA/GS	Lake Hāwea	360614	5074684	P.A/C.GS	Semi-schist
23	LH-CG002	Lake Hāwea	360301	5075361	C.GS	Phyllitic schist
24	LH-CG003	Lake Hāwea	359310	5076159	C.GS	Phyllitic schist

25	LH-CG004	Lake Hāwea	358268	5076492	C.GS	Psammitic schist
26	RS4	Lake Hāwea	357552	5076760	C.GS	Phyllitic schist
27	RS5	Lake Hāwea	357462	5076776	C.GS	Phyllitic schist
28	BHCG-001	Blackstone Hills	407673	5019918	C.GS	Phyllitic schist
29	RS1	Clyde Dam	367280	4995550	B.GS	Phyllitic schist
30	RS2a	Clyde Dam	365225	5004820	B.GS	Mafic schist
31	RS2b	Clyde Dam	365230	5004820	B.GS	Phyllitic schist
32	MCM-001A	Macraes Mine	457600	4974140	C.GS	Massive sch-qtz-py- vein
33	MCM-001B	Macraes Mine	456900	4974950	C.GS	Massive sch-qtz-py- vein
34	MCM-001C	Macraes Mine	456900	4974950	C.GS	Laminated sch-qtz-py
35	MGB-1A	Macraes Mine	463250	4971020	C.GS	Micaceous schist (ore)
36	MGB-1B	Macraes Mine	463250	4971020	C.GS	Micaceous schist (ore)
37	MGB-2	Macraes Mine	463250	4971020	C.GS	Feldspathic schist (ore)
38	MGB-3	Macraes Mine	463250	4971020	C.GS	Micaceous schist (ore)
39	MGB-4	Macraes Mine	463250	4971020	C.GS	Micaceous schist (ore)
40	MGB-5	Macraes Mine	463250	4971020	C.GS	Micaceous schist (ore)
41	MGB-6	Macraes Mine	463250	4971020	C.GS	Micaceous schist (ore)
42	MGB-7	Macraes Mine	463250	4971020	C.GS	Micaceous schist (ore)
43	MGB-8	Macraes Mine	463250	4971020	C.GS	Feldspathic schist (ore)
44	MGM-9	Macraes Mine	463250	4971020	C.GS	Feldspathic schist (ore)
45	MGV-10	Macraes Mine	463250	4971020	C.GS	Micaceous schist (ore)

5.3 Geology of Sample Sites

The Fiddlers Flat section has previously been described in detail by Henne et al. (2011) and Henne and Craw (2012); the Lake Hāwea section by Craw and Norris (1991) and Stallard and Shelley (2005), and the Macraes Mine by Begbie and Craw (2006), Craw (2002), Craw et al. (1999, 2004), de Ronde et al. (2000), MacKenzie et al. (2013), McKeag et al. (1989), Petrie et al.

(2005), and others. The following section on the geology of sample sites draws upon these site detailed studies, my own observations, and generalized studies on mineralogy, metamorphism, and structure of the Otago Schist.

5.3.1 Fiddlers Flat

The Fiddlers Flats section (Fig. 10), is well-exposed along the southwest flowing Manuherikia River where it provides excellent exposures across the metamorphic transition from Torlesse Terrane sedimentary rocks into the Otago Schist. Narrowing in the Fiddlers Flat section is observed compressing the normally >15 km thick Jurassic metamorphic section into an interval approximately only 2 km wide (Henne and Craw 2012).

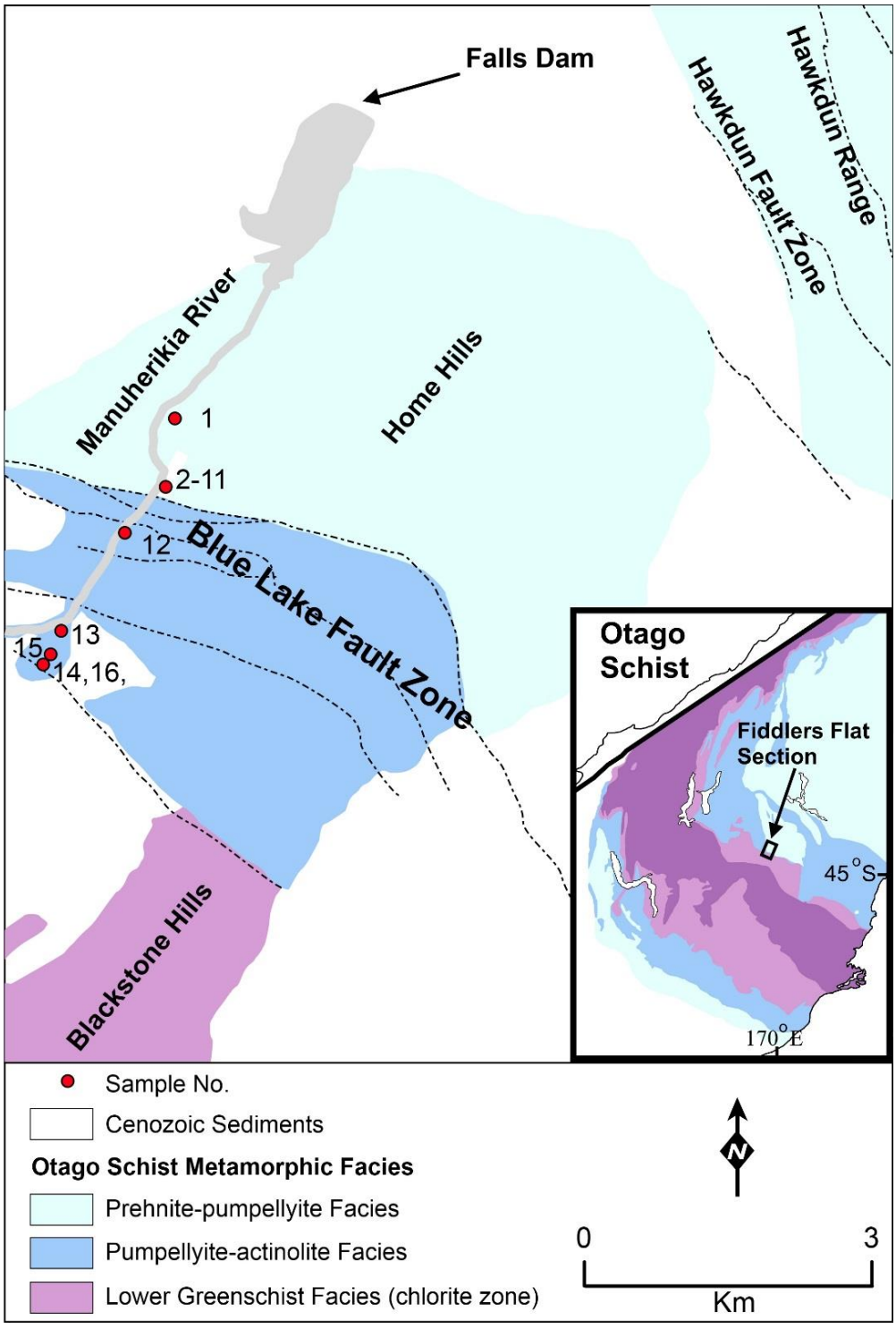

Fig. 10. Fiddles Flat section with metamorphic facies boundaries, traceable faults (dotted lines), and sample locations. Figure based on Henne et al. (2011), Henne and Craw (2012), and Rattenbury and Isaac (2012). Sample abbreviations: 1- FFPP-001, 2- F1-A, 3- F1-B, 4- F1D, 5- F2-A, 6- F2-B, 7- F3, 8- F4, 9- F5-A, 10- F5-B, 11- F5-C, 12- FFB-001, 13- FFPA-001, 14- FFPA-003, 15- FFPA-004, 16- FFPA-005, FFPA-002.

Prehnite–pumpellyite facies turbidites occupy the northern portion of the Fiddlers Flat section (Fig. 10), and represents the lowest metamorphic grade in the area. Rocks belonging to the prehnite-pumpellyite metamorphic facies at outcrop scale are observed as unfoliated graywackes and subordinate argillites (Henne et al. 2011; Henne and Craw 2012) (Figs. 9A, B). Mineralogy of these metasedimentary prehnite-pumpellyite facies rocks is largely consistent with mineralogy reported for prehnite-pumpellyite facies elsewhere in the Torlesse Terrane derived Otago Schist (for example, Bishop 1972). Graywacke assemblages in the prehnite-pumpellyite facies rocks of the Fiddlers Flat section are characterized by the rock-forming minerals quartz, albite, K-mica, chlorite, prehnite, pumpellyite, titanite (discussed further in Chapters 6, 7, and 8), and detrital carbonaceous material (angular and rounded fragments commonly with relict cell structures preserved, albeit in collapsed form; Henne and Craw 2012) (Fig. 9C). Accessory minerals include illite, rutile (discussed further in Chapters 6, 7, and 8), apatite, allanite, biotite, zircon, pyrite ± chalcopyrite, galena, sphalerite, stripnomelane, K-mica, calcite, epidote, K-feldspar, garnet, scheelite (discussed further in Chapter 8), and amphibole (Bishop 1972; Stallard and Shelley 2005; Stallard et al. 2005; Pitcairn et al. 2010; Henne et al. 2011; Henne and Craw 2012; Large et al. 2012). The breakdown of detrital plagioclase, K-feldspar, biotite, garnet, and amphibole is observed throughout the development of the prehnite-pumpellyite facies, with plagioclase being completely albitized early on and K-feldspar, biotite, garnet, and amphibole persisting into the pumpellyite-actinolite facies rocks (Bishop 1972). The disappearance of prehnite marks the onset of the pumpellyite-actinolite facies with incipient development of foliation also coinciding with this metamorphic facies transition (MacKinnon 1983; Turnbull et al. 2001; Henne et al. 2011).

In the Fiddlers Flat section, the northwest striking Blue Lake Fault Zone separates the

prehnite–pumpellyite and pumpellyite–actinolite facies rocks (Figs. 8, 10) (Henne et al. 2011). Directly southwest of the boundary of the prehnite–pumpellyite and pumpellyite–actinolite facies rocks, a zone of complexly sheared 'Broken Formation' rocks occurs (Figs. 8, 10). This rock mass is dominated by boudinaged graywackes and conglomerates that are contained within the matrix of sheared argillites with minor sheared graywackes. A prominent northwest striking shear zone 'the black shear zone' (Henne and Craw 2012), defines the southwestern margin of the broken formation and contains evidence for an enhanced recrystallization of K-mica, and chlorite to form a discontinuous metamorphic foliation, and foliated gouge, in strongly sheared argillite (Fig. 8). Southwest of the black shear zone and outside of the tectonically sheared Broken Formation, pumpellyite–actinolite facies rocks are of typical appearance in the Otago Schist (Henne et al. 2011) (Figs. 9D, E). These schists are fine-grained (10–50 μm) and have a moderate to pervasive foliation (Fig. 9F). Foliation is subparallel to strongly transposed bedding, and at outcrop scale, sedimentary features in these rocks are largely obscured (MacKinnon 1983; Turnbull et al. 2001; Henne et al. 2011) (Figs. 9D, E). Relict lithological variations are preserved (Henne et al. 2011). Massive psammitic schist dominates, with interlayered subordinate pelitic schist layers 1–10 m thick. Syn-metamorphic quartz veins, commonly with minor albite, titanite, K-mica, and chlorite, have been emplaced parallel to the foliation in micaceous horizons (Henne et al. 2011). In these rocks, rare scattered subhedral macroscopic grains of scheelite were also observed in the syn-metamorphic veins (discussed further in Chapters 8). The veins also locally cut across foliation, especially in the psammitic schists. Metamorphic graphite occurs as dusty micron-scale grains that have recrystallized with K-mica and chlorite in the foliation (Fig. 9E). Graywacke/ psammite assemblages are characterized by the rock-forming minerals quartz, albite, K-mica, pumpellyite, titanite (discussed further in Chapters 6, 7, and 8), and actinolite ± chlorite,

stilpnomelane, epidote, and graphite [recrystallized grains (flakes) within the foliation and within syn-metamorphic veins (Henne and Craw 2012; Hu et al. 2015)] (Fig. 9F). Graphite within the pumpellyite-actinolite and greenschist facies rocks of the Otago Schist is thought to have formed from the mobilization of detrital carbonaceous material by metamorphic-hydrothermal fluids (Henne and Craw 2012). Accessory minerals include calcite, rutile (discussed further in Chapters 6, 7 and 8), apatite, allanite, biotite, anorthite, zircon, garnet (spessartine), pyrite, pyrrhotite, ± chalcopyrite, galena, sphalerite, ilmenite, magnetite, scheelite (discussed further in Chapters 8), and amphibole (pargasite) (Bishop 1972; Stallard and Shelley 2005; Stallard et al. 2005; Pitcairn et al. 2010; Henne et al. 2011; Henne and Craw 2012; Large et al. 2012).

5.3.2 Lake Hāwea

The Lake Hāwea section (Fig. 11), the second of two principal sections described in this study, is a well-exposed section along the western shoreline of Lake Hāwea. Road cuttings along Makarora-Lake Hāwea Road, past Dinner Flat exposes fresh unaltered rock (for example, Figs. 9G, H, J, K). This section provides excellent exposures of Torlesse Terrane-derived rocks, across the metamorphic transition from the pumpellyite-actinolite facies through to lower greenschist facies (Figs. 7, 8, 11).

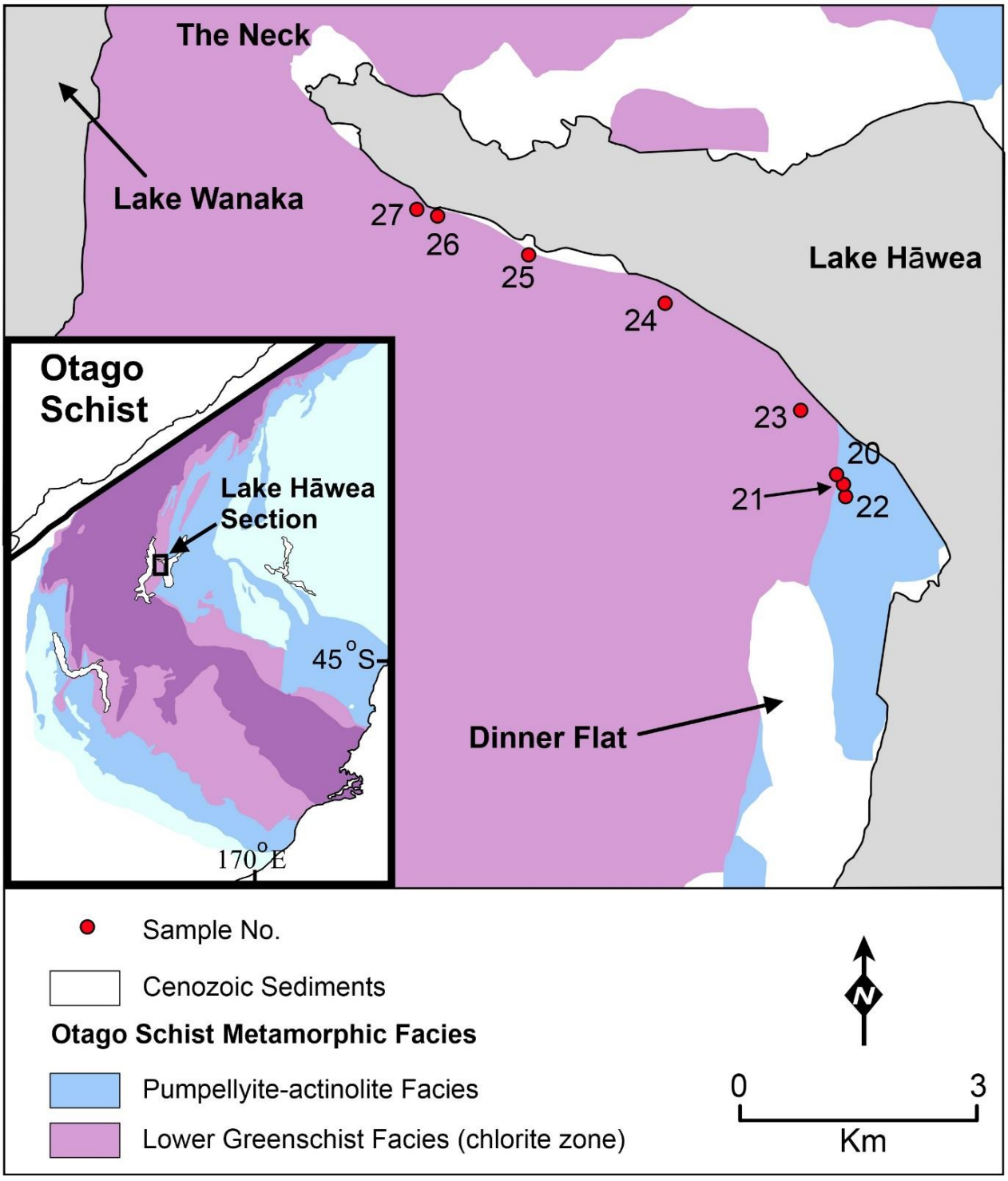

Fig. 11. Lake Hāwea section with metamorphic facies boundaries, and sample locations. Figure based on Pitcairn (2004), and Rattenbury and Isaac (2012). Sample abbreviations: 20- LHPA001, 21- LHPA002, 22 LHPA/GS, 23-LHCG002, 24-LHCG003, 25-LHCG004, 26-RS4, 27-RS5.

Lithologies exposed immediately north of Dinner Flat represent the transition of subgreenschist to greenschist facies rocks in the Otago Schist (Figs. 9G, H, J, K). Psammitic schists with subordinate interlayered phyllitic schists dominate, and at outcrop scale, are observed as moderately well-foliated to pervasively foliated, with local tight folding and incipient development of a second foliation parallel to fold axial surfaces, observed within the greenschist facies lithologies (Craw and Norris 1991; Turnbull et al. 2001; Henne et al. 2011) (Figs. 9I, J, K). Foliation is defined by thin (100-200 μm) laminae of quartz and albite grains (up to 1 cm in length) forming prominent segregations (Figs. 9H, I, L). Detrital quartz and mica are no longer stable at these conditions, having been pervasively recrystallized to metamorphic quartz and micas (Turnbull et al. 2001; Stallard et al. 2005) (Figs. 9I, L). Mineralogy of Torlesse Terrane derived psammitic and argillites lithologies in the lower greenschist facies Otago Schist are characterized by psammitic schist assemblages of quartz, albite, K-mica, chlorite, titanite, actinolite, and clinozoisite ± graphite (Bishop 1972; Craw and Norris 1991; Pitcairn 2004; Stallard and Shelley 2005; Stallard et al. 2005; Pitcairn et al. 2010) (Figs. 9I, L). These rock-forming minerals are associated with accessory amounts of calcite, pumpellyite, apatite, allanite, zircon, pyrite, pyrrhotite ± chalcopyrite, galena, sphalerite, rutile (observed as relict grains within metamorphic titanite; discussed further in Chapters 6, 7, and 8), ilmenite, hematite, spinel, magnetite, scheelite (discussed further in Chapter 8), and amphibole (pargasite) (Bishop 1972; Craw and Norris 1991; Pitcairn 2004; Stallard and Shelley 2005; Stallard et al. 2005; Pitcairn et al. 2010). Syn-metamorphic quartz veins, commonly with minor albite, titanite, chlorite, and epidote, have been emplaced parallel to the foliation in micaceous horizons (Henne et al. 2011) (Fig. 9G). Similar to subgreenschist facies hosted veins, scattered subhedral macroscopic grains of scheelite were also observed in these syn-metamorphic veins (discussed further in Chapters 8).

Syn-metamorphic veins are well documented in the Otago Schist, with their abundance increasing to their maximum concentration in the lower greenschist facies (Cox 1993). These veins occur as swarms of foliation-concordant and foliation-discordant veins approximately 0.5-1 m apart, and typically only persisting for up to 10 m before pinching out (Craw and Norris 1991) (Fig. 9G). These veins are an integral part of the metamorphic host, having been deformed and recrystallized with their host rocks (Craw and Norris 1991 and references therein) (Figs. 9I, K). Vein margins are locally poorly defined with host rock mineralogy largely the same as the veins (Craw and Norris 1991).

5.3.3 Additional Regional Samples

Additional to the detailed studies and sampling programs along the Fiddlers Flat and Lake Hāwea sections (Fig. 7), regional grab samples were taken opportunistically whilst travelling between the two sections (Fig. 7). These samples help fill important gaps in the higher metamorphic grade rocks of the Otago Schist (that is, upper greenschist facies samples taken at Clyde Dam; Fig. 7), and provide extensions of the Fiddlers Flat [Blackstone Hill; Fig. 7] and Lake Hāwea (Lake Hāwea southwestern and southeastern shorelines; Fig. 7) sections.

Pumpellyite–actinolite facies samples obtained from the southwestern and southeastern shorelines of Lake Hāwea (Fig. 7), closely resemble (at the macro and micro-scale) the pumpellyite-actinolite facies samples of the Fiddlers Flat section and the start of the Lake Hāwea section. Metamorphic grade and recrystallization increases towards the west (Fig. 7) in these samples.

Lower greenschist facies samples were obtained from the Blackstone Hills (Fig. 7; approximately 7 km southwest of the Fiddlers Flat section). These samples resemble the lower greenschist facies samples of Lake Hāwea, in terms of appearance (at the macro and micro-scale)

and mineralogy. One obvious difference between the Blackstone Hills samples and those from Lake Hāwea, is the extensive weathering these samples have undergone. This weathering typically has resulted in the breakdown of chlorite and K-mica to clay minerals and the oxidation of Fe-sulfides (presumably, pyrrhotite or pyrite or both) to Fe-oxide minerals. However, Ti-minerals (metamorphic and detrital) appear unaffected by this weathering and resemble those found in the samples from Lake Hāwea.

Upper greenschist (biotite ± garnet) facies samples obtained from Clyde Dam represent the only non-mineralized upper greenschist facies samples obtained during this project (Fig. 7). Psammitic schists with subordinate interlayered phyllitic schists dominate the upper greenschist facies rocks. Samples from Clyde Dam resemble upper greenschist samples described in other studies of the Otago Schist (for example, Brown 1967, Mortimer 2000, Turnbull et al. 2001) (Fig. 9M, N). Textural reconstruction in these upper greenschist facies rocks is observed being greater than the lower greenschist facies samples. Grain size within these schistose rocks is generally coarser than the lower greenschist facies schist, but overall still quite finely grained (25–500 μm) (Fig. 9O). Foliation in these rocks is defined by quartz-albite, mica segregations and polycrystallized quartz veins (Fig. 9O) of variable thickness and length. Mineralogy of Torlesse Terrane derived psammitic and argillites lithologies in the upper greenschist facies Otago Schist is characterized by the rock-forming minerals psammitic schist assemblages of quartz, albite, K-mica, chlorite, titanite, biotite, actinolite, and clinozoisite ± graphite and garnet (Brown 1967; Turnbull et al. 2001; Pitcairn 2004; Pitcairn et al. 2006, 2010) (Fig. 9O). These rock-forming minerals are associated with accessory amounts of calcite, apatite, zircon, pyrrhotite, pyrite ± chalcopyrite, galena, sphalerite, ilmenite, hematite, spinel, and magnetite (Brown 1967; Turnbull et al. 2001; Pitcairn 2004; Pitcairn et al. 2006, 2010). Syn-metamorphic

veins are strongly deformed and recrystallized and form an integral part of the upper greenschist facies rocks.

5.3.4 Mineralized Samples- Macraes Flat

The Macraes Flat area (Fig. 12) is a historical mineral field that produced approximately 1,000 t of scheelite concentrate and 518 Kg of Au, from hard-rock and alluvial sources between 1875 and 1936 (Williamson 1939). Following increases in Au prices during the 1980-90's, new mining developments (Macraes Mine) have occurred in the Macraes Flat area (Fig. 12). Gold prices since the opening of the Macraes Mine in 1990, have remained sufficiently high enough to have maintain Au production from the Macraes operations since its re-opening. Presently, OceanaGold Corporation owns and operates the world-class Macraes Mine, which consists of a series of open pits and underground developments along a regional-scale Early Cretaceous (142-135 Ma; Mortensen et al. 2010) shear zone (The Hyde-Macraes Shear Zone; Figs. 12, 13, 14A). The Macraes Mine is the most significant deposit in the Otago Schist having produced in excess of 70 t of Au (Pitcairn et al. 2014) and containing reserves in excess of 160 t at approximately 1.1 g/t (OceanaGold 2015). Scheelite is currently not recovered during the current mining and processing techniques. However a scoping study has recently been conducted by the owner and operator of the mine to recover scheelite, with results of this study pending.

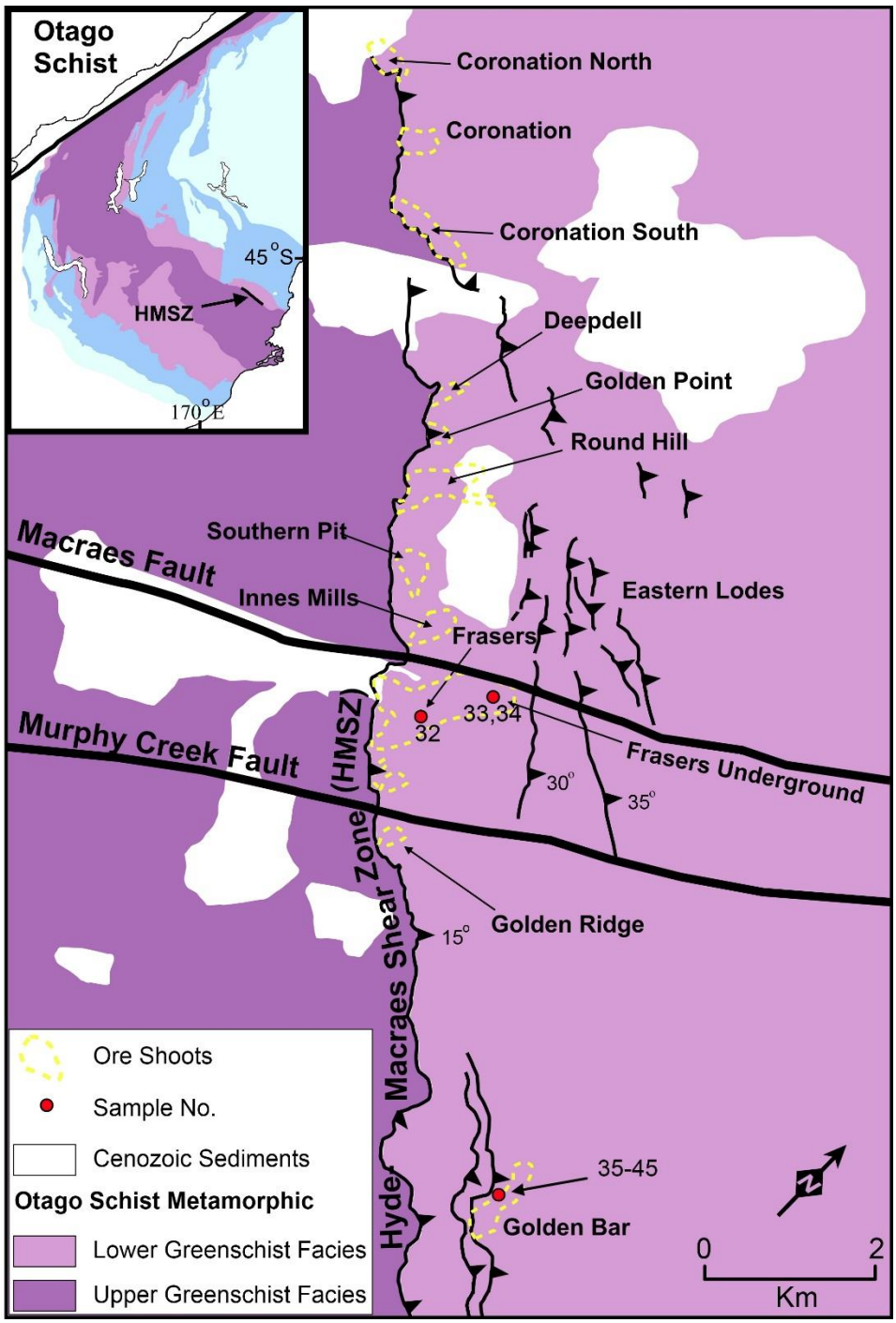

Fig. 12. Macraes Flat with metamorphic facies boundaries, major faults and shear zones, and sample locations. Modified after de Ronde et al. (2000) and OceanaGold Corporation (2010). Sample abbreviations: 32- MCM-001A, 33- MCM-001B, 34- MCM-001C, 35- MGB-1A, 36- MGB-1B, 37- MGB-2, 38 - MGB-3, 39- MGB-4, 40- MGB-5, 41- MGB-6, 42- MGB-7, 43- MGB-8, 44- MGB-9, 45- MGV-10.

Mineralization at Macraes Mine is hosted within lower greenschist facies massive

feldspathic and more fissile micaceous schists (Petrie et al. 2005) (Fig 14B, C, D, E, F) that are juxtaposed against upper greenschist facies schist, along a normal fault, the Footwall Fault (Angus et al. 1997; Craw 2002; Craw et al. 2004; Begbie and Craw 2006) (Figs. 12, 13, 15). Mineralization at Macraes Mine is complex, however, in general consists of foliation parallel mineralized shears (Figs. 14B, C, D, E, F) [and related shear veins (Fig. 14G)] and high angle extensional quartz-carbonate-scheelite veins or 'stockworks' (McKeag et al. 1989; Begbie and Craw 2006; MacKenzie et al. 2013) (Figs. 14I, J). Mineralized shears are typically concentrated in the more micaceous schists and high angle extensional quartz-carbonate±scheelite veins confined to 'pods' of more massive schist (McKeag et al. 1989; Begbie and Craw 2006; MacKenzie et al. 2013).

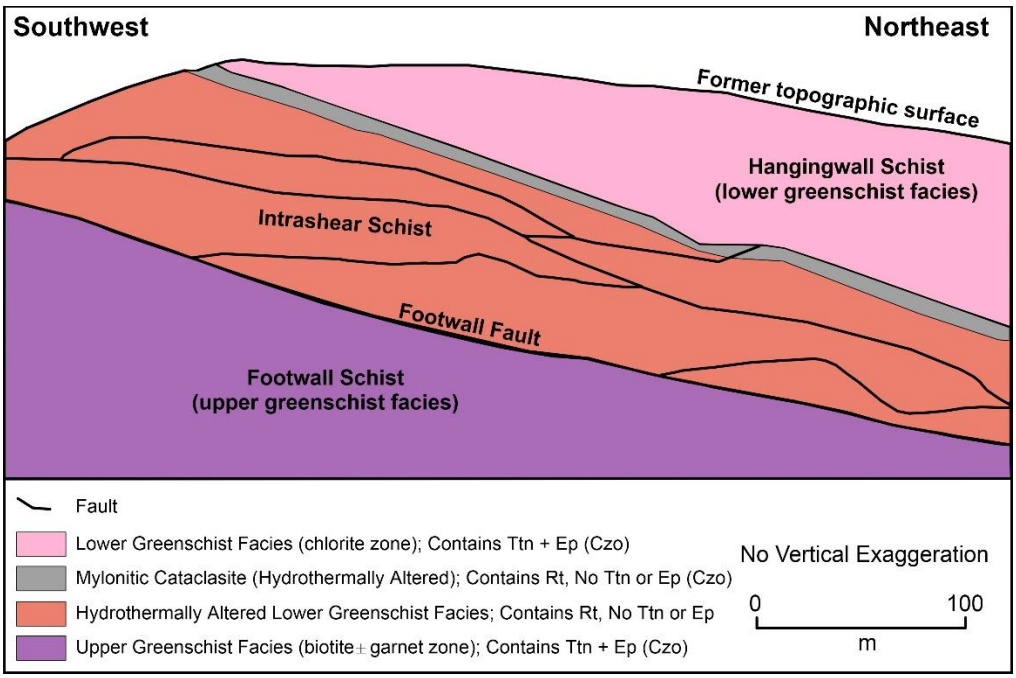

Fig. 13. Cross section through the Hyde-Macraes Shear Zone at the Round Hill mine near Macraes (see Fig. 14), showing the metamorphic-hydrothermally altered Intrashear Schist in-between the lower greenschist facies Hangingwall Fault and the upper greenschist facies Footwall Fault. Mylonitic cataclasite is most common immediately below the Hangingwall Shear. Modified after Craw et al. (1999) and others. Abbreviations are as follows: Ep- Epidote, Rt- Rutile, Ttn- Titanite, Czo- Clinozoisite.

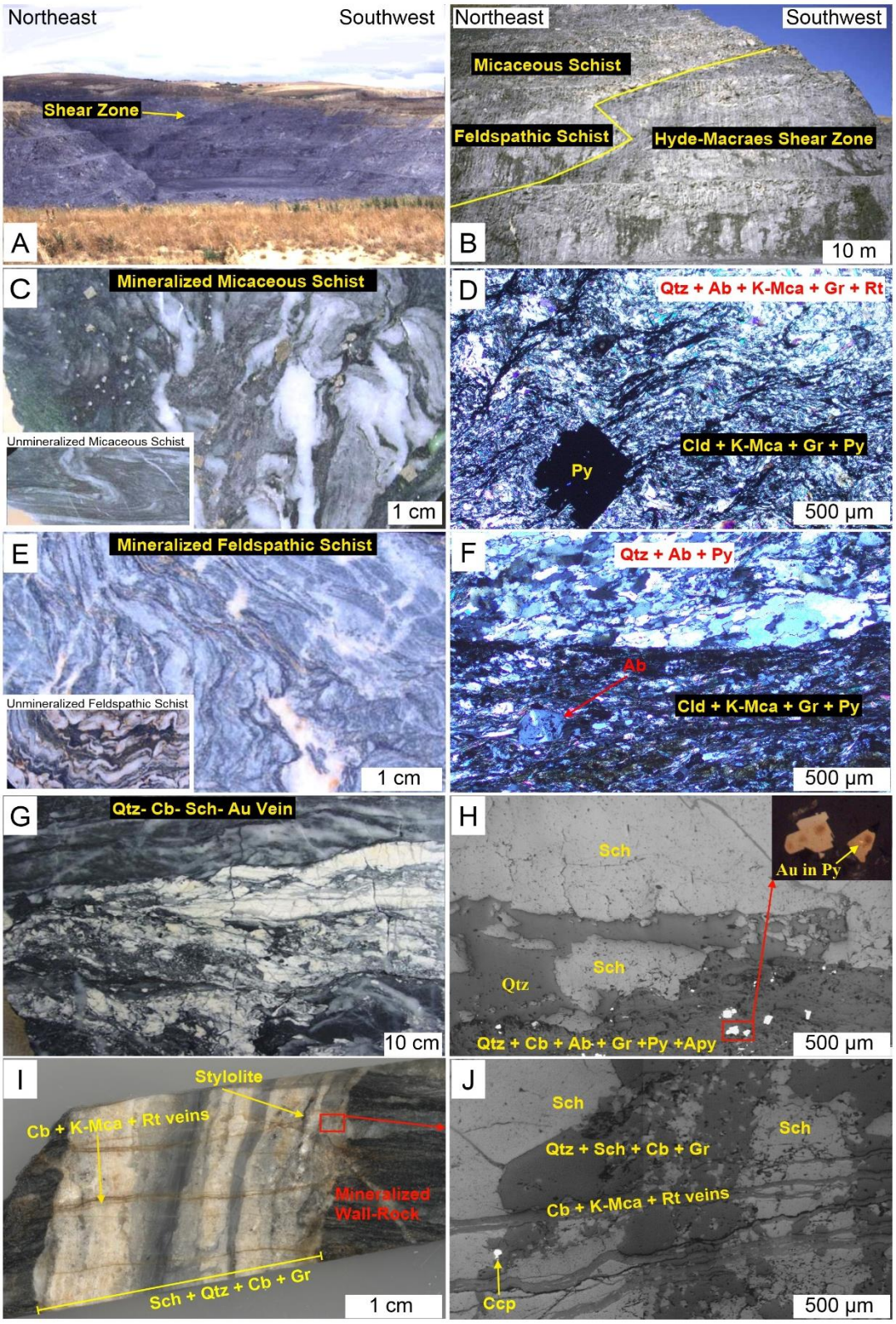

Fig. 14. Shear Zone contacts, major lithologies, and petrology from the mineralized Hyde-Macraes Shear Zone

[modified from Craw (n.d.)]. (A) Hyde-Macraes Shear Zone as exposed in Frasers open pit [modified from Craw (n.d.)], (B) Hyde-Macraes Shear Zone exposed in Frasers open pit and showing the two major lithologies that hosts mineralization (modified from Craw n.d.), (C) mineralized and unmineralized (white box) micaceous schist [modified from Craw (n.d.)], (D) photomicrograph (transmitted light cross-polarized) of mineralized micaceous schist containing abundant chlorite, K-mica, graphite, pyrite ± albite and arsenopyrite. (E) mineralized and unmineralized (white box) feldspathic schist [modified from Craw (n.d.)], (F) photomicrograph (transmitted light cross-polarized) of mineralized feldspathic schist containing abundant segregations of albite, quartz, and pyrite ± arsenopyrite, chlorite, K-mica, and graphite, (G) complex polyphase shear-related quartz-scheelite-gold vein from Frasers Underground [photograph from International Applied Geochemistry Symposium (2013)], (H) photomicrograph (reflected light) of scheelite-bearing shear-related vein, (I) high angle extensional quartz-carbonate-scheelite vein/ stockwork vein from Frasers Underground, (J) photomicrograph (reflected light) of) high angle extensional quartz-carbonate-scheelite vein/ stockwork vein. Abbreviations are as follows: Qtz- Quartz, Ab- Albite, Rt- Rutile, Gr- Graphite, Cld- Chlorite, K-Mca- K-Mica, Py- Pyrite, Cb- Carbonate, Sch- Scheelite, Au- Gold, Apy- Arsenopyrite.

Mineralized shears volumetrically are the major ore type at Macraes Mine (Craw et al. 1999). These mineralized shears typically occur adjacent to the Hangingwall Shear or other well-defined shears associated with shear duplexes (MacKenzie et al. 2013). These mineralized shears are characterized by rotated and recrystallized K-mica, hydrothermal graphite, rutile, and disseminated sulfides, mainly pyrite and arsenopyrite (Craw et al. 1999; Petrie et al. 2005; MacKenzie et al. 2013) (Figs. 14D, F). Gold occurs primarily as micron sized blebs encapsulated in sulfides, as well as along fractures within the sulfides (Craw et al. 1999; Petrie et al. 2005; MacKenzie et al. 2013).

Silicified schist and shear-parallel quartz veins occur as sheared and disrupted lenses within the shears (Craw et al. 1999; Petrie et al. 2005; MacKenzie et al. 2013). The veins are variably mineralized with sulfides (predominantly, arsenopyrite, and pyrite) (McKeag et al. 1989; Craw et al. 1999; MacKenzie et al. 2013; Petrie et al. 2005). Like in the mineralized

shears, Au occurs in the silicified schist and shear-parallel quartz veins, as native Au and as micron sized blebs in sulfides (Fig. 14H). Scheelite is also found as infill in some of these low angle veins (McKeag et al. 1989; Craw et al. 1999; MacKenzie et al. 2013; Petrie et al. 2005) (Figs. 14G, H).

High angle extensional quartz-carbonate±scheelite veins, or 'stockworks' as previously stated are typically confined to 'pods' of more massive schist (MacKenzie et al. 2013). These veins typically strike northeast, oblique to the HMSZ, and are thought to have developed in localized regions of extension along steeply dipping lateral ramps that link northeast -dipping shears and ramps within the shear zone (Begbie and Craw 2006; MacKenzie et al., 2013). Stockwork veins consist of quartz, scheelite, and carbonate, with subordinate K-mica, hydrothermal rutile, sulfide minerals (arsenopyrite and pyrite ± chalcopyrite and bornite), and Au (Craw et al. 1999; Begbie and Craw 2006; MacKenzie et al. 2013) (Figs. 14I, J). The veins are typically laminated in appearance (Fig. 14I), a feature that is thought to record an incremental succession of brecciation and infill events (Begbie and Craw 2006; MacKenzie et al. 2013). Further discussion of the incremental nature of these veins is provided in Chapter 8.

References

ANGUS, P., DE RONDE, C. & SCOTT, J. 1997. Exploration along the hyde macraes shear [abs.]. *New Zealand Minerals and Mining Conference Proceedings*, 1997. 151-157.

BEGBIE, M. & CRAW, D. 2006. Geometry and petrography of stockwork vein swarms, Macraes mine, Otago Schist, New Zealand. *New Zealand Journal of Geology and Geophysics*, 49**,** 63-73.

BISHOP, D. 1972. Progressive metamorphism from prehnite-pumpellyite to greenschist facies in the Dansey Pass area, Otago, New Zealand. *Geological Society of America Bulletin*, 83**,**

3177-3198.

BREEDING, C. M. & AGUE, J. J. 2002. Slab-derived fluids and quartz-vein formation in an accretionary prism, Otago Schist, New Zealand. *Geology,* 30**,** 499-502.

BROWN, E. 1967. The greenschist facies in part of eastern Otago, New Zealand. *Contributions to Mineralogy and Petrology,* 14**,** 259-292.

COX, S. C. 1993. Veins, fluid, fractals, scale & schist: an investigation of fluid-rock interaction during deformation of the Torlesse Terrane, New Zealand. *Ph.D. Thesis,* University of Otago, New Zealand.

CRAW, D. 2002. Geochemistry of late metamorphic hydrothermal alteration and graphitisation of host rock, Macraes gold mine, Otago Schist, New Zealand. *Chemical Geology,* 191**,** 257-275.

CRAW, D. n.d. Macraes gold mine, East Otago, New Zealand. *Department of Geology, University of Otago,* http://www.otago.ac.nz/geology/research/gold/macraes-gold-mine/index.html, Accessed 7th April 2016.

CRAW, D. & NORRIS, R. J. 1991. Metamorphogenic Au-W veins and regional tectonics: Mineralisation throughout the uplift history of the Haast Schist, New Zealand. *New Zealand Journal of Geology and Geophysics,* 34**,** 373-383.

CRAW, D., WINDLE, S. & ANGUS, P. 1999. Gold mineralization without quartz veins in a ductile-brittle shear zone, Macraes Mine, Otago Schist, New Zealand. *Mineralium Deposita,* 34**,** 382-394.

CRAW, D., MACKENZIE, D. & PETRIE, B. 2004. Disseminated gold mineralisation in a schist-hosted mesothermal deposit, Macraes Mine, Otago, New Zealand [abs.]. *Proceedings of the PACRIM 2004 Congress, The Australasian Institute of Mining and*

Metallurgy Publication series, 2004. 135-141.

DE RONDE, C. E. J., FAURE, K., BRAY, C. J. & WHITFORD, D. J. 2000. Round Hill shear zone-hosted gold deposit, Macraes Flat, Otago, New Zealand: evidence of a magmatic ore fluid. *Economic Geology*, 95**,** 1025-1048.

HENNE, A. & CRAW, D. 2012. Synmetamorphic carbon mobility and graphite enrichment in metaturbidites as a precursor to orogenic gold mineralisation, Otago Schist, New Zealand. *Mineralium Deposita*, 47**,** 781-797.

HENNE, A., CRAW, D. & MACKENZIE, D. 2011. Structure of the Blue Lake Fault Zone, Otago Schist, New Zealand. *New Zealand Journal of Geology and Geophysics*, 54**,** 311-328.

HU, S., EVANS, K., CRAW, D., REMPEL, K., BOURDET, J., DICK, J. & GRICE, K. 2015. Raman characterization of carbonaceous material in the Macraes orogenic gold deposit and metasedimentary host rocks, New Zealand. *Ore Geology Reviews*, 70**,** 80-95.

INTERNATIONAL APPLIED GEOCHEMISTRY SYMPOSIUM. 2013. Orogenic gold deposits: deposit models to exploration methodology [Brochure]. *Rotorua, New Zealand***,** 9.

LARGE, R., THOMAS, H., CRAW, D., HENNE, A. & HENDERSON, S. 2012. Diagenetic pyrite as a source for metals in orogenic gold deposits, Otago Schist, New Zealand. *New Zealand Journal of Geology and Geophysics*, 55**,** 137-149.

MACKENZIE, D., FARMER, L. & CRAW, D. 2013. Multi-stage ore formation at the Macraes gold scheelite deposit Otago Schist, New Zealand. *The Australasian Institute of Mining and Metallurgy New Zealand Branch Annual Conference*, 2013. 281-294.

MACKINNON, T. C. 1983. Origin of the Torlesse terrane and coeval rocks, South Island, New

Zealand. *Geological Society of America Bulletin,* 94**,** 967-985.

MCKEAG, S., CRAW, D. & NORRIS, R. 1989. Origin and deposition of a graphitic schist-hosted metamorphogenic Au-W deposit, Macraes, East Otago, New Zealand. *Mineralium Deposita,* 24**,** 124-131.

MORTENSEN, J. K., CRAW, D., MACKENZIE, D. J., GABITES, J. E. & ULLRICH, T. 2010. Age and origin of orogenic gold mineralization in the Otago Schist Belt, South Island, New Zealand: constraints from lead isotope and 40Ar/39Ar Dating Studies. *Economic Geology,* 105**,** 777-793.

MORTIMER, N. 2000. Metamorphic discontinuities in orogenic belts: example of the garnet–biotite–albite zone in the Otago Schist, New Zealand. *International Journal of Earth Sciences,* 89**,** 295-306.

PETRIE, B., CRAW, D. & RYAN, C. 2005. Geological controls on refractory ore in an orogenic gold deposit, Macraes mine, New Zealand. *Mineralium Deposita,* 40**,** 45-58.

PITCAIRN, I. K. 2004. Sources of fluids and metals in orogenic gold deposits: the Otago Schists, New Zealand. *Ph.D. Thesis,* University of Southhampton, United Kingdom.

PITCAIRN, I. K., TEAGLE, D. A. H., CRAW, D., OLIVO, G. R., KERRICH, R. & BREWER, T. S. 2006. Sources of metals and fluids in orogenic gold deposits: insights from the Otago and Alpine Schists, New Zealand. *Economic Geology,* 101**,** 1525-1546.

PITCAIRN, I. K., OLIVO, G. R., TEAGLE, D. A. H. & CRAW, D. 2010. Sulfide evolution during prograde metamorphism of the Otago and Alpine Schists, New Zealand. *The Canadian Mineralogist,* 48**,** 1267-1295.

PITCAIRN, I. K., CRAW, D. & TEAGLE, D. A. 2014. The gold conveyor belt: large-scale gold mobility in an active orogen. *Ore Geology Reviews,* 62**,** 129-142.

RATTENBURY, M. & ISAAC M. 2012. The QMAP 1: 250 000 geological map of New Zealand project. *New Zealand Journal of Geology and Geophysics,* 55**,** 393-405.

STALLARD, A. & SHELLEY, D. 2005. The initiation and development of metamorphic foliation in the Otago Schist, Part 1: competitive oriented growth of white mica. *Journal of Metamorphic Geology,* 23**,** 425-442.

STALLARD, A., SHELLEY, D. & REDDY, S. 2005. The initiation and development of metamorphic foliation in the Otago Schist, Part 2: evidence from quartz grain-shape data. *Journal of Metamorphic Geology,* 23**,** 443-459.

TURNBULL, I., MORTIMER, N. & CRAW, D. 2001. Textural zones in the Haast Schist—a reappraisal. *New Zealand Journal of Geology and Geophysics,* 44**,** 171-183.

WILLIAMSON, J. H. 1939. The geology of the Naseby subdivision, Central Otago, New Zealand. *New Zealand Geological Survey Bulletin,* 39**,** 141 p.

Chapter 6: MAJOR W HOST MINERALS IN THE METASEDIMENTARY ROCKS OF THE OTAGO SCHIST

6.1 Aims

This chapter aims to identify the major W host mineral phase(s) in the metasedimentary rocks of the Otago Schist of varying metamorphic grade, utilizing Laser Ablation Inductively Coupled Plasma Mass Spectrometer (LA-ICP-MS) traverses, combined with reflected and scanning electron microscopy (SEM). This approach is adopted following the methodology of Large et al. (2012) who identified the mineralogical source for Au, As, Ag, Hg, and Sb in the Otago Schist using similar techniques. More detailed discussions of the stability of the major W hosting mineral phases with prograde metamorphism is provided in Chapter 7 and partially in Chapter 8. An additional aim of this chapter is to utilize the laser ablation traverses to identify at what metamorphic grade W becomes depleted in the Otago Schist. This approach is undertaken to assess the previous study of Breeding and Ague (2002) that shows W depletion occurs in the Otago Schist at the subgreenschist-greenschist facies boundary, a premise that forms a cornerstone of this study.

6.2 Introduction

As previously discussed in Chapters 2 and 4, current models for the source of metals enriched in the orogenic Au deposits of the Otago Schist, propose that these metals are sourced from the recrystallisation of enriched mineralogical phase(s) (diagenetic pyrite to pyrrhotite; Au, As, Ag, Hg, and Sb) in the metasedimentary rock of the Otago Schist with increasing metamorphic

grades (Pitcairn et al. 2010; Large et al. 2012). Currently a mineralogical source for W is not defined. However, if the models of Pitcairn et al. (2010) and Large et al. (2012) are correct, a mineralogical source for W should be located within the lowest metamorphic grade rocks with recrystallization of this mineral phase with progressive metamorphism mobilizing W.

Previous literature on mineralogical phases enriched in W (as previously discussed in Chapter 3), combined with known mineralogical compositions of Torlesse Terrane metasediments (as defined in Chapter 5), indicates that the most likely mineralogical source minerals for W are the titanium-rich minerals rutile, ilmenite, and titanite, with chlorite, biotite, K-feldspar, pyroxene, muscovite, garnet, amphibole, and stilpnomelane also potentially being important W hosts.

Identification of the major W-bearing mineral phases in the Otago Schist in this chapter, forms the foundation for the next three chapters that focus on the mobilization of W during mineral recrystallization reactions (Chapters 7 and 9), and the source of W in the turbidite-hosted orogenic Au deposits of the Otago Schist (Chapter 8) and other terranes (Chapter 9).

6.3 Sampling and Methodology

6.3.1 Sample Selection

Samples from the Fiddlers Flat and Lake Hāwea sections were utilized as combined they depict the progressive metamorphism of the major lithologies present (graywackes and argillites) in the Otago Schist and its Torlesse Terrane precursor, from prehnite-pumpellyite facies to lower greenschist facies. In addition, metasedimentary upper greenschist facies (Torlesse Terrane) samples were taken from Clyde Dam. The sampling areas are shown on Figure 7, and individual sample locations can be found in Table 1 and Appendix 1. Detailed descriptions of the local

geology of both major sections (Fiddlers Flat and Lake Hāwea) are provided within Chapter 5, as is a generalized description of the Clyde Dam local.

The samples collected from Fiddlers Flat, Lake Hāwea, and Cylde Dam have protolith compositions ranging from argillite to graywacke, and metamorphic grades ranging from prehnite-pumpellyite to upper greenschist facies. Mineralogical and textural associations in the samples were examined using a combination of reflected light and scanning electron microscopy (SEM). Analytical traverses using LA-ICP-MS were undertaken on representative samples with protolith compositions ranging from argillite to graywacke, and all metamorphic grades [prehnite-pumpellyite (n 14), pumpellyite-actinolite (n 4), lower greenschist (n 7), and upper greenschist facies (n 2)].

6.3.2 Analytical Methods

Analytical instrumentation used in this study includes a Resonetics Resolution laser ablation system equipped with a Coherent COMPex Pro 110 ArF excimer laser, housed at CODES/Earth Sciences, University of Tasmania. The ArF excimer laser operates at a 193 nm wavelength with a 20 ns pulse width and was coupled to an Agilent 7900 quadrupole inductively coupled plasma mass spectrometer (ICP-MS). Laser ablation traverses were performed using a 100 μm beam moving at 60 μm/s relative to the sample. Traverses were conducted perpendicular to the major bedding/foliation and utilized a laser repetition rate of 10 Hz with laser beam energy at the sample interface maintained at approximately 8.5 J/cm^2. Traverses average 30mm in length, approximately equal to 260 sweeps per traverse.

Laser traverses are reported in counts per second (cps) and in the context of this study are not quantifiable. They do, however, provide valuable information on relative concentrations

between other elements at certain periods in time. This combined with petrology along the traverse lines, allows the identification of mineralogical hosts of elements and assessment of which phases are the most significant hosts. In addition, mean laser traverses allow the assessment of relative whole rock concentrations of elements between samples. Therefore in the context of this study, relative concentrations of W between rocks of different metamorphic grades can be compared.

6.4 Results

6.4.1 Relative Concentrations of W in the Metasediments with Increasing Metamorphic Grade

Laser ablation traverses from representative metasedimentary samples, show mean relative W concentrations (cps) in the subgreenschist facies rocks are nearly twice as high as in the greenschist facies rocks (Table 2, Fig. 15A). The decrease in average W cps strongly supports the evidence of Breeding and Ague (2002) that W loss is widespread in greenschist facies rocks from the Otago Schist.

In addition, the highest individual W counts are observed in the prehnite-pumpellyite facies rocks (max 184,000 cps; Table 2, Fig. 15B), and maximum individual W counts systematically decrease with increasing metamorphic grade (Table 2, Fig. 15B). This observation supports the concept that the loss of W is associated with the disappearance of a mineral that contains high W.

Table 2. Mean and maximum values (cps) from laser traverses of metasediments grouped by metamorphic grade.

Metamorphic facies	Prehnite-pumpellyite	Pumpellyite-actinolite	Lower greenschist	Upper greenschist
W- Mean (cps)	4,360	4,640	2,600	2,490
W- Max (cps)	184,000	91,500	44,400	13,900

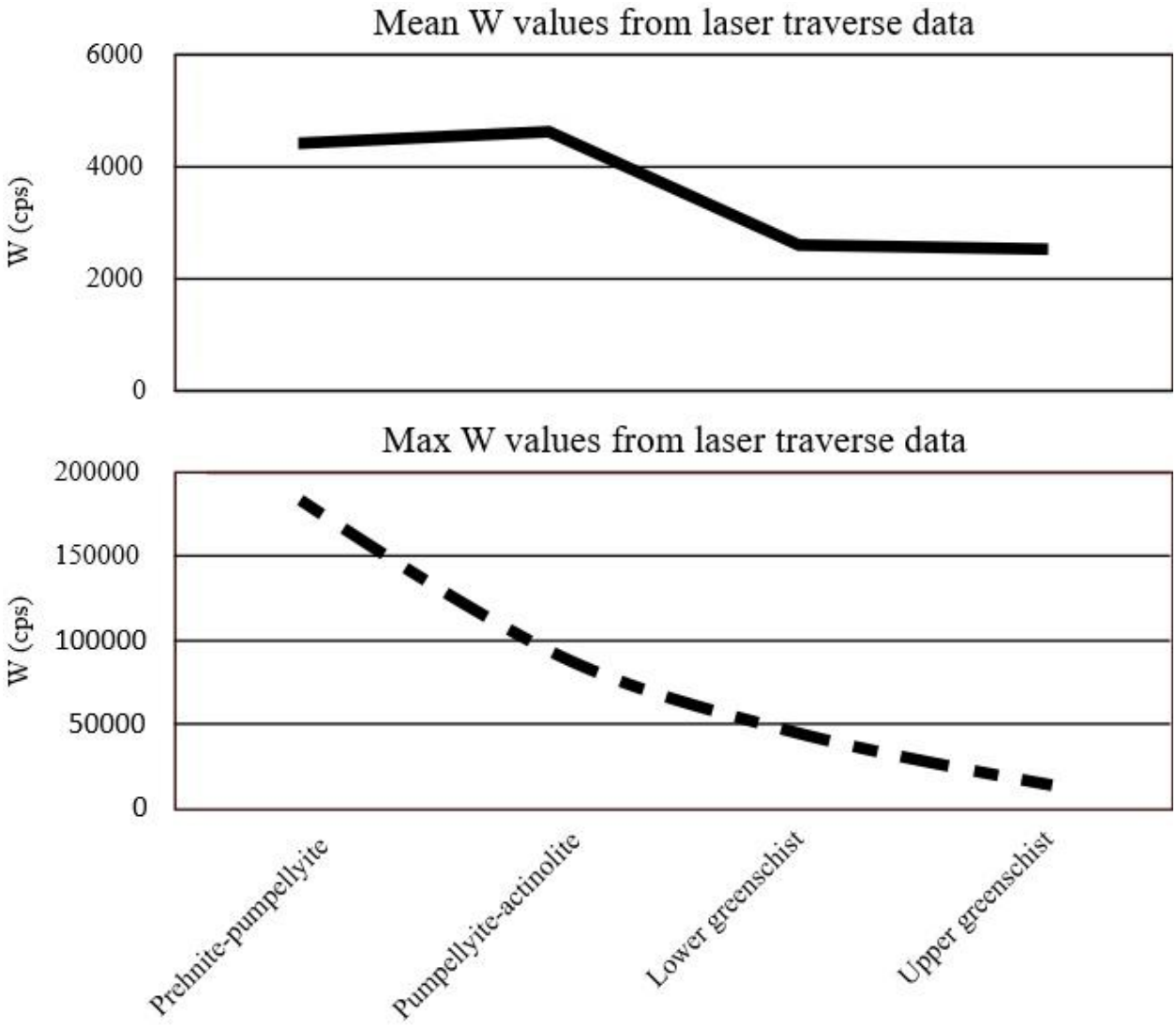

Fig. 15. Mean and maximum relative W concentrations (cps) from laser traverse data from metasediments from varying metamorphic grade.

6.4.2 Identification of W Host Minerals using LA-ICP-MS Traverses

Prehnite-pumpellyite Facies Rocks: Laser ablation traverses completed on representative

graywacke and argillite samples from Fiddlers Flat, show irregular distributions of W at detectable and locally relatively high levels, at the <100µm scale (Figs. 16A, B, C). The majority of high W peaks coincide with high Ti ± Ca peaks, with reflected light microscopy and SEM observing these peaks as corresponding to the laser beam having passed through grains of rutile ± titanite (Figs. 16A, B, C). In addition, rare, yet, prominent corresponding peaks of W, Ca, and Sr that lack peaks of Ti are also observed in the laser ablation traverses, with SEM observing these peaks as corresponding to the laser beam having passed through rare scheelite micrograins (for example, Fig. 16D).

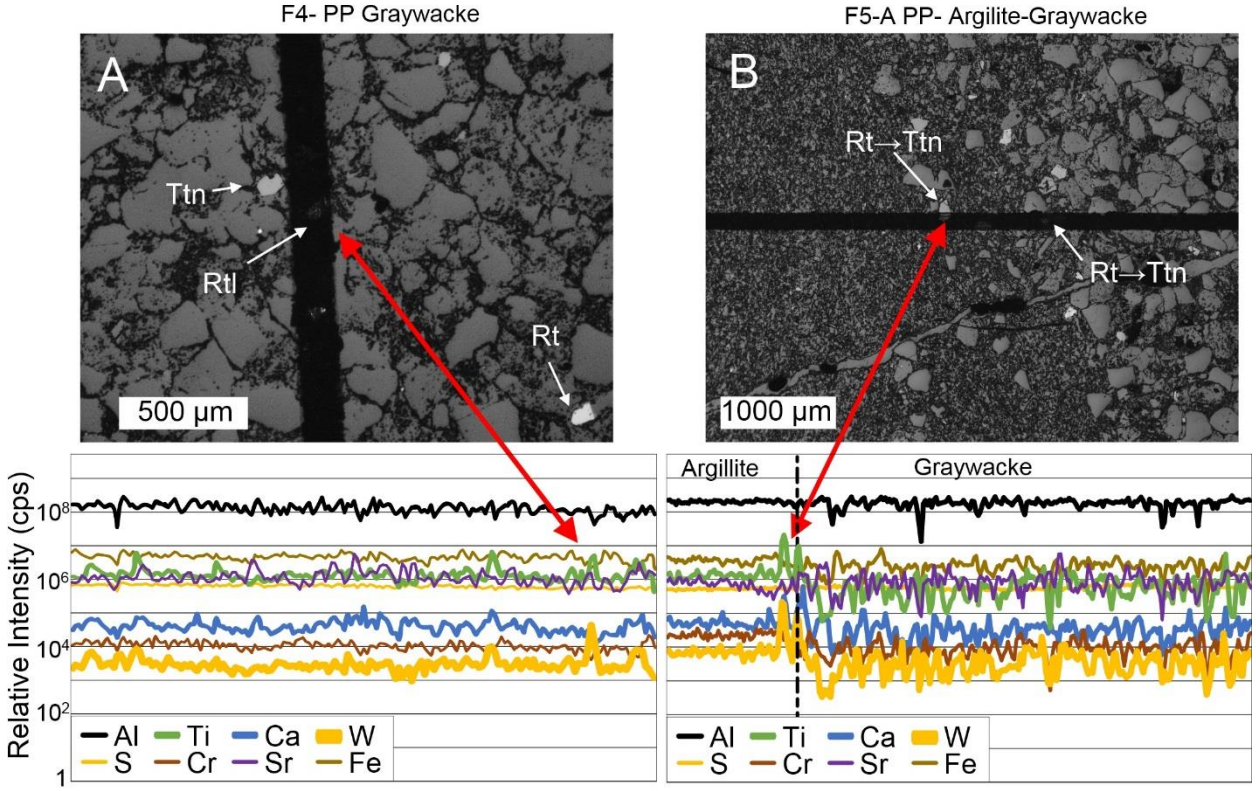

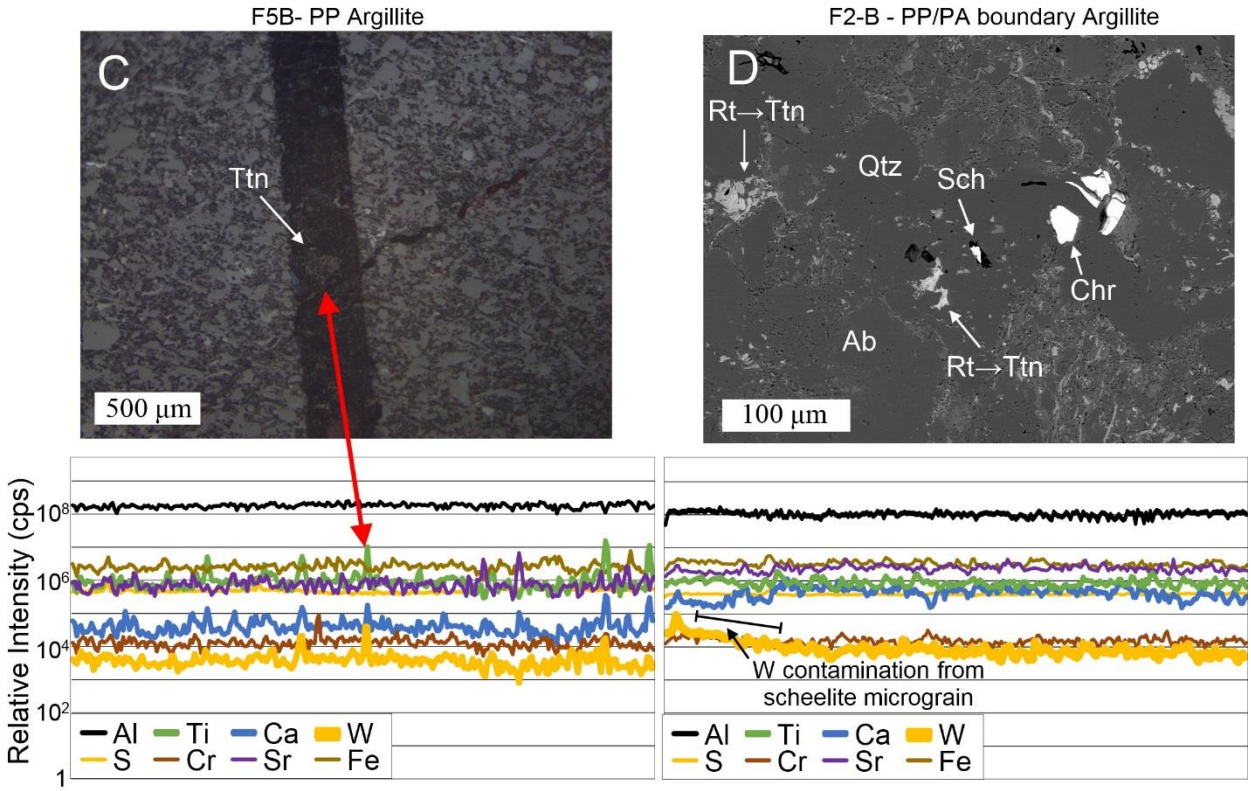

Fig. 16. Upper prehnite-pumpellyite facies, to prehnite-pumpellyite / pumpellyite-actinolite facies boundary, graywacke and argillite samples. Upper images (reflected light or scanning electron) shows a selected area through which the laser traverse passed, with a selected portion of the LA-ICP-MS traverse and selected elements displayed in the lower images. Abbreviations are as follows: Qtz- Quartz, Ab- Albite, Rt- Rutile, Ttn- Titanite, Sch- Scheelite, Chr- Chromite.

Pumpellyite-actinolite Facies rocks: Laser ablation traverses completed on representative graywacke/psammite and argillite/phyllite samples from Lake Hāwea, show irregular distributions of W at detectable and locally relatively high levels (Figs. 17A, B, C). Compared to prehnite-pumpellyite facies, the majority of high W peaks are now observed intimately associated with both Ti and Ca (Figs. 17B, C, D), with high W peaks only associated with peaks in Ti now observed as being quite rare (for example, Fig. 17A). Reflected light microscopy and

SEM of the high W, Ca, and Ti peaks and the rarer W and Ti peaks observed these peaks as corresponding to the laser beam having passed through grains of titanite and rutile, respectively (Figs. 17A, B, C, D). In addition, rare prominent corresponding peaks of W, Ca, and Sr that lack peaks of Ti are also observed in the laser ablation traverses, with SEM observing these peaks as corresponding to the laser beam having passed through rare scheelite micrograins (for example, Fig. 17A).

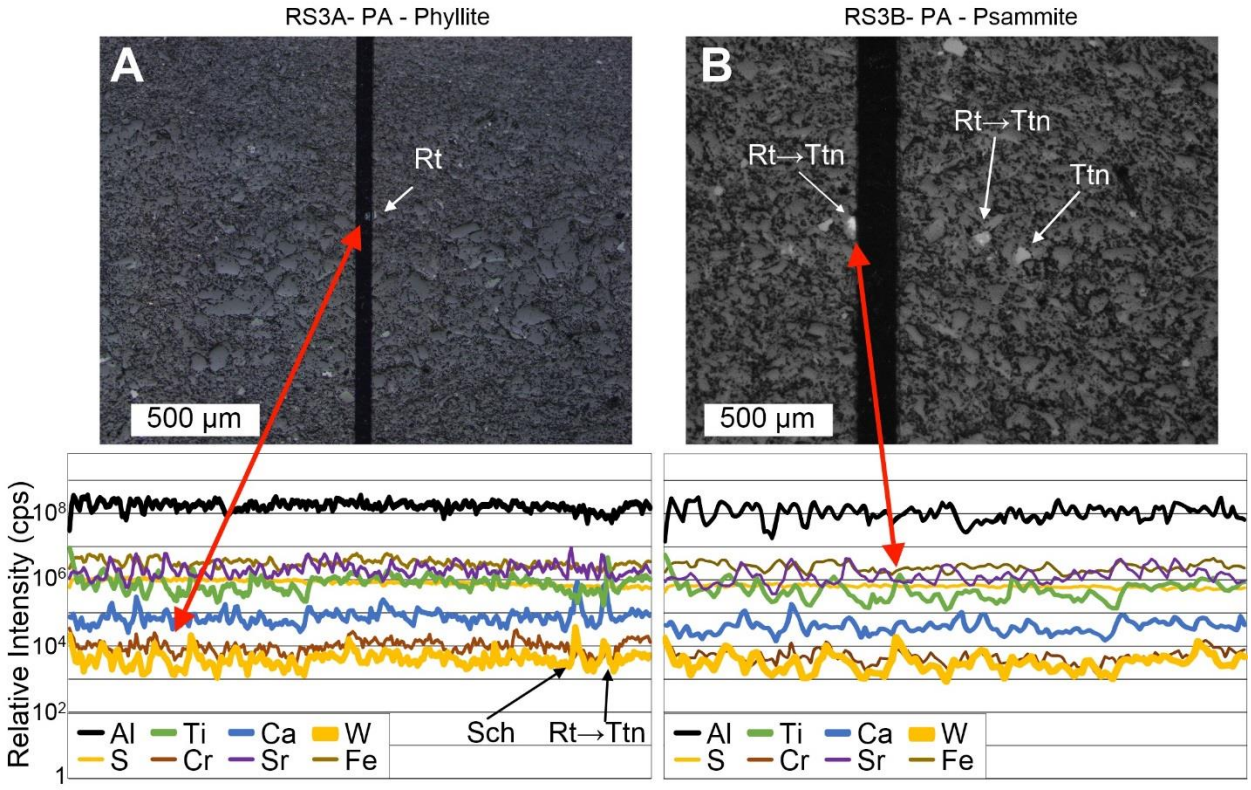

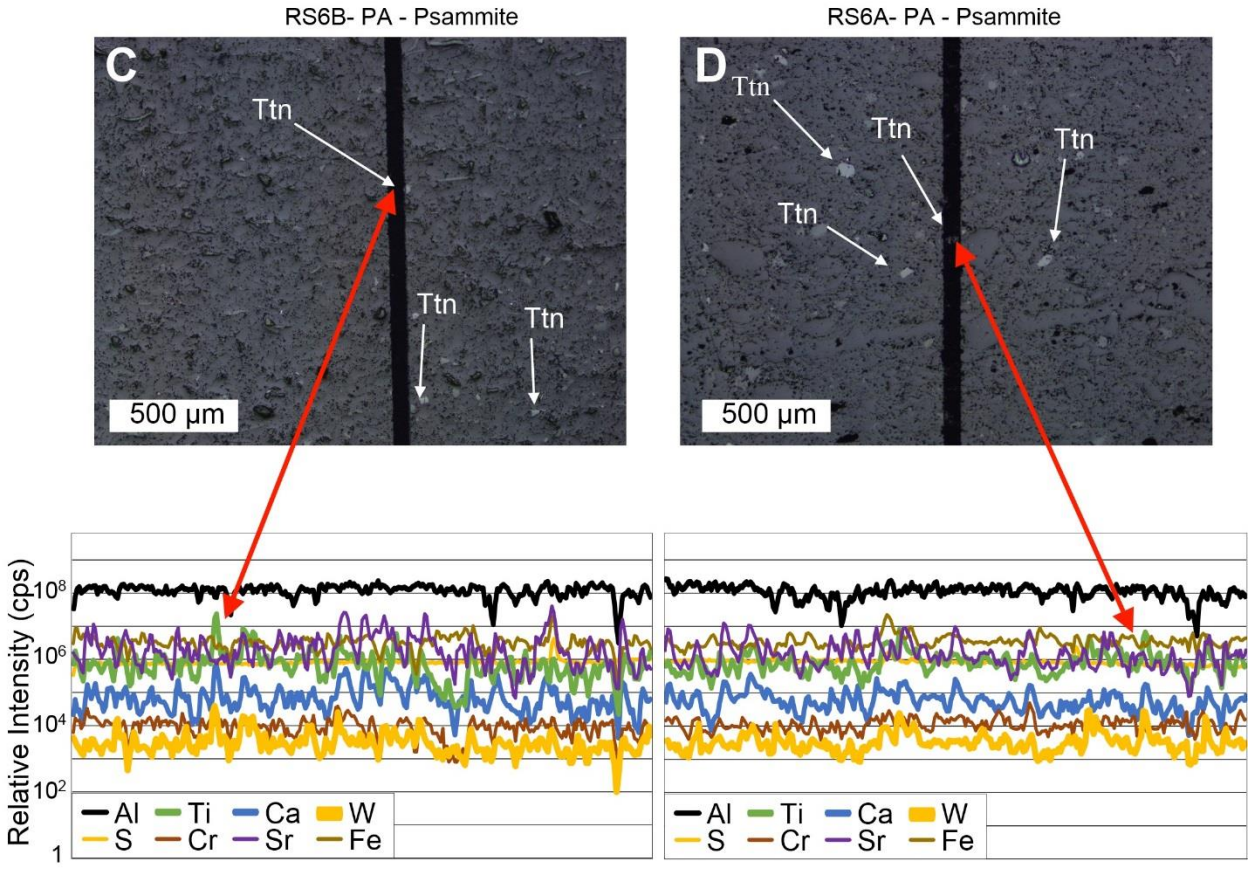

Fig. 17. Pumpellyite-actinolite facies, psammite and pelite samples. Upper images (reflected light) shows a selected area through which the laser traverse passed, with a selected portion of the LA-ICP-MS traverse and selected elements displayed in the lower images. Abbreviations are as follows: Rt- Rutile, Ttn- Titanite, Sch- Scheelite.

Lower Greenschist Facies rocks: Laser ablation traverses completed on representative chlorite-rich micaceous schist samples from Lake Hāwea show extremely heterogeneous distributions of W (Figs. 18A, B, C, D). Tungsten distribution in the chlorite-rich micaceous schists systematically mirrors the segregation laminas of the schist, with W generally below detection limit in quartz-albite segregations and enriched in the mica-rich segregations (Figs. 18A, B, C, D). Within the mica-rich segregations, small W-peaks observed above background-levels correspond to peaks in Ca and Ti (Figs. 18A, B, C, D), with SEM observing the peaks as

corresponding to the laser beam having passed through titanite grains and, sporadically where Ti peaks are enhanced relative to Ca, through rutile relicts within titanite grains (Figs. 18A, C, D).

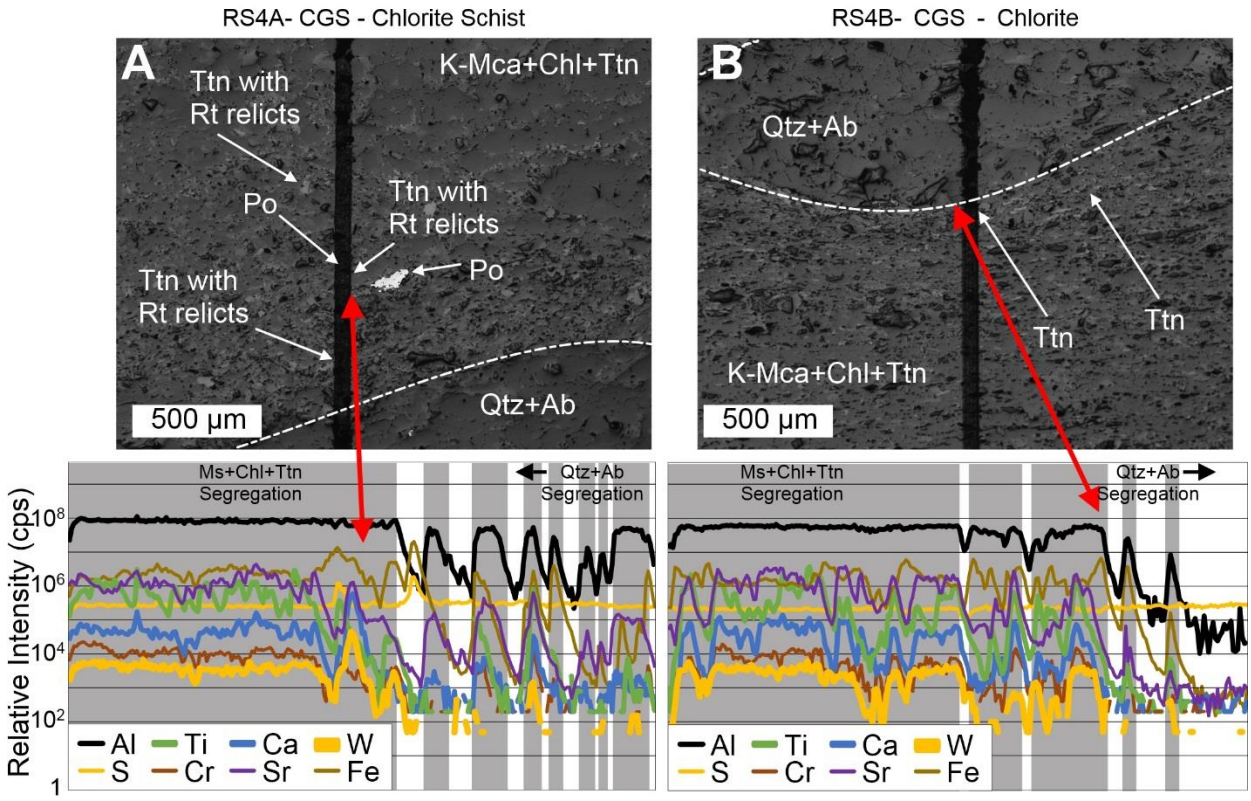

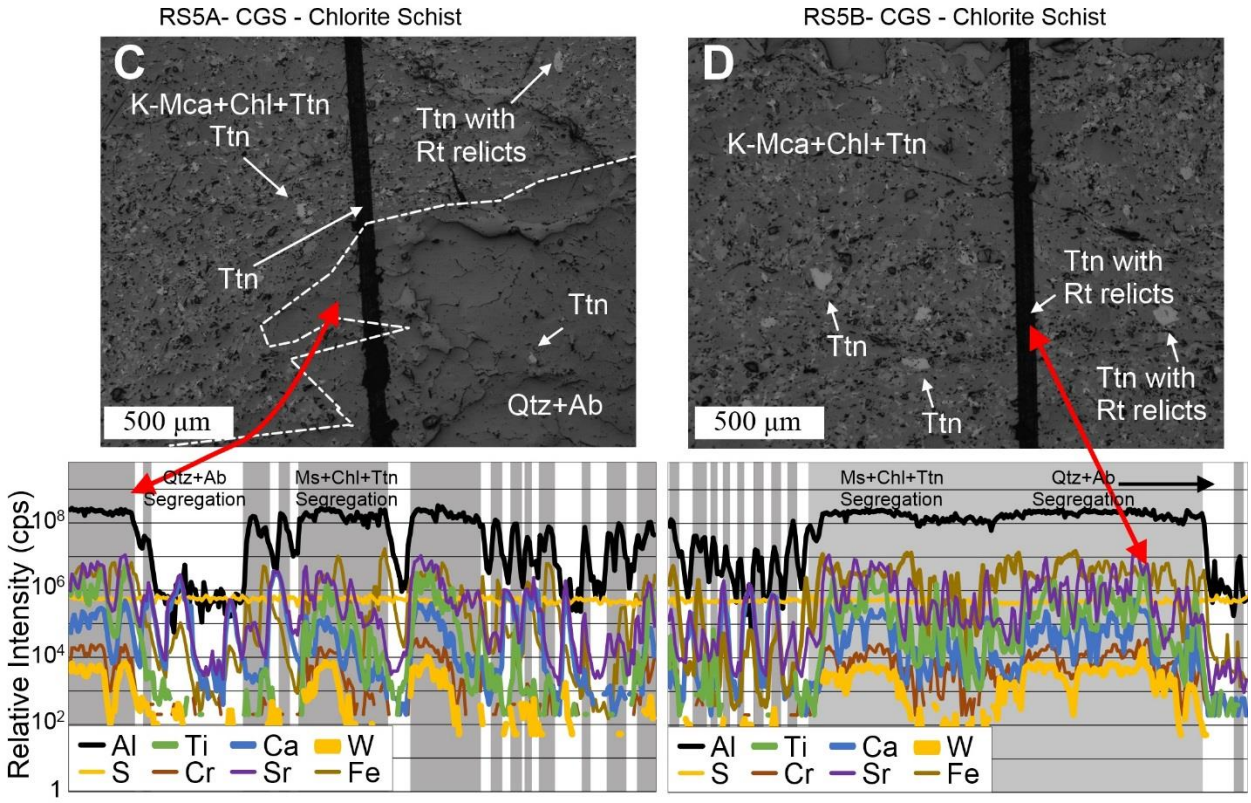

Fig. 18. Lower greenschist facies samples. Upper images (reflected light) shows a selected area through which the laser traverse passed, with a selected portion of the LA-ICP-MS traverse and selected elements displayed in the lower images. Abbreviations are as follows: Qtz- Quartz, Ab- Albite, Rt- Rutile, Ttn- Titanite, K-Mca- K-Mica, Chl- Chlorite, Po- Pyrrhotite.

Upper Greenschist Facies Rocks: Laser ablation traverses completed on representative biotite-bearing micaceous schist samples from Clyde Dam show extremely heterogeneous distributions of W (Figs. 19A, B). Similar to W distribution in the lower greenschist facies samples from Lake Hāwea, W systematically mirrors the segregation laminas of the schist, with W generally below detection limit in quartz-albite segregations and enriched in the mica-rich segregations (Figs. 19A, B). Within the mica-rich segregations, muted W-peaks observed above background-levels correspond to peaks in Ca and Ti (Figs. 19A, B), with SEM observing the

peaks as corresponding to the laser beam having passing through titanite grains. Unlike in the lower greenschist facies samples, W peaks associated with Ti peaks are always associated with dominate Ca peaks (Figs. 19A, B). No rutile relicts are observed within the titanite grains from the upper greenschist facies samples.

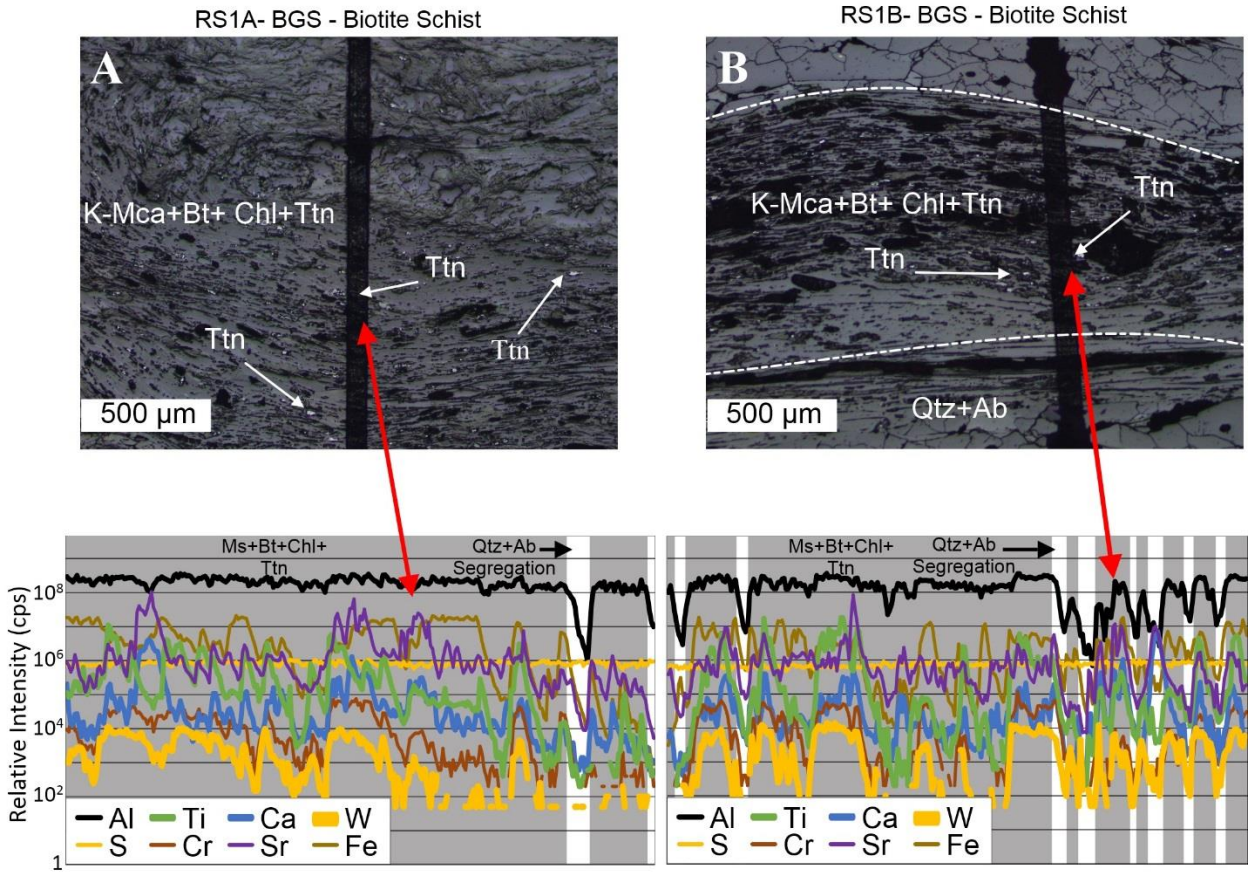

Fig. 19. Upper greenschist facies samples. Upper images (reflected light) shows a selected area through which the laser traverse passed, with a selected portion of the LA-ICP-MS traverse with selected elements displayed in the lower images. Abbreviations are as follows: Qtz- Quartz, Ab- Albite, Ttn- Titanite, K-Mca- K-Mica, Chl-Chlorite, Bt- Biotite.

6.5 Discussion and Conclusions

Laser ablation traverses conducted on samples from the lowest metamorphic grade rocks (prehnite-pumpellyite facies graywackes and argillites), indicates that detrital rutile is the major host of W, with titanite and rare scheelite micrograins being subordinate host phases (Figs. 16A, B, C, D). Calculation of Pearson product-moment correlation coefficients values from the prehnite-pumpellyite facies laser traverses (Table 3), supports the conclusion that rutile is the most important host for W in these rocks. Pearson's correlation values show W is only well correlated with Ti ($r = 0.60$), whilst being poorly correlated with other elements. In samples from increasing metamorphic grades (pumpellyite-actinolite facies to upper greenschist facies), Pearson's correlation values show W is correlated well with the major elements Ti and Ca (Table 3), and variably with the trace elements V, Cr, Sr, Sn, Sb, Ta, and U (Table 3). Correlation of these major elements supports petrological observations along laser traverse lines that identify detrital rutile increasingly becoming a subordinate host for W, with titanite becoming the major host for W by lower greenschist facies conditions (Figs. 18A, B, C, D). Plotting 95 percentile W laser traverse data against Ti/(Ti+Ca), illustrates rutile and titanite are the most important W-host minerals in these rocks (Figs. 20A, B), and confirms that with increasing metamorphic grades rutile becomes a subordinate host for W (Fig. 20B). Petrological observations along laser traverse lines, combined with the bivariate plot (Fig 19A, B, 20B) indicates that rutile relicts are not present within titanite grains at upper greenschist, with detrital rutile likely having been completely recrystallized to titanite at this metamorphic grade. In addition, rare scheelite micrograins were observed within the fabric of subgreenschist and greenschist facies samples (for example, Figs. 16D, 17A), and are illustrated in the bivariate plot (Fig. 20A). Increasing correlations between W and Sr, especially in the greenschist facies quartz-albite metamorphic

segregations (Table 3) most likely reflects the presences of these scheelite micrograins. Other than rutile, titanite, and scheelite, no other mineral phases hosting significant amounts of W have been identified in these rocks (for example, Fig. 20A).

Table 3. Pearson Product Moment Correlation Coefficients for selected elements against W, from different metamorphic grades. Where metamorphic segregations are developed segregations like compositions are grouped.

	W	W	W	W	W	W
Metamorphic facies	Prehnite-pumpellyite	Pumpellyite-actinolite	Lower greenschist	Lower greenschist	Upper greenschist	Upper greenschist
Metamorphic segregation	Not developed	Not developed	Ms+chl+ttn	Qtz-ab	Ms+bt+chl+ttn	Qtz-ab
Mg	0.10	0.07	0.08	0.12	0.02	0.28
Al	0.05	0.03	0.17	0.02	0.35	0.19
S	-0.14	-0.05	-0.04	0.03	-0.09	-0.05
Ca	0.05	0.47	0.56	0.41	0.65	0.39
Ti	0.60	0.64	0.43	0.14	0.62	0.43
V	0.26	0.40	0.48	0.19	0.85	0.53
Cr	0.17	0.34	0.50	0.20	0.76	0.24
Fe	0.05	0.04	0.16	0.02	-0.05	0.31
Co	0.00	0.03	0.12	0.01	-0.04	0.18
As	-0.01	0.05	0.00	0.20	0.14	-0.07
Sr	0.00	0.05	0.27	0.56	0.15	0.45
Sn	0.19	0.51	0.42	0.22	0.75	0.08
Sb	0.05	0.13	0.27	0.29	0.15	0.12
Ta	0.24	0.58	0.48	0.16	0.53	0.38
U	0.09	0.55	0.26	0.10	0.58	0.02

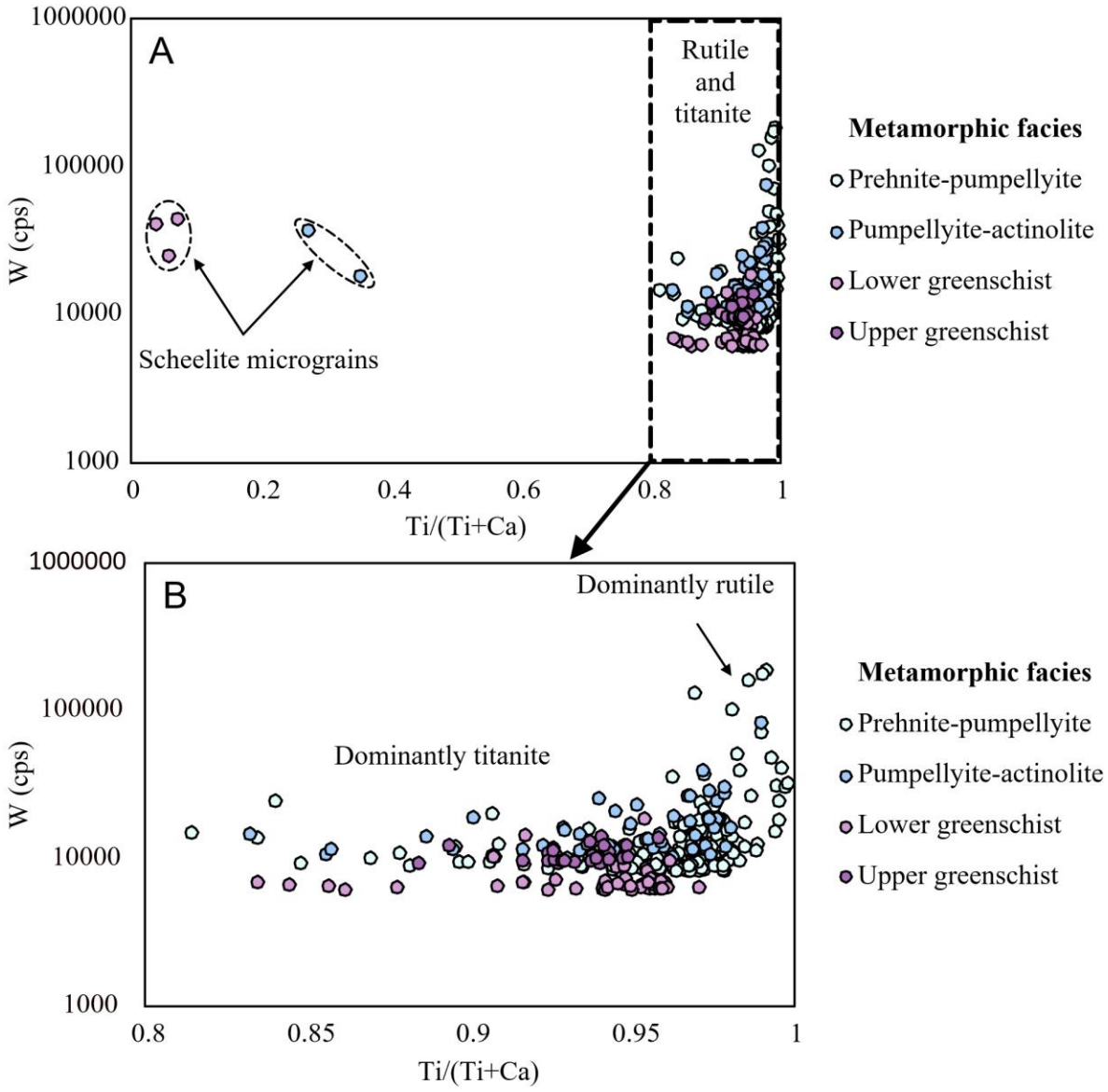

Fig 20. Bivariate plot of MS sweeps with W above the 95 percentile from laser traverse data: W plotted against Ti/(Ti+Ca). (A) Full Ti range shows Ti-Ca minerals, presumably rutile and titanite, are the major hosts of W in the Otago Schist. In addition, Ca-rich low-Ti W phases are identified in the pumpellyite-actinolite and lower greenschist facies samples, interpreted here as scheelite micrograins that were observed at these metamorphic grades. (B) Enlarged plot showing Ti minerals associated with minor amounts of Ca are the dominate hosts of W in the subgreenschsit facies rocks, and that with increasing metamorphic grade Ti-Ca minerals are the major hosts. This parallels laser traverse data combined with petrological observations that observed rutile as the major W host in the subgreenschist facies rocks, transitioning to titanite with increasing metamorphic grade.

This observation that the major host mineral of W in the lowest metamorphic grade samples (detrital rutile) recrystallizes with increasing metamorphic grade, parallels the process by which diagenetic pyrite recrystallizes to pyrrhotite in these rocks (Pitcairn et al. 2006, 2010; Large et al. 2012). This mineral reaction (pyrite to pyrrhotite), as previously discussed in Chapters 2 and 4, is identified as the mineralogical source for Au, As, Ag, Hg, and Sb in the orogenic Au deposits of the Otago Schist (Pitcairn et al. 2006, 2010; Large et al. 2012). The source of W inferred from these models (for example, Pitcairn et al. 2010, Large et al. 2012), as previously discussed in Chapters 4, is an enriched detrital or diagenetic mineral phase, where prograde metamorphism recrystallizes it to another mineral phase(s), releasing W. Identification of detrital rutile enriched in W recrystallizing to titanite with increasing metamorphic grade potentially satisfies this. In addition, mean relative W concentrations (cps) calculated from laser traverses, show W concentration (cps) in the subgreenschist facies rocks are nearly twice as high as in the greenschist facies rocks (Table 2, Fig. 15A). These results parallel previous whole rock W depletions observed occurring at the subgreenschist to greenschist facies transition in the Otago Schist (Breeding and Ague 2002), and support the conclusion that the transition of rutile to titanite enables the mobilization of W and that rutile is the mineralogical source for W in the orogenic deposits of the Otago Schist. Detailed investigations are undertaken in the next two chapters (Chapters 7 and 8) to investigate this idea that detrital rutile is the mineralogical source for W in the orogenic deposits of the Otago Schist.

References

BREEDING, C. M. & AGUE, J. J. 2002. Slab-derived fluids and quartz-vein formation in an accretionary prism, Otago Schist, New Zealand. *Geology*, 30**,** 499-502.

CRAW, D. & NORRIS, R. J. 1991. Metamorphogenic Au-W veins and regional tectonics: mineralisation throughout the uplift history of the Haast Schist, New Zealand. *New Zealand Journal of Geology and Geophysics,* 34**,** 373-383.

HENNE, A. & CRAW, D. 2012. Synmetamorphic carbon mobility and graphite enrichment in metaturbidites as a precursor to orogenic gold mineralisation, Otago Schist, New Zealand. *Mineralium Deposita,* 47**,** 781-797.

HENNE, A., CRAW, D. & MACKENZIE, D. 2011. Structure of the Blue Lake Fault Zone, Otago Schist, New Zealand. *New Zealand Journal of Geology and Geophysics,* 54**,** 311-328.

LARGE, R., THOMAS, H., CRAW, D., HENNE, A. & HENDERSON, S. 2012. Diagenetic pyrite as a source for metals in orogenic gold deposits, Otago Schist, New Zealand. *New Zealand Journal of Geology and Geophysics,* 55**,** 137-149.

PITCAIRN, I. K., TEAGLE, D. A. H., CRAW, D., OLIVO, G. R., KERRICH, R. & BREWER, T. S. 2006. Sources of metals and fluids in orogenic gold deposits: insights from the Otago and Alpine Schists, New Zealand. *Economic Geology,* 101**,** 1525-1546.

PITCAIRN, I. K., OLIVO, G. R., TEAGLE, D. A. H. & CRAW, D. 2010. Sulfide evolution during prograde metamorphism of the Otago and Alpine Schists, New Zealand. *The Canadian Mineralogist,* 48**,** 1267-1295.

STALLARD, A. & SHELLEY, D. 2005. The initiation and development of metamorphic foliation in the Otago Schist, Part 1: competitive oriented growth of white mica. *Journal of Metamorphic Geology,* 23**,** 425-442.

This chapter has been removed for copyright or proprietary reasons.

Published as:
Cave, B. J., Stepanov, A. S., Craw, D., Large, R. R., Halpin, J. A., Thompson, J., 2015. Release of trace elements through the sub-greenschist facies breakdown of detrital rutile to metamorphic titanite in the Otago Schist, New Zealand, Canadian mineralogist, 53(3), 379-400

Chapter 8: A METAMORPHIC MINERAL SOURCE FOR W IN THE TURBIDITE-HOSTED AU GOLD DEPOSITS OF THE OTAGO SCHIST, NEW ZEALAND

8.1 Abstract

The orogenic Au deposits of the Otago Schist, New Zealand, are enriched in a variety of trace elements including Au, As, Ag, Hg, W, and Sb. Previous research on metal sources for these deposits has defined the mineralogical sources for most of these metals, but the mineralogical sources of W are not well-constrained. In this chapter, combined laser ablation inductively coupled plasma mass spectrometry (LA-ICP-MS) traverses and images are utilized to show detrital rutile is the most important host mineral for W in the subgreenschist facies rocks, and that its prograde metamorphic recrystallization to titanite releases significant amounts of W (potentially 0.41 g per ton of rock). Scheelite development closely follows the progression of this W-liberating reaction, with early formation of scheelite micrograins within the fabric of the rock evolving to locally and regionally sourced scheelite-bearing veins. Scheelite from syn-metamorphic veins at Fiddlers Flat and Lake Hāwea shows distinct differences in composition to scheelite from late metamorphic veins at the Macraes Mine, with the Macraes scheelite being enriched in REEs, Y, and Sr. Suggesting that the scheelite at Macraes became enriched due to the liberation of these elements during alteration of the Ca-silicate minerals epidote and titanite by the ore forming fluid. These results are supportive of recent models for orogenic Au mineralization in the Otago Schist, whereby prograde metamorphic recrystallization of diagenetic or detrital metal-rich mineral phases (pyrite to pyrrhotite: Au, As, Ag, Hg, and Sb;

rutile to titanite: W) releases significant amounts of metals into the concurrently developing metamorphic fluids that can be subsequently focused into regional structures and form significant W-bearing orogenic Au deposits.

8.2 Introduction

Orogenic Au deposits are enriched in a characteristic suite of elements including As, Ag, Sb, Te, W, Mo, and Bi, and also contain notably low base-metal contents (Phillips and Groves 1983; Craw 1992; Groves 1993; Groves et al. 1998; Goldfarb et al. 2005; Goldfarb and Groves 2015). Various models have been proposed to account for the source(s) of these metal enrichments, with recent studies suggesting metals mobilized during metamorphism are the most important (Pitcairn et al. 2006, 2014, 2015a, 2015b; Large et al. 2011). However, these studies focus mainly on Au, As, and Sb while the sources of other metals enriched in these deposits are less well constrained.

The Otago Schist of southern New Zealand (Fig. 31) provides an ideal natural laboratory in which to investigate the hypothesis of a metamorphic source for W in orogenic Au deposits. Tungsten-bearing orogenic Au deposits are common in the Otago Schist with a number of deposits having been previously exploited for W, including the currently producing Macraes Au mine. A full range of metamorphic grades is exposed in the schist belt from prehnite-pumpellyite facies metamorphosed graywacke to upper greenschist facies rocks, and this combined with the minor lithological variation in the schists has allowed considerable investigation into the mobility of trace elements during metamorphism and mineralization. Systematic decreases in the same suite of elements enriched in the Otago orogenic deposits are observed in the metasedimentary (Au, As, Ag, Hg, Mo, Sb, and W; Pitcairn et al. 2006) and metabasaltic (Au,

Sb, and Hg; Pitcairn et al. 2015a) rocks of the Otago Schist, with increasing metamorphic grade. These observations have largely led to the prevailing consensus that the metasedimentary country-rocks hosting these deposits are the major metal source, possibly with a subordinate input of Au, Sb, and Hg from metabasalts. Previous investigations on the occurrence of W in the Otago Schist have speculated as to whether W is mobilized from enriched source rocks such as metavolcanics and cherts (Henley et al. 1976; Wood 1983), or from larger volumes of less enriched source rocks, such as the metasedimentary rocks (Paterson and Rankin 1979; Paterson 1982, 1985; Craw and Norris 1991). A systematic decrease in W concentration with metamorphic grade in the metasedimentary rocks (Breeding and Ague 2002; Pitcairn et al. 2006), coupled with the observation that W-bearing mineralization throughout the Otago Schist is not spatially associated with any particular rock type (Craw and Norris 1991) strongly suggests non-enriched metasedimentary rocks are the source rocks for W in the Otago Schist. Diagenetic pyrite is identified as the major mineralogical host for Au, As, Ag, Hg, Mo, and Sb in the lowest metamorphic grade metasedimentary rocks (Pitcairn et al. 2010; Large et al. 2012). Recrystallization of diagenetic pyrite to metamorphic pyrrhotite during regional greenschist facies metamorphism releases these elements into the concurrently developing metamorphic fluids effectively mobilizing them from the sedimentary pile, with focusing of these metal-rich fluids into metamorphic structures resulting in orogenic ore formation (Pitcairn et al. 2006, 2010; Large et al. 2012). Large et al. (2012) reports low concentrations of W in diagenetic pyrite, and therefore W cannot have been produced during the diagenetic pyrite to pyrrhotite transition. Recent research has identified detrital rutile grains in the lowest metamorphic grade precursor rocks (Torlesse Terrane) of the Otago Schist as having high W concentrations (mean 830 ppm) [Cave et al. 2015 (Chapter 7)]. Furthermore, the rutile is observed to recrystallize to relatively

W-depleted metamorphic titanite (mean 76.7 ppm) during regional subgreenschist to lower greenschist facies metamorphism [Cave et al. 2015 (Chapter 7)]. This recrystallization reaction takes place concurrent with the recrystallization of quartz, calcite, and the breakdown of organic matter, with these components providing the additional cations and anions required to convert rutile to titanite, with graphite and water also being produced:

Equation 3 $$TiO_2 + SiO_2 + CaCO_3 + CH_4 \leftrightarrow CaSiTiO_5 + 2C_{graphite} + 2H_2O$$

This mineral transition potentially provides a viable source for W in the orogenic deposits of the Otago Schist. In this chapter, the distribution of W amongst mineral phases in prehnite-pumpellyite and lower greenschist facies metasedimentary rocks of the Torlesse Terrane is evaluated using laser ablation inductively coupled plasma mass spectrometry (LA-ICP-MS) traverses. Results show that detrital rutile, metamorphic titanite, and scheelite are the major W-bearing phases in the Otago Schist and that the transition from detrital rutile to metamorphic titanite (Equation 3) liberates W during regional metamorphism of the Otago Schist. Scheelite development in the Otago Schist is also investigated, with specific focus on the timing of its formation relative to the recrystallization of detrital rutile to metamorphic titanite. Scheelite geochemistry from a variety of vein types and different metamorphic grade rocks is also presented, along with selected REE analyzes of Ca-silicate minerals. Through these approaches a unified model is presented that W (scheelite) in the turbidite-hosted orogenic Au deposits of the Otago Schist, New Zealand, is sourced from the subgreenschist to greenschist facies recrystallization of detrital rutile to metamorphic titanite.

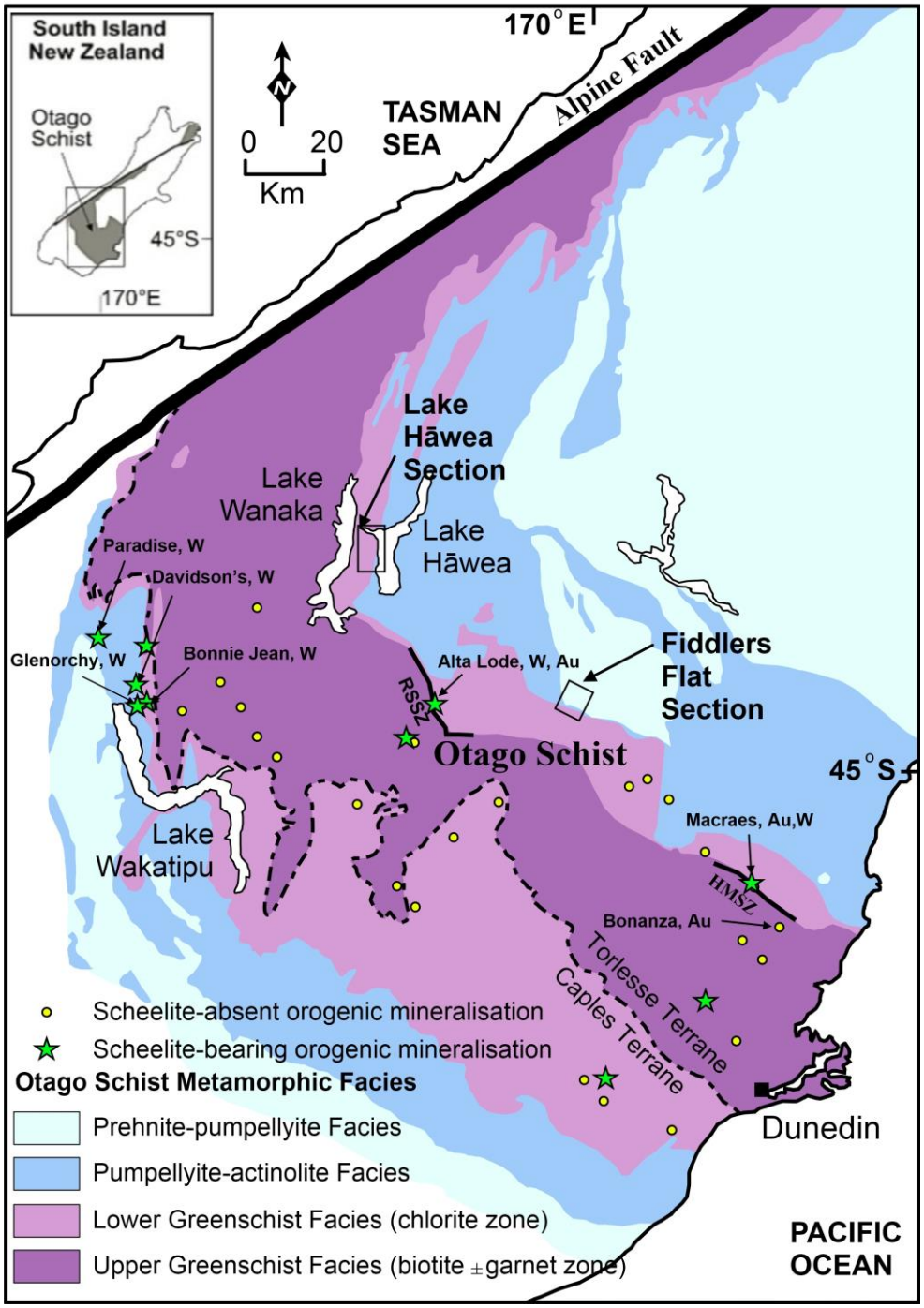

Fig. 31. Geological map of the Otago Schist and Alpine Schist, South Island, New Zealand, showing the Caples and Torlesse terranes, metamorphic facies, sample sections, selected W-bearing and Au-bearing orogenic ore deposits, selected mineralized shear zones, the Alpine Fault – Austro-Pacific plate contact. Modified from Cave et al. [2015 (Chapter 7)]. Abbreviations: HMSZ- Hyde-Macraes Shear Zone, RSSZ- Rise and Shine Shear Zone.

8.3 Geological Setting

8.3.1 Geology of the Otago Schist

Formed during the Mesozoic collision and metamorphism of the Torlesse and Caples terranes, the Otago Schist belt of southern New Zealand (Fig. 31) is predominately comprised of metaturbiditic graywackes and argillites, with subordinate metabasic horizons and ultramafic slices (Turnbull 1979; MacKinnon 1983; Craw 1984; Mortensen et al. 2010). The metamorphic grade of the Otago Schist belt ranges from prehnite-pumpellyite facies to upper greenschist facies (biotite–garnet–albite) in the center of the belt (Fig. 31) (MacKinnon 1983; Craw 1984; Mortimer 2000; Mortensen et al. 2010; Pitcairn et al. 2014, 2015a), equivalent to peak metamorphic conditions of approximately 450°C and 8–10 kbar (Bishop 1972; Yardley 1982; Craw 1998; Pitcairn et al. 2014, 2015a). The increase in metamorphic grade, from prehnite-pumpellyite facies to upper greenschist facies (biotite-garnet-albite), is accompanied in all lithologies by progressive metamorphic recrystallization and foliation development (Bishop 1972; Turnbull et al. 2001; Henne et al. 2011). Prehnite-pumpellyite facies Torlesse Terrane metasediments are typically comprised of quartz, albite, K-mica, chlorite, prehnite, pumpellyite, detrital titanite, and detrital carbonaceous material, and importantly contain trace amounts of detrital rutile and diagenetic pyrite [Cave et al. 2015 (Chapter 7)]. Whereas, upper greenschist facies Torlesse Terrane metasedimentary schists are typically comprised of quartz, albite, K-mica, chlorite, epidote, biotite, titanite, graphite, and garnet (Bishop 1972; Mortimer 2000; Mortensen et al. 2010; Pitcairn et al. 2010), with detrital rutile and diagenetic pyrite having been converted to metamorphic titanite and pyrrhotite, respectively [Pitcairn et al. 2010; Large et al. 2012; Cave et al. 2015 (Chapter 7)]. Argon-Argon dating of the metamorphism of the Otago

Schist suggests metamorphism occurred between 200 to 120 Ma (Little et al. 1999; Gray and Foster 2004; Pitcairn et al. 2010), with the timing of peak metamorphism suggested to have occurred considerably later (at approximately 160-140 Ma) in the higher metamorphic grade rocks than in the lower metamorphic grade rocks (at approximately 180 Ma) (Little et al. 1999; Gray and Foster 2004; Pitcairn et al. 2010). The transition between the higher metamorphic grade core and lower grade flanks has been accentuated by post-metamorphic extensional faulting, some of which was dominated by middle Cretaceous low-angle normal faults that facilitated exhumation of the Otago Schist belt (Deckert et al. 2002; Gray and Foster 2004; MacKenzie and Craw 2005; Mortensen et al. 2010). Extensional deformation continued through the Late Cretaceous and into the Tertiary as a result of the crustal thinning associated with the breakup of Gondwana in the southwest Pacific (Laird and Bradshaw 2004; Landis et al. 2008; Mortensen et al. 2010).

8.3.2 Orogenic Au Mineralization

Orogenic Au mineralization is widespread throughout the greenschist facies (and to a lesser extent, the subgreenschist facies) rocks of the Otago Schist, with over 200 exposed mineralized quartz-carbonate veins being recognized (Fig. 31; Rattenbury and Isaac 2012). Mineralization displays a strong structural control, being hosted in brittle-ductile shear zones and extensional veins formed at relatively shallow crustal levels (Craw et al. 2006; Pitcairn et al. 2014). Two discrete and relatively short-lived mineralizing events are recognized as being responsible for the majority of orogenic Au mineralization in the Otago Schist (one occurring between 142 and 135 Ma, and the other occurring between 106 and 101 Ma), with both events generating brittle-ductile shear zones and extensional veins (Mortensen et al. 2010). Comprising a series of open

pits and underground developments, along a regional-scale Early Cretaceous (142-135 Ma) shear zone (The Hyde-Macraes Shear Zone; Fig. 31), the Macraes Mine is the most significant deposit in the Otago Schist having produced in excess of 70 t Au (Pitcairn et al. 2015a) and containing reserves in excess of 160 t Au at approximately 1.1 g/t (OceanaGold 2015). In addition to Au at the Macraes Mine, a variety of other trace elements (including As, Sb, Hg, Se, Mo, W, Cr, and Bi) are enriched in the ore, a feature that is common in orogenic mineralization in the Otago Schist (McKeag et al. 1989; Craw 1992, 2002; Craw et al. 1999; Pitcairn et al. 2006, 2010, 2014, 2015a). Scheelite, which hosts the W enrichments in these deposits, is recorded as an accessory mineral (and occasionally ore mineral) in over 170 localities throughout the Otago Schist (Rattenbury and Isaac 2012). Previous W production from the Otago Schist is estimated to be in excess of 3,000 tons with the bulk of this derived from the mines surrounding Glenorchy, and the Macraes Mine (Fig. 31) (Williamson 1939; Mutch 1969).

8.4 Material and Analytical Methods

8.4.1 Sample Selection

Night time surveys using a shortwave UV light were carried out along the two well exposed metamorphic sections, Fiddlers Flat and Lake Hāwea (Fig. 31) in order to identify the occurrence of scheelite. Scheelite was observed and sampled from both of these sections, and also from auriferous veins in the Macraes Mine (Macraes underground). Detailed descriptions of the local geology of both major sections (Fiddlers Flat and Lake Hāwea) are provided within Chapter 5, with the reader directed to this chapter for further background information on the sections. The occurrence of scheelite at Macraes Mine has previously been discussed by Begbie and Craw (2006) with details on the general mineralization in the Macraes Mine deposits

reported in McKeag et al. (1989), Craw et al. (1999, 2004), de Ronde et al. (2000), Craw (2002), and Petrie et al. (2005).

The samples collected from Fiddlers Flat and Lake Hāwea have protolith compositions ranging from argillite to graywacke, and metamorphic grades ranging from prehnite-pumpellyite to upper greenschist facies. Mineralogical and textural associations in the samples were examined using a combination of reflected light and scanning electron microscopy (SEM). Trace element compositions of Ca-silicate minerals and scheelite from Fiddlers Flat, Lake Hāwea, and Macraes Mine were determined by LA-ICP-MS. Analytical traverses using LA-ICP-MS were undertaken on representative prehnite-pumpellyite facies and lower greenschist facies samples to understand element distributions, with LA-ICP-MS images subsequently being made over areas showing detrital rutile partially recrystallized to metamorphic titanite.

8.4.2 Analytical Methods

Analytical instrumentation used in this chapter includes a Resonetics Resolution laser ablation system equipped with a Coherent COMPex Pro 110 ArF excimer laser, housed at CODES/Earth Sciences, University of Tasmania. The ArF excimer laser operates at a 193 nm wavelength with a 20 ns pulse width and was coupled to an Agilent 7900 quadrupole inductively coupled plasma mass spectrometer (ICP-MS). Quantitative LA-ICP-MS trace element analyzes were performed on scheelite and Ca-silicate minerals (titanite, epidote, albite, and apatite) with ablation beam sizes of 19 and 15 μm, respectively. Laser repetition rate for scheelite analyzes was typically 10 Hz and laser beam energy at the sample interface was maintained at 1.92 J/cm^2, repetition rates for Ca-silicate analyzes was typically 5 Hz with laser beam energy at the sample interface maintained at 3.5 J/cm^2. Each analysis was pre-ablated with five laser pulses to remove the surface contamination. Once the pre-ablation had washed out (20 s) then a blank gas was

analyzed for 30 s followed by 60 s of sample ablation for scheelite, and 50 s of sample ablation for Ca-silicates. All data reduction calculations and error propagations were undertaken within Microsoft Excel® via macros designed at the University of Tasmania. Data reduction was undertaken using stoichiometric values of Ca as the internal standard for scheelite, titanite, epidote, and apatite, and stoichiometric values of Al for albite. Glass standard NIST612 was used as the primary calibration standard (using GeoReM preferred values: http://georem.mpch-mainz.gwdg.de/), with synthetic basalt glass standard GSD-1g as the secondary standard (using GeoReM preferred values: http://georem.mpch-mainz.gwdg.de/).

The primary calibration standard was analyzed with an 80 μm beam and a laser repetition rate of either 5 or 10 Hz depending on whether the laser session was analyzing Ca-silicates or scheelite, respectively. These analyzes were conducted at the beginning-and-end of the session and at hourly intervals throughout to account for instrument drift. The secondary calibration standard was analyzed with ablation spot size and laser repetition rates matching the unknowns throughout the analytical session. Samples were initially quantified on the primary standard NIST612 at a larger spot size, then a secondary standard correction was applied based on analyzes of the secondary standard GSD-1g at the same conditions as the unknowns to correct for differences in spot size. Precision on replicate analyzes of basalt glass standard BCR-2g at spot sizes the same as the unknowns, showed that following the application of the spot size correction factor (based on GSD-1g), all elements were within 10% of reported concentrations for BCR-2g. Typical detection limits for unknown Ca-silicate samples using three standard deviations of the background signal (99% confidence) for 15 μm spots were 900 ppm for Ca, 70 ppm for Na, 35 ppm for K, 5 ppm for Al, 0.5 ppm for Gd, Sm, and Nd, 0.2 ppm for Yb, Er, Dy, and Eu, and 0.05 ppm for Lu, Tm, Ho, Tb, Pr, Ce, La, Y, and Sr. Whilst typical detection limits

for unknown scheelite samples using three standard deviations of the background signal (99% confidence) for 19 μm spots were 0.8 ppm for Na, 0.05 ppm for Mn and Mo, and 0.02 ppm for Sr, Y, La, Ce, Pr, Nd, Sm, Eu, Gd, Tb, Dy, Ho, Er, Tm, Yb, Lu, U, and Pb.

Laser ablation traverses were performed using a 100 μm beam moving at 60 μm/s relative to the sample. Traverses were conducted perpendicular to the major bedding/foliation and utilized a laser repetition rate of 10 Hz with laser beam energy at the sample interface maintained at approximately 8.5 J/cm^2. Trace element maps were produced for rutile and titanite grains by ablating sets of parallel laser lines in a grid across areas of interest. Laser lines were ablated using a beam size of 5 μm and a repetition rate of 10 Hz, with laser beam energy at the sample interface maintained at approximately 3.5 J/cm^2. Spacing between the lines was kept constant at the same size as the laser beam, with the line speed kept at 5 μm/s and a sweep time of 0.239 s.

8.5 Results

8.5.1 Identification of W Host Minerals using LA-ICP-MS

Subgreenschist facies rocks: Laser ablation traverses completed on representative graywacke and argillite samples from Fiddlers Flat and Lake Hāwea show irregular distributions of W at detectable and locally relatively high levels, at the <100 μm scale (Figs. 32A, B, C). The majority of high W peaks are coincidental with high Ti ± Ca peaks (Figs. 32A, B), indicating the laser beam as having passed through grains of rutile ± titanite. Laser ablation trace element mapping of subgreenschist facies samples confirms rutile and titanite as hosting relatively high levels of W compared to the other rock-forming minerals (Figs. 33, 34). Titanite associated with the recrystallization of detrital rutile is observed having significantly lower levels of W than the rutile (Figs. 33, 34). Additionally, rare prominent coincidental peaks of W, Ca, and Sr are also

observed in the laser ablation traverses, corresponding to the laser passing through scheelite micrograins (Fig. 32C). The concentrations of W in detrital rutile vary from 17.5 to 11,150 ppm with mean values of 830 ppm [Cave et al. 2015 (Chapter 7)].

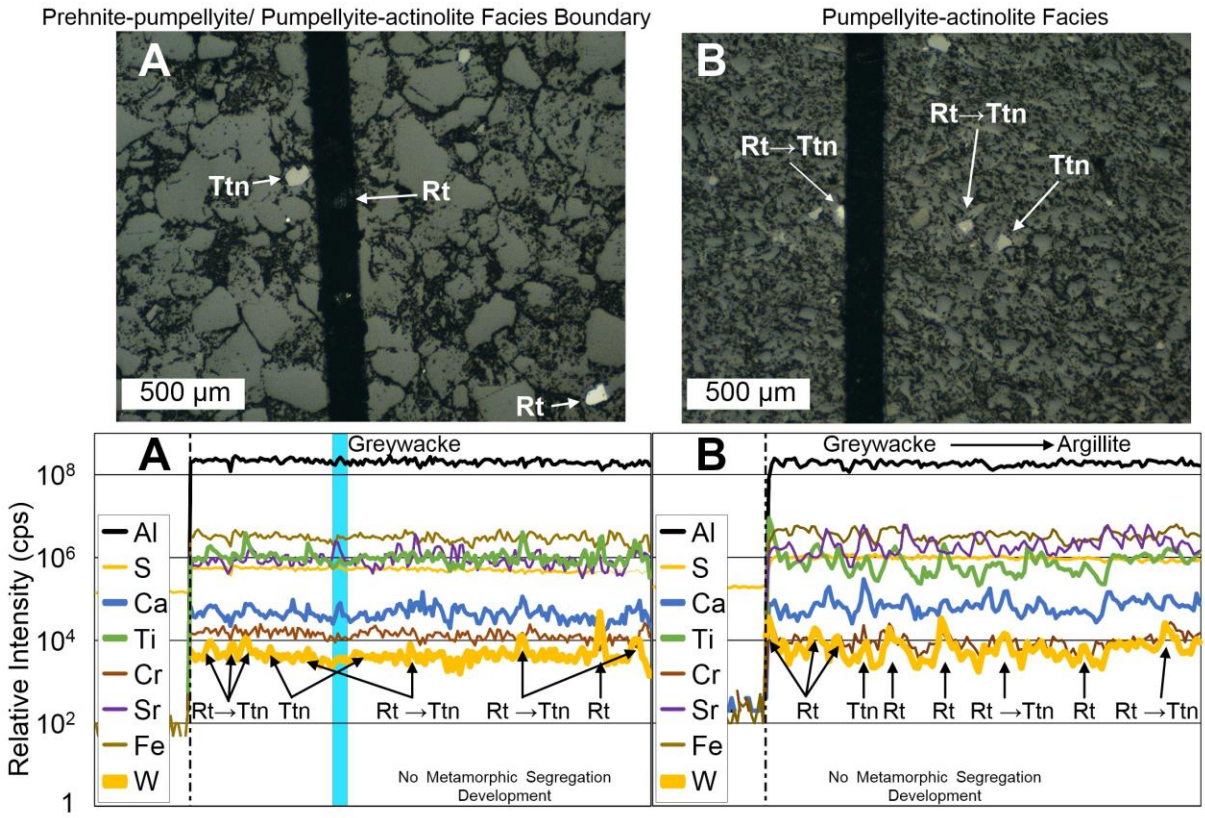

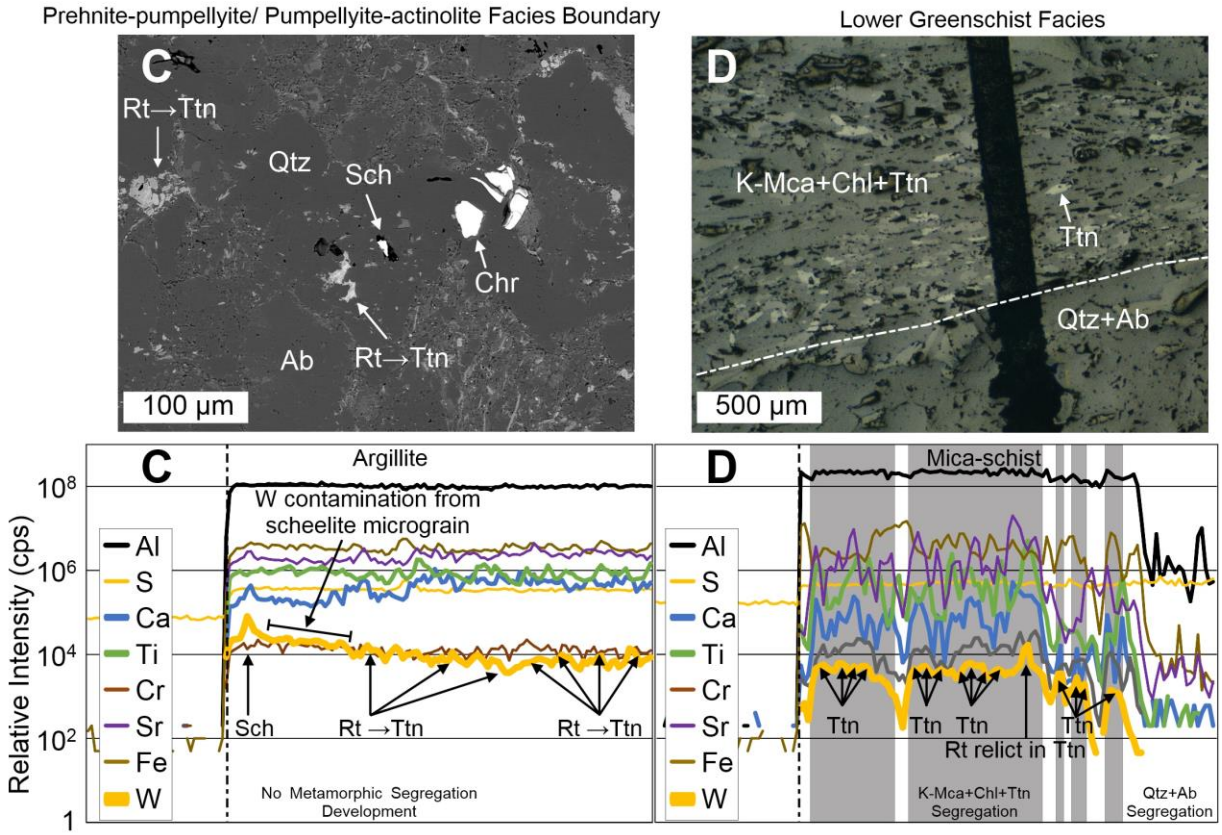

Fig. 32. (A) Graywacke sample (F5-B) from the prehnite-pumpellyite / pumpellyite-actinolite facies boundary along the Fiddlers Flat section. Upper image (reflected light) shows a selected area through which the laser traverse passed, with the entire LA-ICP-MS traverse with selected elements displayed in the lower image. (B) Interbedded graywacke-argillite, lower pumpellyite-actinolite facies sample (RS-3) from the Lake Hāwea section. Upper image (reflected light) shows a selected area through which the laser traverse passed, with the entire LA-ICP-MS traverse with selected elements displayed in the lower image. (C) Argillite sample (F2-B) from the prehnite-pumpellyite / pumpellyite-actinolite facies boundary along the Fiddlers Flat section. Upper image (scanning electron) shows a scheelite micrograin within the fabric of the argillite away from the laser traverse (not shown in picture), with the entire LA-ICP-MS traverse completed on this sample with selected elements displayed in the lower image and observed intersecting a scheelite micrograin. (D) Mica schist, lower greenschist facies sample (RS-5) from the Lake Hāwea section. Upper image (reflected light) shows a selected area through which the laser traverse passed, with the entire LA-ICP-MS traverse with selected elements displayed in the lower image. Mineral abbreviations Rt- rutile, Ttn- titanite, Sch- scheelite, Cb- carbonate, K-Mca- K-mica, Chl- chlorite, Qtz- quartz, Ab- albite, Chr- chromite.

Lower greenschist facies rocks: Laser ablation traverses completed on representative micaceous schist samples from Lake Hāwea show extremely heterogeneous distributions of W (Fig. 32D). Tungsten distribution in the micaceous schists systematically mirrors the segregation laminae of the schist, with W below detection limit in quartz-albite segregations and enriched in the mica-rich segregations (Fig. 32D). Within the mica-rich segregations, muted W-peaks observed above background-levels correspond to peaks in Ca and Ti (Fig. 32D) corresponding to the laser passing through titanite, and sporadically where Ca peaks are minor, through rutile relicts within titanite. The concentrations of W in metamorphic titanite vary from 4.7 to 233 ppm with mean values of 76.7 ppm, whereas W concentrations in detrital titanite vary from 0.9 to 97 ppm with mean values of 15.9 ppm [Cave et al. 2015 (Chapter 7)].

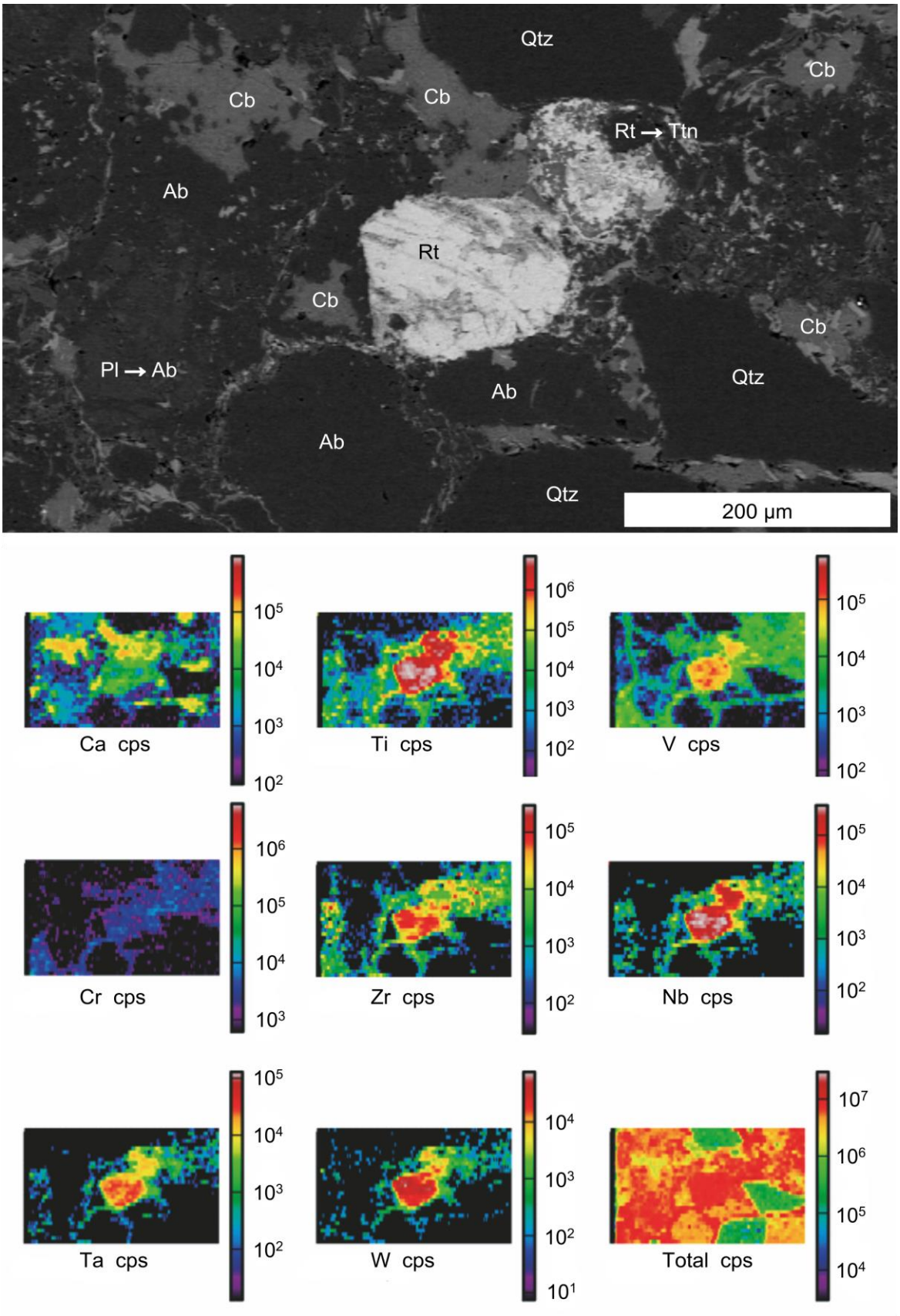
Qtz
Cb
Cb
Cb
Rt → Ttn
Ab
Rt
Cb
Cb
Pl → Ab
Ab
Qtz
Ab
Qtz
200 µm
Ca cps
Ti cps
V cps
Cr cps
Zr cps
Nb cps
Ta cps
W cps
Total cps

Fig 33. Scanning electron image (above) of pumpellyite-actinolite facies graywacke sample (F1-B) from the Fiddlers Flat section, with selected LA-ICP-MS counts per second elemental maps (below). This sample displays varying recrystallization of rutile to titanite, with metamorphic titanite observed with much lower counts relative to rutile, for a range of elements including W, V, Cr, Zr, Nb, and Ta, consistent with mass-balance calculations performed by Cave et al. [2015 (Chapter 7)] for this mineral reaction in the Otago Schist. Tungsten, Nb, Ta, Cr, and Zr, are all relatively enriched in the grain boundaries surrounding rutile breakdown to titanite, possibly suggesting local mobilization of these element into local grain boundary fluids. Mineral abbreviations Rt- rutile, Ttn-titanite, Cb- carbonate mineral, Zrn- zircon, Ab- albite, Qtz- quartz, Pl- plagioclase.

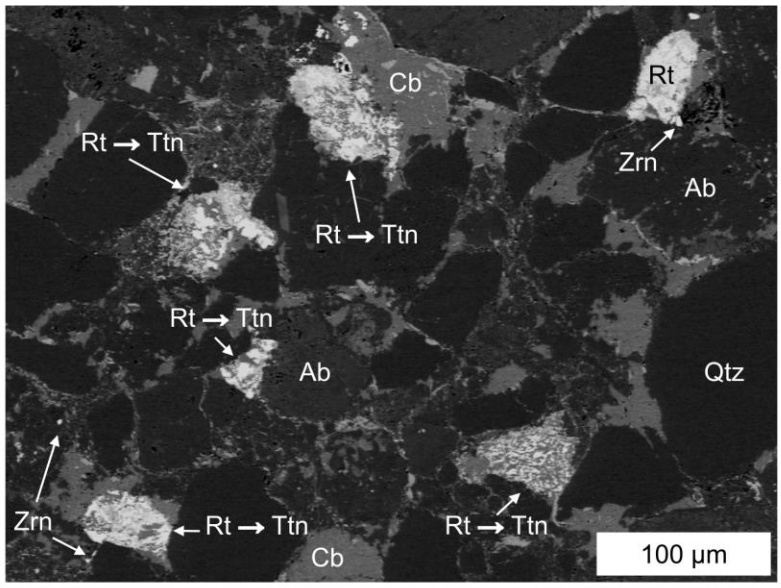
Cb
Rt
Rt → Ttn
Zrn
Ab
Rt → Ttn
Rt → Ttn
Ab
Qtz
Zrn
Rt → Ttn
Cb
Rt → Ttn
100 µm

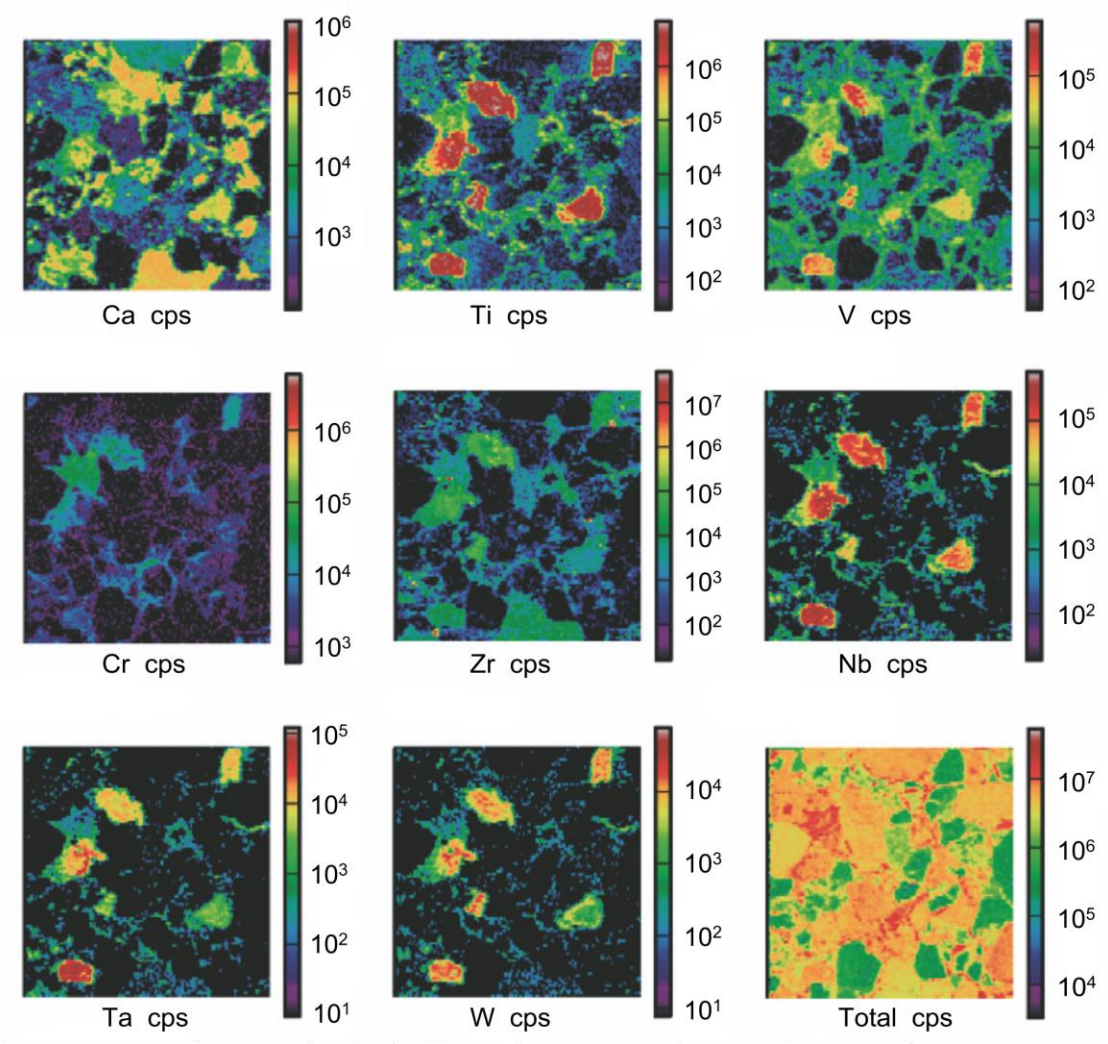
Ca cps
Ti cps
V cps
Cr cps
Zr cps
Nb cps
Ta cps
W cps
Total cps

Fig. 34- Scanning electron image (above) of pumpellyite-actinolite facies graywacke sample (F1-B) from the Fiddlers Flat section, with selected LA-ICP-MS counts per second elemental maps (below). This sample displays almost the entire spectrum of recrystallization of detrital rutile grains to metamorphic titanite observed in the pumpellyite-actinolite facies rocks. Metamorphic titanite forming from the recrystalization is observed in this image with much lower relative counts than rutile, for a range of elements including W, V, Cr, Zr, Nb, and Ta; all of which are observed being relatively enriched in the grain boundaries surround rutile breakdown to titanite, possibly suggesting local mobilization of these element into local grain boundary fluids. Mineral abbreviations Rt- rutile, Ttn-titanite, Cb- carbonate mineral, Zrn- zircon, Ab- albite, Qtz- quartz.

8.5.2 Scheelite Occurrence in the Otago Schist

Prehnite-pumpellyite facies samples used in this study come from the Fiddlers Flat section, near the boundary between prehnite-pumpellyite and pumpellyite-actinolite facies. Scanning electron microscopy (SEM) of graywacke and argillite samples revealed rare disseminated scheelite micrograins (for example, Fig. 35A) throughout both lithologies. Scheelite in the prehnite-pumpellyite facies samples was observed as subhedral grains ranging in size from < 1 to 3 µm (Figs. 35A, 36) and associated with the rock-forming and accessory minerals, albite, titanite, epidote, and pargasite.

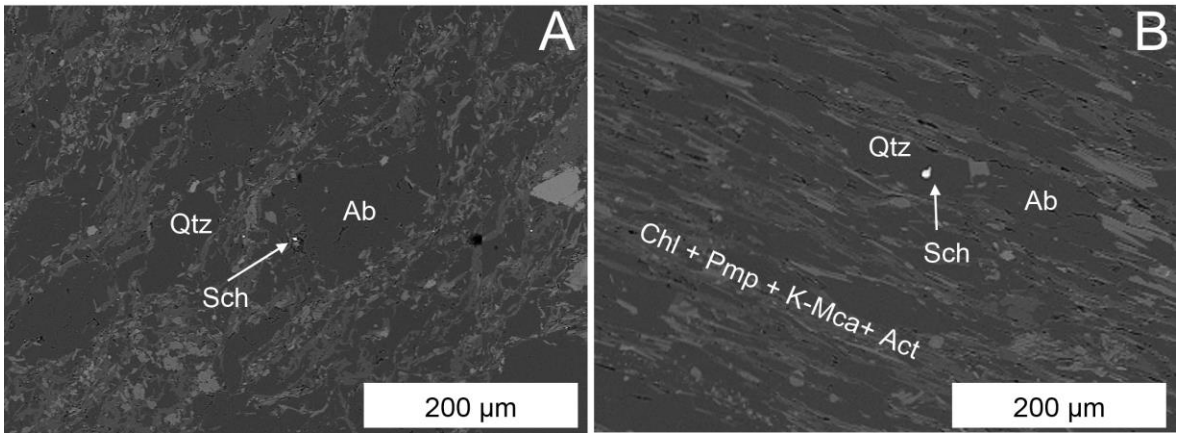

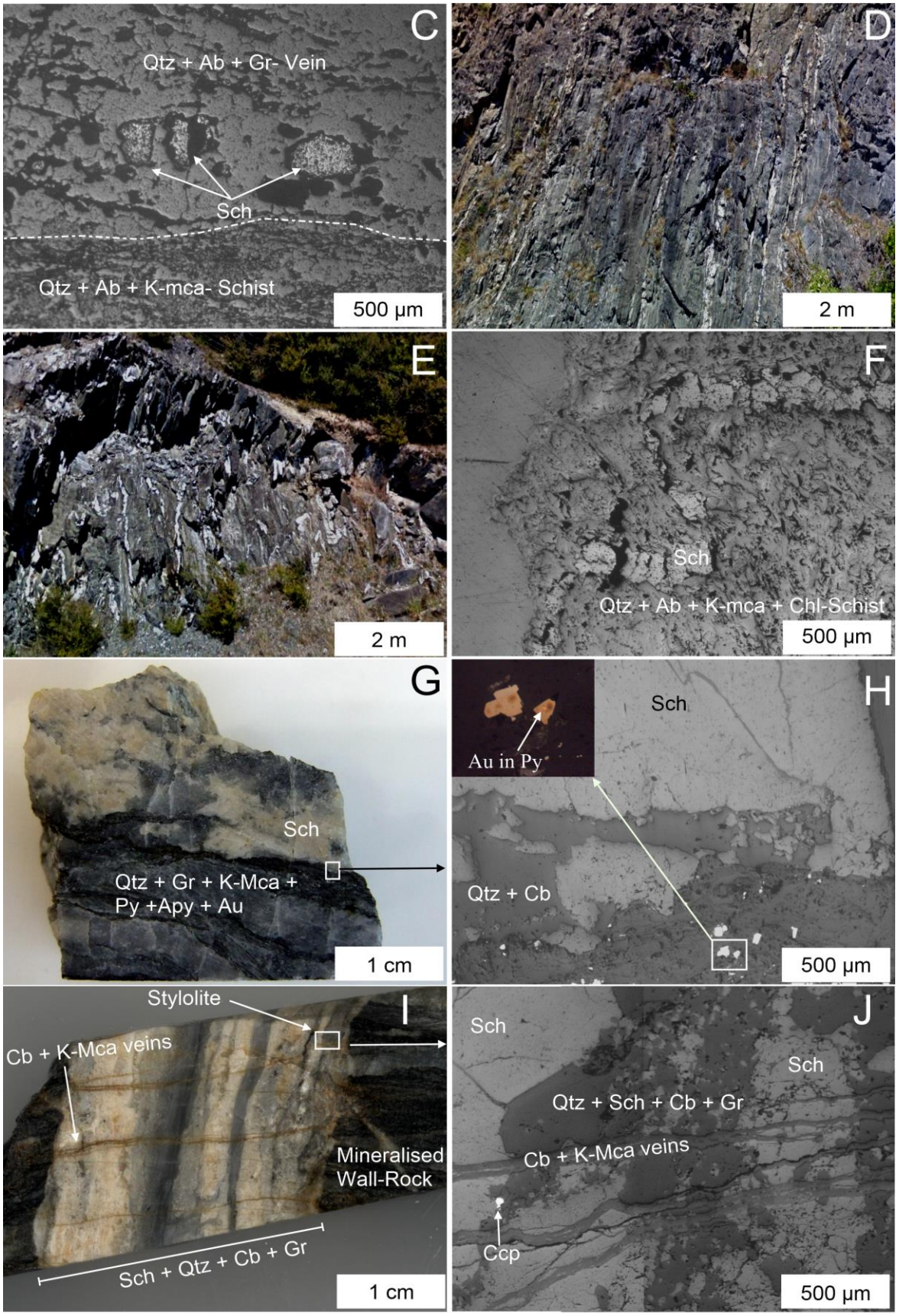
C
Qtz + Ab + Gr- Vein
Sch
Qtz + Ab + K-mca- Schist
500 µm
D
2 m
E
2 m
F
Sch
Qtz + Ab + K-mca + Chl-Schist
500 µm
G
Sch
Qtz + Gr + K-Mca +
Py +Apy + Au
1 cm
H
Sch
Au in Py
Qtz + Cb
500 µm
I
Stylolite
Cb + K-Mca veins
Mineralised
Wall-Rock
Sch + Qtz + Cb + Gr
1 cm
J
Sch
Sch
Qtz + Sch + Cb + Gr
Cb + K-Mca veins
Ccp
500 µm

Fig. 35. (A)- Scanning electron image of prehnite-pumpellyite facies graywacke sample (FFB-001A) from the Fiddlers Flat section, with scheelite micrograin approximately 2 microns in diameter. (B) Scheelite micrograin in upper pumpellyite-actinolite facies schist sample (LHPA-001A) from the Lake Hāwea section. (C) Scattered scheelite grains in foliation concordant vein in upper pumpellyite-actinolite facies schist (FFPA-003) from the Fiddlers Flat section. (D) Quartz-albite-chlorite-epidote veins at approximately the pumpellyite-actinolite/ lower greenschist metamorphic facies boundary along the Lake Hāwea section; these veins contain scattered scheelite grains. (E) Quartz-albite-chlorite-epidote veins at lower greenschist facies further along the Lake Hāwea section, showing deformation with the host schist rocks; these veins contain scattered scheelite grains. (F) Folded scheelite vein in lower greenschist facies schist sample (LHCG-004) from the Lake Hāwea section. (G) Massive scheelite-rich vein sample (MCM-001B) from Macraes underground mine (drift 2M2). (H) Insert of (G), with reflected microscopy showing the relationship between scheelite and Au (within pyrite) in this sample. (I) Laminated quartz-scheelite-carbonate vein sample (MCM-002) with subordinate carbonate and quartz from Macraes underground mine (drift 2E). (J) Insert of (I), with reflected microscopy showing differing texture of scheelite and its relationship with carbonate-K-mica veins. Mineral abbreviations Sch- scheelite, Cb- Carbonate, K-Mca- K-mica, Qtz- quartz, Ab- albite, Gr- graphite, Ccp- chalcopyrite.

Pumpellyite-actinolite facies samples from the Fiddlers Flat and Lake Hāwea sections are classified using the degree of foliation development into lower and upper pumpellyite-actinolite facies, following Cave et al. [2015 (Chapter 7)]. Scheelite in the lower pumpellyite-actinolite facies rocks was observed as rare subhedral micrograins ranging in size from < 1 μm up to 10 μm and associated with the rock-forming and accessory minerals, albite, titanite, epidote, and pargasite. In the upper pumpellyite-actinolite facies rocks, scheelite was observed as rare subhedral micrograins (3-20 μm; Fig. 35B) associated with the rock-forming and accessory minerals, albite, titanite, epidote, and actinolite. In these rocks, scattered subhedral macroscopic grains (up to 5,000 μm in diameter) of scheelite were also observed in rare 0.5-10 cm wide foliation-parallel quartz-albite-epidote±titanite veins (Figs. 35C, 36) and rare 0.5-10 cm wide semi-continuous foliation-discordant quartz-albite-epidote±titanite veins.

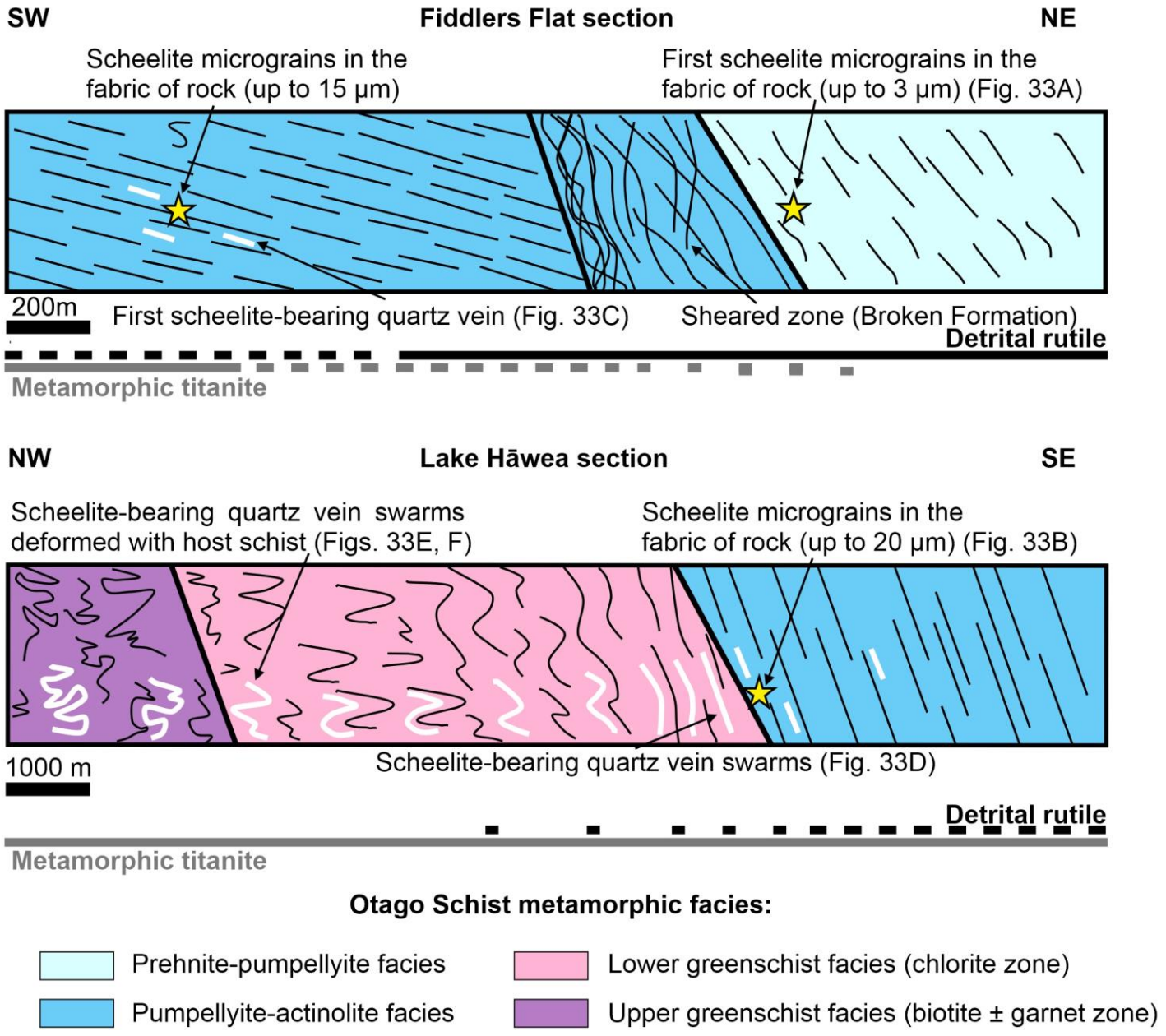
SW
Fiddlers Flat section
NE
Scheelite micrograins in the fabric of rock (up to 15 µm)
First scheelite micrograins in the fabric of rock (up to 3 µm) (Fig. 33A)
S
200m
First scheelite-bearing quartz vein (Fig. 33C)
Sheared zone (Broken Formation)
Detrital rutile
Metamorphic titanite
NW
Lake Hāwea section
SE
Scheelite-bearing quartz vein swarms deformed with host schist (Figs. 33E, F)
Scheelite micrograins in the fabric of rock (up to 20 µm) (Fig. 33B)
1000 m
Scheelite-bearing quartz vein swarms (Fig. 33D)
Detrital rutile
Metamorphic titanite
Otago Schist metamorphic facies:
Prehnite-pumpellyite facies
Lower greenschist facies (chlorite zone)
Pumpellyite-actinolite facies
Upper greenschist facies (biotite ± garnet zone)

Fig. 36. Sketch section through the Fiddlers Flat and Lake Hāwea sections from lowest metamorphic grade (right) to the highest metamorphic grade (left). Sections show overall metamorphic fabric and bedding (thin black lines) in the lowest metamorphic grade rocks, along with major faults (thick black lines), scheelite-bearing quartz veins (thick white lines) and selected locations with scheelite micrograins within the fabric of the rock (yellow stars). Fiddlers Flat and Lake Hāwea sections based on the work of Henne et al. (2012) and Pitcairn (2004), respectively.

Lower greenschist facies samples used in this study are derived from the Lake Hāwea section. Macroscopic scheelite is first observed in quartz-albite-chlorite-epidote veins along the Lake Hāwea section at approximately the pumpellyite-actinolite/ lower greenschist metamorphic facies boundary (Figs. 35D, 36). These veins occur as swarms of foliation-concordant and foliation-discordant veins approximately 0.5-1 m apart, and typically only persisting for up to 10 m before pinching out (Fig. 35D) (Craw and Norris 1991). These veins are an integral part of the metamorphic host, having been deformed and recrystallized with their host rocks (Figs. 35E, F, 36) (Craw and Norris 1991, and references therein). Scheelite also occurs in the fabric of the lower greenschist facies rocks as rare subhedral micrograins (3-20 μm) associated with quartz and albite.

Macraes Mine samples. Scheelite-bearing stockwork veins from the Macraes underground mine, collected along drifts 2M2 (MCM-001B) and 2E (MCM-002) have been investigated. Sample MCM-001B consists of a massive scheelite vein with subordinate carbonate and quartz, which is cut by a quartz-carbonate-graphite vein with abundant arsenopyrite and pyrite ± chalcopyrite, and Au (Figs. 35G, H). Sample MCM-002 is a laminated quartz-scheelite-carbonate vein with subordinate hydrothermal rutile, sulfide minerals (arsenopyrite and pyrite ± chalcopyrite, and bornite), and Au (Figs. 35I, J). Individual laminae occur parallel to the vein margins and are defined by either variations in grain size, thin bands of scheelite, or wall-rock schist, or stylolites, similar to the observations of Begbie and Craw (2006) (Fig. 35I). Scheelite

adjacent to the laminae is commonly heavily fragmented, with scheelite distal from the laminae margins being more well-formed and massive (Fig. 35J). Later calcite-K-mica veins cross-cut the scheelite-carbonate-quartz vein parallel to metamorphic foliation (Figs. 35I, J). Abundant sulfides (arsenopyrite and pyrite ± chalcopyrite, and bornite) are associated with scheelite (Fig. 35J).

8.5.3 Chemical Composition of Scheelite

Trace element analyzes of scheelite samples investigated in this chapter reveal two distinct populations (Fig. 37A, Appendix 2). The first population comprising all samples from Fiddlers Flat and Lake Hāwea (syn-metamorphic scheelite; Fig. 37A) is characterized by relatively high HREE (Tb-Lu) /LREE (La-Gd) ratios (1.0-23, mean 5.2) together with relatively low concentrations of Sr (160-1,320 ppm, mean 646 ppm), Y (1.7-133 ppm, mean 27 ppm), and ∑REEs (0.95-64 ppm, mean 13.1 ppm). The second population, which consists of all samples from the Macraes Mine (late-metamorphic scheelite; Fig. 37A) is characterized by relatively low HREE/LREE ratios (0.21-0.52, mean 0.34) together with relatively high concentrations of Sr (3,240-13,400 ppm, mean 7,610 ppm), Y (39-1,250 ppm, mean 217 ppm), and ∑REEs (51-2,540 ppm, mean 336 ppm). These distinct populations of scheelite are further divisible into four types based on subtle differences in their REE-normalized patterns (Fig. 37B). Table 6 contains min, max, and mean values (ppm) for trace elements of different scheelite types (Type-A, B, C, and D) from Fiddlers Flat, Lake Hāwea, and Macraes Mine, with combined values for scheelite types when observed at more than one locality (for example, Type-A at Fiddlers Flat and Lake Hāwea) also shown.

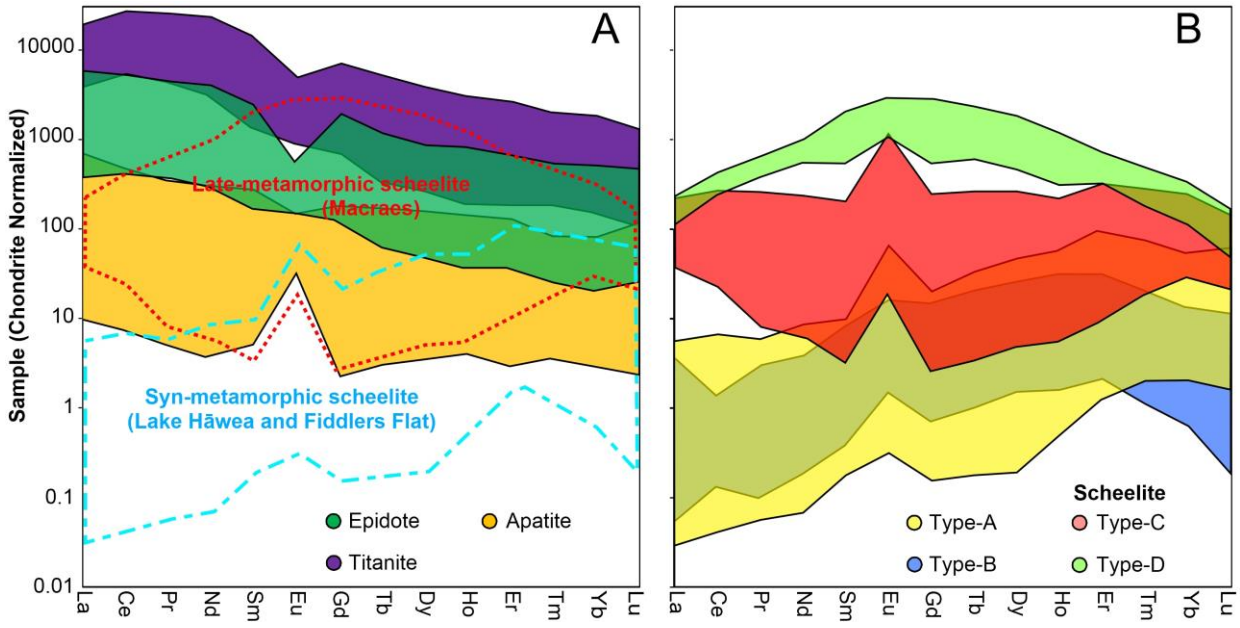

Fig. 37. (A) Chondrite normalized REE plots showing variations between syn-metamorphic scheelites, late-metamorphic scheelites, epidote, titanite, and apatite. Chondrite normalized values, normalize, to the chondrite values of Evensen et al. (1978). (B) Chondrite normalized REE plots, showing scheelite min-max value field for all types. Type-A and –B patterns are exclusively from Fiddlers Flat and Lake Hāwea sections (syn-metamorphic scheelites), and Types-C and –D are exclusively from Macraes Mine (late-metamorphic scheelites).

Type-A scheelite is found in the cores of scheelite grains from foliation concordant and foliation discordant veins from Fiddlers Flat (for example, Fig. 38), and in the cores and rims of scheelite grains from Lake Hāwea. Type-A scheelite is characterized by concave-downward REE-normalized patterns with prominent peaks at Eu and Er (Fig. 37B), and high HREE/LREE ratios. Compared to the other types of scheelite characterized in this chapter, this scheelite variant contains the highest mean concentrations of Mo (Fig. 39), relatively high concentrations of Pb, and relatively low concentrations of Y (Figs. 10A, B, C, D), ∑REEs (Fig. 40B), Sr (Figs. 39, 40A), and Mn, as well as Na that is generally below detection limit (<0.8 ppm). Gd/Lu-normalized ratios are the lowest of all scheelite types characterized in this chapter (Fig. 42), and La/Sm-normalized ratios range between 0.12 and 1.8 (Fig. 42).

Table 6. Minimum, maximum, and mean ($\bar{x}$), values for scheelite (sch) types (A, B, C, and D) from Fiddlers Flat (FF), Lake Hāwea (LH), Macraes Mine sample MCM-001B1 (MC1), and Macraes Mine sample MCM-002 (MC2). Chondrite normalized values normalized to the chondrite values of Evensen et al. (1978), except Y which was normalized against chondrite value of McDonough and Sun (1995).

Sch Type	A	A	A	A	A	A	A	A	A	B	B	B	C	C	C	D	D	D
Value	Min	Max	x̄	Min	Max	x̄	Min	Max	x̄	Min	Max	x̄	Min	Max	x̄	Min	Max	x̄
Unit	ppm	ppm	ppm	ppm	ppm	ppm	ppm	ppm	ppm	ppm	ppm	ppm	ppm	ppm	ppm	ppm	ppm	ppm
n	49	49	49	64	64	64	15	15	15	25	25	25	46	46	46	6	6	6
Locality	LH	LH	LH	FF & LH	FF & LH	FF & LH	FF	FF	FF	FF	FF	FF	MC2 &MC1	MC2 &MC1	MC2 &MC1	MC2	MC2	MC2
Na	<0.8	25.1	N/A	<0.8	25.1	N/A	<0.8	25.0	N/A	<0.8	7.7	N/A	0.75	72	16.5	33	178	119
Mn	0.91	3.2	1.8	0.11	3.2	1.5	0.11	1.8	0.64	<0.05	0.89	N/A	2.0	13.1	5.0	1.3	2.9	2.1
Sr	515	1,130	717	331	1,320	753	331	1,320	871	160	879	372	4,100	13,400	8,070	3,240	5,410	4,090
Y	1.7	133	35	1.7	133	29	5.4	22.0	11.5	6.3	45	19.6	39	526	134	410	1,250	855
Mo	0.44	1.2	0.82	0.44	1.2	0.80	0.44	1.1	0.73	0.07	1.3	0.47	<0.05	0.30	0.09	0.11	0.26	0.15
La	<0.02	1.3	0.39	<0.02	1.3	0.34	0.04	0.30	0.16	<0.02	0.79	0.10	10.0	44	21	15.6	44	33
Ce	0.02	3.9	0.91	0.02	3.9	0.79	0.15	0.70	0.39	0.07	1.1	0.32	14.7	149	45	117	266	214
Pr	<0.02	0.57	0.15	<0.02	0.57	0.13	0.02	0.10	0.06	0.01	0.28	0.08	0.89	24	5.4	37	65	52
Nd	<0.02	3.8	0.73	<0.02	3.8	0.65	0.12	0.63	0.37	0.08	1.8	0.64	2.8	94	22	287	478	342
Sm	<0.02	1.8	0.33	<0.02	1.8	0.29	0.06	0.22	0.16	0.08	1.3	0.45	0.54	30	6.8	113	314	180
Eu	0.01	3.2	0.69	0.01	3.2	0.63	0.19	0.67	0.45	0.09	0.89	0.33	0.84	69	8.3	79	144	115
Gd	<0.02	4.4	0.73	<0.02	4.4	0.65	0.16	0.75	0.38	0.19	3.7	1.4	0.60	48	9.6	137	505	268
Tb	0.01	1.2	0.21	0.01	1.2	0.18	0.05	0.14	0.09	0.04	0.74	0.32	0.13	8.6	1.8	24	81	46

Dy	0.05	12.6	2.4	0.05	12.6	2.1	0.43	1.3	0.88	0.54	6.9	3.0	1.2	67	13.3	133	436	270
Ho	0.03	3.6	0.80	0.03	3.6	0.67	0.14	0.39	0.27	0.15	1.9	0.82	0.32	12.8	2.7	19.9	62	41
Er	0.21	14.3	3.6	0.21	14.3	3.0	0.44	1.8	1.00	0.42	5.9	2.4	1.4	43	9.3	41	129	93
Tm	0.05	1.9	0.60	0.05	1.9	0.49	0.06	0.24	0.12	0.04	0.47	0.21	0.44	6.5	1.5	3.3	12.9	8.2
Yb	0.45	10.5	4.5	0.33	10.5	3.6	0.33	1.6	0.71	0.13	2.1	0.74	4.8	37	11.1	11.3	52	32
Lu	0.08	1.3	0.66	0.04	1.3	0.52	0.04	0.18	0.07	0.01	0.27	0.07	0.59	3.1	1.2	0.63	3.6	2.2
Pb	1.2	83	17.4	<0.02	83	13.4	<0.02	1.7	0.57	<0.02	1.0	N/A	3.6	43	14.5	4.7	8.6	6.2
U	<0.02	1.6	0.22	<0.02	1.6	0.18	<0.02	0.08	N/A	<0.02	0.17	N/A	0.01	5.2	2.3	0.01	0.09	0.04
∑REE	0.95	64	16.7	0.95	64	14.0	2.4	8.7	5.1	2.3	25	10.9	51	590	159	1,130	2,540	1,700
∑LREE	0.07	18.7	3.9	0.07	18.7	3.5	0.85	3.1	2.0	0.87	8.9	3.4	41	438	118	894	1,780	1,200
∑HREE	0.88	45	12.8	0.88	45	10.5	1.6	5.6	3.1	1.4	17.5	7.6	10.1	158	41	234	759	492
HREE/LREE	2.0	23	7.7	1.2	23	6.3	1.2	1.8	1.6	1.0	5.1	2.4	0.21	0.49	0.33	0.26	0.52	0.40
LaN/SmN	0.12	1.8	0.76	0.12	1.8	0.73	0.30	1.2	0.66	0.02	2.1	0.20	0.36	20	4.6	0.05	0.25	0.13
GdN/LuN	0.01	0.49	0.11	0.01	1.0	0.25	0.42	1.0	0.67	0.49	7.6	3.4	0.08	5.7	1.1	7.1	29	18.3

.

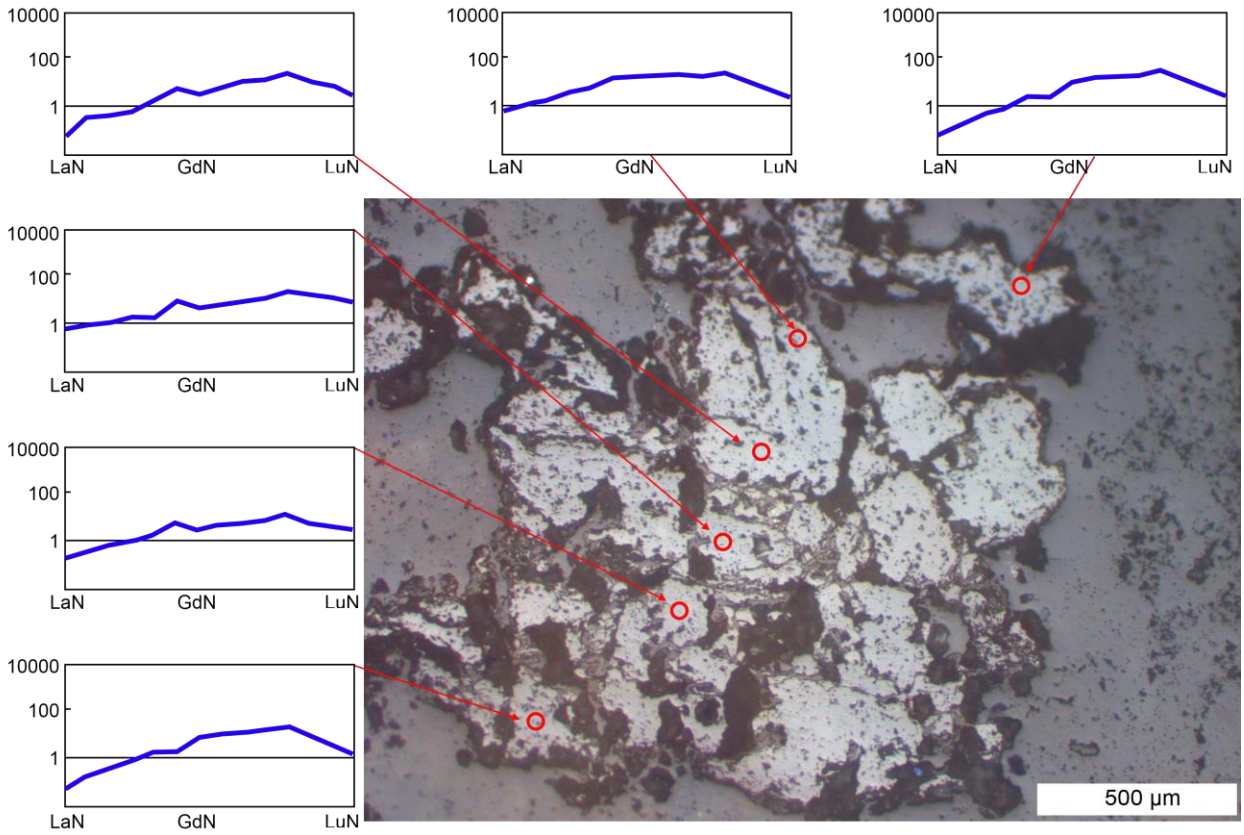

Fig. 38. Scheelite grain within semi-continuous foliation-discordant quartz-albite-epidote±titanite vein sample (FFPA-003) hosted within upper pumpellyite-actinolite facies schist from the Fiddlers Flat section. Red circles indicate site of laser ablation with the REE-normalized pattern of each spot shown. REE-normalized patterns show gradual transition (core to rim) from Type-A to Type-B scheelite.

Type-B scheelite is exclusively found in rims surrounding Type-A scheelite in foliation concordant and foliation discordant veins at Fiddlers Flat (Fig. 38). REE-normalized patterns of Type-B scheelite are very similar to Type-A scheelite (Fig. 36B), except that the two prominent peaks at Eu and Er defining Type-A scheelite are replaced with a plateau between Eu and Er corresponding to higher Gd, Tb, Dy, and Ho values, and the HREEs Tm, Yb, and Lu being relatively depleted (Fig. 36B). Type-B scheelite is characterized by relatively high concentrations of Mo (Fig. 39), and relatively low concentrations of Sr (Figs. 39, 40A), Y (Figs. 40A, B, C, D), Pb, ∑REEs (Fig. 40B), ∑LREEs (Figs. 40C, 41), and ∑HREEs (Figs. 40D, 41).

Gd/Lu-normalized ratios relative to Type-A scheelite are high (Fig. 42), whereas La/Sm-normalized ratios in Type-B scheelite are similar to those of Type-A scheelite (Fig. 42).

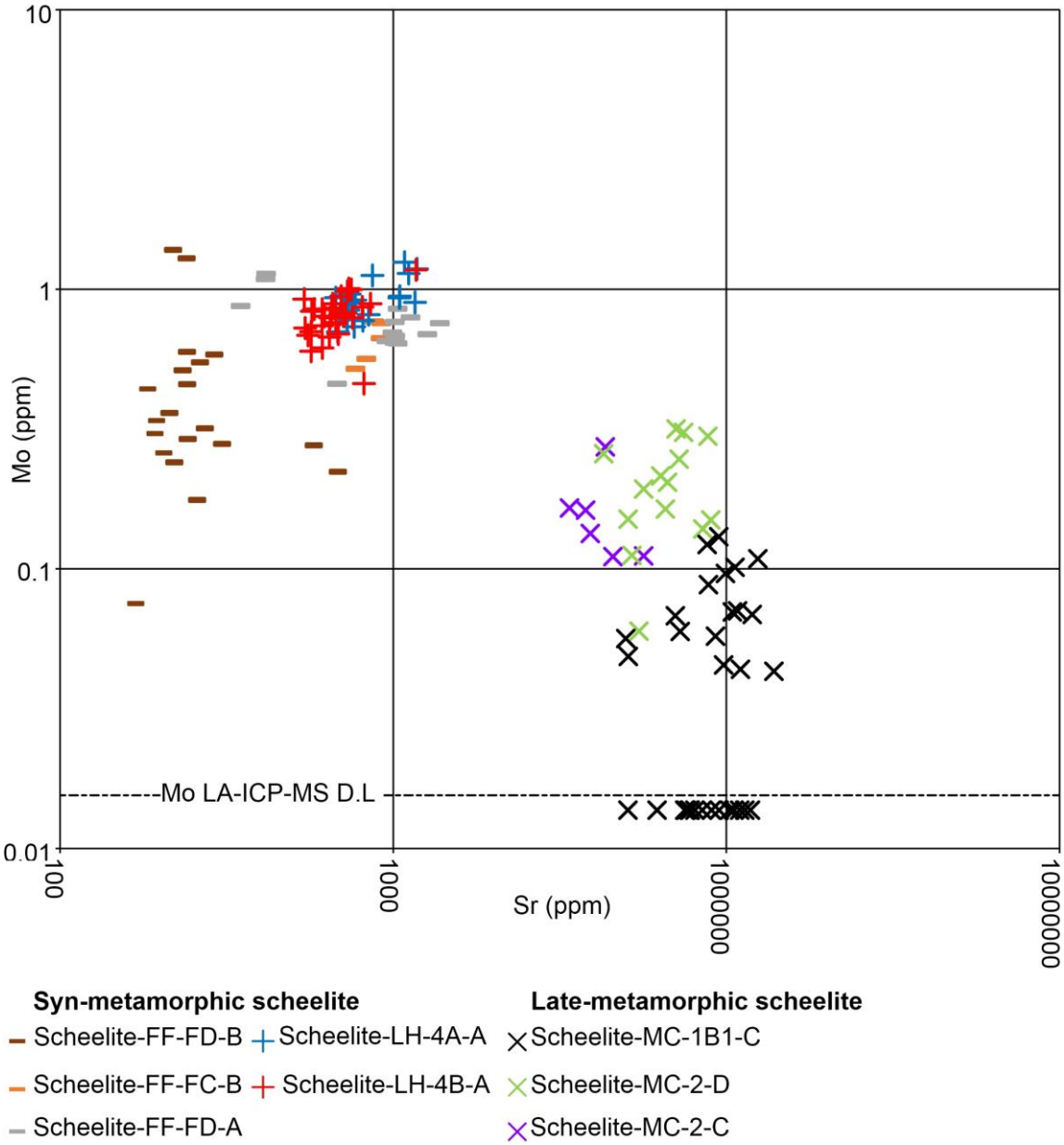

Fig. 39. Concentrations of molybdenum versus strontium in syn-metamorphic and late-metamorphic scheelites. Strontium concentrations allow discrimination between these two varieties in this chapter with late-metamorphic scheelites being relatively enriched in strontium (>3,200 ppm) compared to the syn-metamorphic scheelites (<1,300 ppm). Abbreviations in legend: FF- Fiddlers Flat, LH- Lake Hāwea, and MC- Macraes Mine. FD and FC in Fiddlers Flat scheelite indicates scheelite hosted in either foliation discordant or concordant veins, respectively. 4A, 4B, 2,

and 1B1 in Lake Hāwea and Macraes scheelites refers to sample numbers LHCG-004A, LHCG-004B, MCM-002, and MCM-001B, respectively. A, B, C, and D in scheelites refers to scheelite types.

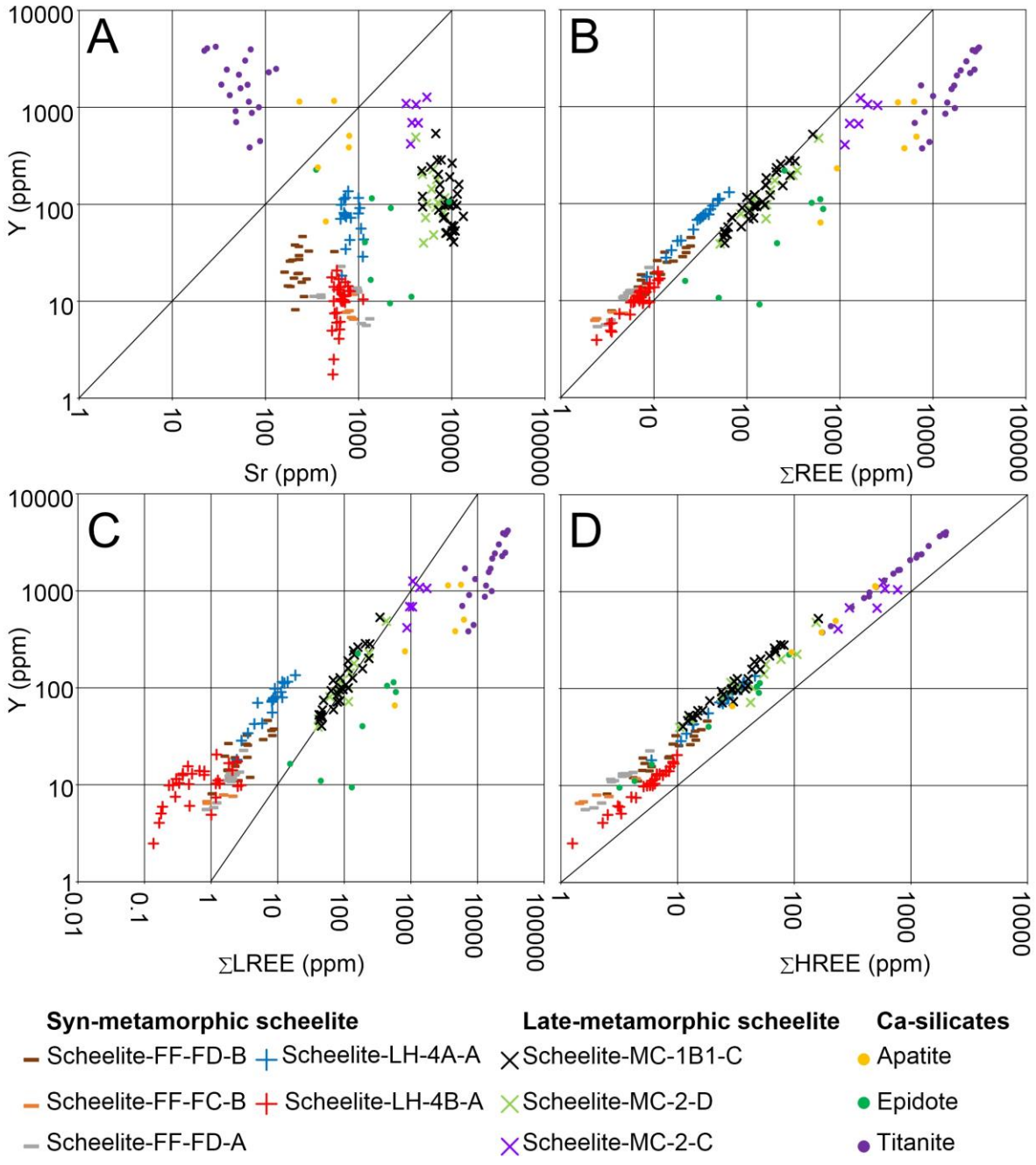

Fig. 40- Plots showing yttrium concentrations in scheelite varieties (syn-metamorphic and late-metamorphic) versus (A) strontium, (B) ∑REEs, (C) ∑LREEs, and (D) ∑HREEs. Abbreviations as per Fig 39.

Type-C scheelite is the dominant scheelite type observed in samples analyzed from

Macraes Mine (MCM-001B and MCM-002). In scheelite sample MCM-002, Type-C scheelite is observed within the core of the scheelite band closest to the wall-rock and in the core-and-rim of scheelite band further towards the middle of the vein (Fig. 43). The normalized REE patterns of the Type-C scheelite are typically flat to concave-upwards (relatively depleted in MREEs) with a prominent peak at Eu (Fig. 37B). Compared to the other types of scheelite characterized in this chapter, Type-C scheelite has the highest concentrations of Sr (Figs. 39, 40A), Pb, and U, relatively high concentrations of Y (Figs. 40A, B, C, D), ∑REEs (Fig. 40B), ∑LREEs (Figs. 40C, 41), ∑HREEs (Figs. 40D, 41), Na, and Mn. Gd/Lu-normalized ratios for Type-C scheelite display considerable variation, varying between 0.08 and 5.7 (Fig. 42). Mean (La/Sm)n ratios in Type-C are observed as being the highest of all scheelite types with considerable variation occurring between minimum and maximum values (Fig. 42).

Type-D scheelite is observed exclusively in the scheelite sample MCM-002, occurring in the rims (either-side) of the scheelite band closest to the wall-rock (Fig. 43). Type-D scheelites are characterized by concave-downwards REE-normalized patterns with the apex at Eu (Fig. 37B). Compared to the other types of scheelites characterized in this chapter, Type-D scheelites contain the highest concentrations of Y (Figs. 40A, B), ∑REEs (Fig. 40B), ∑LREEs (Figs. 40C, 41), ∑HREEs (Figs. 40D, 41), and Na, with relatively high concentrations of Sr (Figs. 39, 40A), Mn, and Pb, and relatively low concentrations of U and Mo (Fig. 39). High (Gd/Lu)n ratios are observed in Type-D scheelite relative to the other scheelite types, and are negatively correlated with (Gd/Lu)n ratios (Fig. 41).

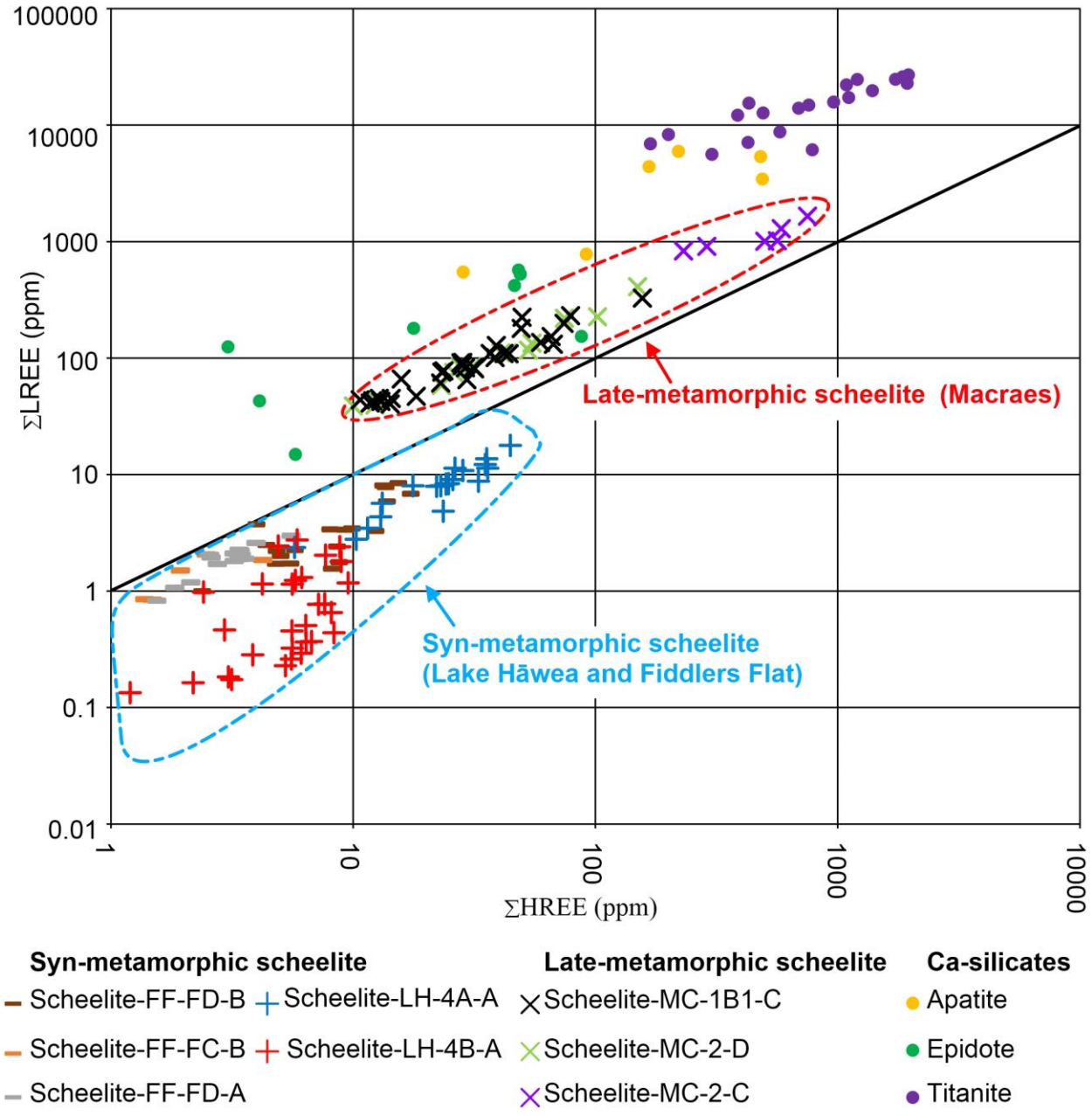

Fig. 41. Concentrations of ∑LREEs against ∑HREEs in scheelite varieties and Ca-silicate minerals, titanite, epidote, and apatite. Abbreviations as per Fig. 39.

Scheelite trace element concentrations and types reported from Macraes Mine (Type-C and Type-D) in this chapter, resembles limited scheelite data previously reported from the Macraes Mine [that is, Farmer et al. (2012)]. Scheelite types (Type-C and Type-D) from the Macraes Mine closely resemble scheelite REE-normalized patterns observed from a variety of

vein hosted Au-W deposits; including the hydrothermal veins of the Archean Au deposits in the Kalgoorlie-Norseman greenstone belt of Western Australia (Ghaderi et al. 1999; Brugger et al. 2000), the Paleoproterozoic Björkdal Au deposit of northern Sweden (Roberts et al. 2006), the Paleozoic turbidite-hosted Au deposits of Nova Scotia, Canada (Dostal et al. 2009).

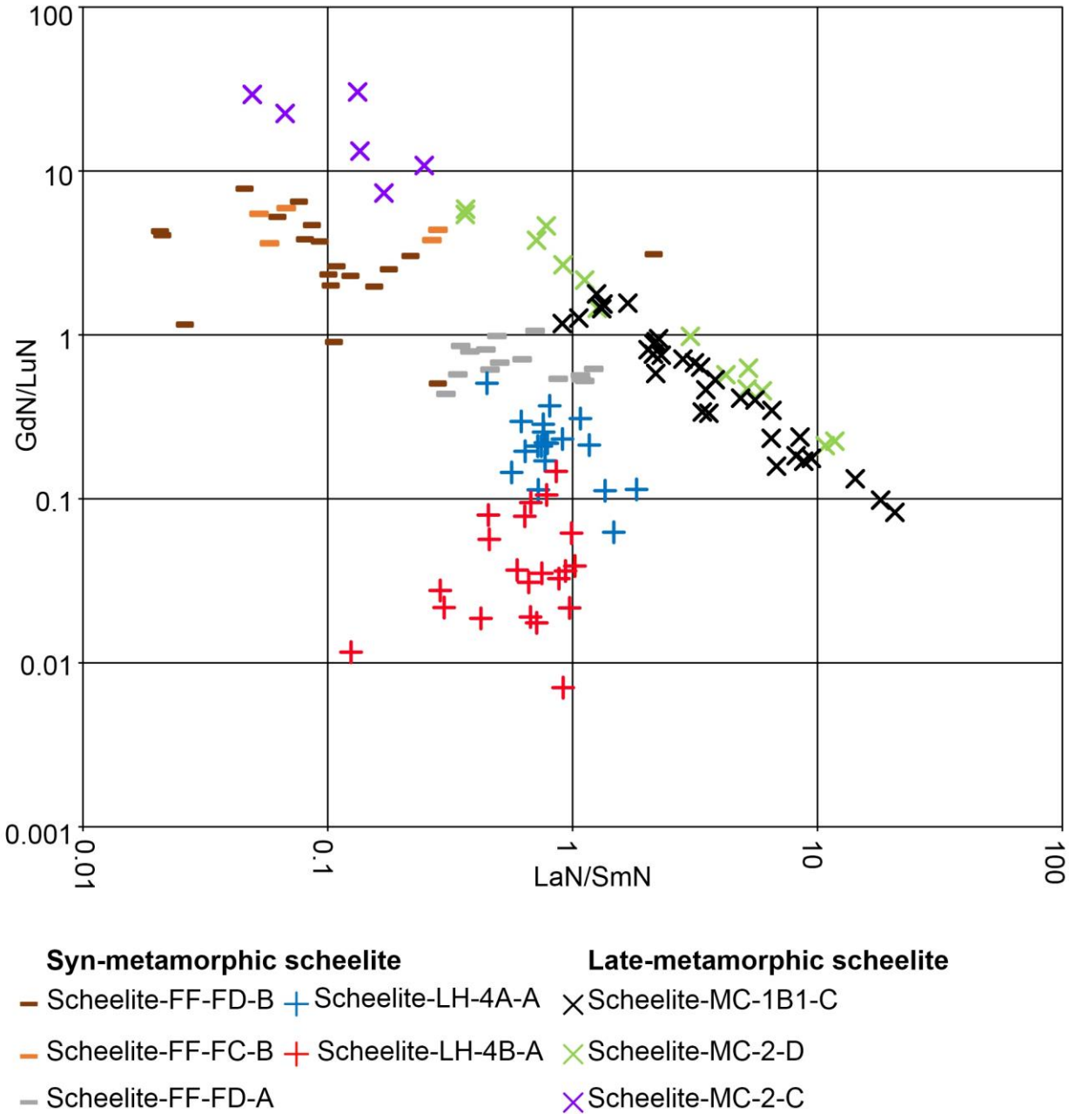

Fig 42. Gd/Lu_N versus La/Sm_N diagram for syn-metamorphic and late-metamorphic scheelite. La/Sm_N values

increase concurrent with decreasing Gd/Lu_N ratios during fractional precipitation of scheelite (Brugger et al. 2000). Abbreviations as per Fig. 39.

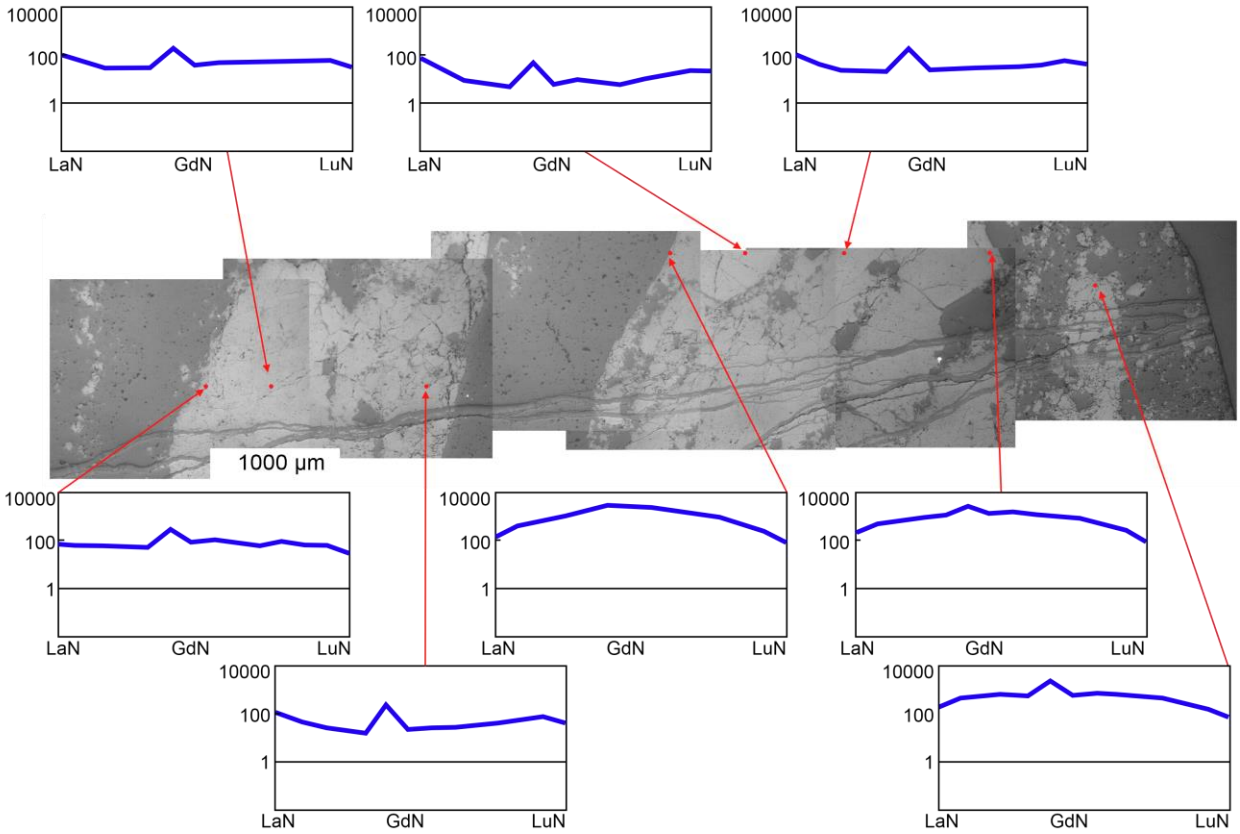

Fig. 43. Scheelite bands in a stockwork vein sample (MCM-002) from Macraes underground mine (drift 2E). Red dots indicate site of laser ablation with the REE-normalized pattern of each spot shown. REE-normalized patterns show complicated transition zoning between the various types of scheelite. Interpretation of the geochemistry of the late-metamorphic scheelite is complicated with a combination of numerous scenarios likely contributing to the observed difference and transition between individual types. Pulses of distinct fluid phases are recorded by laminated scheelite veins (MCM-002) with, input from the breakdown of REE-bearing minerals, co-precipitation of REE-incorporating vein minerals, fractional crystallization of scheelite, dissolution and remobilization of scheelite (as evidenced from the transition of inclusion-free, well formed scheelite to heavily-fractured scheelite near the laminae margins), all likely contributing to the observed differences between the two types.

8.5.4 Selected Trace Element Concentrations in Titanite, Epidote, Apatite, and

Albite

Table 7 contains min, max, and mean values (ppm) for select trace elements of selected Ca-silicate minerals (titanite, epidote, albite, and apatite) from lower and upper greenschist facies samples that were analyzed using LA-ICP-MS techniques, with all analyzes shown in Appendix 2. Epidote in these samples is characterized by moderate to high concentrations of Sr (Fig. 40A), together with low concentrations of Y (Figs. 40A, B, C, D) and ∑REEs (Fig. 40B), with LREEs being dominant over HREEs (Fig. 41) as reflected in their very low HREE/LREE ratios. Titanite in contrast is characterized by low concentrations of Sr (Fig. 40A), high concentrations of Y (Figs. 40A, B, C, D), and extremely high concentrations of ∑REEs (Fig. 40B), with LREEs also dominating over HREEs (Fig. 41) generating very low HREE/LREE ratios. Apatite is characterized by low to moderate concentrations of Sr (Fig. 40A) and Y (Figs. 40A, B, C, D), together with moderate to high concentrations of ∑REEs (Fig. 40B), with LREEs again being dominant over HREEs (Fig. 41) producing very low HREE/LREE ratios. Albite contains low concentrations of Sr, and very low Y and ∑REEs with analyzes predominantly below detection limit.

Table 7. Minimum, maximum, and mean ($\bar{x}$), values for epidote, titanite, apatite, and albite from regional lower greenschist and upper greenschist facies samples. Chondrite normalized values normalized to the chondrite values of Evensen et al. (1978), except Y which was normalized against chondrite values of McDonough and Sun (1995).

Mineral	Epidote	Epidote	Epidote	Titanite	Titanite	Titanite	Apatite	Apatite	Apatite	Albite	Albite
Value	min	max	$\bar{x}$	min	max	$\bar{x}$	min	max	$\bar{x}$	min	max
Unit	ppm	ppm	ppm	ppm	ppm	ppm	ppm	ppm	ppm	ppm	ppm
n	8	8	8	20	20	20	6	6	6	7	7
Na	<70	1100	194	<70	238	113	<70	817	433	71,100	73,700
Al	108,000	123,600	116,000	4,900	7,500	6,300	<5.0	61	15	Std	Std
K	<35	246	111	<35	81	N/A	<35	<35	N/A	211	343
Ca	Std	Std	Std	Std	Std	Std	Std	Std	Std	<900	<900
Sr	350	9,400	2,700	22	130	60	231	794	528	6.5	72
Y	9.2	222	75	377	4,100	2,000	65	1,100	573	<0.05	0.49
La	2.8	150	54	904	3,600	2,300	93	1,100	575	<0.05	<0.05
Ce	5.6	286	116	2,800	12,800	7,600	252	2,800	1,500	<0.05	0.05
Pr	0.64	31	13.7	373	1,920	1,080	33	382	215	<0.05	<0.05
Nd	2.3	133	55	1,300	8,300	4,470	149	1,610	975	<0.50	<0.50
Sm	0.92	39	13.6	181	1,810	838	26	354	202	<0.50	<0.50
Eu	2.1	8.1	4.4	46	241	127	8.2	29	20	<0.20	<0.20
Gd	0.60	35	14.0	118	1,300	588	26	333	176	<0.50	0.31
Tb	0.14	6.2	2.0	12.4	165	72	2.5	42	21	<0.05	<0.05

Dy	1.1	39	12.9	63	890	394	12.3	223	109	<0.20	0.24
Ho	0.27	8.5	2.6	11.1	153	70	2.3	41	20	<0.05	0.04
Er	0.65	22	7.8	34	417	197	6.6	109	53	<0.20	<0.20
Tm	0.12	2.2	0.96	4.86	49	24	0.67	13.6	6.0	<0.05	<0.05
Yb	0.63	13.9	5.9	39	293	157	3.8	83	35	<0.20	0.29
Lu	<0.05	2.9	0.88	6.6	33	19.24	0.76	12.2	5.0	<0.05	0.06
YN	5.9	141	48	240	2,640	1,260	41	727	365	N/A	N/A
∑REE	21	658	304	6,400	31,500	18,000	616	6,680	3,950	N/A	N/A
∑LREE	15.6	609	271	6,100	29,600	17,100	587	6,460	3,700	N/A	N/A
∑HREE*	3.1	89	33	171	1,980	934	29	495	249	N/A	N/A
∑HREE/∑LREE	0.02	0.54	0.18	0.02	0.12	0.05	0.03	0.13	0.07	N/A	N/A
LaN/SmN	0.31	11.2	4.0	0.82	6	2.34	0.83	2.50	2.0	N/A	N/A
GdN/LuN*	0.21	8.7	3.1	1.7	7	3.6	1.2	8.8	5.2	N/A	N/A

8.6 Discussion

8.6.1 Host Minerals for W during Prograde Metamorphism

The results reported in this chapter indicate that in subgreenschist facies graywackes and argillites, detrital rutile is the major host of W with titanite and rare scheelite micrograins being subordinate host phases (Figs. 32A, B, C, 34A). With increasing prograde metamorphism from prehnite-pumpellyite facies to lower greenschist facies, detrital rutile recrystallizes to metamorphic titanite [Equation 3; Cave et al. 2015 (Chapter 7)]. This is demonstrated in the laser ablation traverse data, which show that in lower greenschist facies samples rutile is rare and the main W host is titanite (Fig. 32D). Additionally, rare scheelite micrograins were observed within the fabric of subgreenschist and greenschist facies samples (Fig. 32C). No other minerals hosting W in these rocks have been identified and this, combined with the observation that W is mobilized during recrystallization of rutile to titanite [Cave et al. 2015 (Chapter 7)], suggests that W is released from the metasedimentary rocks during the progression from subgreenschist to greenschist facies metamorphism.

8.6.2 Development of Scheelite during Prograde Metamorphism

Scheelite is observed in prehnite-pumpellyite facies graywackes and argillites as micrograins (< 1 to 3 μm) within the fabric of the rock (for example, Figs. 35A, 36). The scheelite micrograins are first observed in the same rocks where recrystallization of detrital rutile to metamorphic titanite begins. The size of the largest scheelite micrograins within the fabric of the rock increases with increasing metamorphic grade and with the extent of progress of the detrital rutile to metamorphic titanite reaction (Equation 3), with the largest scheelite micrograins

observed at the pumpellyite-actinolite/lower greenschist facies boundary (up to 20 μm; Figs. 35B, 36). This spatial and temporal link indicates that scheelite development is most likely linked to W release during the rutile-titanite reaction (Equation 3). Laser ablation inductively coupled plasma mass spectrometry (LA-ICP-MS) imaging of the incomplete recrystallization of rutile to titanite shows local transportation of W away from the reaction interface (Figs. 33, 34). Undeformed scheelite-bearing veins occur near the pumpellyite-actinolite/lower greenschist facies boundary (Figs. 35C, D). At lower greenschist facies, scheelite is more abundant in veins than in the host rock, with these veins being deformed and recrystallized at this metamorphic grade (for example, Figs. 35E, F).

Samples of scheelite-bearing stockwork veins from Macraes underground operations closely resemble those described by Begbie and Craw (2006). Formation of these veins is ascribed to incremental pulses of metamorphic fluids produced at depth into shallow-level incremental late-stage-metamorphic extensional structures (Begbie and Craw 2006; Pitcairn et al. 2014). Individual laminae record the incremental growth of the stockwork veins (for example, Fig. 35I), with remobilization of scheelite during subsequent incremental growth in samples MCM-001B and MCM-002 demonstrated by the fragmented texture of scheelite adjacent the laminae (for example, Figs. 35I, J).

8.6.3 Controls on the Chemical Variation in Scheelite

Scheelite ($CaWO_4$) forms a complete solid solution with powellite ($CaMoO_4$), with Mo^{6+} able to substitute for W^{6+} (Barabanov 1971; Raimbault et al. 1993). Additionally, scheelite can incorporate significant amounts of REEs, Sr, and Y with these elements able to substitute for Ca^{2+} (Cottrant 1981; Raimbault et al. 1993; Ghaderi et al. 1999; Brugger et al. 2002). Trace element geochemistry of scheelite in this chapter reveals subtle differences between sample

locations and vein types, with variations in the trace elements, Y, Sr, LREEs, and HREEs, and the low concentrations of Mo being the most interesting. Molybdenum concentrations in scheelite from all locations are very low (<2.3 ppm), with scheelite from Macraes Mine containing lower concentrations than scheelite from Fiddlers Flat and Lake Hāwea (Fig. 39). The occurrence of graphite in all veins suggests that the fluids were relatively reduced, particularly at Macraes, thus explaining the low Mo concentrations, as transportation of Mo^{6+} requires oxidizing conditions (Rempel et al. 2009).

Strontium concentrations clearly discriminate between syn-metamorphic vein scheelite precipitated from Fiddlers Flat and Lake Hāwea, and late-metamorphic vein scheelite from the Macraes Mine (Figs. 39, 40A). Macraes scheelites are enriched in Sr (>3,200 ppm) compared to the syn-metamorphic scheelites (<1,320 ppm). Significant depletions of Sr (and Y) were noted by Paterson and Rankin (1979) in the altered wall-rock surrounding the Glenorchy Mine compared to the un-altered host-rocks, leading Paterson and Rankin (1979) to propose that the relatively high concentrations of Sr observed in the Glenorchy scheelites were sourced from the breakdown of Ca-silicates during wall-rock alteration by the W-bearing fluid. At the Macraes Mine Ca-silicate minerals titanite and epidote have been replaced by a variety of secondary minerals including rutile, siderite, chlorite, K-mica, and calcite, due to interaction between the host rocks and the metal-rich ore forming fluids (Craw et al. 1999; Craw 2002). Analyzes of the major Ca-silicates present in un-altered regional greenschist facies samples, shows that epidote contains abundant Sr (mean 2,720 ppm), with apatite, titanite, and albite also containing Sr but at much lower concentrations (Table 7). Suggesting that the high Sr contents of the Macraes scheelite resulted from Sr released during alteration of epidote during mineralization. Lower Sr concentrations in the syn-metamorphic scheelites could reflect the near-equilibrium relationship

these veins share with their host rocks as shown by the mineralogy of the veins and lack of vein margin alteration selvages (Craw and Norris 1991), with the Sr being preferentially hosted by epidote, titanite, and apatite (Figs. 39, 40A). Variations in Sr content of syn-metamorphic scheelite between different vein locations (Figs. 39, 40A) likely relates to local variations in the host rock or vein mineralogy.

Yttrium concentrations in the scheelites of this chapter also vary substantially (1.7-1,245 ppm; Figs. 40A, B, C, D), with the Macraes scheelite showing higher Y concentrations than the syn-metamorphic scheelites (Figs. 40A, B, C, D). Like Sr, Y is also depleted surrounding the scheelite lodes of Glenorchy (Paterson and Rankin 1979) suggesting that Y and Sr enrichments in late-metamorphic scheelites may be sourced from the breakdown of Ca-silicates during wall-rock alteration by the W-bearing fluid. Yttrium contents in epidote are lower than those in Macraes scheelite (Fig. 40A) and therefore although the breakdown of epidote is suggested as being the source of the Sr, it is not likely the source of Y. Titanite however has significant Y contents (mean Y content of 1,980 ppm; Fig. 40A) and its replacement by rutile during alteration at Macraes is suggested as having liberated the Y that is enriched in the Macraes scheelite. Similarly to Sr, variations in Y concentrations in the syn-metamorphic scheelites most likely relates to local variations in the host rock or vein mineralogy (Figs. 40A, B, C, D). Yttrium displays good positive correlations with REEs (Figs. 40B, C, D), attesting to Y having the same charge as REE^{3+} and a similar ionic radius in eightfold coordination (1.015 Å), falling near Ho (1.02 Å) (Ghaderi et al. 1999). Macraes scheelites show strong positive correlations between Y, LREEs, HREEs, and REEs (Figs. 40B, C, D). Similar trends are observed in syn-metamorphic scheelites for REEs and HREEs (Figs. 40B, D) but less so for LREEs (Fig. 40C), with syn-metamorphic scheelites observed being depleted in LREEs in relation to Y and HREEs (Figs.

40C, 41). Trace element analyzes from Macraes scheelite (both Type-C or Type-D) reveal these scheelites are heavily enriched in REEs and have HREE/LREE ratios close to one (0.7-2.1, mean 1.4; Fig. 40). As previously discussed, titanite and epidote have undergone recrystallization to form rutile and siderite, respectively, during the hydrothermal alteration at Macraes. Both titanite and epidote in regional un-altered greenschist facies samples contain significant amounts of REEs at extremely high LREE/HREE ratios (Fig. 41), and it is suggested that similarly to Sr and Y, the Macraes scheelite is enriched in REEs released during alteration of Ca-silicates in the course of mineralization.

Rare earth element patterns in scheelite are primarily thought to be inherited from the precipitating fluid (Sylvester and Ghaderi 1997; Ghaderi et al. 1999; Brugger et al. 2000; Dostal et al. 2009; Peng et al. 2010; Song et al. 2014). Several parameters can affect the partitioning of REEs between scheelite and the fluid including temperature, pressure, the composition of the hydrothermal fluid, and the REE speciation in the fluid (Brugger et al. 2008; Song et al. 2014). Limited published data are available on the solubility and partitioning of REEs between fluids and scheelite, with most previous research assuming that all REEs have similar partitioning coefficients (Song et al. 2014). Hence, decoupling between LREE and HREE in scheelite is an interesting feature (Song et al. 2014).

Syn-metamorphic scheelites from both locations (Fiddlers Flat and Lake Hāwea) irrespective of scheelite type (Type-A or Type-B; Figs. 37A, B) reveal strong decoupling of LREEs and HREEs with strong enrichments in HREEs relative to LREEs (1.3-23, mean 5.2; Fig. 41). Available experimental data on REE fractionation in fluids shows the addition of ligands (for example, F-, Cl-) in relatively small concentrations [0.3–1.5 m (mol/kg H_2O)] can have a significant effect in enhancing REE solubilities (Williams-Jones et al. 2012, Tsay et al. 2014, and

references therein), with different ligands producing characteristic REE patterns due to preferential dissolution of either LREEs or HREEs (Tsay et al. 2014). Chloride complexes are shown to preferentially fractionate LREEs (Migdisov et al. 2009) and therefore cannot explain the observed HREE/LREE ratios. Fluorine is assumed to be present based on observation of fluorapatite in the syn-metamorphic veins along the Lake Hāwea section (Smith and Yardley 1999). Theoretical studies on fluorine complexes (Haas et al. 1995) have suggested that fluorine preferentially fractionates HREEs, potentially explaining the high HREE/LREE ratios (Fig. 41). However, recent experimental studies show that these models significantly overestimate the stability of REE fluoride species with increasing temperatures, in particular HREEs (Migdisov et al. 2009; Williams-Jones et al. 2012). An alternative explanation for the decoupling of LREEs and HREEs could be the early precipitation of an LREE bearing phase that sequesters the bulk of the LREEs. Analyzes of the major Ca-silicate minerals observed in regional un-altered greenschist facies samples, reveals that epidote, titanite, and apatite all contain significant amounts of REEs at extremely high LREE/HREE ratios (Fig. 41, Table 7). Early precipitation of these mineral phases would explain the high HREE/LREE ratios observed in the syn-metamorphic scheelites (Table 6). Additionally this mechanism likely provides an explanation for the observed decoupling between Y and LREEs, with LREEs preferentially incorporated into titanite, epidote, and apatite over Y (Fig. 40C).

Subtle differences in normalized REE patterns in scheelite allows for the distinction of two types of syn-metamorphic scheelite, Type-A and Type-B; that occur in the cores-and-rims of scheelite, respectively (for example, Fig. 38). Transition between the two types is gradual (Fig. 38), and is characterized by relative decreases in the HREEs Tm, Yb, and Lu, and relative increases in the HREEs Tb, Dy, Ho, and the LREEs Gd to form a plateau between Eu and Er

(Fig. 38). Assuming, as most previous researchers have, that scheelite/fluid partitioning coefficients are similar for all REEs (Song et al. 2014 and references therein), these REE-normalized patterns indicate the fluid precipitating the scheelite is progressively enriched in the HREEs Tb, Dy, Ho, and the LREE, Gd. As discussed previously, this could be explained by the gradual sequestering of LREEs in Ca-silicates contemporaneous with scheelite growth.

The occurrence at Macraes of two types (Type-C and Type-D) of scheelite and multiple transitions between them provides further evidence for incremental growth, with fluids precipitating the scheelite interpreted from scheelite geochemistry, as fluctuating between relatively MREE-depleted fluids (Type-C) and relatively MREE-enriched fluids (Type-D). Scheelite (Gd/Lu)N and (La/Sm)N ratios potentially record complex fractional crystallization patterns. However, interpretation of these patterns is complicated by a combination of numerous competing and complementary scenarios that likely significantly contributed to the observed difference and transition between individual types (Figs. 42, 43). Such factors include pulses of distinct fluid phases, input from the breakdown of REE-bearing minerals, co-precipitation of REE-incorporating vein minerals, dissolution and remobilization of scheelite, and fractional precipitation of scheelite.

Positive Eu anomalies are shown in all scheelite types (Type-A, Type-B, Type-C, and Type-D, Fig. 37A, B). Reduced fluid conditions and inherited anomalies from the breakdown of minerals (typically, plagioclase), are the two predominant explanations for decoupling between Eu and the other REE in scheelite (Brugger et al. 2000; Castorina 2008; Farmer et al. 2012). Plagioclase recrystallization could potentially explain the anomalies in the syn-metamorphic scheelite, with Cave et al. (2015) (Chapter 7, Fig 22) showing hosts rocks of this mineralization are only slightly higher metamorphic grade than where plagioclase is completely recrystallised.

In the Macraes Mine, however, the host rocks are significantly higher than plagioclase stability in the Otago Schist (shown in chapter 7, Fig. 22) and analyses of other Ca-silicate minerals shows no Eu anomaly in any of the phases (Fig. 37A). Thus at Macraes Mine, Eu anomalies are likely a result of the fluid being reduced. This is consistent with the previously discussed occurrence of graphite and low Mo concentrations in scheelite at Macraes Mine, and throughout the Otago Schist.

8.6.4 Mass of W Mobilized from the Recrystallization of Detrital Rutile to Metamorphic Titanite

The mass of metals (Au, As, Hg, and Sb) and fluids (metamorphic H_2O) produced per ton of rock metamorphosed from protolith to amphibolite facies has previously been calculated using whole-rock metal concentrations by Pitcairn et al. (2014) for the Otago and Alpine Schists (Table 8). These values were applied by Pitcairn et al. (2014) to calculate the volume of source rock required for the Macraes deposit with calculated volumes of amphibolite facies source rock ranging from 0.5 km^3 for Ag to 41 km^3 for Au. The mass-balance was applied to the currently active Southern Alps of New Zealand in order to quantify the metals mobilized during active orogenesis (Pitcairn et al. 2014). Results showed that from the advection of a 10 km wide and 5 km deep section of starting material through an orogeny at a rate of 0.01 m/yr for 1 Myrs, over 1,127 t Au, 10.1 Mt As, 47,000 t Hg, 560,000 t Sb, and 14,000 Mt H_2O were mobilized (Pitcairn et al. 2014) (Table 8). The mass of W produced from the complete conversion of rutile to titanite is easily calculated (Table 8), using a mass-balance reaction (Equation 4 in Table 8) involving only the critical elements in Equation 3. Assuming rutile has a mean W concentration of 830 ppm and metamorphic titanite 76.7 ppm [Cave et al. 2015 (Chapter 7)], together with a conservative rutile volume abundance of 0.1% [based on computer processing of backscatter

electron mount scans and W concentrations in protolith samples from Pitcairn et al. (2006)], a source rock density of 2.7 t/m^3 and rutile density equaling 4.23 t/m^3; approximately 0.41 g of W is released per ton of rock that has undergone the complete conversion of rutile to titanite (Table 8). These results are similar to those reported in Pitcairn et al. (2006) based on whole-rock concentrations. Advection of the same volume/mass of source rocks as per Pitcairn et al. (2014) for 1 Myrs would result in excess of 553,500 t of W being mobilized from the recrystallization of rutile to titanite (Table 8). It is clear that not all the mobilized metals find their way into orogenic deposits in the Otago Schist. Significantly more metal is mobilized during orogenesis of the whole Otago Schist, or the whole of the currently active Southern Alps than is observed trapped in deposits, and efficient fluid focusing and chemical trapping are perhaps more important controls on the formation of orogenic deposits than other factors, for example, the composition of the source rocks [for example, Pitcairn et al. (2014)].

Table 8. Mass-balance parameters and calculated W produced from the advection of a 10 km wide × 5 km deep section of starting material (source rock) through an orogeny (and complete conversion of rutile to titanite) at a rate of 0.01 m/yr for 1, 2, 3, 4, and 5 Myrs. Shown below for comparison are the calculated masses of mobilized Au, As, Hg, Sb, and H_2O, that Pitcairn et al. (2014) calculated using the same source area, orogeny rate, and periods of time as was used in this chapter when calculating the mass of W produced from the source area.

Mass-balance parameters and results:

Equation 4 $100\ g\ TiO_2 + 70.2\ g\ CaO + 75.23\ g\ SiO_2 \leftrightarrow CaSiTiO_5$

Mass-balance	Unit	Value
Measured mean detrital rutile	ppm	830
Mean metamorphic titanite calculated from mean rutile composition and mass-balance equation	ppm	339

(Equation 4) (that is, a dilution factor of 2.45 being applied to the mean rutile composition)		
Measured mean metamorphic titanite	ppm	76.7
Calculated loss of W per 100g of rutile converted to metamorphic titanite	g	0.02623
Volume percent rutile in lowest metamorphic grade metasediments[1]	%	0.1
Rutile density	t/m^3	4.23
Source rock density[2]	t/m^3	2.7
Convergence rate[2]	m/yr	0.01
Source area length[2]	m	10,000
Source area depth[2]	m	5,000
Volume through orogen[2]	m^3/yr	500,000
Mass through orogen[2]	t/yr	1,350,000

[1]Conservative value based on scanning electron imaging and petrographic observations. [2] Same parameters used by Pitcairn et al. (2014)

Mass produced from rutile to titanite recrystallization reaction from source area (t/Myr)						
	(g/t)	1	2	3	4	5
W	**0.41**	**553,500**	**1,107,000**	**1,660,500**	**2,214,000**	**2,767,500**

Comparison against calculated values by Pitcairn et al. (2014) for other elements in the Otago Schist

Mass produced from source area passing through amphibolite facies metamorphism (t/Myr) from Pitcairn et al. (2014)						
	(g/t)	1	2	3	4	5
Au	0.0008	1,127	2,254	3,380	4,507	5,634
As	7.52	10,157,057	20,314,114	30,471,171	40,628,228	50,785,285
Hg	0.04	47,728	95,456	143,184	190,912	238,640
Sb	0.42	568,763	1,137,527	1,706,290	2,275,054	2,843,817
Met H_2O	10,581	1.4E + 10	2.9E + 10	4.3E + 10	5.7E + 10	7.1E + 10

8.6.5 Sources of W and Implications for Formation of Orogenic Au Deposits in the

Otago Schist

Systematic depletion of W in the metasedimentary rocks of the Otago Schist with increasing metamorphic grade has been previously reported (Breeding and Ague 2002; Pitcairn et al. 2006), with the major W depletion event in the Otago Schist occurring between subgreenschist and greenschist facies conditions (Breeding and Ague 2002). Results from this chapter show that this depletion is caused by W liberation due to recrystallization of detrital rutile to the metamorphic titanite (Fig. 36) [Cave et al. 2015 (Chapter 7)], with the mass-balance calculation above indicating that over 1,100t of W is mobilized from every km^3 of subgreenschist facies rock metamorphosed to higher grades (Table 8). The W liberated by breakdown of rutile is shown to move away from the rutile grains (Figs. 33, 34) and is related to the development of scheelite micrograins (for example, Fig. 35A). With increasing metamorphism, the scheelite becomes incorporated into syn-metamorphic veins that form as a result of localized (up to tens of meters) advection of fluid and silica from local diffusion of material, and from the wall rock (Cox 1993; Pitcairn et al. 2014). These syn-metamorphic veins are well documented in the Otago Schist, with their abundance increasing to their maximum concentration in the lower greenschist facies (Cox 1993). As the metamorphic grade increases, these veins are observed being increasingly deformed and recrystallized (Figs. 35E, F), eventually being incorporated in the coarse-grained, segregated amphibolite facies schist rocks (Craw and Norris 1991; Cox 1993; Pitcairn et al. 2006, 2014). As is suggested for Au (Pitcairn et al. 2014), W in the form of scheelite that was mobilized into these veins, would be finally removed from the rock by metamorphic fluids produced at the greenschist and amphibolite transition (Pitcairn et al. 2014). As such, the reaction that mobilizes W from rutile occurs between subgreenschist and greenschist facies, but W is finally removed from the rock by

dissolution of scheelite in deformed recrystallized veins by fluids produced at the greenschist-amphibolite facies phase boundary.

Focusing of these metal-rich metamorphic fluids to shallower levels through the regionally extensive Hyde–Macraes Shear Zone resulted in the formation of the Macraes Mine (Craw 2002; Pitcairn et al. 2014), with Au-scheelite stockwork veins forming as a result of local extensional-shears resulting from the development of the through going shear (Begbie and Craw 2006). Consistent with the interpretations of Begbie and Craw (2006), trace element contents in scheelite suggest multiple pulses of W-bearing fluids causing incremental precipitation of scheelite in the stockwork veins at Macraes Mine (for example, Fig. 43). Wall-rock alteration and leaching of Sr, Y, and REEs (at high LREE/HREE) from the Ca-silicates titanite (Y and REEs) and epidote (Sr and REEs) by the W-rich fluid is thought to account for trace element differences between the late-metamorphic and syn-metamorphic scheelites (Figs. 37A, 40A, B, C, D, 41). Similar processes are suggested to have depleted wall rocks and enriched scheelite in Sr at the Glenorchy Scheelite Mine (Paterson and Rankin 1979).

Enrichments of both Au and W are common within the metal signatures of orogenic Au deposits within the Otago Schist. However, the relative concentration of the two elements varies significantly forming, for example, the Au-rich, W-poor mineralized veins of Bonanza, Shotover, and Nenthorn (Craw and Norris 1991) and the W-rich, Au-poor mineralized veins of Glenorchy, Paradise, and Bonnie Jean (Craw and Norris 1991) (Fig. 31). Potential explanations for this decoupling include 1) differences in the Au:W ratio in the metamorphic fluid produced at depth due to source rock compositional variation where, for example, Au-rich, W-poor deposits (for example, Bonanza, Shotover, and Nenthorn) may reflect an original sedimentary environment(s) with low rutile contents, or 2) variation in the efficiency of extraction of these elements from the

high grade rocks into the metamorphic fluid, or 3) variation in the conditions of formation of the mineralized veins (P, T, pH, redox, host-rock composition) which influence the deposition of either element, or 4) a combination of some or all of these factors. Further work is required to resolve this.

8.6.6 Potential Implications for Exploration

The application of indicator minerals to vector towards mineral deposits is a well-documented and routinely undertaken procedure in exploration for many styles of ore deposits including orogenic Au. Scheelite previously has been shown by McClenaghan et al. (2014) as being a useful indicator mineral for W-Mo skarns systems, with McClenaghan et al. (2014) utilizing scheelite grainsize fractions within till sediments to vector towards deposits of known W-Mo mineralization.

The geochemical differences (for example, Mo, Sr, Y, and REEs) between scheelite forming from local sources (syn-metamorphic scheelite) and those that were derived from the late-metamorphic focusing of fluids on a regional scale to lower crustal levels (Macraes scheelite) shown in this chapter could be a useful vector to Au mineralization. Combination of scheelite trace element geochemistry and the scheelite grain size fraction technique of McClenaghan et al. (2014), may prove to be a valuable tool in exploring for significant orogenic Au-W deposits in the Otago Schist: with scheelite geochemistry able to distinguish between formation via local process (likely to be uneconomical; for example, Lake Hāwea) and that which has formed from the focusing of fluids along regional structures to lower levels and interaction with wallrocks (potentially economical; for example, Macraes Mine), and the scheelite grain size fraction technique of McClenaghan et al. (2014) able to vector towards the source.

8.7 Conclusion

The orogenic Au deposits of the Otago Schist, New Zealand, are enriched in a variety of trace elements including W, Au, As, Ag, Hg, and Sb. Systematic depletions of W, Au, As, Ag, Hg, and Sb (along with others) in the metasedimentary rocks of the Otago Schist has previously been shown occurring with increasing metamorphic grade. Mobilization, and the source of Au, As, Ag, Hg, and Sb in the orogenic Au deposits of the Otago Schist, is ascribed to the recrystallization of metal-rich diagenetic pyrite to pyrrhotite with prograde metamorphism. A similar mineralogical source for W, prior to this chapter, however, was not constrained. This chapter shows detrital rutile is the mineralogical source for W (scheelite) in the orogenic Au deposits of the Otago Schist, with prograde metamorphic recrystallization (under subgreenschist to greenschist facies conditions) to titanite, releasing significant amounts of W (potentially 0.41 g per ton of rock). The development of scheelite in these rocks closely follows the progression of this W-liberating reaction, with scheelite micrograins formed early within the fabric of the rock. Scheelite is observed, with increasing metamorphism, being incorporated into locally derived metamorphic veins. These scheelite-bearing veins, with further increases in metamorphic grade, are increasingly deformed and recrystallized, and scheelite that was mobilized into these veins, would be removed from the rock by metamorphic fluids produced at the greenschist to amphibolite transition. Geochemically, scheelite from syn-metamorphic veins at Fiddlers Flat and Lake Hāwea displays distinct compositional differences, with scheelite from late metamorphic veins at the Macraes Mine enriched in REEs, Y, and Sr. Suggesting that the scheelite at Macraes became enriched due to liberation of these elements during alteration of Ca-silicate minerals by the ore forming fluid, with titanite (Y and REEs) and epidote (Sr and REEs) being the most important sources. These results are supportive of recent models for orogenic Au

mineralization in the Otago Schist whereby prograde metamorphic recrystallization of diagenetic or detrital metal-rich mineral phases (pyrite to pyrrhotite: Au, As, Ag, Hg, and Sb; rutile to titanite: W) releases significant amounts of metals into the concurrently developing metamorphic fluids that can be subsequently focused into regional structures and form significant W-bearing orogenic Au deposits.

References

BARABANOV, V. 1971. Geochemistry of tungsten. *International Geology Review*, 13**,** 332-344.

BEGBIE, M. & CRAW, D. 2006. Geometry and petrography of stockwork vein swarms, Macraes mine, Otago Schist, New Zealand. *New Zealand Journal of Geology and Geophysics*, 49**,** 63-73.

BISHOP, D. 1972. Progressive metamorphism from prehnite-pumpellyite to greenschist facies in the Dansey Pass area, Otago, New Zealand. *Geological Society of America Bulletin*, 83**,** 3177-3198.

BREEDING, C. M. & AGUE, J. J. 2002. Slab-derived fluids and quartz-vein formation in an accretionary prism, Otago Schist, New Zealand. *Geology*, 30**,** 499-502.

BRUGGER, J., LAHAYE, Y., COSTA, S., LAMBERT, D. & BATEMAN, R. 2000. Inhomogeneous distribution of REE in scheelite and dynamics of Archaean hydrothermal systems (Mt. Charlotte and Drysdale gold deposits, Western Australia). *Contributions to Mineralogy and Petrology*, 139**,** 251-264.

BRUGGER, J., MAAS, R., LAHAYE, Y., MCRAE, C., GHANDERI, M., COSTA, S., LAMBERT, D., BATEMAN, R. & PRINCE, K. 2002. Origins of Nd–Sr–Pb isotopic

variations in single scheelite grains from Archaean gold deposits, Western Australia. *Chemical Geology,* 182**,** 203-225.

BRUGGER, J., ETSCHMANN, B., POWNCEBY, M., LIU, W., GRUNDLER, P. & BREWE, D. 2008. Oxidation state of europium in scheelite: tracking fluid–rock interaction in gold deposits. *Chemical Geology,* 257**,** 26-33.

CAVE, B. J., STEPANOV, A. S., CRAW, D., LARGE, R. R., HAPLIN, J. A. & THOMPSON, J. 2015. Release of trace elements through the sub-greenschist facies breakdown of detrital rutile to metamorphic titanite in the Otago Schist, New Zealand. *The Canadian Mineralogist,* 53**,** 379-400.

CASTORINA, F., MASI, U., PADALINO, G. & PALOMBA, M. 2008. Trace-element and Sr-Nd isotopic evidence for the origin of the Sardinian fluorite mineralization (Italy). *Applied Geochemistry,* 23**,** 2906-2921.

COTTRANT, J. F. 1981. Cristallochimie et géochimie des terres rares dans la scheelite: application à quelques gisements français. *Unpublished Ph.D. thesis,* University of Paris, France.

COX, S. C. 1993. Veins, fluid, fractals, scale & schist: an investigation of fluid-rock interaction during deformation of the Torlesse Terrane, New Zealand. *Unpublished Ph.D. Thesis,* University of Otago, New Zealand.

CRAW, D. 1984. Lithologic variations in Otago Schist, Mt Aspiring area, northwest Otago, New Zealand. *New Zealand Journal of Geology and Geophysics,* 27**,** 151-166.

CRAW, D. 1992. Fluid evolution, fluid immiscibility and gold deposition during Cretaceous-Recent tectonics and uplift of the Otago and Alpine Schist, New Zealand. *Chemical Geology,* 98**,** 221-236.

CRAW, D. 1998 Structural boundaries and biotite and garnet ‘isograds’ in the Otago and Alpine Schists, New Zealand. *Journal of Metamorphic Geology,* 16**,** 395-402.

CRAW, D. 2002. Geochemistry of late metamorphic hydrothermal alteration and graphitisation of host rock, Macraes gold mine, Otago Schist, New Zealand. *Chemical Geology,* 191**,** 257-275.

CRAW, D. & NORRIS, R. J. 1991. Metamorphogenic Au-W veins and regional tectonics: Mineralisation throughout the uplift history of the Haast Schist, New Zealand. *New Zealand Journal of Geology and Geophysics,* 34**,** 373-383.

CRAW, D., WINDLE, S. & ANGUS, P. 1999. Gold mineralization without quartz veins in a ductile-brittle shear zone, Macraes Mine, Otago Schist, New Zealand. *Mineralium Deposita*, 34**,** 382-394.

CRAW, D., MACKENZIE, D. & PETRIE, B. 2004. Disseminated gold mineralisation in a schist-hosted mesothermal deposit, Macraes Mine, Otago, New Zealand [abs.]. *Proceedings of the PACRIM 2004 Congress, The Australasian Institute of Mining and Metallurgy Publication series*, 2004. 135-141.

CRAW, D., BEGBIE, M. & MACKENZIE, D. 2006 Structural controls on Tertiary orogenic gold mineralization during initiation of a mountain belt, New Zealand. *Mineralium Deposita*, 41**,** 645-659.

DE RONDE, C. E. J., FAURE, K., BRAY, C. J. & WHITFORD, D. J. 2000. Round Hill shear zone-hosted gold deposit, Macraes Flat, Otago, New Zealand: evidence of a magmatic ore fluid. *Economic Geology,* 95**,** 1025-1048.

DECKERT, H., RING, U. & MORTIMER, N. 2002. Tectonic significance of Cretaceous bivergent extensional shear zones in the Torlesse accretionary wedge, central Otago

Schist, New Zealand. *New Zealand Journal of Geology and Geophysics,* 45**,** 537-547.

DOSTAL, J., KONTAK, D. & CHATTERJEE, A. K. 2009. Trace element geochemistry of scheelite and rutile from metaturbidite-hosted quartz vein gold deposits, Meguma Terrane, Nova Scotia, Canada: genetic implications. *Mineralogy and Petrology,* 97**,** 95-109.

EVENSEN, N., HAMILTON, P. J. & O'NIONS, R. 1978. Rare-earth abundances in chondritic meteorites. *Geochimica Cosmochimica Acta,* 42**,** 1199-1212.

FARMER, L., PALIN, M., MOORE, J., TEAGLE, D. A. H. & STIRLING, C. 2012. The geochemistry and isotopic signature of scheelite from the Macraes orogenic gold deposit. *AusIMM NZ Branch Annual Conference, Rotorua, New Zealand,* 2012**,** 145-153.

GHADERI, M., PALIN, J. M., CAMPBELL, I. H. & SYLVESTER, P. J. 1999. Rare earth element systematics in scheelite from hydrothermal gold deposits in the Kalgoorlie-Norseman region, Western Australia. *Economic Geology,* 94**,** 423-437.

GOLDFARB, R. J. & GROVES, D. I. 2015. Orogenic gold: common or evolving fluid and metal sources through time. *Lithos,* 233**,** 2-26.

GOLDFARB, R. J., BAKER, T., DUBE, B., GROVES, D. I., HART, C. J. & GOSSELIN, P. 2005. Distribution, character, and genesis of gold deposits in metamorphic terranes. *Economic Geology 100th Anniversary Volume***,** 407-450.

GRAY, D. & FOSTER, D. 2004. 40Ar /39Ar thermochronologic constraints on deformation, metamorphism and cooling/exhumation of a Mesozoic accretionary wedge, Otago Schist, New Zealand. *Tectonophysics,* 385**,** 181-210.

GROVES, D. I., GOLDFARB, R. J., GEBRE-MARIAM, M., HAGEMANN, S. G. & ROBERT, F. 1998. Orogenic gold deposits: a proposed classification in the context of their crustal

distribution and relationship to other gold deposit types. *Ore Geology Reviews,* 13**,** 7-27.

HAAS, J. R., SHOCK, E. L. & SASSANI, D. C. 1995. Rare earth elements in hydrothermal systems: estimates of standard partial molal thermodynamic properties of aqueous complexes of the rare earth elements at high pressures and temperatures. *Geochimica Cosmochimica Acta*, 59**,** 4329-4350.

HEIMANN, A., SPRY, P. G. & TEALE, G. S. 2005 Zincian spinel associated with metamorphosed Proterozoic base-metal sulfide occurrences, Colorado: a re-evaluation of gahnite composition as a guide in exploration. *The Canadian Mineralogist*, 43**,** 601-622.

HENLEY, R., NORRIS, R. & PATERSON, C. 1976. Multistage ore genesis in the New Zealand geosyncline a history of post-metamorphic lode emplacement. *Mineralium Deposita,* 11**,** 180-196.

HENNE, A. & CRAW, D. 2012. Synmetamorphic carbon mobility and graphite enrichment in metaturbidites as a precursor to orogenic gold mineralisation, Otago Schist, New Zealand. *Mineralium Deposita*, 47**,** 781-797.

HENNE, A., CRAW, D. & MACKENZIE, D. 2011. Structure of the Blue Lake Fault Zone, Otago Schist, New Zealand. *New Zealand Journal of Geology and Geophysics*, 54**,** 311-328.

LAIRD, M. & BRADSHAW, J. 2004. The break-up of a long-term relationship: the Cretaceous separation of New Zealand from Gondwana. *Gondwana Research,* 7**,** 273-286.

LANDIS, C., CAMPBELL, H., BEGG, J., MILDENHALL, D., PATERSON, A. M. & TREWICK, S. 2008. The Waipounamu Erosion Surface: questioning the antiquity of the New Zealand land surface and terrestrial fauna and flora. *Geological Magazine,* 145**,** 173-197.

LARGE, R. R., BULL, S. W. & MASLENNIKOV, V. V. 2011. A carbonaceous sedimentary source-rock model for Carlin-type and orogenic gold deposits. *Economic Geology,* 106**,** 331-358.

LARGE, R., THOMAS, H., CRAW, D., HENNE, A. & HENDERSON, S. 2012. Diagenetic pyrite as a source for metals in orogenic gold deposits, Otago Schist, New Zealand. *New Zealand Journal of Geology and Geophysics,* 55**,** 137-149.

LITTLE, T. A., MORTIMER, N. & MCWILLIAMS, M. 1999. An episodic Cretaceous cooling model for the Otago-Marlborough Schist, New Zealand, based on 40Ar/39Ar white mica ages. *New Zealand Journal of Geology and Geophysics,* 42**,** 305-325.

MACKENZIE, D. & CRAW, D. 2005. Structural and lithological continuity and discontinuity in the Otago Schist, Central Otago, New Zealand. *New Zealand Journal of Geology and Geophysics,* 48**,** 279-293.

MACKINNON, T. C. 1983. Origin of the Torlesse terrane and coeval rocks, South Island, New Zealand. *Geological Society of America Bulletin,* 94**,** 967-985.

MCCLENAGHAN, B., SEAMAN, A., PARKHILL, M. & PRONK, A. 2014. Till geochemical signatures associated with the Sisson W-Mo deposit, New Brunswick, Canada. *Atlantic Geology,* 50**,** 116-137.

MCDONOUGH, W. F. & SUN, S. S. 1995. The composition of the Earth. *Chemical Geology,* 120**,** 223-253.

MCKEAG, S., CRAW, D. & NORRIS, R. 1989. Origin and deposition of a graphitic schist-hosted metamorphogenic Au-W deposit, Macraes, East Otago, New Zealand. *Mineralium Deposita,* 24**,** 124-131.

MIGDISOV, A. A., WILLIAMS-JONES, A. & WAGNER, T. 2009. An experimental study of

the solubility and speciation of the Rare Earth Elements (III) in fluoride-and chloride-bearing aqueous solutions at temperatures up to 300 C. *Geochimica et Cosmochimica Acta,* 73**,** 7087-7109.

MORTENSEN, J. K., CRAW, D., MACKENZIE, D. J., GABITES, J. E. & ULLRICH, T. 2010. Age and origin of orogenic gold mineralization in the Otago Schist Belt, South Island, New Zealand: constraints from lead isotope and 40Ar/39Ar Dating Studies. *Economic Geology,* 105**,** 777-793.

MORTIMER, N. 2000. Metamorphic discontinuities in orogenic belts: example of the garnet–biotite–albite zone in the Otago Schist, New Zealand. *International Journal of Earth Sciences,* 89**,** 295-306.

MUTCH, A. R. 1969. The Scheelite Resources of the Glenorchy District West Otago, New Zealand. *New Zealand Geological Survey Report,* 40**,** 68 p.

OCEANA GOLD. 2015. Updated resource & reserve statement March 2015. *OceanaGold,* https://www.oceanagold.com/wp-content/uploads/OceanaGold-Announces-Updated-Resource-Reserve-Statement.pdf. Accessed 7th April 2016.

PATERSON, C. J. 1982. Oxygen isotopic evidence for the origin and evolution of a scheelite ore-forming fluid, Glenorchy, New Zealand. *Economic Geology,* 77**,** 1672-1687.

PATERSON, C. J. 1986. Controls on gold and tungsten mineralization in metamorphic-hydrothermal systems, Otago, New Zealand. *Geological Association of Canada Special Paper,* 32**,** 25-39.

PATERSON, C. J. & RANKIN, P. C. 1979. Trace element distribution in the schist surrounding a quartz-scheelite lode, Glenorchy, New Zealand. *New Zealand Journal of Geology and Geophysics,* 22**,** 329-338.

PENG, J., ZHANG, D., HU, R., WU, M., LIU, X., QI, L. & YU, Y. 2010. Inhomogeneous distribution of rare earth elements (REEs) in scheelite from the Zhazixi W-Sb Deposit, Western Hunan and its geological implications. *Geological Review,* 56**,** 810-819.

PETRIE, B., CRAW, D. & RYAN, C. 2005. Geological controls on refractory ore in an orogenic gold deposit, Macraes mine, New Zealand. *Mineralium Deposita,* 40**,** 45-58.

PHILLIPS, G. N. & GROVES, D. I. 1983. The nature of Archaean gold-bearing fluids as deduced from gold deposits of Western Australia. *Journal of the Geological Society of Australia,* 30**,** 25-39.

PITCAIRN, I. K. 2004. Sources of fluids and metals in orogenic gold deposits: the Otago Schists, New Zealand. *Unpublished Ph.D. Thesis,* University of Southhampton, United Kingdom.

PITCAIRN, I. K., TEAGLE, D. A. H., CRAW, D., OLIVO, G. R., KERRICH, R. & BREWER, T. S. 2006. Sources of Metals and Fluids in Orogenic Gold Deposits: Insights from the Otago and Alpine Schists, New Zealand. *Economic Geology,* 101**,** 1525-1546.

PITCAIRN, I. K., OLIVO, G. R., TEAGLE, D. A. H. & CRAW, D. 2010. Sulfide evolution during prograde metamorphism of the Otago and Alpine Schists, New Zealand. *The Canadian Mineralogist,* 48**,** 1267-1295.

PITCAIRN, I. K., CRAW, D. & TEAGLE, D. A. 2014. The gold conveyor belt: large-scale gold mobility in an active orogen. *Ore Geology Reviews,* 62**,** 129-142.

PITCAIRN, I. K., CRAW, D. & TEAGLE, D. A. 2015a. Metabasalts as sources of metals in orogenic gold deposits. *Mineralium Deposita, 50***,** 373-390.

PITCAIRN, I., SKELTON, A. & WOHLGEMUTH-UEBERWASSER, C. 2015b. Mobility of gold during metamorphism of the Dalradian in Scotland. *Lithos,* 233**,** 69-88.

RATTENBURY, M. & ISAAC M. 2012. The QMAP 1: 250 000 geological map of New Zealand project. *New Zealand Journal of Geology and Geophysics,* 55**,** 393-405.

RAIMBAULT, L., BAUMER, A., DUBRU, M., BENKERROU, C., CROZE, V. & ZAHM, A. 1993. REE fractionation between scheelite and apatite in hydrothermal conditions. *American Mineralogist,* 78**,** 1275-1285.

REMPEL, K. U., WILLIAMS-JONES, A. E. & MIGDISOV, A. A. 2009. The partitioning of molybdenum (VI) between aqueous liquid and vapour at temperatures up to 370 C. *Geochimica et Cosmochimica Acta,* 73**,** 3381-3392.

ROBERTS, S., PALMER, M. R. & WALLER, L. 2006. Sm-Nd and REE characteristics of tourmaline and scheelite from the Björkdal gold deposit, northern Sweden: evidence of an intrusion-related gold deposit? *Economic Geology,* 101**,** 1415-1425.

SMITH, M. & YARDLEY, B. 1999. Fluid evolution during metamorphism of the Otago Schist, New Zealand: (II) influence of detrital apatite on fluid salinity. *Journal of Metamorphic Geology,* 17**,** 187-194.

SONG, G., QIN, K., LI, G., EVANS, N. J. & CHEN, L. 2014. Scheelite elemental and isotopic signatures: implications for the genesis of skarn-type W-Mo deposits in the Chizhou area, Anhui Province, eastern China. *American Mineralogist,* 99**,** 303-317.

STALLARD, A. & SHELLEY, D. 2005. The initiation and development of metamorphic foliation in the Otago Schist, Part 1: competitive oriented growth of white mica. *Journal of Metamorphic Geology,* 23**,** 425-442.

SYLVESTER, P. J. & GHADERI, M. 1997. Trace element analysis of scheelite by excimer laser ablation-inductively coupled plasma-mass spectrometry (ELA-ICP-MS) using a synthetic silicate glass standard. *Chemical Geology,* 141**,** 49-65.

TSAY, A., ZAJACZ, Z. & SANCHEZ-VALLE, C. 2014. Efficient mobilization and fractionation of rare-earth elements by aqueous fluids upon slab dehydration. *Earth and Planetary Science Letters,* 398**,** 101-112.

TURNBULL, I. 1979. Petrography of the Caples terrane of the Thomson Mountains, northern Southland, New Zealand. *New Zealand Journal of Geology and Geophysics,* 22**,** 709-727.

TURNBULL, I., MORTIMER, N. & CRAW, D. 2001. Textural zones in the Haast Schist—a reappraisal. *New Zealand Journal of Geology and Geophysics,* 44**,** 171-183.

WILLIAMS-JONES, A. E., MIGDISOV, A. A. & SAMSON, I. M. 2012. Hydrothermal mobilisation of the rare earth elements–a tale of "ceria" and "yttria". *Elements,* 8**,** 355-360.

WILLIAMSON, J. H. 1939. The geology of the Naseby subdivision, Central Otago, New Zealand. *New Zealand Geological Survey Bulletin,* 39**,** 141 p.

WOOD, B. 1983. Widespread scheelite in Mesozoic schists of South Island, New Zealand [abs.]. *In: Proceedings and Abstracts, Pacific Science Congress,* 1983**,** 258.

YARDLEY, B. D. 1982. The early metamorphic history of the Haast Schists and related rocks of New Zealand. *Contributions to Mineralogy and Petrology,* 81**,** 317-327.

Chapter 9: THE SOURCE OF W IN TURBIDITE-HOSTED OROGENIC AU MINERALIZATION: IMPLICATIONS FOR METAMORPHIC PROCESSES AND METAL SOURCES IN THE MEGUMA (CAN) AND BENDIGO-BALLARAT (AUS) TERRANES

9.1 Abstract

Turbidite-hosted orogenic Au deposits are commonly enriched in W, along with a variety of other trace elements including As, Ag, Hg, and Sb. Previous research on metal sources for these deposits has defined the sources for most of these metals. Sources are well-constrained for Au, As, Ag, Hg, and Sb, with the metamorphic recrystallization of sedimentary pyrite (to metamorphic pyrrhotite) having been shown to mobilize these metals. The mineralogical source for W, however, is not so well-constrained. Recently, the recrystallization of detrital rutile (to metamorphic titanite) has been shown to mobilize and be the source of W in the turbidite-hosted orogenic Au deposits of the Otago Schist, New Zealand. In this chapter, the rigor of the recent source model for W in the turbidite-hosted orogenic Au mineralization of the Otago Schist (Chapter 8) is evaluated, through investigating the availability of W through prograde metamorphic mineral recrystallization in two additional turbidite-hosted orogenic Au provinces; one containing orogenic Au mineralization with associated subordinate W (Meguma Terrane, Canada) and the other containing orogenic Au mineralization without associated W (Bendigo-Ballarat Terrane, Australia). Similar to the Otago Schist, in both of these terranes, detrital rutile

is identified as being the most important host mineral for W in the lowest metamorphic grade rocks, and its prograde metamorphic recrystallization (to ilmenite) releases significant amounts of W (1.9 g and 0.18 g of W per ton of rock, Meguma Terrane and Bendigo-Ballarat Terrane, respectively). This release of W in the Meguma Terrane is likely the source of W in the orogenic Au deposits. The lack of W in the orogenic Au deposits of the Bendigo-Ballarat Terrane might reflect the Au in these deposits as being sourced from lower greenschist facies metasediments (Castlemaine metasediments), and potentially precludes previous models that have suggested source rocks for Au in these deposits as being either Castlemaine metasediments at the greenschist-amphibolite transition or underlying Cambrian volcano-sedimentary rocks. However, the lack of scheelite in the Bendigo-Ballarat Terrane could also result from other factors, such as variations in the conditions of formation of the mineralized veins (P, T, pH, redox, host-rock composition) that may not favor the transport and/or precipitation of W. These factors were unable to be resolved in this study. Results presented within this study are supportive of recent models for turbidite-hosted orogenic Au mineralization, whereby prograde metamorphic recrystallization of diagenetic or detrital metal-rich mineral phases [pyrite to pyrrhotite, Au, As, Ag, Hg, and Sb; rutile to titanite (Chapter 8) or ilmenite (this chapter), W] can release significant amounts of these metals into the concurrently developing metamorphic fluids that can be subsequently focused into regional structures and form orogenic Au ± W deposits.

9.2 Introduction

Turbidite-hosted orogenic Au deposits are a well-studied, important source for global Au (Phillips and Groves 1983; Craw 1992; Groves et al. 1998; Goldfarb et al. 2005). Typically, turbidite-hosted orogenic Au deposits are enriched in a characteristic suite of elements including

As, Ag, Sb, Te, W, Mo, and Bi, and also contain notably low base-metal contents (Goldfarb and Groves 2015, and references therein). Various models have been proposed to account for the source(s) of these metal enrichments, with recent studies conducted in the Otago Schist of New Zealand providing compelling evidence for a coherent metamorphic source model for these deposits [Pitcairn et al. 2006, 2010, 2014, 2015a; Large et al. 2012; Cave et al. accepted (Chapter 8)]. The sources for Au, As, Ag, Hg, Sb, and W, are well-constrained in the Otago Schist, with metamorphic recrystallization of diagenetic/ detrital metal-rich mineral phases such as pyrite to pyrrhotite, and rutile to titanite releasing significant amounts of Au, As, Ag, Hg, and Sb, and W, respectively [Pitcairn et al. 2010; Large et al. 2012; Cave et al. accepted (Chapter 8)]. Several studies conducted in other turbidite-dominated orogenic belts around the world, have reported similar trace element depletions associated with prograde metamorphism (for example, Dalradian Orogeny, Scotland; Pitcairn et al. 2015b) and trace element releases during the conversion of diagenetic pyrite to pyrrhotite (for example, the Bendigo-Ballarat Terrane, Australia; Large et al. 2009, 2011; Thomas et al. 2011), suggesting that turbidite-hosted Au deposits are formed by similar processes and metals sources. However, the same attention has not been afforded to the source of W, and the reason(s) why some Au deposits are enriched in W while others are not.

The availability of W through prograde metamorphic mineral recrystallization was identified by Cave et al. [accepted (Chapter 8)] as being crucial in the formation of W bearing mineralization in the Otago Schist. In this chapter, the availability of W during prograde metamorphic mineral recrystallization is assessed in two additional turbidite-hosted orogenic Au provinces, one containing orogenic Au mineralization with associated subordinate W (Meguma Terrane) and the other containing orogenic Au mineralization without associated W (Bendigo-

Ballarat Terrane). This approach is taken to investigate if protolith mineralogy and recrystallization mineral reactions control the presence or absence of W in turbidite-hosted orogenic mineralization world-wide. Similar to the investigation of Cave et al. [accepted (Chapter 8)], laser ablation inductively coupled plasma mass spectrometry (LA-ICP-MS) traverses are undertaken on low metamorphic grade and high metamorphic grade samples (from both terranes) to evaluate the distribution of W amongst mineral phases, and subsequently quantitative LA-ICP-MS spot analyzes are performed on the major W-bearing mineral phases to characterize trace element concentrations in them. Petrological observations of the W-host phases are combined with the quantitative spot analyzes to perform simple mass-balance calculations to assess the significance of any potential liberation of W. Implications for the source of metals in Meguma and Bendigo-Ballarat terranes is subsequently discussed in light of these observations, as are the implications on the source of metals in turbidite-hosted orogenic Au deposits. A key assumption in this study is that the orogenic systems in the Meguma (CAN) and Bendigo-Ballarat (AUS) terranes, formed via similar processes to those in the Otago Schist (NZ).

9.3 Geological Setting

The Meguma and Bendigo-Ballarat terranes are located in southern Nova Scotia, eastern Canada and central Victoria, southeastern Australia, respectively (Figs. 44, 45). These terranes formed as a result of accretionary processes along the active continental margins of Gondwana (Bierlein et al. 2004), and share many similarities with the Mesozoic accretionary Otago Schist of southern New Zealand. Orogenic Au is recognized in both terranes, with hard-rock Au production from the Bendigo-Ballarat Terrane being the most significant (791 t; Wilde 1989), while subordinate

hard-rock Au production is also recorded in the Meguma Terrane (47 t; Ryan and Smith 1998). Tungsten in the form of scheelite is present in orogenic mineralization in the Meguma Terrane and previously during periods of high metal prices and/or strategic value, W was exploited from these deposits (< 62 t; Fisher 1984). Tungsten enrichments are not recognized in orogenic Au mineralization in the Bendigo-Ballarat Terrane, other than in those that have undergone post-tectonic intrusion-related modification (for example, Maldon; Ciobanu et al. 2010, Fu et al. 2014).

9.3.1 Meguma Terrane

The Meguma Terrane of southern Nova Scotia, eastern Canada, is the most outboard terrane of the Canadian Appalachian Orogen (Fig. 44) (Murphy et al. 2009; White and Barr 2010) and is separated from the adjacent but non-correlatable peri-Gondwanan Avalon Terrane by the east to west trending Cobequid-Chedabucto Fault Zone or Minas Fault Zone (Fig. 44) (Murphy et al. 2009). The Meguma Terrane is composed of a thick (~11–13 km) sequence of variably metamorphosed early Cambrian (Terreneuvian, but the base is not exposed) to early Ordovician (Floian) turbiditic metasandstone and slate (Goldenville and Halifax Groups), and a much thinner sequence of Early Silurian to Early Devonian slate, quartzite, and metavolcanic rocks (Rockville Notch Group) (White 2008, 2010; White and Barr 2010, 2012; White et al. 2012; Pothier et al. 2015). These rocks were deformed and metamorphosed during the Early to Middle Devonian Neoacadian Orogeny, and intruded by numerous, late syn- to post-tectonic, mainly Middle to Late Devonian, peraluminous granitic plutons (for example, South Mountain Batholith) (Clarke and Carruzzo 2007; White and Barr 2010).

The early Cambrian to lower Ordovician metasedimentary rocks are divisible into two principle units: the lower turbiditic Goldenville Group composed of dominantly metasandstone

with subordinate metasiltsone, and slate, and the overlying Halifax Group that is dominated by metamorphosed black mudstones, with subordinate fine-grained metasandstone and metasiltstone (White 2008; White and Barr 2010; Hilchie and Jamieson 2014). Both of these Groups have been subdivided into regionally mappable formations and the previous establishment of a metal-rich transitional zone between the Goldenville and Halifax Groups (for example, Zentilli et al. 1986) was shown to be incorrect (White 2010; White and Barr 2010, 2012; Pothier et al. 2015).

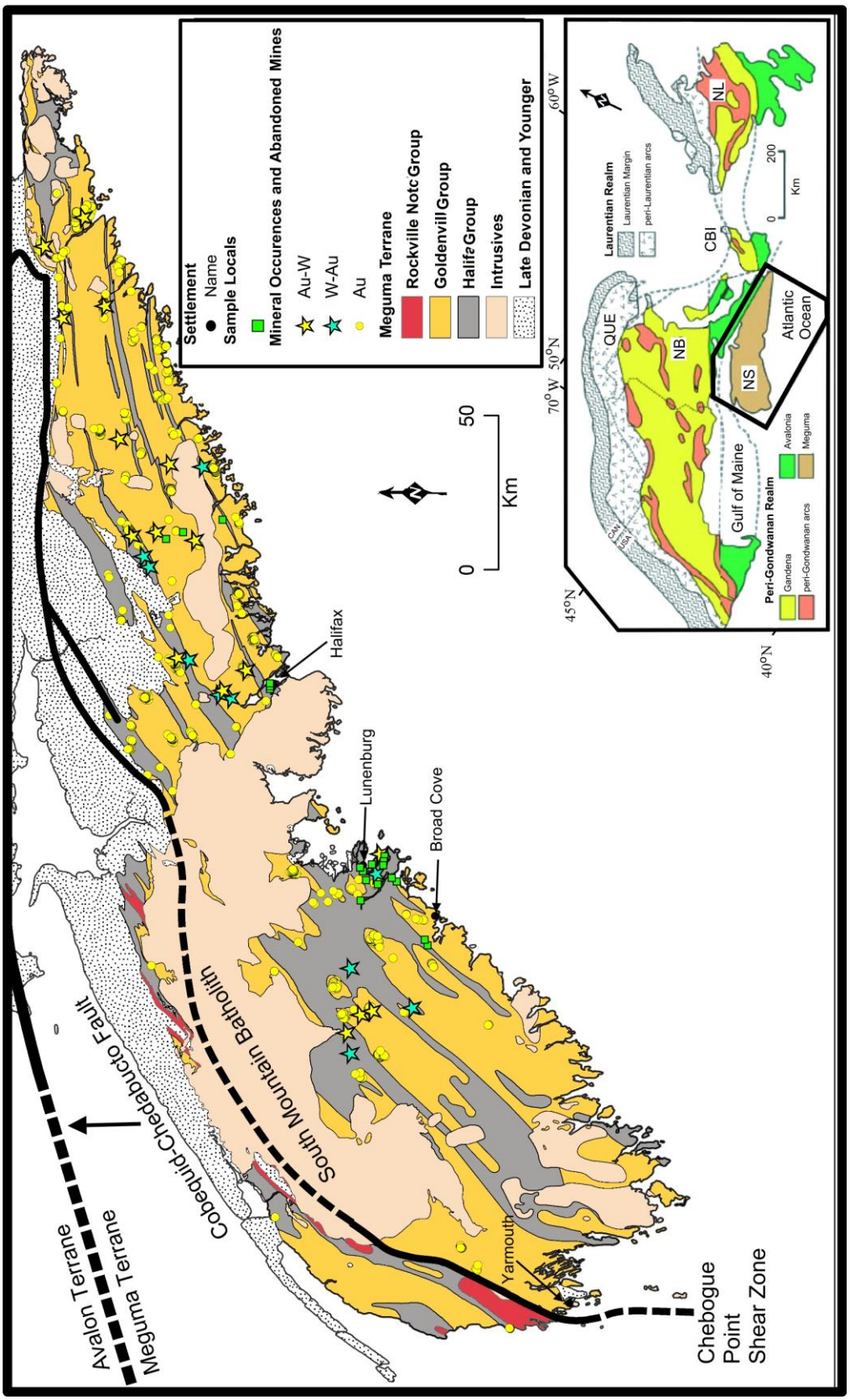
Settlement
Name
Sample Locals
Mineral Occurences and Abandoned Mines
Au-W
W-Au
Au
Meguma Terrane
Rockville Notch Group
Goldenville Group
Halifax Group
Intrusives
Late Devonian and Younger
Halifax
Lunenburg
Broad Cove
Yarmouth
South Mountain Batholith
Cobequid-Chedabucto Fault
Avalon Terrane
Meguma Terrane
Chebogue Point Shear Zone
0
50
Km
70° W
50°N
60° W
45°N
40°N
QUE
NB
NS
NL
CBI
Gulf of Maine
Atlantic Ocean
Laurentian Realm
Laurentian Margin
peri-Laurentian arcs
Peri-Gondwanan Realm
Gandena
peri-Gondwanan arcs
Avalonia
Meguma
0
200
Km

Fig. 44. Regional geology of the Meguma Terrane, showing: selected settlements, sample locations, major lithoteconic units, and orogenic mineral occurrences. Modified from White and Barr (2012), and references therin.

Horne and Pelley (2006) suggested that gold districts occur throughout the Goldenville and Halifax Groups, with no indication that stratigraphic position has any control in their distribution. Instead, they concluded that the key factor in gold mineralization is the presence of tight fold hinges. Such anticlinal hinges are more common in the Goldenville Group than in the overlying Halifax Group at the current level of exposure, and hence so are the gold districts. In contrast, some stratigraphic control of gold districts is suggested by comparing their distribution to the stratigraphy established by White (2010) and White and Barr (2012), where numerous Au ± W showings are located in the upper part of the Goldenville Group (White and Barr 2012).

The Goldenville, Halifax, and Rockville Notch Groups were regionally metamorphosed and deformed during the Neoacadian Orogeny. Traditionally, this event was considered to be part of the Acadian Orogeny (for example, Keppie and Dallmeyer 1995; Culshaw and Lee 2006) but has been renamed to distinguish the deformation and metamorphism observed in the Meguma Terrane from that related to the older and probably unrelated Acadian Orogeny that occurred elsewhere in the northern Appalachian Orogen (Hibbard et al. 2007; White and Barr 2012). Detailed radiometric studies indicate that the regional deformation and greenschist facies metamorphism associated with the Neoacadian Orogeny occurred between approximately 406-388 Ma (Reynolds et al. 1973; Muecke et al. 1988; Kontak et al. 1998; Hicks et al. 1999; Morelli et al. 2005) during the docking of the Meguma Terrane with Avalonia.

Regional metamorphic grade varies across the Meguma Terrane and ranges from lower greenschist to amphibolite facies (Jamieson et al. 2012), equivalent to peak metamorphic conditions of approximately 500 °C and 3–8 kbar (Taylor and Schiller 1966). Deformation was

associated with regional metamorphism and produced a series of N-S and NE-SW-trending, chevron- and box-style, upright folds with wavelengths approximately 1,000-2,000 m (Horne and Culshaw 2001; Culshaw and Lee 2006; White and Barr 2010; Hilchie and Jamieson 2014). Accompanying this phase of folding was the development of a strong, axial-planar, slaty cleavage (S1) in the fine-grained slate and metasiltstones, and a spaced (disjunctive) solution cleavage in metasandstone (Hilchie and Jamieson 2014).

These regional structures and related metamorphism were overprinted locally by contact metamorphism up to hornblende-hornfels facies around the late syn- to post-tectonic (with respect to the Neoacadian Orogeny) South Mountain Batholith and other smaller plutons (Jamieson et al. 2012; White and Barr 2012). In addition, younger thermal and deformational events are locally recorded, mainly associated with shear zones at approximately 370 Ma and 325 (White and Barr 2012) and there is evidence for post-intrusive flexural slip folding coaxial with the earlier folds (Horne and Culshaw 2001; Hilchie and Jamieson 2014).

Titanium-rich minerals ilmenite, rutile, and anatase are locally abundant in the Goldenville and Halifax Groups (up to 8, 2, and 4 %, respectively; Haysom et al. 1997; Pelley 2007). Clarke and Carruzzo (2007) on describing rutile morphologies in the Goldenville and Halifax Groups metasediments separated them into four varieties: (1) an anhedral to subhedral poikilitic variety (Rt M1), (2) a variety in complex intergrowth with ilmenite, (3) an anhedral variety with a distinctive “fingerprint” texture (Rt M3), and (4) a blocky, subhedral, inclusion-poor (Rt M4). Similarly, Clarke and Carruzzo (2007) separated ilmenite into three varieties based on their morphologies in Goldenville and Halifax Groups metasediments: (1) a variety characterized by abundant inclusions (Ilm M1), (2) a variety with complex intergrowths with rutile (Ilm M2), and (3) a variety with a fingerprint” texture (Ilm M3). Similarities between the

texture of rutile and ilmenite grains are acknowledged by Clarke and Carruzzo (2007) as is the possibility that these represent different stages of recrystallization reactions (for example, Rt M1 recrystallizing to Rt M2 /Ilm M2). Haysom et al. (1997) in describing ilmenite grains in the Meguma metasediments, suggests the most common variety of ilmenite grains are observed as lathes (ranging between 500– 5,000µm) of which are envisaged as forming prior-to or contemporary with regional prograde metamorphism, as evidenced by alignment of lathes parallel to cleavage (Haysom et al. 1997). A transition from rutile to ilmenite in Cunard Formation (Halifax Group) rocks has previously been documented in the contact aureole surrounding the intrusion of the Halifax Pluton (South Mountain Batholith) at approximately the biotite-in isograd (Hilchie and Jamieson 2014), and by Taylor and Schiller (1966) at the transition of lower (chlorite) to upper (biotite) greenschist facies affected by regional metamorphism. Anatase is also recognized in the Cunard Formation (Halifax Group) in a variety of different morphologies. Fine-grained aggregates of anatase are observed replacing ilmenite after peak metamorphism (Haysom et al. 1997). Anhedral to subhedral anatase crystals occurring in fine-grained aggregates are also recognized in the Cunard Formation (Halifax Group), these fine-grained aggregates are often found in contact (commonly mantling) with or inside sulfide minerals, and are envisaged to reflect excess TiO_2 during regional prograde metamorphism (Haysom et al. 1997).

Orogenic type Au -mineralization is widespread throughout the greenschist facies Goldenville and Halifax Groups rocks of the Meguma Terrane, with over 60 past-producing orogenic-type Au mines (Fig. 44) (Kontak et al. 1990, 2001; Horne and Culshaw 2001; Morelli et al. 2005). Two styles of orogenic-type mineralization are recognized in the Meguma Terrane; these being vein Au deposits (for example, the Ovens Au district and the Dufferin Mine) and

disseminated Au deposits (for example, Tourquoy Deposit), of which vein-style Au deposits form the overwhelming majority of the orogenic-type Au occurrences (Morelli et al. 2005) and are the focus of this chapter. Both styles of mineralization are observed having a strong structural control and occur within or in close proximity to anticlinal fold hinges and one another (Kontak et al. 1990, 2001; Horne and Culshaw 2001; Morelli et al. 2005; Horne and Pelley 2006).

Radiometric age dating ($^{40}Ar/^{39}Ar$) obtained from vein-filled amphibole and mica, from several orogenic-type Au deposits in the Meguma Terrane most commonly yields ages between 380 and 362 Ma (for example, Kontak et al. 1990, 1993, 1998), which coincides with regional plutonism in the Meguma Terrane. Recent Re-Os age dates obtained by Morelli et al. (2005) from arsenopyrite grains in auriferous veins from two Au occurrence (The Ovens and the Dufferin Mine), have yielded two discrete ages broadly coincident with regional Neoacadian metamorphism (The Ovens, 407 ± 4 Ma) and the intrusion South Mountain Batholith (Dufferin Mine, 380 ± 3 Ma), indicating that at least two discrete ages of auriferous vein emplacement have occurred in the Meguma Terrane, potentially recording episodic mineralization or remobilization over a period of some 15 to 30 Ma (Morelli et al. 2005; Sangster and Smith 2007).

Vein Au deposits are predominantly comprised of quartz with subordinate amounts of various carbonates and sulfides [arsenopyrite (dominant), pyrite, pyrrhotite, chalcopyrite, and galena ± sphalerite and molybdenite], together with rare chlorite, albite, muscovite, biotite, amphibole, tourmaline, garnet, epidote, rutile, scheelite, gold, and Bi-Ag tellurides (Kontak et al. 1993; Kontak and Smith 1993; Morelli et al. 2005; Dostal et al. 2009). Scheelite, although not currently recognized as a mineral of economic significance in the Meguma Terrane, is observed as a trace or accessory mineral phase in at least 26 orogenic-type vein Au occurrences

throughout the Meguma Terrane. Scheelite mineralization is most commonly observed within bedding concordant veins (flexural-slip, buckled, and saddle reefs) that are located near the crest of a large anticline or along the limbs of a large anticline, or both. Scheelite, however, is also noted as occurring within bedding-discordant veins at numerous locations (Fisher, 1984). Scheelite has been documented to occur in Ca-silicate nodules in southwestern Nova Scotia and has been attributed to skarnitization related to hydrothermal alteration from adjacent plutonic units (for example, Chatterjee and Keppie 1981) or fluids related to regional metamorphism (Reid 2005). Timing of scheelite mineralization relative to other vein minerals is contentious with arguments for both early (Miller 1974; Miller et al. 1976; Fisher 1984) and late (Kontak and Smith 1993; Dostal et al. 2009) precipitation of scheelite being proposed. However, the presence of non-vein scheelite in Ca-silicate nodules suggests that metamorphic fluids played an important role in its formation.

The source of metals in the Meguma Terrane is currently a point of contention, with four sources currently proposed to account for the metals enriched in the Meguma orogenic-type occurrences, these being; metals directly from a granitic source, metals sourced from the lower crust or mantle, metals sourced from the country-rock Goldenville and Halifax Groups metasedimentary rocks and mobilized by either magmatic or deep crustal metamorphic fluids driven by magmatic or metamorphic heat, and a hybrid model that proposes a combination of all or some of these previously stated sources (Mawer 1985, 1986, 1987; Hy and Williams 1986; Smith and Kontak 1986; Kontak and Smith 1987, 1988a, 1988b, 1989, 1993; Kontak et al. 1990, 1993; Kontak and Archibald 2002; Sangster and Smith 2007).

9.3.2 Bendigo-Ballarat Terrane

The Bendigo-Ballarat Terrane of central Victoria, southeastern Australia, forms part of

the western sub-province of the extensive Paleozoic Lachlan Fold Belt (Jia, 2002) and is separated from the adjacent and correlatable Late Cambrain Stawell Zone (West), and the Silurian to Early Devonian Melbourne Zone (East) by the Avoca Fault and the Mt William Fault, respectively (Gray and Foster 1998; Fergusson 2003; Raine 2005) (Fig. 45). Basement rocks in the Bendigo-Ballarat Terrane are dominated by four lithotectonic units: (1) the Early to Middle Ordovician Castlemaine Group metasediments, (2) Cambrain metavolcanics and metasediments, (3) Lower Devonian to Upper Silurian S-type and I-type granites, and (4) Carboniferous to Middle Devonian S-type and I-type granites (Fig. 45) (Keays 1987; Bierlein et al. 1998).

The Early to Middle Ordovician Castlemaine Group metasediments form the majority of outcropping basement rocks in the Bendigo-Ballarat Terrane and consists of a thick succession (>3,000 m maximum thickness) of mass flow deposited sandstone and mudstone, with lesser suspension deposited black shale (Fergusson and Vandenberg 2003; Bull and Large 2014). Lithostratigraphic units are difficult to recognize due to the monotonous nature of the sequence (Fergusson and Vandenberg, 2003). However, subdivision of the Group into six biostratigraphic stages (Lancefieldian, Bendigonian, Chewtonian, Castlemainian, Yapeenian, and Darriwilian) and nineteen zones is possible using unique graptolites preserved in black shales (VandenBerg and Cooper 1992; Willman 2007). Importantly, hosted within the Castlemaine Group, are the orogenic Au deposits of the Bendigo-Ballarat Terrane.

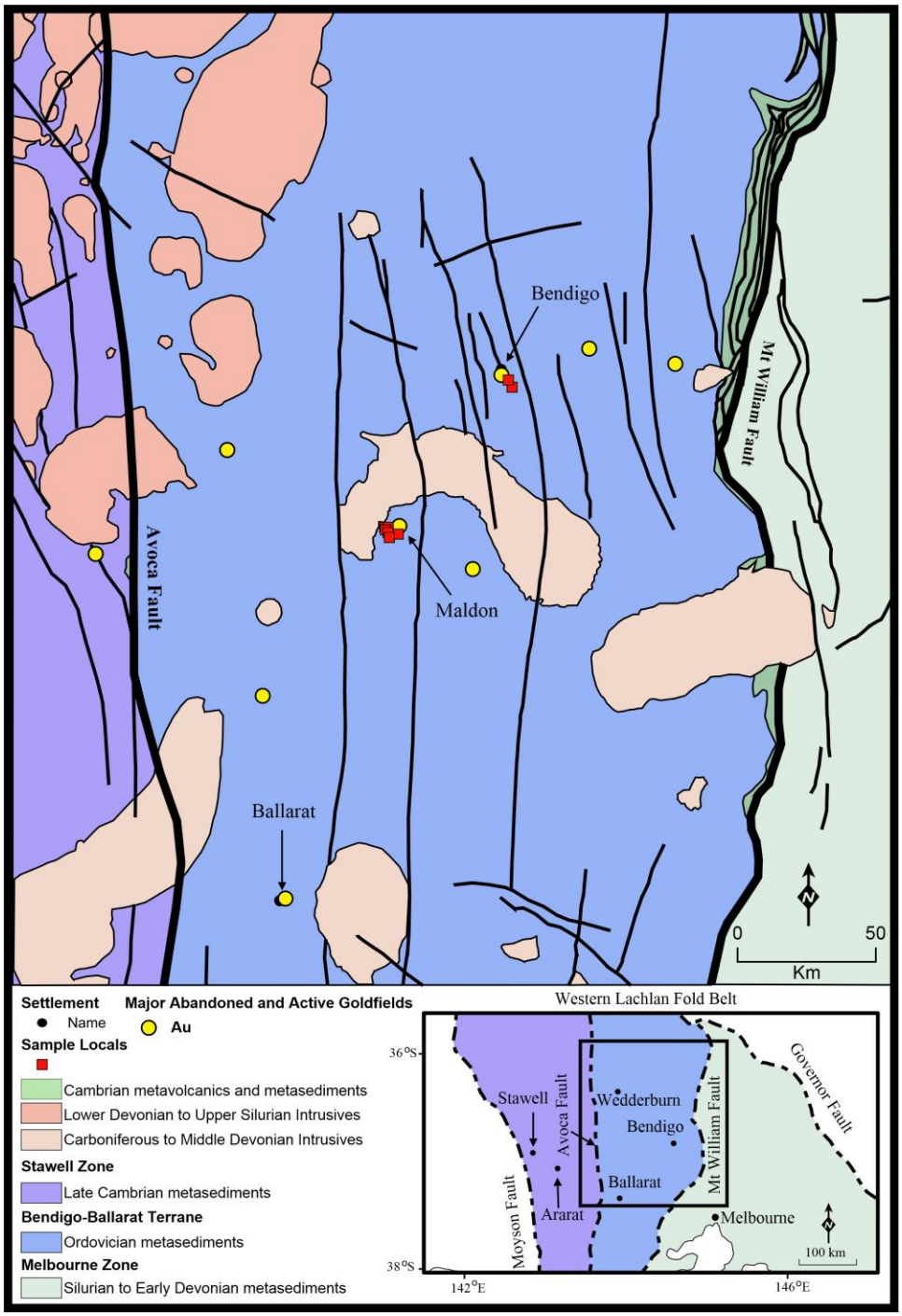

Fig. 45. Regional geology of the Bendigo-Ballarat Terrane, showing: selected settlements, sample locations, major lithoteconic units, and selected major abandon or active goldfields. Aspects from Bierlein et al. (2000, 2004), Vandenberg et al. (2000), and Thomas et al. (2011).

Deformation in the Bendigo-Ballarat Terrane is complex with multiple phases of

deformation recognized, however, most orogenic-Au mineralization is associated with deformational events relating to the Benambran Orogeny (at approximately 455-440 Ma; VandenBerg et al. 2000). Onset of the Benambran Orogeny regionally metamorphosed [prehnite-pumpellyite to lower greenschist facies at current erosion-level; equivalent to peak metamorphic conditions of approximately 360 °C and 4 kbar (Offler et al. 1998)]. Deformation was associated with regional metamorphism) and deformed the Early Cambrian to Middle Ordovician units into a series of broadly N-S to NW-SE-trending, tight chevron- and box-style, upright to steeply west-dipping folds with wavelengths approximately 150-500m (Cox et al. 1991; Gray and Wilman 1991). Accompanying this folding was the development of a strong, axial-planar, crenulation cleavage in the fine-grained slate and black shales (VandenBerg et al. 2000; Shaubs and Wilson 2002; Raine 2005, and references therein). Folding in the Bendigo-Ballarat Terrane accompanied the development of steeply to moderately west-dipping and east-dipping reverse faults with the development of some reverse fault zones associated with orogenic Au mineralization (Cox et al. 1991). Intrusion of the post-tectonic Early to Late Devonian S-type and I-type granites in the Bendigo-Ballarat Terrane resulted in minor contact metamorphism of the Castlemaine Group metasediments, immediately surrounding the granites and remobilization of Au from earlier orogenic veins (Ciobanu et al. 2010; Fu et al. 2014).

Documentation of titanium-rich minerals phases in the Castlemaine Group is limited. However, rutile is noted as a detrital mineral phase in the regionally metamorphosed Castlemaine Group metasediments (for example, Bierlein et al. 2000). In the contact metamorphosed Castlemaine Group metasediments, surrounding the Harcourt Granite, rutile is not noted, however, the presence of ilmenite is (for example, Bierlein et al. 2000).

Orogenic-type Au mineralization is widespread throughout the subgreenschist and lower

greenschist facies Castlemaine Group rocks of the Bendigo-Ballarat Terrane, with historically greater than 790 t of Au being recovered from hard-rock mining operation in the Bendigo-Ballarat Terrane (Fig. 45). Similar to the Meguma Terrane, two main styles of orogenic-type mineralization are recognized in the Bendigo-Ballarat Terrane; these being, vein Au deposits (for example, Bendigo) and disseminated Au deposits (for example, Fosterville). Vein-style Au deposits form the overwhelming majority of the orogenic-type Au occurrences and like in the Meguma Terrane both styles of mineralization are observed having a strong structural control and occur within or in close proximity to anticlinal fold hinges and reverse faults (VandenBerg et al. 2000).

Radiometric age dating ($^{40}Ar/^{39}Ar$) obtained from whole-rock (mica) and *in situ* Re-Os (sulfides) analyzes from various orogenic Au deposits, suggests two major stages of mineralization were experienced in the Bendigo-Ballarat Terrane, one at approximately 445 Ma and the other at 380-370 Ma; consistent with ages for the Benambran Orogeny and the intrusion of post-tectonic granitoids into the Bendigo-Ballarat Terrane, respectively (Bierlein et al. 2001; Phillips et al. 2012). Another possible subordinate mineralizing event is also suggested as occurring at approximately 410–400 Ma (Phillips et al. 2012).

Vein Au deposits in the Bendigo-Ballarat Terrane are predominantly comprised of quartz with subordinate amounts of various carbonates and sulfides (predominantly pyrite and arsenopyrite, with subordinate galena, sphalerite, chalcopyrite, and pyrrhotite), together with chlorite, siderite, sericite, muscovite, albite, apatite, sillimanite, muscovite, and gold (Willman and Wilkinson 1992, and references therein). Significant W enrichments are not recognized in any orogenic Au mineralization in the Bendigo-Ballarat Terrane that has not undergone later overprinting related to the intrusion of the post-tectonic Early to Late Devonian S-type and I-type

granites. Tungsten enrichments in these intrusion-modified deposits in the Bendigo-Ballarat Terrane is found in the form of scheelite (for example, Maldon; Fu et al. 2014, and references therein).

The source of metals in the Bendigo-Ballarat Terrane similar to the Meguma Terrane is a major point of contention, with two major sources currently proposed to account for the metals enriched in the Bendigo-Ballarat orogenic occurrences, these being; metals sourced from the Cambrian volcano-sedimentary rocks with a significant proportion derived from the oceanic basalts (Keays and Scott 1976; Bierlein et al. 1998; Willman et al. 2010), or metals sourced from the country-rock Castlemaine Group metasedimentary rocks and mobilized at either the greenschist-amphibolite facies transition (Lisitsin and Pitcairn 2015) or more "shallowly" at greenschist facies conditions (Thomas et al. 2011; Large et al. 2011).

9.4 Material and Analytical Methods

9.4.1 Sample Selection

Following the approaches of Cave et al. [accepted (Chapter 8)], low and high metamorphic grade equivalents (contact and regional metamorphic) of the Goldenville and Halifax Groups metasediments were sampled from a various location throughout Nova Scotia (Appendix 1, Fig. 44). Similarly regionally metamorphosed subgreenschist to lower greenschist and contact metamorphosed (up to K-feldspar zone) Castlemaine Group metasediments were sampled from drillholes in the Bendigo goldfield and in mine adits-and-road cuttings around Maldon (mine adits: Nuggetty Reef and Liscotts Reef), respectively (Appendix 1, Fig. 45). Only subgreenschist and lower greenschist facies rocks are exposed at current erosion levels and in drill holes, thus the approach of sampling contact metamorphosed samples to represent upper

greenschist facies and amphibolite facies rocks was adopted.

Mineralogical and textural associations in these samples were examined using a combination of reflected light microscopy and SEM on samples of either argillite/siltstone or greywacke/psammite protolithology, and encompassing the entire span of metamorphic (regional and contact) grade ranges observed in each terrane. Subsequent to this, LA-ICP-MS traverses were undertaken on representative lowest and highest metamorphic grade samples, from each terrane, to understand element distribution among mineral phases, especially W. Trace element compositions of Ti-oxide minerals were quantitatively determined by LA-ICP-MS techniques for representative facies samples of different metamorphic grades.

Rutile (TiO_2) identified in this chapter is done so based on chemical composition and optical properties. Titanium dioxide (TiO_2) is present in nature as several different polymorphs [for example, akaogiite, TiO_2(II), TiO_2(B), TiO_2(H), TiO_2(R), TiO_2(OI), and TiO_2(OII)]. However, in sedimentary environments, rutile, brookite, and anatase are the most abundant polymorphs, with the presence of the other phases unlikely. The possibility that some of the grains identified as rutile by optical and geochemical means could in fact be anatase, brookite, or other TiO_2 phases is acknowledged. As such, the term "rutile" in this paper could encompass all TiO_2 polymorphs.

9.4.2 Analytical Methods

Analytical instrumentation used in this chapter includes a Resonetics Resolution laser ablation system equipped with a Coherent COMPex Pro 110 ArF excimer laser, housed at CODES/Earth Sciences, University of Tasmania. The ArF excimer laser operates at a 193 nm wavelength with a 20 ns pulse width and was coupled to an Agilent 7900 quadrupole inductively coupled plasma mass spectrometer (ICP-MS). Quantitative LA-ICP-MS trace element (Al, Ti, V,

Cr, Mn, Fe, Zr, Nb, Hf, Ta, and W) analyzes were performed on rutile and ilmenite with an ablation beam size of 9 μm. Laser repetition rate for rutile and ilmenite analyzes was typically 5 Hz and laser beam energy at the sample interface was maintained at 2.60 J/cm^2. Each analysis was pre-ablated with three laser pulses to remove the surface contamination. Once the pre-ablation had washed out (20 s) then a blank gas was analyzed for 30 s followed by 25 s of sample ablation. All data reduction calculations and error propagations were undertaken within Microsoft Excel® via macros designed at the University of Tasmania. Data reduction was undertaken using stoichiometric values of Ti as the internal standard for rutile and ilmenite. Synthetic basalt glass standard GSD-1g was used as the primary calibration standard (using GeoReM preferred values: http://georem.mpch-mainz.gwdg.de/), with glass standard NIST610 as the secondary standard (using GeoReM preferred values: http://georem.mpch-mainz.gwdg.de/).

The primary calibration standard was analyzed with a 74 μm beam and a laser repetition rate of either 5 Hz. These analyzes were conducted at the beginning-and-end of the session, and at hourly intervals throughout to account for instrument drift. The secondary calibration standard was analyzed with ablation spot size and laser repetition rates matching the unknowns throughout the analytical session. Samples were initially quantified on the primary standard GSD-1g at a larger spot size, then a secondary standard correction was applied based on analyzes of the secondary standard NIST610 at the same conditions as the unknowns to correct for differences in spot size. Precision on replicate analyzes of basalt glass standard BCR-2g at spot sizes the same as the unknowns, showed that following the application of the spot size correction factor (based on GSD-1g), all elements were within 10% of reported concentrations for BCR-2g (using GeoReM preferred values: http://georem.mpch-mainz.gwdg.de/). Typical detection limits

for unknown samples using three standard deviations of the background signal (99% confidence) for 9 μm spots were 200 ppm for Fe, 8 ppm for Al, 5 ppm for Mn, 1 ppm for V and Cr, 0.2 ppm for Zr, Nb, Hf, and W, and 0.1 ppm for Ta.

Laser ablation traverses were performed using a 100 μm beam moving at 60 μm/s relative to the sample. Traverses were conducted perpendicular to the major bedding/foliation and utilized a laser repetition rate of 10 Hz with laser beam energy at the sample interface maintained at approximately 8.5 J/cm^2.

9.5 Results

9.5.1 Rutile and Ilmenite Textures in the Meguma Terrane

Regional metamorphosed lower greenschist facies samples used in this study consist of Goldenville and Halifax Group metasediments derived from Lunenburg, Dublin Shore, Bayport, LaHave, and the Ovens areas (Fig. 44). Mineral assemblage in the studied samples are characterized by the rock-forming minerals quartz, muscovite, chlorite, albite ± epidote, graphite, calcite, spessartite, and plagioclase. Accessory minerals include epidote, calcite, spessartite, plagioclase, rutile (<1-5 %), apatite, allanite, zircon, titanite, pyrite, pyrrhotite, arsenopyrite, ± chalcopyrite, galena, sphalerite, and magnetite.

In the lowest metamorphic grade samples (lower greenschist) of both the Halifax and Goldenville Groups, rutile is the major Ti-mineral phase present. Rutile in these samples displays a range of textures and mineral associations. In selected samples of Halifax Group slates and psammites, heavy mineral bands parallel to relict bedding contain rutile along with zircon and apatite (Fig. 46A). Rutile in these bands typically occurs as small (3-50 μm) anhedral to subhedral poikilitic grains (Fig. 46B), however, rare euhedral to subhedral rounded grains (Fig.

46C) are also present, occasionally with anhedral to euhedral rutile laths adjoining them (Fig. 46D). Scanning electron microscopy (SEM) of these euhedral to subhedral rounded grains under high contrast settings commonly reveals zoning patterns truncated by grain boundaries (Fig. 46C). Zoning is also occasionally recognized in the anhedral to subhedral poikilitic grains with zoning patterns also observed being truncated by grain boundaries (Fig. 46E). Rutile in these samples is also observed as anhedral polycrystalline rims around euhedral to subhedral, moderate to well-rounded silicate mineral grains (for example, quartz), and polycrystalline quartz that itself rims subhedral sulfide minerals (pyrite or pyrrhotite; Fig. 46F). Under high contrast settings on the SEM these polycrystalline rims show no zoning patterns. Rutile in Goldenville Group samples is typically observed as large (20- 300 μm) subhedral poikilitic unzoned grains orientated parallel to the main metamorphic foliation (Fig. 46G); rutile mantling and infill textures observed in the Halifax Group metasediments are also present in Goldenville Group samples.

Regional metamorphosed upper greenschist facies samples used in this study consist of Goldenville and Halifax Group metasediments derived from Broad Cove, Tangier Mine, Mooseland, and Mooseriver (Fig. 44). Mineral assemblage in the studied samples are characterized by the rock-forming minerals quartz, muscovite, biotite, chlorite, albite, actinolite ± epidote, graphite, calcite, and spessartite. Accessory minerals include ilmenite (<1-5 %), rutile, apatite, allanite, zircon, pyrite, pyrrhotite, arsenopyrite, ± chalcopyrite, galena, sphalerite, and magnetite. Ilmenite in these samples is the dominant Ti-mineral present with rutile observed as a sub-ordinate mineral phase. Ilmenite grains are typically anhedral to subhedral poikilitic in morphology and vary from 3-500 μm in diameter [with larger grains being found within Goldenville Group samples (Fig. 46I)]. Ilmenite grains typically are closely associated with

biotite (Fig. 46H). However, biotite in some samples is completely (or partially) recrystallized to chlorite. Rutile in the upper greenschist facies is typically observed as very fine lathes along ilmenite grain boundaries (Fig. 46I), however, occasionally rutile is observed as relict grains (Fig. 46J), texturally dissimilar to the lath rutile observed along grain boundaries.

Contact metamorphosed samples used in this study consist of Halifax Group metasediments derived from around the Halifax Pluton, located in the city of Halifax (Fig. 44). Hornfels samples were dominantly obtained between the bitotite-in and K-feldspar-in isograds. Mineral assemblages in the studied samples are characterized by the rock-forming minerals quartz, muscovite, biotite, plagioclase, ± cordierite, andalusite, and graphite. Accessory minerals include chlorite, albite, rutile/ ilmenite (<1-5 %), apatite, allanite, monazite, zircon, pyrite, pyrrhotite, arsenopyrite, ± chalcopyrite, galena, sphalerite, and magnetite.

Samples obtained outside of the biotite-in isograd are mineralogically and texturally indistinguishable from the regional lower greenschist facies samples, apart from lacking rutile grains subhedral to euhedral in morphology. At approximately the biotite-in isograd, minor replacement of rutile by ilmenite is observed (Fig. 46K), with ilmenite replacement observed becoming more pronounced in samples of increasing metamorphic grade (from Figs. 46K, L through to M). Ilmenite grains well-above the biotite-in isograd and just before the K-feldspar-in isograd, are observed being almost entirely recrystallized to ilmenite with only rare relict rutile observed within them (Fig. 46M). Ilmenite grains are texturally similar to those of the regional biotite greenschsit facies samples and are typically anhedral to subhedral poikilitic in morphology (for example, Fig. 46M). Similar to the regional upper greenschist facies samples, ilmenite is closely associated with biotite (Fig. 46L, M), whereas chlorite is associated with rutile below the biotite-in isograd.

9.5.2 Rutile and Ilmenite Textures in the Bendigo-Ballarat Terrane

Regional metamorphosed subgreenschist to lower greenschist facies samples used in this study consist of Castlemaine Group metasediments derived from drillholes (259W1, NBD186, and NBD005) from the Bendigo Goldfield (Fig. 45). Mineral assemblage in the studied samples are characterized by the rock-forming minerals quartz, muscovite, chlorite, and albite ± graphite. Accessory minerals include kaolin, calcite, rutile (0.05%), plagioclase, apatite, allanite, zircon, xenotime, monazite, and pyrite. Rutile is the major titanium-rich mineral observed in the regionally metamorphosed subgreenschist to lower greenschist samples, albeit occurring as a trace mineral phase (0.05%). In selected samples of Castlemaine Group sandstones and mudstones, heavy mineral bands parallel to relict bedding structures are preserved with rutile observed (albeit as a very minor phase) along with zircon, xenotime, monazite, allanite, and apatite (Figs. 46N, O). In samples not containing heavy-mineral bands, rutile is observed disseminated throughout. Rutile occurs typically as small (2-20 μm; up to 50 μm) euhedral to subhedral, moderate to well-rounded grains (Fig. 46P) that are occasionally fractured (Fig. 46Q). High contrast SEM revealed no obvious zoning patterns (Figs. 46P, Q).

Contact metamorphosed samples used in this study consist of Castlemaine Group metasediments derived from Linscotts Reef and Nuggetty Reef Mines, and along the Mt Tarrengower Road. Hornfels samples were dominantly obtained between the bitotite-in and K-feldspar-in isograds surrounding the Harcourt Granite (Fig. 45). Mineral assemblages in the studied samples are characterized by the rock-forming minerals quartz, muscovite, biotite, and albite, ± chlorite, cordierite, and graphite. Accessory minerals include ilmenite (0.05-0.1 %), apatite, zircon, pyrrhotite, chalcopyrite, arsenopyrite, ± K-feldspar, pyroxene, grossular, and chalcopyrite. Ilmenite is the major titanium-rich mineral phase present (typically <0.1%) in these

samples, and is typically observed as small to medium-sized (2-50 μm; up to 150 μm) subhedral to anhedral grains (Figs. 46R, S, T). Ilmenite is commonly observed within these samples occurring in alignment with other ilmenite grains (Figs. 46S, T) and the heavy minerals apatite and zircon (Fig. 46R). Ilmenite commonly displays a close association with biotite (Figs. 46S, T). Rutile is commonly observed along ilmenite grain margins and occasionally within ilmenite grains (Figs. 46R, S, T).

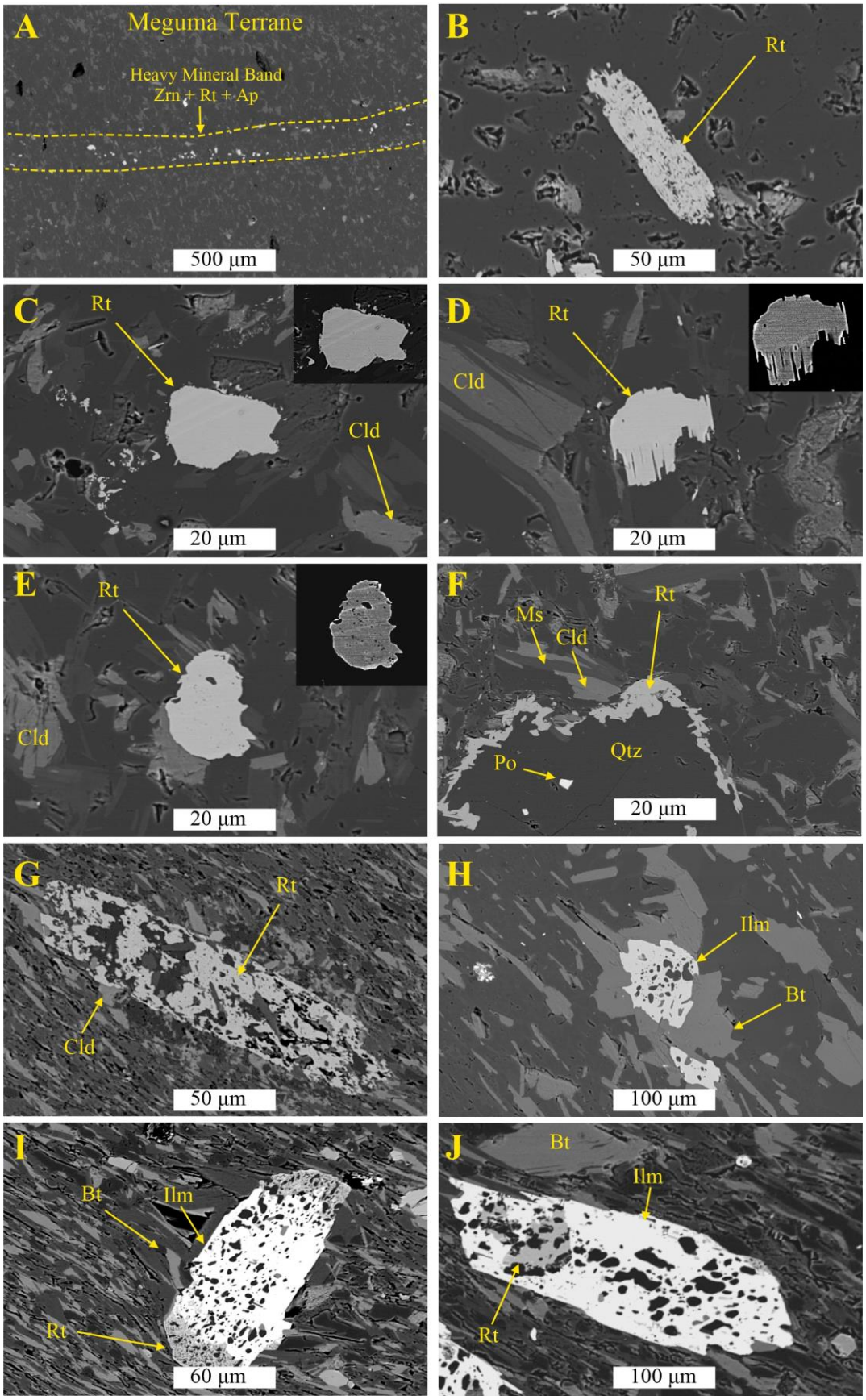
A
Meguma Terrane
Heavy Mineral Band
Zrn + Rt + Ap
500 µm
B
Rt
50 µm
C
Rt
Cld
20 µm
D
Rt
Cld
20 µm
E
Rt
Cld
20 µm
F
Ms
Cld
Rt
Qtz
Po
20 µm
G
Rt
Cld
50 µm
H
Ilm
Bt
100 µm
I
Bt
Ilm
Rt
60 µm
J
Bt
Ilm
Rt
100 µm

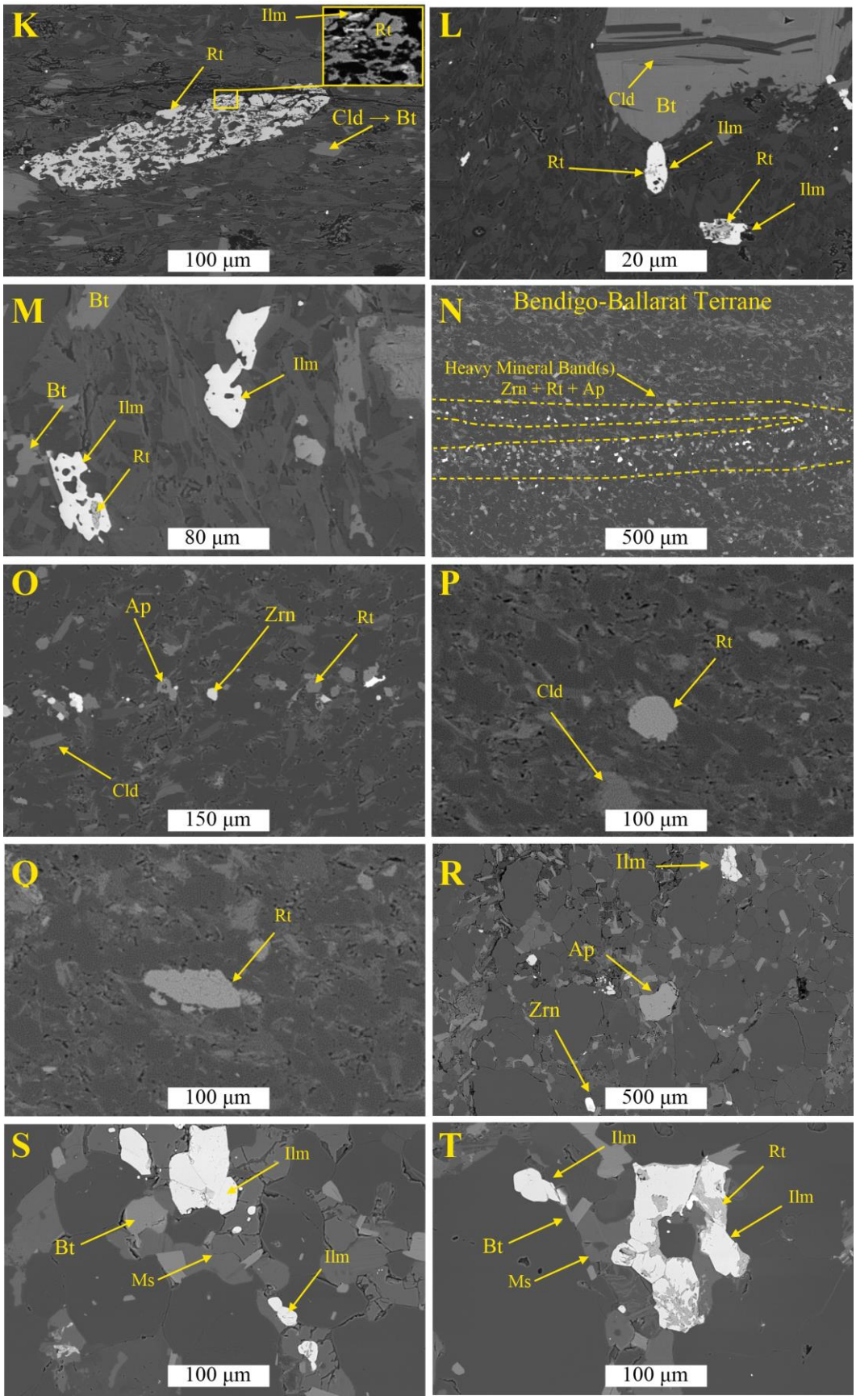
K
Ilm
Rt
Rt
Cld → Bt
100 µm
L
Cld
Bt
Ilm
Rt
Rt
Ilm
20 µm
M
Bt
Ilm
Bt
Ilm
Rt
80 µm
N
Bendigo-Ballarat Terrane
Heavy Mineral Band(s)
Zrn + Rt + Ap
500 µm
O
Ap
Zrn
Rt
Cld
150 µm
P
Rt
Cld
100 µm
Q
Rt
100 µm
R
Ilm
Ap
Zrn
500 µm
S
Ilm
Bt
Ms
Ilm
100 µm
T
Ilm
Rt
Ilm
Bt
Ms
100 µm

Fig. 46. Scanning electron images of mineralogical texture within the Meguma (A-M) and Bendigo-Ballarat terranes (N-T). *Meguma Terrane*: (A) Heavy mineral band (highlighted) in lower greenschist facies Halifax Group slate (CUN-03) containing zircon, rutile, apatite, and other minerals. (B) Anhedral poikilitic rutile grain containing inclusions of muscovite, chlorite and quartz, in regionally metamorphosed lower greenschist facies Halifax Group psammite (CUN-13). (C) Rounded rutile grain within regionally metamorphosed lower greenschist facies Halifax Group slate (CUN-03). Rounded rutile grain displaying prominent zonation patterns under SEM; zonation is truncated by the rounded grain boundaries. (D) Rounded anhedral slightly poikilitic rutile grain, with subhedral to euhedral fine laths adjoining it, within regionally metamorphosed lower greenschist facies Halifax Group slate (CUN-03). (E) Rounded slightly poikilitic rutile grain, with very minor subhedral to euhedral rutile laths adjoining it, within regionally metamorphosed lower greenschist facies Halifax Group slate (CUN-03). Prominent zonation patterns are observed under SEM, with zonation being truncated by the rounded grain boundaries. (F) Polycrystalline rutile mantling quartz and pyrrhotite in regionally metamorphosed lower greenschist facies Halifax Group psammite (CUN-13). (G) Subhedral poikilitic rutile grain containing inclusions of muscovite, chlorite, and quartz, in regionally metamorphosed lower greenschist facies Goldenville Group psammite/ argillite (MG-3). (H) Anhedral poikilitic ilmenite grain containing inclusions of muscovite and quartz, and mantled by biotite, in regionally metamorphosed upper greenschist facies Goldenville Group psammite (MG-7). (I) Rotated subhedral poikilitic ilmenite grain containing inclusions of muscovite, chlorite, biotite, and quartz, in regionally metamorphosed upper greenschist facies Goldenville Group psammite (CUN-14). Anhedral to subhedral rutile laths are observed along ilmenite grain boundaries. (J) Subhedral poikilitic ilmenite grain containing inclusions of muscovite, chlorite, biotite, and quartz, in regionally metamorphosed upper greenschist facies Goldenville Group psammite (CUN-15). Rare rutile relict grains are observed within some ilmenite grains, and are textural dissimilar to the commonly observed rutile laths that grow along ilmenite grain boundaries. (K) Subhedral poikilitic rutile grain containing inclusions of muscovite, chlorite (with minor recrystallization to biotite), and quartz, in hornfelsed (biotite-in isograd) Halifax Group shale (KIL-E04P). Rutile shows very minor recrystallization to ilmenite (insert). (L) Subhedral poikilitic ilmenite grain containing inclusions of muscovite, biotite (with minor inclusions of muscovite and chlorite), rutile, and quartz, in hornfelsed (above biotite-in isograd) Halifax Group shale (SS). (M) Subhedral poikilitic ilmenite grain containing inclusions of muscovite, biotite, quartz, and rare rutile, in hornfelsed (well-above the biotite-in isograd) Halifax Group shale (OEC11-2B). *Bendigo-Ballarat Terrane:* (N) Rare heavy

mineral band (highlighted) in regionally metamorphosed lower greenschist facies Castlemaine Group psammite (259W1-798), containing zircon, rutile, apatite, and other minerals. (O) Enlargement of the heavy mineral band shown in Fig. 46N. (P) Rounded rutile grain within regionally metamorphosed lower greenschist facies Castlemaine Group psammite (NBD005-140.1). Rutile grains commonly display minor fracturing. (Q) Subhedral rutile grain within regionally metamorphosed lower greenschist facies Castlemaine Group psammite (NBD005-140.1). Rutile grains commonly display rounding and minor fracturing. (R) Rare heavy mineral band (highlighted) in hornfelsed (well-above the biotite-in isograd) Castlemaine Group psammite (H8), containing zircon, apatite, ilmenite, and other minerals. (S) Band containing ilmenite and phyllosilicate minerals (for example, muscovite and biotite) in hornfelsed (well-above the biotite-in isograd) Castlemaine Group psammite (H9B). Not shown in this picture is that these bands run parallel to rare heavy mineral bands (for example, Fig. 46R). (T) Ilmenite grains in hornfelsed (well-above the biotite-in isograd) Castlemaine Group psammite (H9B). Ilmenite displays an intricate relationship to rutile. Rutile is most commonly observed along the edges of the ilmenite grains. Mineral abbreviations: Zrn- zircon, Rt- rutile, Ap-apatite, Cld- chloritoid, Ms- muscovite, Qtz- quartz, Po- pyrrhotite, Bt- biotite, Ilm- ilmenite.

9.5.3 Laser Lines and Major-hosts of W through Prograde Regional and Contact Metamorphism

Meguma Terrane: Laser ablation traverses completed on representative lower greenschist facies Goldenville and Halifax gGroups metasediments samples, show irregular distributions of W at detectable and locally relatively high levels, at the <100 μm scale (Fig. 47A). The most anomalous of these relatively high levels of W, form prominent peaks that are commonly coincidental with peaks of Ti and Ta (Fig. 47A). Reflected microscopy and SEM conducted along the laser traverses observed the laser beam as having passed through grains of rutile at periods of coincidental relatively high levels of W, Ti, and Ta (Fig. 47A).

Laser ablation traverses completed on representative regionally metamorphosed upper greenschist facies and biotite-in contact metamorphosed Goldenville and Halifax Groups metasediments samples, similarly shows irregular distributions of W at detectable and locally

relatively high levels, at the <100 μm scale (Fig. 47B). The most anomalous of these relatively high levels of W, form prominent peaks that are commonly coincidental with peaks of Ti, Fe, and Ta (Fig. 47B). Reflected microscopy and SEM conducted along the laser traverses observed the laser beam as having passed through grains of ilmenite at periods of coincidental relatively high levels of W, Ti, Fe, and Ta (Fig. 47B).

Bendigo-Ballarat Terrane: Laser ablation traverses completed on representative lower greenschist facies Castlemaine Group metasediments samples, show irregular distributions of W at detectable and locally relatively high levels, at the <100 μm scale (Fig. 47C). The most anomalous of these relatively high levels of W, form prominent peaks that are often observed being coincidental with peaks of Ti and Ta (Fig. 47C). Reflected microscopy and SEM conducted along the laser traverses observed the laser beam as having passed through grains of rutile at periods of coincidental relatively high levels of W, Ti, and Ta (Fig. 47C).

Laser ablation traverses completed on representative contact metamorphosed (above the biotite-in isograd) Castlemaine Group metasediments samples, similarly shows irregular distributions of W at detectable and locally relatively high levels, at the <100 μm scale (Fig. 47D). The most anomalous of these relatively high levels of W, form prominent peaks that are often observed being coincidental with peaks of Ti, Fe, and Ta (Fig. 47D). Reflected microscopy and SEM conducted along the laser traverses observed the laser beam as having passed through grains of ilmenite at periods of coincidental relatively high levels of W, Ti, Fe, and Ta (Fig. 47D)

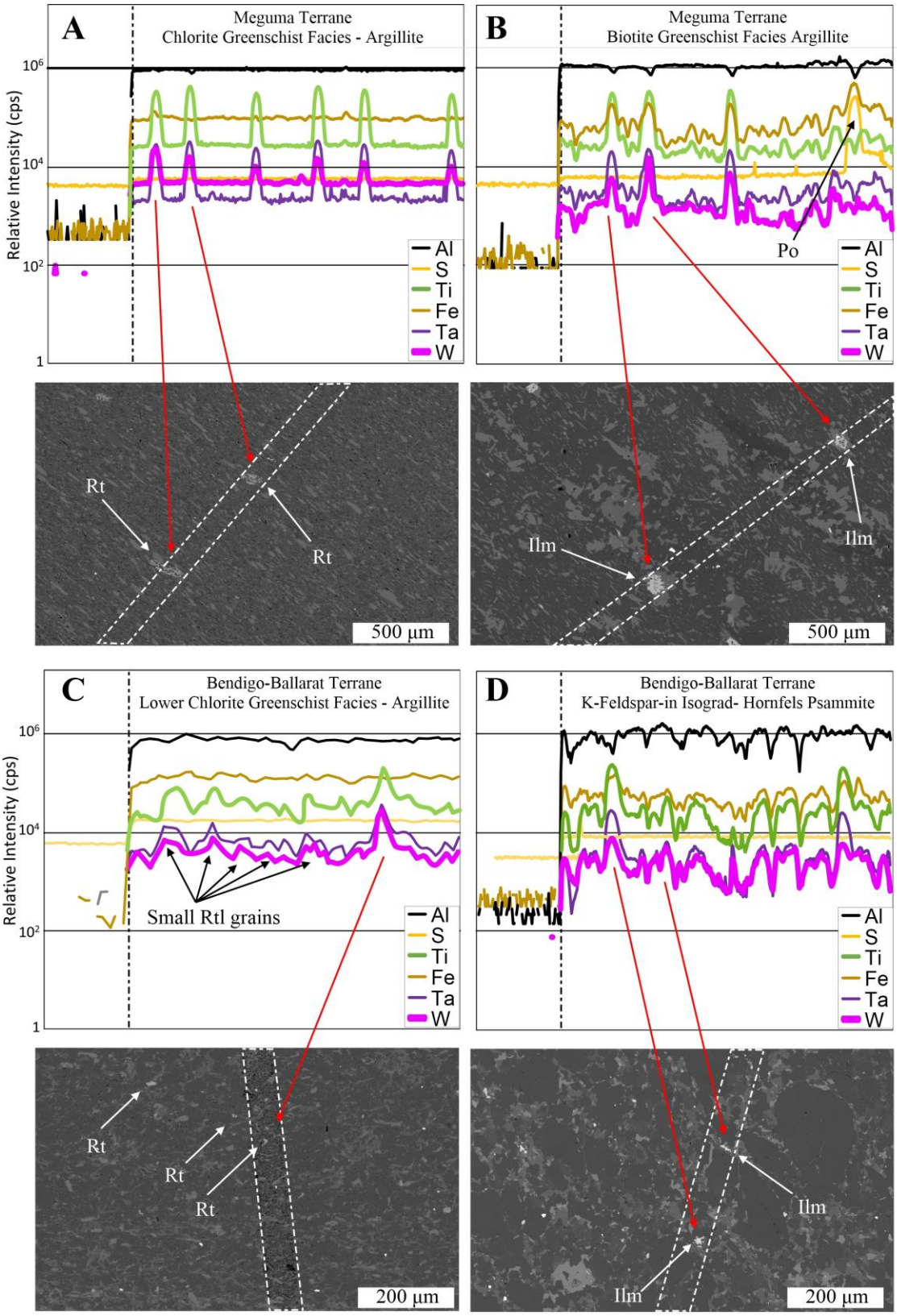

Fig. 47. Laser ablation inductively coupled plasma mass spectrometry (LA-ICP-MS) traverses on low metamorphic

grade and high metamorphic grade samples from the Meguma and Bendigo-Ballarat terranes, showing the distribution of selected elements. *Meguma Terrane:* (A) Regionally metamorphosed lower greenschist facies Goldenville Group argillite (MG3). Upper image shows entire LA-ICP-MS traverse, lower image (SEM) shows a selected area through which the laser traverse passed, with rutile grain transect highlighted on both the upper and lower image. (B) Regionally metamorphosed upper greenschist facies Goldenville Group psammite (MG-7). Upper image shows entire LA-ICP-MS traverse, lower image (SEM) shows a selected area through which the laser traverse passed, with ilmenite grain transect highlighted on both the upper and lower image. *Bendigo-Ballarat Terrane:* (C) Regionally metamorphosed lower greenschist facies Castlemaine Group argillite/ psammite (NBD005-140.1). Upper image shows entire LA-ICP-MS traverse, lower image (SEM) shows a selected area through which the laser traverse passed, with rutile grain transect highlighted on both the upper and lower image. (D) Hornfelsed (well-above the biotite-in isograd) Castlemaine Group psammite (H8). Upper image shows entire LA-ICP-MS traverse, lower image (SEM) shows a selected area through which the laser traverse passed, with ilmenite grain transect highlighted on both the upper and lower image. Mineral abbreviations: Rt- rutile, Ilm- ilmenite.

9.5.4 Chemical Composition of Rutile and Ilmenite

Meguma Terrane: Trace element analyzes of rutile grains located in the heavy minerals bands of Halifax Group and large rutile grains in the Goldenville Group, reveal great heterogeneity between individual grains with minimum and maximum values (Appendix 2, Table 9, Fig. 48) for some elements showing up to three orders of magnitude variation (for example, W). Mean concentrations of trace elements (Table 9, Fig. 48) reveal rutile grains are characterized by high concentrations (500-3,500 ppm) of V, Fe, and Nb, moderate amounts (100-500 ppm) of Cr, Zr, Ta, and W, and trace amounts (1-50 ppm) of Mn and Hf.

Table 9. Min, max, mean, and median compositions (ppm), for Meguma Terrane and Bendigo-Ballarat Terrane, rutile and ilmenite.

MEGUMA		V	Cr	Mn	Fe	Zr	Nb	Hf	Ta	W
	Min	38	<8.0	2.2	812	3.7	166	<0.6	4.4	1.2
	Max	3,695	1168	420	25,868	1,670	25,711	83	1,841	3,501
	Mean	858	278	45	3,543	333	1,894	16.6	128	257
Rutile n 83	Median	930	166	8.8	1,685	150	1,508	8.8	92	126
	Min	5.0	<6.5	13,257	220,341	<0.67	218	<0.43	18.8	0.76
	Max	180	389	107,512	351,224	268	898	7.0	115	43
	Mean	39	N/A	71,534	277,814	35	490	N/A	62	19.8
Ilmenite n 80	Median	24	N/A	82,810	271,887	16.6	467	N/A	64	17.8

BENDIGO		V	Cr	Mn	Fe	Zr	Nb	Hf	Ta	W
	Min	60	14.4	3.6	464	8.2	722	0.40	24	3.4
	Max	3,628	3,398	67	4,658	1,478	8,805	80	1,408	1,636
	Mean	1,094	685	N/A	2,588	415	3,329	19.0	243	462
Rutile n 40	Median	788	329	N/A	2,317	293	2,119	10.3	96	251
	Min	67	20	5,698	277,601	0.06	466	<0.13	62	2.8
	Max	441	308	16,799	358,339	8.8	880	0.65	115	44
	Mean	313	159	7,647	333,967	1.9	778	N/A	91	23
Ilmenite n 48	Median	334	153	6,548	337,898	1.7	797	N/A	90	23

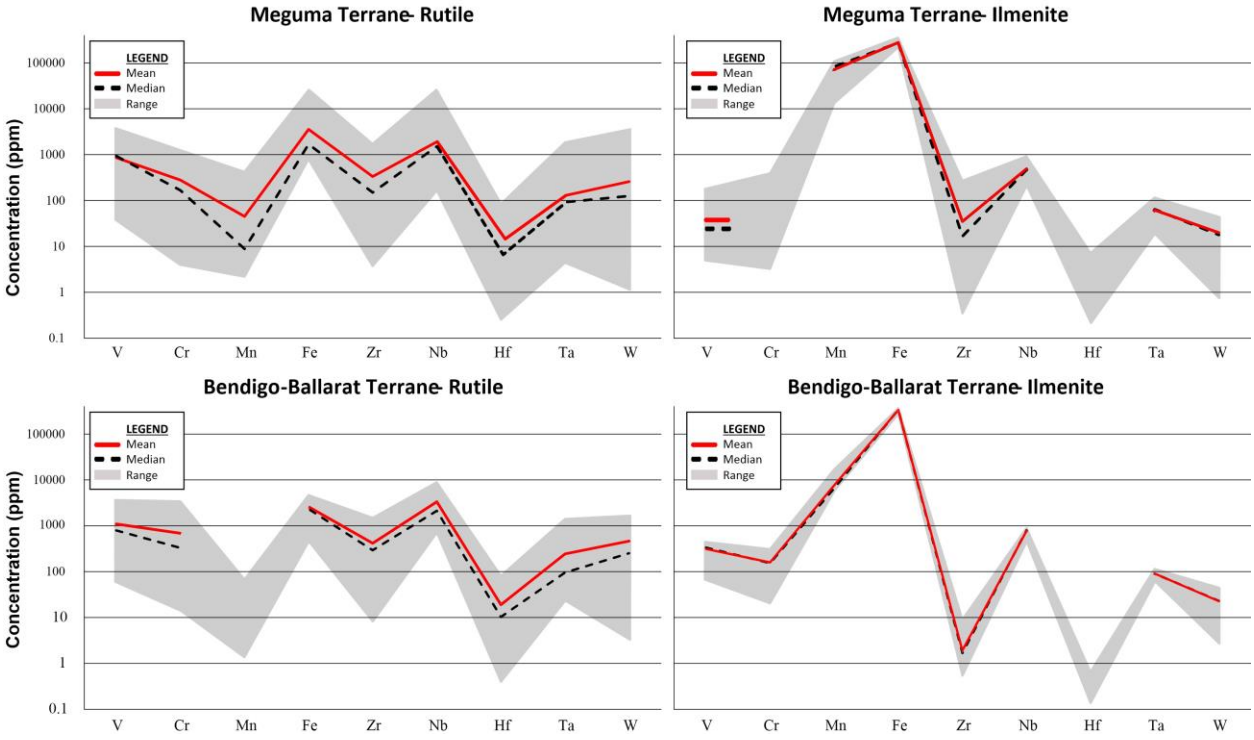

Fig. 48. Trace element concentrations of detrital rutile and metamorphic ilmenite as determined by LA-ICP-MS analyzes. BDL values replaced with half-detection limit values when calculating mean, if greater than half of the dataset are above detection limit. Images show the range between the minimum and maximum values, the median value (dotted line), and the mean value (red solid line). Calculation of mean and median for some elements (for example, Hf, Cr, and Mn) in rutile and ilmenite was not possible, as greater than half the dataset are BDL.

Individual trace element analyzes of ilmenite grains reveals a greater degree of homogeneity between grains compared to the rutile analyzes, however, overall they are still quite heterogeneous (Appendix 2, Table 9, Fig. 48). Mean trace elements concentrations (Table 9, Fig. 48) reveal ilmenite grains are characterized by extremely high concentrations (70,000-280,000 ppm) of Fe and Mn, moderate amounts (approximately 500 ppm) of Nb, minor amounts (approximately 60 ppm) of Ta and trace amounts (1-50 ppm) of V, Zr, and W. Whereas Hf and Cr concentrations were commonly below the detection limit (BDL) for the LA-ICP-MS technique.

Bendigo-Ballarat Terrane: Trace element analyzes of rutile grains located in the heavy minerals bands and disseminated throughout the matrix of the Castlemaine Group metasediments, reveals heterogeneity between individual grains with minimum and maximum values (Table 9, Fig. 48). Mean concentrations of trace elements (Table 9, Fig. 48) reveal rutile grains are characterized by high concentrations (500-3,500 ppm) of V, Cr, Fe, and Nb, moderate amounts (100-500 ppm) of Zr, Ta, and W, and trace amounts (1-50 ppm) of Hf. Whereas Mn concentrations were commonly below the detection limit (BDL) for the LA-ICP-MS technique.

Trace element analyzes of ilmenite grains reveals good homogeneity between individual grains (Table 9, Fig. 48), especially compared to the rutile analyzes and ilmenite analyzes from the Meguma Terrane (Table 9, Fig. 48). Mean trace elements concentrations (Table 9, Fig. 48) reveal ilmenite grains are characterized by extremely high concentrations (approximately 334,000 ppm) of Fe, high concentrations of Mn and Nb (700-7,700 ppm), moderate amounts (100-500 ppm) of V and Cr, Minor amounts (50-100 ppm) of Ta and trace amounts (2-25 ppm) of Zr and W. Whereas Hf concentrations were commonly below the detection limit (BDL) for the LA-ICP-MS technique.

9.6 Discussion

9.6.1 Major Hosts Minerals for W during Prograde Metamorphism of the Meguma and Bendigo- Ballarat Terranes

Results reported in this chapter indicate that in lowest metamorphic grade metasedimentary rocks of the Meguma Terrane (Goldenville and Halifax Groups) and Bendigo-Ballarat Terrane (Castlemaine Group), rutile is the major host mineral of W (Figs. 47A, C). In contrast, ilmenite is the major host mineral of W in the contact metamorphosed and regionally

metamorphosed (above the biotite-in isograd) metasedimentary rocks, of both terranes (Figs. 47B, D).

In addition, mean W concentrations are an order of magnitude greater in rutile than in ilmenite (Fig. 48, Table 9). No other minerals hosting W have been identified in these rocks. Similar results have been reported in the Otago Schist, where rutile and titanite are the most important hosts for W in low and high metamorphic grade metasedimentary rocks, respectively [Cave et al. accepted (Chapter 8)].

9.6.2 Metamorphic Alteration of Rutile, and the Metamorphic Recrystallization of Rutile to Ilmenite

Rutile grains from the Meguma Terrane show five distinct textural and/or mineral associations under SEM. (1) Rare euhedral to subhedral rounded grains, occasionally with truncated zoning under high contrast SEM (Fig. 46C), are observed within the heavy mineral bands of lower greenschist facies Halifax Group slates (Fig. 46A), and are interpreted as detrital in origin. In addition, located within the heavy mineral bands of lower greenschist facies Halifax Group slates and argillites, and disseminated throughout both Halifax and Goldenville Group metasediments, are (2) anhedral to subhedral poikilitic grains (Fig. 46B). These grains have previously been described in investigations of the Meguma Terrane as being of ‘fingerprint/net’ (Clarke and Carruzzo 2007) or ‘moth-eaten’ (Fisher 1984) texture. Truncated zoning is occasionally observed (under high contrast SEM) in anhedral to subhedral poikilitic grains (Fig. 46E) of the Halifax Group slates. These anhedral to subhedral poikilitic rutile grains, have likely formed from detrital rutile grains, via pseudomorphic (coupled) dissolution–re-precipitation processes. This origin is suggested based upon the observations of these grains within heavy mineral bands (Fig. 46B), and the preservation of truncated zoning in some grains (Fig. 46E).

Pseudomorphic (coupled) dissolution–re-precipitation of detrital rutile grains to form poikilitic rutile grains of similar morphologies to those observed in the Meguma Terrane, has previously been described in the low metamorphic grade metasandstones of the Moeda Formation (Minas Supergroup, Quadrilátero Ferrífero, Minas Gerais, Brazil; Koglin et al. 2015). In general, fluid–rock interactions aid the coupled dissolution–re-precipitation process (Putnis and Austrheim 2010), as such, the observed truncated, zoned anhedral-to-subhedral poikilitic grains (Fig. 46E) in only the Halifax Group slates, likely attests to lower intrinsic permeabilities in these lithologies aiding in their preservation (for example, larger fluid volumes are able to pass through the more permeable argillites than the slates, resulting in a greater degree of replacement in detrital rutile grains from these lithologies). (3) Polycrystalline rutile rimming detrital quartz grains (and other silicate minerals), and rimming polycrystalline quartz that itself rims sulfide minerals [pyrrhotite and pyrite], is also observed in lower greenschist facies Halifax and Goldenville metasediments (Fig. 46F). One possible explanation for this texture is that it represents the complete dissolution of detrital rutile and precipitation of authigenic rutile around metamorphic quartz and sulfide minerals, and in voids (for example, similar to Type-2 rutile documented by Koglin et al. 2015). A lack of rutile or ilmenite mantles (forming after rutile mantles) in available upper greenschist facies Halifax and Goldenville Group samples, however, complicates its interpretation, as such, the origin of this rutile texture is presently unknown. In regionally and contact metamorphosed Halifax and Goldenville Group metasediments above the biotite-in isograd, (4) fine lathes of rutile are observed and have been extensively documented around ilmenite grains (for example, Haysom et al. 1997), with their origin recognized as being as a result of retrograde recrystallization of ilmenite. (5) Rare rutile relict grains are observed within some ilmenite grains (Fig. 46J) in the Halifax and Goldenville Group metasediments, with

these considered to represent the incomplete recrystallization of rutile to ilmenite with prograde metamorphism (both contact and regional).

Rutile within the Castlemaine Group metasediments of the Bendigo-Ballarat Terrane appears to have undergone a simpler metamorphic history, with rutile recognized in two distinct morphologies. (1) Rare euhedral to subhedral, moderate to well-rounded grains (for example, Fig. 46P) that are occasionally fractured (for example, Fig. 46Q). These grains typically occur in rare heavy mineral bands (Figs. 46N, O) and disseminated throughout the lower greenschist facies metasediments. As per previous investigations (for example, Bierlein et al. 2000), these euhedral to subhedral, moderate to well-rounded grains are interpreted as being detrital in origin. In addition, (2) rutile is observed in the contact metamorphosed (above the biotite-in isograd) Castlemaine Group metasediments along ilmenite grain margins and occasionally within ilmenite grains, with this rutile representing retrograde recrystallization of ilmenite.

Evidence for rutile (detrital and authigenic) recrystallizing to ilmenite during prograde metamorphism (regional and/or contact) is abundant in both the Meguma Terrane and Bendigo-Ballarat metasediments [for example, rutile relict grains in ilmenite (Fig. 46J), ilmenite replacement becoming more pronounced with increasing metamorphic grade (Figs. 46K, L, M), rutile and ilmenite observed as distinct mineral grains within heavy mineral bands, in the lowest and highest grade samples, respectively (Figs. 46O, R)]. Numerous mineral reactions in the literature describe the recrystallization reaction of rutile to ilmenite (Force 1991, and reference therein). In metasedimentary rocks containing high Al_2O_3/CaO and FeO/MgO ratios, rutile is stable until upper greenschist facies (biotite and garnet zones), where it recrystallizes to yield ilmenite (Force 1991). In such rocks, chlorite may recrystallize and provide the additional cations (Fe ± Mn) and anions (O) required to convert rutile to ilmenite, with silicate mineral(s)

and H_2O also being produced, for example:

$$Rutile + Chlorite <-> Ilmenite + Silicate\ Mineral(s) + H_2O \qquad (Reaction\ 1)$$

The metasedimentary rocks in the Halifax, Goldenville, and Castlemaine Groups all contain high Al_2O_3/CaO and FeO/MgO ratios (Fig. 49). Chlorite and biotite, in both terranes are observed in close association with rutile (Figs. 46E, K) and ilmenite (Figs. 46H, L, M), respectively. This close association suggests that reaction (1) is an appropriate reaction to describe the transition of detrital and authigenic rutile to metamorphic ilmenite in the metasedimentary rocks of the Meguma and Bendigo-Ballarat terranes. In addition, the close association of biotite with ilmenite in both terranes, suggests biotite is the major silicate mineral produced in Reaction 1. Supply of Fe, Mn, and O to the reaction front is paramount to the transformation of rutile to ilmenite. Putnis and Austrheim (2010) highlighted the role hydrous fluids play during any metamorphic reaction (the exception being at high temperatures) involving dissolution, material transport, and precipitation (Willner et al. 2013). Thermal breakdown of chlorite during prograde metamorphism (Reaction 1) releases significant amounts of metamorphic H_2O (Tomkins 2010). Fluids produced during the mineral transition of chlorite to biotite in the Meguma and Bendigo-Ballarat terranes, would have provided sufficient fluid flow to allow the effective transportation of the cations Fe and Mn to the rutile-ilmenite interface. The generation of porosity is an integral aspect of the dissolution, material transport, and precipitation mechanism (Putnis et al. 2005; Putnis and Austrheim 2010). Based on molar volume differences between rutile and ilmenite, an overall increase in volume is implied if all Ti dissolved from rutile is precipitated as ilmenite. Positive volume changes resulting from mineral replacement reactions often generate significant porosity through inducing fracturing in the product and parent phases (Ruiz-Agudo et al. 2014). Although no evidence of this is preserved

(possibly obscured by retrograde alteration) in the rocks of the Meguma or Bendigo-Ballarat terranes, this mechanism was likely in operation in both these terranes. In addition, in the Meguma Terrane pseudomorphic (coupled) dissolution–re-precipitation of detrital rutile grains (Fig. 46C) to poikilitic rutile grains (Fig. 46B) has increased the overall porosity of the grains and increased the surface area of the mineral-reaction interface. Both porosity-forming mechanisms would have allowed (either together or singularly) the fluids produced by the transition of chlorite to biotite to effectively transport Fe and Mn to the rutile-ilmenite interface, resulting in the complete conversion of rutile to ilmenite, in both terranes.

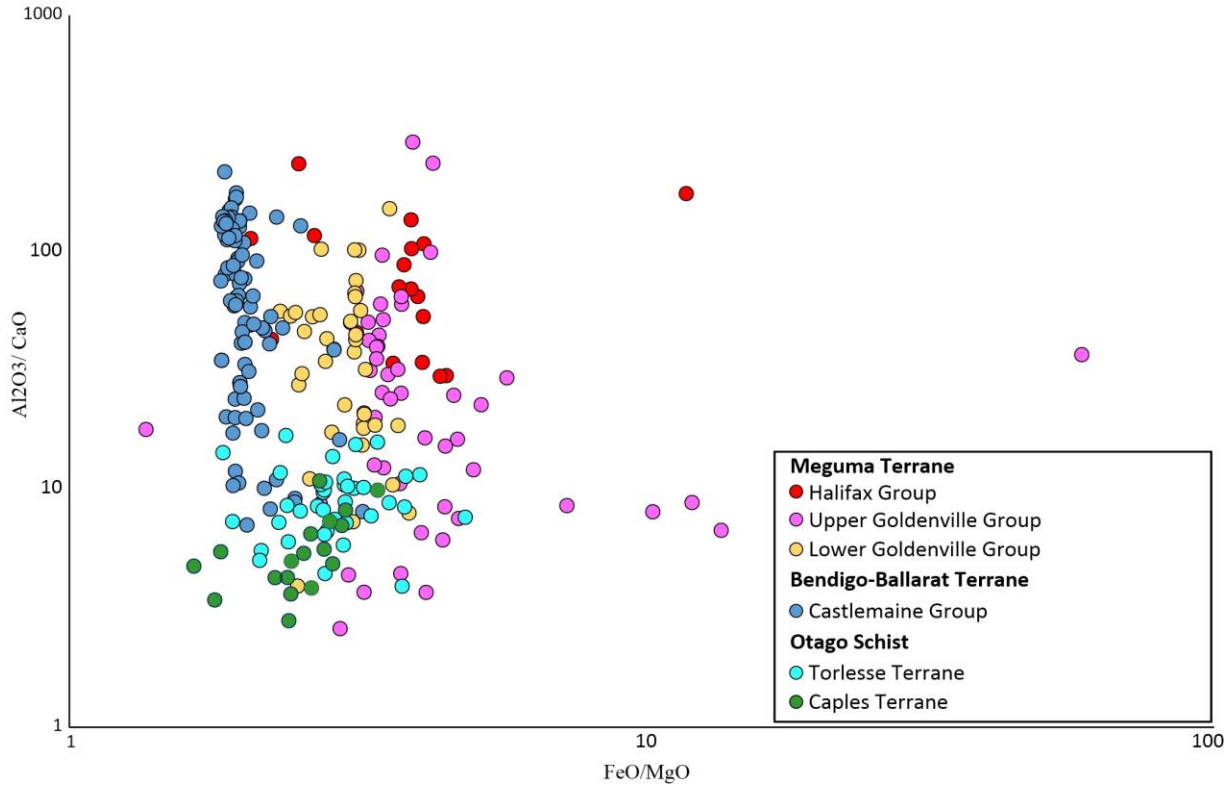

Fig. 49. Whole rock Al_2O_3/CaO ratios plotted against whole rock FeO/MgO ratios from representative metasedimentary samples from the Meguma Terrane, Bendigo-Ballarat Terrane, and Otago Schsit. Data obtained from White and Goodwin (2011) and Zentilli et al. (1986) for the Meguma Terrane, Bull and Large (2014) for the Bendigo-Ballarat Terrane, and Pitcairn (2004) for the Otago Schist.

9.6.3 Release of Trace Elements in the Meguma and Bendigo-Ballarat Terranes during the Rutile to Ilmenite Transition

Rutile (authigenic and/or detrital) in the Meguma and Bendigo-Ballarat terranes is observed recrystallizing to metamorphic ilmenite at the biotite-in isograd during prograde metamorphism (contact and/or regional). Trace element analyzes have highlighted significant differences in the chemical abundance of elements in detrital rutile and metamorphic ilmenite (Fig. 48). A similar recrystallizing reaction of detrital rutile to metamorphic titanite is observed in Otago Schist to release significant amounts of metals (V, Cr, Zr, Nb, Ta, and W) during its recrystallization reaction [Cave et al. 2015 (Chapter 7)]. The release of W during this mineral recrystallization reaction is proposed to be the source of W in the orogenic mineralization of the Otago Schist [Cave et al. accepted (Chapter 8)]. Assessment of whether trace elements were released, retained, or sourced externally during the recrystallization of rutile to ilmenite was undertaken following similar mass balance techniques as outlined by Lucassen et al. (2010) and Cave et al. [2015 (Chapter 7)]. The assumptions of Lucassen et al. (2010) and Cave et al. [2015 (Chapter 7)] are generally adopted, differing slightly to reflect the differences between the mineral reactions of rutile to titanite and rutile to ilmenite. Key assumptions involved in these calculations are: Ti contents of rutile grains (authigenic and/or detrital) completely transfer to metamorphic ilmenite, mean trace element analyzes of rutile are representative, and measurements of trace element contents in metamorphic ilmenite are representative. A dilution factor of 1/1.90 was then applied to the mean trace element concentrations of rutile, to yield expected mean concentration of trace elements in metamorphic ilmenite (Table 10) following the methods of Gresens (1967), Lucassen et al. (2010), and Cave et al. [2015 (Chapter 7)], with this dilution factor based on 100 g of rutile (TiO_2) requiring 80.05 g FeO and 9.77 g MnO for the

complete conversion of rutile (TiO_2) to ilmenite [$Fe_{(0.89)}Mn_{(0.11)}TiO_3$; Equation 5]. As previously discussed, the addition of mass and reduction in density in the dilution factor reaction, predicts an overall increase in volume will be observed if all Ti dissolved from rutile is precipitated as ilmenite. Typically, metamorphic ilmenite grains are observed being larger in size than the rutile grains (in similar lithologies), in both terranes, suggesting this reaction is appropriate.

Equation 5

$$100\ g\ TiO_2\ + 80.05\ g\ FeO + 9.77\ g\ MnO <-> 189.82\ g\ \ Fe_{(0.89)}Mn_{(0.11)}TiO_3$$

Calculated metamorphic ilmenite trace element values were then normalized against measured metamorphic ilmenite trace element values (Table 10, Fig. 50). Values >1, <1, and approximately 1, indicate an element was released, sourced externally, and retained, respectively. Indicated as typically being released, are the elements V, Cr, Zr, Nb, Ta, and W, whereas Mn and Fe require external input (Fig. 50). The external source(s) for Mn and Fe, as previously discussed, is likely the recrystallization of chlorite to biotite (Reaction 1). The orogenic Au deposits of the Meguma Terrane, similar to those in the Otago Schist contain enrichments of W. The release of W during the transition of rutile to metamorphic ilmenite (Fig. 50) potentially provides a source for W in the orogenic Au deposits of the Meguma Terrane, similar to those in the Otago Schist where the transition of rutile to metamorphic titanite is the source of W [Cave et al. accepted (Chapter 8)]. The lack of W in the orogenic Au deposits of the Bendigo-Ballarat Terrane, however, complicates this. A feature that is discussed further in the subsequent discussion subsections.

Table 10. Calculated trace element releases for the recrystallization of rutile to ilmenite, in the Meguma and Bendigo-Ballarat terranes.

Meguma Terrane	V	Cr	Mn	Fe	Zr	Nb	Hf	Ta	W
Rutile (mean ppm)	858	278	45	3,543	333	1,894	16.6	128	257
Ilmenite (mean ppm)	39	N/A	71,534	277,814	35	490	N/A	62	19.8
Calculated ilmenite (mean ppm)	452	146	24	1,865	175	997	9	67	136
Calculated ilmenite normalized to measured metamorphic ilmentite	11.6	N/A	0.0003	0.007	5.0	2.0	N/A	1.09	6.8

Bendigo- Ballarat Terrane	V	Cr	Mn	Fe	Zr	Nb	Hf	Ta	W
Rutile (mean ppm)	1,094	685	N/A	2,588	415	3,329	19.0	243	462
Ilmenite (mean ppm)	313	159	7,647	333,967	1.9	778	N/A	91	23
Calculated ilmenite (mean ppm)	576	361	N/A	1,362	219	1,752	10	128	243
Calculated ilmenite normalized to measured metamorphic ilmentite	1.8	2.3	N/A	0.004	114	2	N/A	1.4	10.7

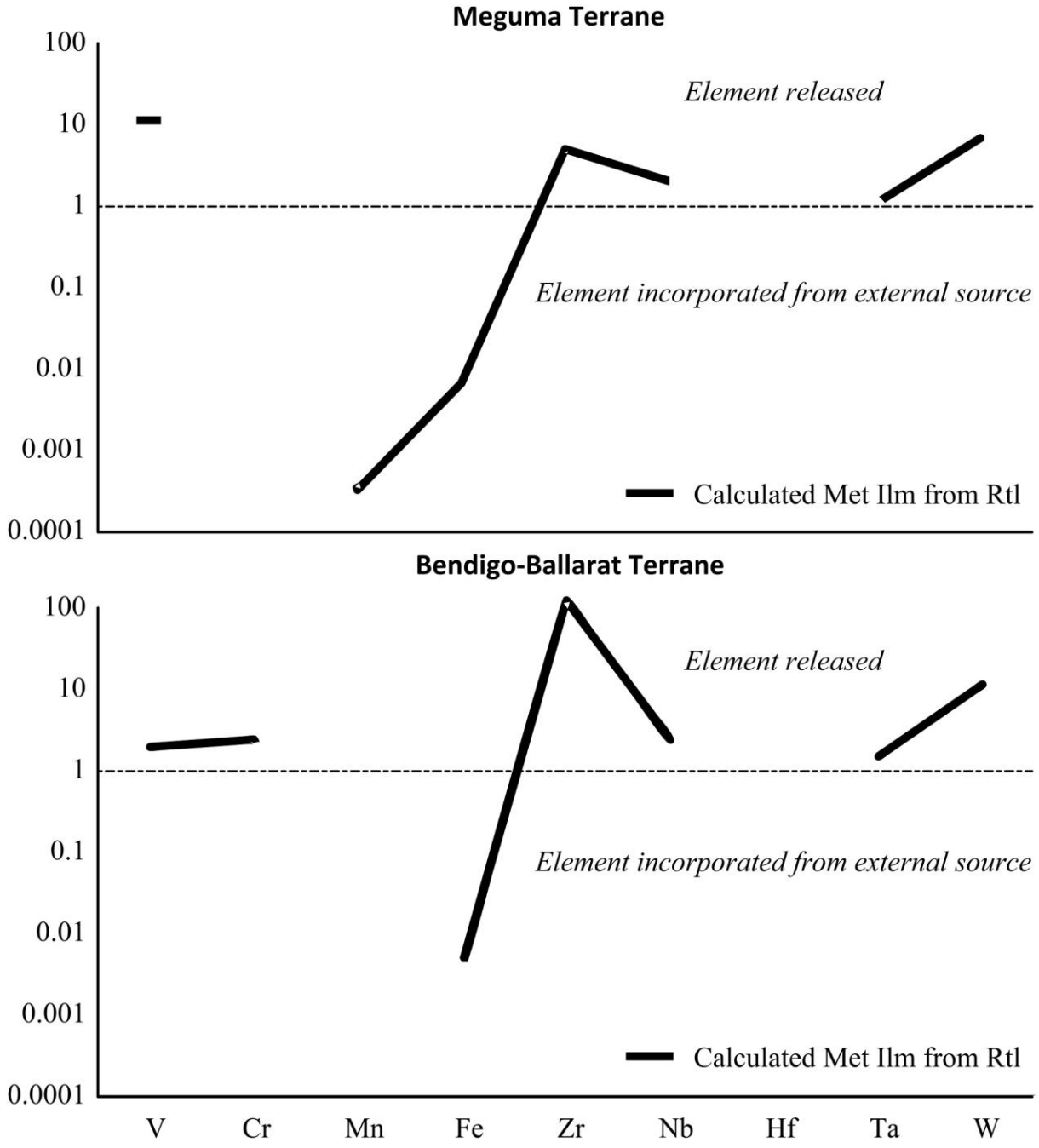

Fig. 50. Mean calculated trace element values for metamorphic ilmenite forming after rutile calculated using the 1/1.9 dilution factor, normalized against mean measured metamorphic ilmenite composition. Elements plotting above the mean measured metamorphic ilmenite normalization line are suggested to have been released during the mineral transition, elements plotting on or very close to the line are suggested as being retained and elements plotting below the mean measured metamorphic ilmenite normalization line are suggested as being incorporated

from an external source. Calculation of mean values for some trace elements weren't possible in some instances for rutile or ilmenite, or both, hence calculating trace element releases wasn't possible for all elements.

9.6.4 Mass of W Mobilized from the Recrystallization of Detrital Rutile to Metamorphic Ilmenite

Calculating the mass of metals and fluids mobilized during prograde metamorphism is a common approach undertaken to understand the volumes of source rocks needed to produce ore deposits [for example, Pitcairn et al. 2006, 2014, 2015a; Cave et al. accepted (Chapter 8)]. The mass of W produced from the complete conversion of rutile to ilmenite is easily calculated (Table 11), using a mass balance reaction (Equation 5). Assuming rutile and metamorphic ilmenite mean W concentrations as reported in Table 9 are representative, together with conservative rutile volume abundance of 1 and 0.05% (based on computer processing of backscatter electron mount scans) for the Meguma and Bendigo-Ballarat terranes, respectively, a source rock density of 2.7 t/m^3, and a rutile density equaling 4.23 t/m^3; approximately 1.9 g and 0.18 g of W is released per ton of rock that has undergone the complete conversion of rutile to ilmenite in the Meguma and Bendigo-Ballarat terranes, respectively (Table 11). These results fall either side of the 0.41 g of W released per ton of rock in the Otago Schist that has undergone the complete conversion of rutile to titanite [Cave et al. accepted (Chapter 8)]. Comparison of the advection of the same volume/mass of source rocks as per Cave et al. [accepted (Chapter 8)] for 1 Myrs would result in excess of 2,565,000 and 243,000 tons of W being mobilized from the recrystallization of rutile to ilmenite, in the Meguma and Bendigo-Ballarat terranes, respectively (Table 11). It is clear that not all the mobilized W finds its way into orogenic deposits in the Meguma and Bendigo-Ballarat terranes. Indeed significant W-bearing minerals are entirely absent from the orogenic deposits of the Bendigo-Ballarat terranes. Efficient fluid focusing and

chemical trapping are suggested as being the most important controlling factors on the formation of orogenic deposits (Pitcairn et al. 2014). Clearly the occurrence of orogenic deposits in both the Meguma and Bendigo-Ballarat terranes eliminates a lack of efficient fluid focusing in both terranes. Availability of Ca through wall-rock alteration is a proposed mode of W (scheelite) precipitation in the orogenic Au deposits of the Otago Schist [Paterson and Rankin 1979; Paterson 1982, 1986; McKeag et al. 1989; Cave et al. accepted (Chapter 8)]. In comparison to the Otago Schist, the Meguma and Bendigo-Ballarat terranes are generally relatively CaO poor (Fig. 51), thus chemical trapping may have been less efficient within these terranes. The majority of scheelite-bearing deposits in the Meguma Terrane are found hosted within the upper part of the Goldenville Group (Fisher 1984; Zentilli et al. 1986; Dostal et al. 2009) that is distinctly enriched in CaO compared to the bulk CaO concentrations of the Halifax and Goldenville Groups (Fig. 51). Furthermore, locally numerous calc-silcate nodules and rare beds (up to 0.5 m wide) are present within the Goldenville Group and to a lesser extent in the Halifax Group, and are occasionally observed containing scheelite (Mitchell 2003; Reid 2005). This provides further evidence that a major limiting factor for the formation of scheelite in the Meguma Terrane is likely the availability of Ca through wall-rock alteration. The lack of significant W-bearing minerals in the orogenic deposits of the Bendigo-Ballarat Terrane, may have also resulted from inefficient chemical trapping. Assuming as appears to be the case in the Otago Schist and Meguma Terrane that the availability of Ca through wall-rock alteration is an important factor on the presence of scheelite in orogenic mineralization in the terranes, whole rock CaO values in the Bendigo-Ballarat Terrane should be consistently low. Comparison of whole rock CaO values in the Bendigo-Ballarat Terrane to those in the Meguma Terrane shows the Bendigo-Ballarat Terrane rocks do contain low bulk CaO concentrations, similar to those in the Halifax and

Goldenville Groups (excluding the upper Goldenville Group) (Fig. 51). However, minor calcerous units are present within the Castlemaine metasediments (Fig. 51), some of which host orogenic Au mineralization (Bull and Large, 2014), and yet no significant W-bearing mineral phases (scheelite) are observed within these either, suggesting that the lack of scheelite in the Bendigo-Ballarat deposits might be controlled by other factors.

Table 11. Mass balance parameters and results, showing the mass of W produced from the advection of 10 km wide × 5 km deep section of starting material (source rock) through an orogeny (and complete conversion of rutile to ilmenite) at a rate of 0.01 m/yr for 1, 2, 3, 4, and 5 Myrs. Shown below for comparison are values calculated by Cave et al. [accepted (Chapter 8)] for W produced in the Otago Schist. Cave et al. [accepted (Chapter 8)] calculations were made using the advection of the same volume of source rocks, orogeny rate, and periods of time as was used to calculate the mass of W produced in the Meguma Terrane and Bendigo-Ballarat Terrane from the source area.

Mass balance parameters and results:

Equation 5 $100\ g\ TiO_2\ + 80.05\ g\ FeO + 9.77\ g\ MnO <-> Fe_{(0.89)}Mn_{(0.11)}TiO_3$

Mass Balance	Unit	Value
Measured mean detrital rutile (Meguma Terrane)	ppm	257
Measured mean detrital rutile (Bendigo-Ballarat Terrane)	ppm	462
Mean metamorphic ilmenite calculated from mean rutile composition (Meguma Terrane) and mass-balance equation (Equation 5) (that is, a dilution factor of 1.90 being applied to the mean rutile composition)	ppm	136
Mean metamorphic ilmenite calculated from mean rutile composition (Bendigo-Ballarat Terrane) and mass-balance equation (Equation 5) (that is, a dilution factor of 1.90 being applied to the mean rutile composition)	ppm	243
Measured mean metamorphic ilmenite (Meguma Terrane)	ppm	19.8
Measured mean metamorphic ilmenite (Bendigo-Ballarat Terrane)	ppm	23
Calculated loss of W per 100g of rutile converted to metamorphic ilmenite (Meguma Terrane)	g	0.0121

Calculated loss of W per 100g of rutile converted to metamorphic ilmenite (Bendigo-Ballarat Terrane)	g	0.0228
Volume percent rutile in lowest metamorphic grade metasediments[1] (Meguma Terrane)	%	1.0
Volume percent rutile in lowest metamorphic grade metasediments[1] (Bendigo-Ballarat Terrane)	%	0.05
Rutile density	t/m^3	4.23
Source rock density[2]	t/m^3	2.7
Convergence rate[2]	m/yr	0.01
Source area length[2]	m	10,000
Source area depth[2]	m	5,000
Volume through orogen[2]	m^3/yr	500,000
Mass through orogen[2]	t/yr	1,350,000

[1]Conservative value based on scanning electron imaging and petrographic observations. [2] Same parameters used by Cave et al [accepted (Chapter 8)].

Mass produced from rutile to ilmenite recrystallization reaction in the Meguma Terrane from source area (t/Myr)						
	(g/t)	1	2	3	4	5
W	1.90	2,565,000	5,130,000	7,695,000	10,260,000	12,825,000

Mass produced from rutile to ilmenite recrystallization reaction in the Bendigo-Ballarat Terrane from source area (t/Myr)						
	(g/t)	1	2	3	4	5
W	0.18	243,000	486,000	729,000	972,000	1,215,000

Comparison against values calculated for the mass of W mobilized in the Otago Schist by Cave et al [accepted (Chapter 8)].

Mass produced from rutile to titanite recrystallization reaction in the Otago Schist from source area (t/Myr)						
	(g/t)	1	2	3	4	5
W	0.41	553,500	1,107,000	1,660,500	2,214,000	2,767,500

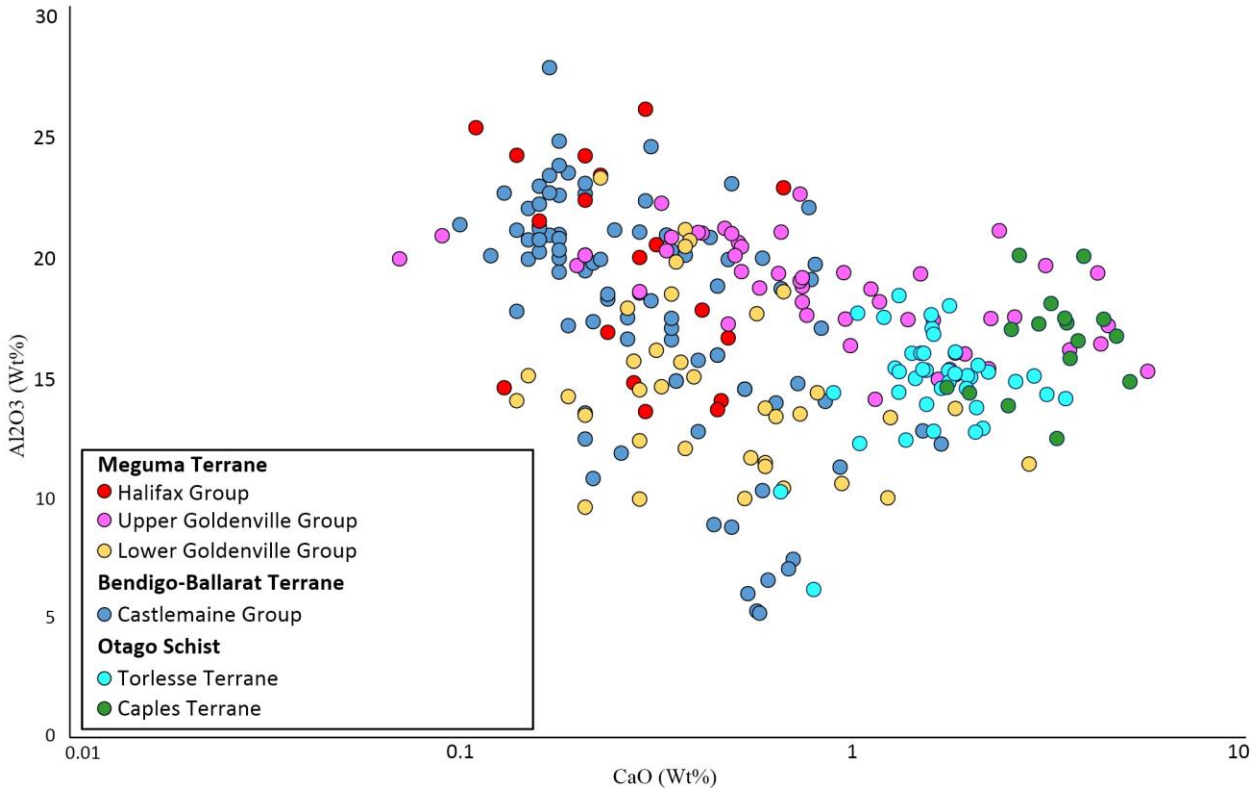

Fig. 51. Whole rock values for Al_2O_3 and CaO plotted against one another, from representative metasedimentary samples from the Meguma Terrane, Bendigo-Ballarat Terrane, and Otago Schist. Data obtained from White and Goodwin (2011) and Zentilli et al. (1986) for the Meguma Terrane, Bull and Large (2014) for the Bendigo-Ballarat Terrane, and Pitcairn (2004) for the Otago Schist.

9.6.5 Likely Sources of Metals in the Meguma and Bendigo-Ballarat Terranes

Results, as previously discussed, indicate that a significant amount of W is mobilized from the metasedimentary rocks of the Meguma Terrane during the metamorphic recrystallization of rutile to ilmenite (Fig. 49 and Table 11). The restriction of orogenic Au-W deposits in the Meguma Terrane to greenschist facies rocks (Sangster and Smith 2007), coupled with the observed significant release of W at this metamorphic grade is indicative that the W in these deposits is likely sourced from the recrystallization of rutile to ilmenite at the biotite-in isograd. The sources for other metals commonly enriched (Au, Sb, As, Te, and Ag) in other

turbidite-hosted orogenic Au deposits around the world, has recently been suggested as being derived from the metamorphic recrystallization of diagenetic pyrite to pyrrhotite, (Pitcairn et al. 2006, 2010, 2014; Large et al. 2007, 2011, 2012; Thomas et al. 2011). In addition, the composition of diagenetic pyrite forming in open oceans is suggested as being a function of age (Gregory et al. 2015; Large et al. 2015), with diagenetic pyrite from other sedimentary rocks of similar age to those of the Meguma Terrane being enriched in Au, As, Ag, Te, and other elements. In the Meguma Terrane, the distribution and texture of pyrrhotite indicates its formation from the recrystallization of diagenetic pyrite during regional greenschist facies metamorphism (Haysom et al. 1997; Clarke et al. 2009). Thus, the metals enriched within the orogenic deposits of the Meguma Terrane (Au, As, Ag, Te, and W) can be explained by the recrystallization of metal-rich diagenetic (pyrite) and detrital (rutile) minerals with regional ± contact metamorphism.

Problematic to this study is why W is not enriched in the Bendigo-Ballarat Terrane orogenic Au deposits, when it is indicated as being mobilized during the metamorphic recrystallization of rutile to ilmenite (Table 11, Fig. 49). However, this mobilization of W assumes that Castlemaine Group metasediments were the source rocks and that they reached at least the biotite-in isograd, during regional metamorphism, as the major orogenic Au event pre-dates the intrusives (Bierlein et al. 2001; Phillips et al. 2012). Deep seismic surveys (Cayley et al. 2011) conducted across the Bendigo-Ballarat Terrane do indicate that a significant portion of the Castlemaine Group metasediments have likely experienced upper greenschist to amphibolite facies conditions (Willman et al. 2010; Lisitsin and Pitcairn 2015), with the metamorphic recrystallization of diagenetic pyrite to metamorphic pyrrhotite at this transition recently suggested as being the source for Au, Sb, As, Te, and Ag in these orogenic deposits (Lisitsin and

Pitcairn 2015). However, other studies (Large et al. 2011; Thomas et al. 2011) have observed the recrystallization of diagenetic pyrite to pyrrhotite in organic-rich metasedimentary units of Castlemaine Group metasediments at lower greenschist facies conditions, with the organic-rich metasedimentary units lowering $f(O_2)$ conditions promoting lower recrystallization temperatures (Hall 1986). Thus, the lack of W in the orogenic Au deposits of the Bendigo-Ballarat Terrane favors a metals source for these deposits from lower stratigraphic levels of the Castlemaine Group metasedimentary rocks (that is below the deposits) with mobilization of the metals occurring at lower greenschist facies conditions (Thomas et al. 2011; Large et al. 2011). The lack of W in these deposits potentially further precludes previous models that have suggested source rocks for Au in these deposits as being either Castlemaine metasediments at the greenschist-amphibolite transition (Lisitsin and Pitcairn 2015) or underlying Cambrian metavolcano-sedimentary (Keays and Scott 1976; Bierlein et al. 1998; Willman et al. 2010). Reasoning for this preclusion of the underlying Cambrian metavolcano-sedimentary rocks as a metals source, is that any metal-rich fluids derived from these rocks would have to travel through Castlemaine metasediments that have experienced upper greenschist to amphibolite facies conditions, and hence the orogenic Au deposits should contain scheelite. However, the lack of scheelite in the Bendigo-Ballarat Terrane could also result from other factors, such as variations in the conditions of formation of the mineralized veins (P, T, pH, redox, host-rock composition) that may not favor the transport and/or precipitation of W. These factors were unable to be resolved in this study, with further work required on this.

9.6.6 Implications for the Sources of Metals in Turbidite-hosted Orogenic Au Deposits

Interpretation of results presented within this paper, supports current models for metals

sources in turbidite-hosted orogenic Au deposits, with metals in these deposits being derived from the prograde metamorphic recrystallization of diagenetic or detrital metal-rich mineral phases [pyrite to pyrrhotite, Au, As, Ag, Hg, and Sb (Pitcairn et al. 2006, 2010, 2014, 2015b; Large et al. 2007, 2009, 2011, 2012; Steadman et al. 2013; Gregory et al. 2015); rutile to titanite/ilmenite W (Cave et al. [accepted (Chapter 8)], this chapter)]. In addition, this study suggests that whole-rock compositions of the source and host rocks, can potentially be important in terms of the metamorphic grade metals mobilized and metals precipitated, respectively. The metamorphic recrystallization of pyrite to pyrrhotite is suggested as being the most important source for Au, As, Ag, Hg, and Sb. The conversion of pyrite to pyrrhotite is well-defined as being facilitated by the availability of organic carbon and Fe^{2+} (for example, from silicates), and the presence of water, as outlined in the following reactions (Ferry 1981; Hoschek 1984; Thomas et al. 2011):

Equation 6 $2\,FeS_2 + 2H_2O + C <-> 2FeS + 2H_2S + CO_2$, and

Equation 7 $FeS_2 + Fe^{2+} + 0.5C + H_2O <-> 2FeS + H^+ + 0.5CO_2$

Thus, in rocks containing abundant organic carbon and available Fe^{2+} that interact with meteoric or metamorphic fluids (for example, organic-rich pyritic shales being metamorphosed) pyrite commonly recrystallizes to pyrrhotite at lower to upper greenschist facies conditions (Large et al. 2011), with increasing amounts of organic carbon lowering $f(O_2)$ conditions promoting lower recrystallization temperatures (Hall 1986) and mobilizing important metals (Au, As, Ag, Hg, and Sb) at lower metamorphic grades.

The metamorphic recrystallization of rutile to titanite or ilmenite, similarly, is suggested as being the most important source for W [Cave et al. accepted (Chapter 8), this chapter]. The conversion of rutile to titanite or ilmenite is facilitated by the availability of the Ca, Si, and O,

and Fe, Mn, and O, respectively, and the presence of water [Cave et al. 2015 (Chapter 7), this chapter]. Bulk country-rock compositions (that is, Al_2O_3/CaO and FeO/MgO ratios), as discussed previously, controls the recrystallization product of rutile and, as such, the metamorphic grade that this reaction takes place. For example, in the Bendigo-Ballarat and Meguma terranes the metasedimentary rocks contain high FeO/MgO and Al_2O_3/CaO ratios (Fig. 49), thus rutile recrystallizes to ilmenite at upper greenschist facies. Whereas in the Otago Schist the combination of low FeO/MgO and Al_2O_3/CaO ratios (Fig. 49) has resulted in rutile recrystallizing to titanite at subgreenschist-lower greenschist facies conditions. Thus, in source rocks containing high FeO/MgO and Al_2O_3/CaO ratios, rutile will recrystallize to ilmenite at upper greenschist facies and mobilize W, whereas in rocks containing low FeO/MgO and Al_2O_3/CaO ratios rutile will recrystallize to titanite at subgreenschist facies and mobilize W.

9.7 Conclusion

Turbidite-hosted orogenic Au deposits, are commonly enriched in W, along with a variety of other trace elements including Au, As, Ag, Hg, and Sb. Prograde metamorphism of metasedimentary rocks and the accompanying recrystallization of sedimentary pyrite (to metamorphic pyrrhotite) has been shown to mobilize and be the source of Au, As, Ag, Hg, and Sb in these deposits. A similar mineralogical source for W, has recently been shown in the Otago Schist of southern New Zealand (Chapter 8), with detrital rutile in the metasediments recrystallizing to metamorphic titanite and mobilizing W. This chapter shows in the more pelitic rocks of the Meguma and Bendigo-Ballarat terranes, detrital rutile recrystallizes to metamorphic ilmenite at upper greenschist facies conditions. Tungsten is mobilized during this recrystallization reaction and based on modal mineral abundances significant amounts of W are

released (1.9 g and 0.18 g of W per ton of rock, Meguma Terrane and Bendigo-Ballarat Terrane, respectively). The release of W during the recrystallization of rutile to ilmenite is likely the source of W in the orogenic Au deposits of the Meguma Terrane. The lack of W in the orogenic Au deposits of the Bendigo-Ballarat Terrane possibly reflects the source of these deposits as being the lower greenschist facies metasediments. Recrystallization of sedimentary pyrite to pyrrhotite occurs in these rocks at a lower metamorphic grade owning to the organic-rich metasedimentary units lowering $f(O_2)$ conditions promoting lower recrystallization temperatures. This lack of W in the Bendigo-Ballarat Terrane, potentially precludes previous models that have suggested source rocks for Au as being either Castlemaine metasediments at the greenschist-amphibolite transition or underlying Cambrian volcano-sedimentary rocks. However, the lack of scheelite in the Bendigo-Ballarat Terrane could also result from other factors, such as variations in the conditions of formation of the mineralized veins (P, T, pH, redox, host-rock composition) that may not favor the transport and/or precipitation of W. These factors were unable to be resolved in this study. Results presented within this study are supportive of recent models for turbidite-hosted orogenic Au mineralization, whereby prograde metamorphic recrystallization of diagenetic or detrital metal-rich mineral phases [pyrite to pyrrhotite, Au, As, Ag, Hg and Sb; rutile to titanite (Chapter 8) or ilmenite (this chapter), W] can release significant amounts of these metals into the concurrently developing metamorphic fluids that can be subsequently focused into regional structures and form orogenic Au ± W deposits.

References

BIERLEIN, F., ARNE, D., BROOME, J., & RAMSAY, W. 1998. Metatholeiites and interflow sediments from the Cambrian Heathcote greenstone belt, Australia; sources for gold

mineralization in Victoria? *Economic Geology,* 93**,** 84-101.

BIERLEIN, F., ARNE, D., MCKNIGHT, S., LU, J., REEVES, S., BESANKO, J., MAREK, J. & COOKE, D. 2000. Wall-rock petrology and geochemistry in alteration halos associated with mesothermal gold mineralization, central Victoria, Australia. *Economic Geology,* 95**,** 283-311.

BIERLEIN, F., ARNE, D., KEAY, S. & MCNAUGHTON, N. 2001. Timing relationships between felsic magmatism and mineralisation in the central Victorian gold province, southeast Australia. *Australian Journal of Earth Sciences,* 48**,** 883-899.

BIERLEIN, F. P., CHRISTIE, A. B. & SMITH, P. K. 2004. A comparison of orogenic gold mineralisation in central Victoria (AUS), western South Island (NZ) and Nova Scotia (CAN): implications for variations in the endowment of Palaeozoic metamorphic terrains. *Ore Geology Reviews,* 25**,** 125-168.

BULL, S. W. & LARGE, R. R. 2014. Setting the stage for the genesis of the giant Bendigo ore system. *Geological Society, London, Special Publications,* 393**,** 161-187.

CAVE, B. J., STEPANOV, A. S., CRAW, D., LARGE, R. R., HAPLIN, J. A. & THOMPSON, J. 2015. Release of trace elements through the sub-greenschist facies breakdown of detrital rutile to metamorphic titanite in the Otago Schist, New Zealand. *The Canadian Mineralogist,* 53**,** 379-400.

CAVE, B. J., PITCAIRN, I. K., CRAW, D., LARGE, R. R., THOMPSON, J. & JOHNSON, S. C. accepted. A metamorphic mineral source for tungsten in the turbidite-hosted orogenic gold deposits of the Otago Schist, New Zealand. *Mineralium Deposita*.

CAYLEY, R. A., KORSCH, R. J., MOORE, D. H., COSTELLOE, R. D., NAKAMURA, A., WILLMAN, C. E., RAWLING, T. J., MORAND, V. J., SKLADZIEN, P. B. & O'SHEA,

P. J. 2011. Crustal architecture of central Victoria: results from the 2006 deep crustal reflection seismic survey. *Australian Journal of Earth Sciences,* 58**,** 113-156.

CHATTERJEE, A. & KEPPIE, J. 1981. Polymetallic mineralization in the endo-and exo-contact of the Wedgeport Pluton, Yarmouth County. *Nova Scotia Department of Mines and Energy,* Report ME 1981-001**,** 43-46.

CIOBANU, C. L., BIRCH, W. D., COOK, N. J., PRING, A. & GRUNDLER, P. V. 2010. Petrogenetic significance of Au–Bi–Te–S associations: the example of Maldon, Central Victorian gold province, Australia. *Lithos,* 116**,** 1-17.

CLARKE, D. B. & CARRUZZO, S. 2007. Assimilation of country-rock ilmenite and rutile in the South Mountain Batholith, Nova Scotia, Canada. *The Canadian Mineralogist,* 45**,** 31-42.

CLARKE, D. B., ERDMANN, S., SAMSON, H., & JAMIESON, R. A. 2009. Contamination of the South Mountain Batholith by sulfides from the country rocks. *The Canadian Mineralogist,* 47**,** 1159-1176.

COX, S., WALL, V., ETHERIDGE, M. & POTTER, T. 1991. Deformational and metamorphic processes in the formation of mesothermal vein-hosted gold deposits—examples from the Lachlan Fold Belt in central Victoria, Australia. *Ore Geology Reviews,* 6**,** 391-423.

CRAW, D. 1992. Fluid evolution, fluid immiscibility and gold deposition during Cretaceous-Recent tectonics and uplift of the Otago and Alpine Schist, New Zealand. *Chemical Geology,* 98**,** 221-236.

CULSHAW, N. & LEE, S. K. 2006. The Acadian fold belt in the Meguma Terrane, Nova Scotia: cross sections, fold mechanisms, and tectonic implications. *Tectonics,* 25**,** TC3007.

DOSTAL, J., KONTAK, D. J., & CHATTERJEE, A. 2009. Trace element geochemistry of

scheelite and rutile from metaturbidite-hosted quartz vein gold deposits, Meguma Terrane, Nova Scotia, Canada: genetic implications. *Mineralogy and Petrology,* 97**,** 95-109.

FERGUSSON, C. 2003. Ordovician–Silurian accretion tectonics of the Lachlan fold belt, southeastern Australia. *Australian Journal of Earth Sciences,* 50**,** 475-490.

FERGUSSON, C. & VANDENBERG, A. 2003. Ordovician—the development of craton-derived deep-sea turbidite successions. *Victorian Division, Geological Society of Australia,* Special Publication 23**,** 97-115.

FERRY, J. M. 1981. Petrology of graphitic sulfide-rich schists from south-central Maine: an example of desulfidation during prograde regional metamorphism. *American Mineralogist,* 66**,** 908-930.

FISHER, B. E. 1984. A regional investigation of scheelite occurrences in the Meguma Group of Nova Scotia. *Unpublished B.Sc. Thesis,* Dalhousie University, Canada**,** 201 p.

FORCE, E. R. 1991. Geology of titanium-mineral deposits. *Geological Society of America,* Special Paper 259**,** 112 p.

FU, B., MERNAGH, T. P., FAIRMAID, A. M., PHILLIPS, D. & KENDRICK, M. A. 2014. CH4-N2 in the Maldon gold deposit, central Victoria, Australia. *Ore Geology Reviews,* 58**,** 225-237.

GOLDFARB, R. J. & GROVES, D. I. 2015. Orogenic gold: Common or evolving fluid and metal sources through time. *Lithos,* 233**,** 2-26.

GOLDFARB, R. J., BAKER, T., DUBE, B., GROVES, D. I., HART, C. J. & GOSSELIN, P. 2005. Distribution, character, and genesis of gold deposits in metamorphic terranes. *Economic Geology 100th Anniversary Volume***,** 407-450.

GRAY, D. R. & FOSTER, D. A. 1998. Character and kinematics of faults within the turbidite-dominated Lachlan Orogen: implications for tectonic evolution of eastern Australia. *Journal of Structural Geology,* 20**,** 1691-1720.

GRAY, D. & WILLMAN, C. 1991. Deformation in the Ballarat Slate Belt, central Victoria, and implications for the crustal structure across southeast Australia. *Australian Journal of Earth Sciences,* 38**,** 171-201.

GREGORY, D. D., LARGE, R. R., HALPIN, J. A., BATURINA, E. L., LYONS, T. W., WU, S., DANYUSHEVSKY, L., SACK, P. J., CHAPPAZ, A. & MASLENNIKOV, V. V. 2015. Trace element content of sedimentary pyrite in black shales. *Economic Geology,* 110**,** 1389-1410.

GRESENS, R. L. 1967. Composition-volume relationships of metasomatism. *Chemical Geology,* 2**,** 47-65.

GROVES, D. I., GOLDFARB, R. J., GEBRE-MARIAM, M., HAGEMANN, S. G. & ROBERT, F. 1998. Orogenic gold deposits: a proposed classification in the context of their crustal distribution and relationship to other gold deposit types. *Ore Geology Reviews,* 13**,** 7-27.

HALL, A. 1986. Pyrite-pyrrhotine redox reactions in nature. *Mineralogical Magazine,* 50**,** 223-229.

HAYSOM, S., HORNE, R. & PE-PIPER, G. 1997. The opaque mineralogy of metasedimentary rocks of the Meguma Group, Beaverbank-Rawdon area, Nova Scotia. *Atlantic Geology***,** 33.

HIBBARD, J. P., VAN STAAL, C. R. & MILLER, B. V. 2007. Links among Carolinia, Avalonia, and Ganderia in the Appalachian peri-Gondwanan realm. *Geological Society of America Special Papers,* 433**,** 291-311.

HICKS, R. J., JAMIESON, R. A. & REYNOLDS, P. H. 1999. Detrital and metamorphic 40Ar/39Ar ages from muscovite and whole-rock samples, Meguma Supergroup, southern Nova Scotia. *Canadian Journal of Earth Sciences,* 36**,** 23-32.

HILCHIE, L. & JAMIESON, R. 2014. Graphite thermometry in a low-pressure contact aureole, Halifax, Nova Scotia. *Lithos,* 208**,** 21-33.

HORNE, R. & CULSHAW, N. 2001. Flexural-slip folding in the Meguma group, Nova Scotia, Canada. *Journal of Structural Geology,* 23**,** 1631-1652.

HORNE, R. & PELLEY, D. 2006. Geological transect of the Meguma terrane from Centre Musquodoboit to Tangier. *Nova Scotia Department of Natural Resources,* Report ME 2007-001**,** 71-89.

HOSCHEK, G. 1984. Alpine metamorphism of calcareous metasediments in the Western Hohe Tauern, Tyrol: mineral equilibria in COHS fluids. *Contributions to Mineralogy and Petrology,* 87**,** 129-137.

HY, C. & WILLIAMS, P. 1986. Meguma quartz veins: Tangier area. *10th Annual Open House and Review of Activities, Nova Scotia Department of Mines and Energy,* Information Series Number 10**,** 202-205.

JAMIESON, R. A., HART, G., CHAPMAN, G., TOBEY, N. & MURPHY, B. J. 2012. The contact aureole of the South Mountain Batholith in Halifax, Nova Scotia: geology, mineral assemblages, and isograds. *Canadian Journal of Earth Sciences,* 49**,** 1280-1296.

JIA, Y., 2002, Nitrogen Isotope Characteristics of Orogenic Lode Gold Deposits and Terrestrial Reservoirs. *Unpublished Ph.D. Thesis,* University of Saskatchewan, Canada.

KEAYS, R. & SCOTT, R. 1976. Precious metals in ocean-ridge basalts; implications for basalts as source rocks for gold mineralization. *Economic Geology,* 71**,** 705-720.

KEAYS, R. R. 1987. Principles of mobilization (dissolution) of metals in mafic and ultramafic rocks — The role of immiscible magmatic sulphides in the generation of hydrothermal gold and volcanogenic massive sulphide deposits. *Ore Geology Reviews,* 2**,** 47-63.

KEPPIE, J. & DALLMEYER, R. 1995. Late Paleozoic collision, delamination, short-lived magmatism, and rapid denudation in the Meguma Terrane (Nova Scotia, Canada): constraints from 40Ar/39Ar isotopic data. *Canadian Journal of Earth Sciences,* 32**,** 644-659.

KOGLIN, N., ZEH, A., CABRAL, A. R., DECKER, M. & GOMES JR, A. A. S. 2015. Alteration and formation of rutile in aqueous fluids: evidence from microstructures, trace-elements and U–Pb Ages [abs.]. *SGA Biennial Meeting, 13th, Nancy, France, 2015, Proceedings,* 2**,** 595-598.

KONTAK, D. J. & ARCHIBALD, D. A. 2002. 40Ar/39Ar dating of hydrothermal biotite from high-grade gold ore, Tangier gold deposit, Nova Scotia: further evidence for 370 Ma gold metallogeny in the Meguma Terrane. *Economic Geology,* 97**,** 619-628.

KONTAK, D. & SMITH, P. 1987. Alteration haloes and their implications for gold mineralization in the Meguma zone, Nova Scotia. *Nova Scotia Department of Natural Resources,* Report ME 1987-001**,** 65-74.

KONTAK, D. & SMITH, P. 1988a. Meguma gold studies IV: Chemistry of vein mineralogy. *Nova Scotia Department of Natural Resources,* Report ME 1988-001**,** 85-100.

KONTAK, D. & SMITH, P. 1988b. Meguma gold studies VI: Integrated model for the genesis of Meguma-hosted lode gold deposits. *Nova Scotia Department of Natural Resources,* Report ME 1988-001**,** 11-119.

KONTAK, D. & SMITH, P. 1989. Fluid inclusion study of quartz vein polytypes in the Beaver

Dam gold deposit: Meguma terrane, Nova Scotia, Canada [abs.]. *Pan-American Conference on Research on Fluid Inclusions, 2nd, Virginia, United States of America,* 1989**,** 38.

KONTAK, D. J. & SMITH, P. K. 1993, A metaturbidite-hosted lode gold deposit: the Beaver Dam deposit, Nova Scotia; I. vein paragenesis and mineral chemistry. *The Canadian Mineralogist,* 31**,** 471.

KONTAK, D. J., SMITH, P. K., KERRICH, R. & WILLIAMS, P. F. 1990. Integrated model for Meguma Group lode gold deposits, Nova Scotia, Canada. *Geology,* 18, 238-242.

KONTAK, D. J., SMITH, P. K. & REYNOLDS, P. H. 1993. Geology and 40 Ar/39 Ar geochronology of the Beaver Dam gold deposit, Meguma Terrane, Nova Scotia, Canada; evidence for mineralization at 370 Ma. *Economic Geology,* 88**,** 139-170.

KONTAK, D. J., HORNE, R. J., SANDEMAN, H., ARCHIBALD, D. & LEE, J. K. 1998. 40Ar/39Ar dating of ribbon-textured veins and wall-rock material from Meguma lode gold deposits, Nova Scotia: implications for timing and duration of vein formation in slate-belt hosted vein gold deposits. *Canadian Journal of Earth Sciences,* 35**,** 746-761.

KONTAK, D. J., HORNE, R. J. & SMITH, P. 2001. Meguma gold deposits, Nova Scotia: overview of past work with implications for future work. *The Gangue, Geological Association of Canada, Mineral Deposits Division Newsletter,* 71**,** 1–9.

LARGE, R. R., MASLENNIKOV, V. V., ROBERT, F., DANYUSHEVSKY, L. V. & CHANG, Z. 2007. Multistage sedimentary and metamorphic origin of pyrite and gold in the giant Sukhoi Log deposit, Lena gold province, Russia. *Economic Geology,* 102**,** 1233-1267.

LARGE, R. R., DANYUSHEVSKY, L., HOLLIT, C., MASLENNIKOV, V., MEFFRE, S., GILBERT, S., BULL, S., SCOTT, R., EMSBO, P. & THOMAS, H. 2009. Gold and trace

element zonation in pyrite using a laser imaging technique: implications for the timing of gold in orogenic and Carlin-style sediment-hosted deposits. *Economic Geology,* 104**,** 635-668.

LARGE, R. R., BULL, S. W. & MASLENNIKOV, V. V. 2011. A Carbonaceous sedimentary source-rock model for Carlin-type and orogenic gold deposits. *Economic Geology,* 106**,** 331-358.

LARGE, R., THOMAS, H., CRAW, D., HENNE, A. & HENDERSON, S. 2012. Diagenetic pyrite as a source for metals in orogenic gold deposits, Otago Schist, New Zealand. *New Zealand Journal of Geology and Geophysics,* 55**,** 137-149.

LARGE, R. R., GREGORY, D. D., STEADMAN, J. A., TOMKINS, A. G., LOUNEJEVA, E., DANYUSHEVSKY, L. V., HALPIN, J. A., MASLENNIKOV, V., SACK, P. J. & MUKHERJEE, I. 2015. Gold in the oceans through time. *Earth and Planetary Science Letters,* 428**,** 139-150.

LISITSIN, V. A. & PITCAIRN, I. K. 2015. Orogenic gold mineral systems of the Western Lachlan Orogen (Victoria) and the Hodgkinson Province (Queensland): crustal metal sources and cryptic zones of regional fluid flow. *Ore Geology Reviews,* 76, 280-295.

MAWER, C. 1985. Origin of bedding-concordant auriferous quartz veins, Meguma Terrane, Nova Scotia. *Atlantic Geology,* 21**,** 1-9.

MAWER, C. 1986. The bedding-concordant gold-quartz veins of the Meguma Group, Nova Scotia: turbidite-hosted gold deposits. *Geological Association of Canada, Special Paper,* 32**,** 135-148.

MAWER, C. 1987. Mechanics of formation of gold-bearing quartz veins, Nova Scotia, Canada. *Tectonophysics,* 135**,** 99-119.

MCKEAG, S., CRAW, D. & NORRIS, R. 1989. Origin and deposition of a graphitic schist-hosted metamorphogenic Au-W deposit, Macraes, East Otago, New Zealand. *Mineralium Deposita,* 24**,** 124-131.

MILLER, C., GRAVES, M. C. & ZENTILLI, M. 1976. Scheelite mineralization of southeastern Nova Scotia. *Geological Survey of Canada,* Paper no. 76-1A**,** 331-332.

MILLER, C. K. 1974. Scheelite Mineralization in the Region of the Moose River Gold District, Halifax County, Nova Scotia. *Unpublished B.Sc. Thesis,* Dalhousie University, Canada**,** 57 p.

MITCHELL, F. 2003. Metamorphic petrology of calc-silicate nodules from greenschist facies to migmatite grade, Liverpool-Pubnico area, Nova Scotia. *Unpublished B.Sc. Thesis,* Acadia University, Canada**,** 95 p.

MORELLI, R. M., CREASER, R. A., SELBY, D., KONTAK, D. J. & HORNE, R. J. 2005. Rhenium-Osmium geochronology of arsenopyrite in Meguma Group gold deposits, Meguma Terrane, Nova Scotia, Canada: Evidence for multiple gold-mineralizing events. *Economic Geology,* 100**,** 1229-1242.

MUECKE, G., ELIAS, P. & REYNOLDS, P. 1988. Hercynian/Alleghanian overprinting of an Acadian terrane: 40 Ar/39 Ar studies in the Meguma zone, Nova Scotia, Canada. *Chemical Geology: Isotope Geoscience section,* 73**,** 153-167.

MURPHY, B., WALDRON, J. W., WHITE, C. E., BARR, S. M., SIMONETTI, A. & HEAMAN, L. M. 2009. Provenance of the Meguma terrane, Nova Scotia: rifted margin of early Paleozoic Gondwana. *Canadian Journal of Earth Sciences,* 46**,** 1-8.

OFFLER, R., MCKNIGHT S. & MORAND V. 1998. Tectonothermal history of the western Lachlan Fold Belt, Australia—insights from white mica studies. *Journal of Metamorphic*

Geology, 16**,** 531-540.

PATERSON, C. J. 1982. Oxygen isotopic evidence for the origin and evolution of a scheelite ore-forming fluid, Glenorchy, New Zealand. *Economic Geology,* 77**,** 1672-1687.

PATERSON, C. J. 1986. Controls on gold and tungsten mineralization in metamorphic-hydrothermal systems, Otago, New Zealand. *Geological Association of Canada Special paper,* 32**,** 25-39.

PATERSON, C. J. & RANKIN, P. C. 1979. Trace element distribution in the schist surrounding a quartz-scheelite lode, Glenorchy, New Zealand. *New Zealand Journal of Geology and Geophysics,* 22**,** 329-338.

PELLEY, D. 2007. Magnetic mineralogy and susceptibility of magnetostratigraphic/stratigraphic subdivisions of the Goldenville Group, eastern shore Nova Scotia. *Unpublished B.Sc. Thesis,* Dalhousie University, Canada, 47 p.

PHILLIPS, G. N. & GROVES, D. I. 1983. The nature of Archaean gold-bearing fluids as deduced from gold deposits of Western Australia. *Journal of the Geological Society of Australia,* 30**,** 25-39.

PHILLIPS, D., FU, B., WILSON, C. J., KENDRICK, M., FAIRMAID, A. & MILLER, J. M. 2012. Timing of gold mineralisation in the western Lachlan Orogen, SE Australia: a critical overview. *Australian Journal of Earth Sciences,* 59**,** 495-525.

PITCAIRN, I. K. 2004. Sources of fluids and metals in orogenic gold deposits: The Otago Schists, New Zealand. *Unpublished Ph.D Thesis,* University of Southhampton, United Kingdom, 362 p.

PITCAIRN, I. K., TEAGLE, D. A. H., CRAW, D., OLIVO, G. R., KERRICH, R. & BREWER, T. S. 2006. Sources of Metals and Fluids in Orogenic Gold Deposits: Insights from the

Otago and Alpine Schists, New Zealand. *Economic Geology,* 101**,** 1525-1546.

PITCAIRN, I. K., OLIVO, G. R., TEAGLE, D. A. H. & CRAW, D. 2010. Sulfide evolution during prograde metamorphism of the Otago and Alpine Schists, New Zealand. *The Canadian Mineralogist,* 48**,** 1267-1295.

PITCAIRN, I. K., CRAW, D. & TEAGLE, D. A. H. 2014. The gold conveyor belt: large-scale gold mobility in an active orogen. *Ore Geology Reviews,* 62**,** 129-142.

PITCAIRN, I. K., CRAW, D. & TEAGLE, D. A. H 2015a. Metabasalts as sources of metals in orogenic gold deposits. *Mineralium Deposita,* 50**,** 373-390.

PITCAIRN, I. K., SKELTON, A. & WOHLGEMUTH-UEBERWASSER, C. 2015b. Mobility of gold during metamorphism of the Dalradian in Scotland. *Lithos,* 233**,** 69-88.

POTHIER, H. D., WALDRON, J. W., WHITE, C. E., DUFRANE, S. A. & JAMIESON, R. A. 2015. Stratigraphy, provenance and tectonic setting of the Lumsden Dam and Bluestone Quarry formations (Lower Ordovician), Halifax Group, Nova Scotia, Canada. *Atlantic Geology,* 51**,** 51-83.

PUTNIS, A. & AUSTRHEIM, H. 2010. Fluid-induced processes: metasomatism and metamorphism. *Geofluids,* 10**,** 254-269.

PUTNIS, C. V., TSUKAMOTO, K. & NISHIMURA, Y. 2005. Direct observations of pseudomorphism: compositional and textural evolution at a fluid-solid interface. *American Mineralogist,* 90**,** 1909-1912.

RAINE, M. D. 2005. Polyphase deformation and the structural controls on economic gold occurences within the Bendigo gold field, central Victoria, Australia. *Unpublished Ph.D Thesis,* James Cook University, Australia, 193 p.

REID, C. 2005. Metamorphism of the Southern Meguma terrane and emplacement of the

Barrington Passage and Quinan Plutons, southwestern Nova Scotia. *Unpublished M.Sc. Thesis,* Acadia University, Canada, p. 211.

REYNOLDS, P., KUBLICK, E. & MUECKE, G. 1973. Potassium-argon dating of slates from the Meguma Group, Nova Scotia. *Canadian Journal of Earth Sciences,* 10**,** 1059-1067.

RUIZ-AGUDO, E., PUTNIS, C. & PUTNIS, A. 2014. Coupled dissolution and precipitation at mineral–fluid interfaces. *Chemical Geology,* 383**,** 132-146.

RYAN, R. & SMITH, P. 1998, A review of the mesothermal gold deposits of the Meguma Group, Nova Scotia, Canada. *Ore Geology Reviews,* 13**,** 153-183.

SANGSTER, A. L. & SMITH, P. K. 2007. Metallogenic summary of the Meguma gold deposits, Nova Scotia. *in Goodfellow, W.D. (Ed.), Mineral Deposits of Canada: a Synthesis of Major Deposit-Types, District Metallogeny, the Evolution of Geological Provinces, and Exploration Methods: Geological Association of Canada, Mineral Deposits Division, Special Publication,* 5**,** 723-732.

SCHAUBS, P. M. & WILSON, C. J. 2002. The relative roles of folding and faulting in controlling gold mineralization along the Deborah Anticline, Bendigo, Victoria, Australia. *Economic Geology,* 97**,** 351-370.

SMITH, P. & KONTAK, D. 1986. Meguma gold studies: advances in geological insight as an aid to gold exploration. *Nova Scotia Department of Mines and Energy Information Series,* 12**,** 105-113.

STEADMAN, J. A., LARGE, R. R., MEFFRE, S. & BULL, S. W. 2013. Age, origin and significance of nodular sulfides in 2680Ma carbonaceous black shale of the Eastern Goldfields Superterrane, Yilgarn Craton, Western Australia. *Precambrian Research,* 230**,** 227-247.

TAYLOR, F. & SCHILLER, E. 1966. Metamorphism of the Meguma group of Nova Scotia. *Canadian Journal of Earth Sciences,* 3**,** 959-974.

THOMAS, H. V., LARGE, R. R., BULL, S. W., MASLENNIKOV, V., BERRY, R. F., FRASER, R., FROUD, S. & MOYE, R. 2011. Pyrite and pyrrhotite textures and composition in sediments, laminated quartz veins, and reefs at Bendigo gold mine, Australia: insights for ore genesis. *Economic Geology,* 106**,** 1-31.

TOMKINS, A. G. 2010. Windows of metamorphic sulfur liberation in the crust: implications for gold deposit genesis. *Geochimica et Cosmochimica Acta,* 74**,** 3246-3259.

VANDENBERG, A. & COOPER, R. 1992. The Ordovician graptolite sequence of Australasia. *Alcheringa,* 16**,** 33-85.

VANDENBERG, A., WILLMAN, C., MAHER, S., SIMONS, B., CAYLEY, R., TAYLOR, D., MORAND, V., MOORE, D. & RADOJKOVIC, A. 2000. The Tasman fold belt system in Victoria: East Melbourne, Victoria. *Geological Survey of Victoria Special Publication,* 462 p.

WHITE, C. E. 2008. Defining the stratigraphy of the Meguma Supergroup in southern Nova Scotia: where do we go from here. *Atlantic Geology,* 44**,** 58.

WHITE, C. E. 2010. Stratigraphy of the Lower Paleozoic Goldenville and Halifax groups in southwestern Nova Scotia: *Atlantic Geology,* 46**,** 136-154.

WHITE, C. E. & BARR, S. M. 2010. Lithochemistry of the Lower Paleozoic Goldenville and Halifax groups, southwestern Nova Scotia, Canada: Implications for stratigraphy, provenance, and tectonic setting of the Meguma terrane. *Geological Society of America Memoirs,* 206**,** 347-366.

WHITE, C. E. & BARR, S. M. 2012. Meguma Terrane revisited: stratigraphy, metamorphism,

paleontology, and provenance. *GAC-MAC 2012 St. John's post meeting field guide summary, Geoscience Canada,* 39**,** 8-12.

WHITE, C. E. & GOODWIN, T. A. 2011. Lithogeochemistry, petrology, and the acid-generating potential of the Goldenville and Halifax groups and associated granitoid rocks in metropolitan Halifax Regional Municipality, Nova Scotia, Canada. *Atlantic Geology,* 47**,** 158-184.

WHITE, C. E., PALACIOS, T., JENSEN, S. & BARR, S. 2012. Cambrian–Ordovician acritarchs in the Meguma terrane, Nova Scotia, Canada: resolution of early Paleozoic stratigraphy and implications for paleogeography. *Geological Society of America Bulletin,* 124**,** 1773-1792.

WILDE, A. R. 1989. A review of gold mineralisation in Eastern Australia - May 1988. *Bureau of Mineral Resources,* Record 1989/030**,** 132 p.

WILLMAN, C. E. 2007. Regional structural controls of gold mineralisation, Bendigo and Castlemaine goldfields, Central Victoria, Australia. *Mineralium Deposita,* 42**,** 449-463.

WILLMAN, C. E., KORSCH, R., MOORE, D., CAYLEY, R., LISITSIN, V., RAWLING, T., MORAND, V. & O'SHEA, P. 2010. Crustal-scale fluid pathways and source rocks in the Victorian gold province, Australia: insights from deep seismic reflection profiles. *Economic Geology,* 105**,** 895-915.

WILLNER, A. P., MASSONNE, H. J., BARR, S. M., & WHITE, C. E. 2013. Very low-to low-grade metamorphic processes related to the collisional assembly of Avalonia in SE Cape Breton Island (Nova Scotia, Canada). *Journal of Petrology,* 54**,** 1849-1874.

ZENTILLI, M., GRAVES, M. C., MULJA, T., MACINNIS, I. & MATHESON, J. R. 1986. Geochemical characterization of the Goldenville-Halifax Transition of the Meguma

Group of Nova Scotia. *Nova Scotia Department of Mines and Energy,* Preliminary Report ME 1986-001**,** 237 p.

Chapter 10: SUMMARY OF MAJOR CONCLUSIONS

10.1 Aims

This chapter aims to provide a concise summary of the major findings presented within this thesis.

10.2 On the Source of W in Turbidite-hosted Orogenic Au Deposits

This study has identified that in the lowest metamorphic grade metasedimentary rocks of the Otago Schist, Meguma Terrane, and Bendigo-Ballarat Terrane, the major W host mineral phase was detrital rutile.

Detrital rutile was observed in all study areas (Otago Schist, Meguma Terrane, and Bendigo-Ballarat Terrane), recrystallizing under prograde metamorphism and releasing W. In the calcareous rocks of the Otago Schist, detrital rutile recrystallizes to metamorphic titanite at subgreenschist to lower greenschist facies conditions. Whereas in the more pelitic rocks of the Bendigo-Ballarat and Meguma Terranes, detrital rutile recrystallizes to metamorphic ilmenite at approximately the biotite-in isograd.

Based on conservative estimates of rutile volume abundance in the lowest metamorphic grade metasediments in all of the study areas, significant amounts of W are released (0.41 g, 1.9 g, and 0.18 g of W per ton of rock, in the Otago Schist, Meguma Terrane, and Bendigo-Ballarat Terrane, respectively) during the metamorphic recrystallization of rutile to titanite or ilmenite.

In the Otago Schist the development of scheelite closely followed the progression of the W-liberating reaction (rutile to titanite), with scheelite micrograins forming early within the fabric of the rock, and increasing in size with increasing metamorphic grade. Scheelite is

observed with increasing metamorphism (upper pumpellyite-actinolite to lower greenschist facies), being incorporated into locally derived metamorphic veins. These scheelite-bearing veins, with further increases in metamorphic grade, are increasingly deformed and recrystallized, and scheelite that was mobilized into these veins, would be removed from the rock by metamorphic fluids produced at the upper greenschist to amphibolite transition.

Metal-rich metamorphic fluids produced at the upper greenschist – amphibolite facies transition zone, from either the remobilization of earlier scheelite (Otago Schist) or mobilization from the rutile to ilmenite recrystallization reaction (Meguma Terrane), is the source of W in the orogenic deposits of the Otago Schist and Meguma Terrane.

It is clear from mass-balance calculations presented within this thesis that significantly larger amounts of W are mobilized from the metasedimentary country rocks than is observed in orogenic deposits. Precipitation of scheelite in the Meguma Terrane appears controlled somewhat by the presence of more calcerous lithologies, with the majority of scheelite-bearing deposits in the Meguma Terrane hosted within the upper part of the Goldenville Group (Fisher 1984; Zentilli et al. 1986; Dostal et al. 2009) that are distinctly enriched in CaO compared to the bulk CaO concentrations of the Halifax and Goldenville Groups. Furthermore, locally numerous Ca-silicate nodules and rare beds (up to 0.5 m wide) are present within the Goldenville Group and to a lesser extent in the Halifax Group, and are occasionally observed containing scheelite (Mitchell 2003; Reid 2005). This further suggests that a major limiting factor for the formation of scheelite in the Meguma Terrane might have been the availability of Ca through wall-rock alteration.

Wall-rock alteration and its importance in the precipitation of scheelite has previously been reported in the W-bearing deposits of Glenorchy (Otago Schist) (for example, Paterson and

Rankin 1979). Here alteration of Ca-silicate minerals by the W-rich metamorphic fluid, provides the additional Ca required to precipitate scheelite ($CaWO_4$), along with providing trace amounts of Sr and Y. Results presented within this thesis suggest the same process occurred at the Macraes Mine (Otago Schist), with the alteration of Ca-silicate minerals (metamorphic titanite and epidote), providing the additional Ca for the precipitation of scheelite ($CaWO_4$). In addition, alteration of these Ca-silicate minerals at Macraes Mine has provided trace amounts of REEs, Sr, and Y to the scheelite.

The lack of W in the orogenic deposits of the Bendigo-Ballarat Terrane, possibly reflects the source of these deposits as being the lower greenschist facies metasediments (with recrystallization and mobilization of W, in these rocks likely occurring at upper greenschist facies). This lack of W in the orogenic deposits of the Bendigo-Ballarat Terrane, potentially precludes previous models that have suggested source rocks for Au in these deposits as being either Castlemaine metasediments at the greenschist-amphibolite transition or underlying Cambrian volcano-sedimentary rocks. However, the lack of scheelite in the Bendigo-Ballarat Terrane could also result from other factors, such as variations in the conditions of formation of the mineralized veins (P, T, pH, redox, host-rock composition) that may not favor the transport and/or precipitation of W. These factors were unable to be resolved in this study.

The results presented within this thesis support recent models for turbidite-hosted orogenic Au mineralization, whereby prograde metamorphic recrystallization of diagenetic or detrital metal-rich mineral phases [pyrite to pyrrhotite, Au, As, Ag, Hg, and Sb; rutile to titanite or ilmenite, W] can release significant amounts of these metals into the concurrently developing metamorphic fluids that can be subsequently focused into regional structures and form orogenic Au ± W deposits.

References

DOSTAL, J., KONTAK, D. J., & CHATTERJEE, A. 2009. Trace element geochemistry of scheelite and rutile from metaturbidite-hosted quartz vein gold deposits, Meguma Terrane, Nova Scotia, Canada: genetic implications. *Mineralogy and Petrology,* 97**,** 95-109.

FISHER, B. E. 1984. A regional investigation of scheelite occurrences in the Meguma Group of Nova Scotia. *Unpublished B.Sc. Thesis,* Dalhousie University, Canada**,** 201 p.

MITCHELL, F. 2003. Metamorphic petrology of calc-silicate nodules from greenschist facies to migmatite grade, Liverpool-Pubnico area, Nova Scotia. *Unpublished B.Sc. Thesis,* Acadia University, Canada**,** 95 p.

PATERSON, C. J. & RANKIN, P. C. 1979. Trace element distribution in the schist surrounding a quartz-scheelite lode, Glenorchy, New Zealand. *New Zealand Journal of Geology and Geophysics,* 22**,** 329-338.

REID, C. 2005. Metamorphism of the Southern Meguma terrane and emplacement of the Barrington Passage and Quinan Plutons, southwestern Nova Scotia. *Unpublished M.Sc. Thesis,* Acadia University, Canada**,** p. 211.

ZENTILLI, M., GRAVES, M. C., MULJA, T., MACINNIS, I. & MATHESON, J. R. 1986. Geochemical characterization of the Goldenville-Halifax Transition of the Meguma Group of Nova Scotia. *Nova Scotia Department of Mines and Energy,* Preliminary Report ME 1986-001**,** 237 p.